



UNIVERSITY OF AGRONOMIC SCIENCES  
AND VETERINARY MEDICINE OF BUCHAREST  
FACULTY OF LAND RECLAMATION  
AND ENVIRONMENTAL ENGINEERING



# SCIENTIFIC PAPERS

SERIES E

LAND RECLAMATION, EARTH OBSERVATION &  
SURVEYING, ENVIRONMENTAL ENGINEERING

VOLUME VIII



2019  
BUCHAREST

# SCIENTIFIC PAPERS

SERIES E

LAND RECLAMATION, EARTH OBSERVATION &  
SURVEYING, ENVIRONMENTAL ENGINEERING

VOLUME VIII





UNIVERSITY OF AGRONOMIC SCIENCES  
AND VETERINARY MEDICINE OF BUCHAREST  
FACULTY OF LAND RECLAMATION  
AND ENVIRONMENTAL ENGINEERING

# SCIENTIFIC PAPERS

SERIES E

LAND RECLAMATION, EARTH OBSERVATION &  
SURVEYING, ENVIRONMENTAL ENGINEERING

VOLUME VIII

2019  
BUCHAREST

## EDITORIAL BOARD

**General Editor:** Ana VÎRSTA

**Executive Editor:** Mirela Alina SANDU

**Members:** Mariana Cătălina CĂLIN, Carmen CÎMPEANU,  
Claudiu Sorin DRAGOMIR, Raluca MANEA, Patricia MOCANU,  
Sevastel MIRCEA, Tatiana OLINIC, Gabriel POPESCU, Augustina TRONAC

### PUBLISHERS:

**University of Agronomic Sciences and Veterinary Medicine of Bucharest, Romania -  
Faculty of Land Reclamation and Environmental Engineering**

Address: 5 9 Marasti Blvd., District 1, Zip code 011464 Bucharest, Romania  
Phone: + 40 213 1830 75, E-mail: conference@fifim.ro, Webpage: www.fifim.ro

### CERES Publishing House

Address: 29 Oastei Street, District 1, Bucharest, Romania  
Phone: + 40 21 317 90 23, E-mail: edituraceres@yahoo.com, Webpage: www.editura-ceres.ro

### Copyright 2019

*To be cited: Scientific Papers. Series E. LAND RECLAMATION, EARTH  
OBSERVATION & SURVEYING, ENVIRONMENTAL ENGINEERING, Vol. VIII, 2019*

*The publishers are not responsible for the content of the scientific papers and opinions  
published in the Volume. They represent the authors' point of view.*

**Print ISSN 2285-6064, CD-ROM ISSN 2285-6072, Online ISSN 2393-5138, ISSN-L 2285-6064**

### International Database Indexing:

Web of Science Core Collection (Emerging Sources Citation Index)  
Index Copernicus; Ulrich's Periodical Directory (ProQuest); PNB (Polish Scholarly Bibliography);  
Scientific Indexing Service; Cite Factor (Academic Scientific Journals) Scipio; OCLC; Research Bible

## SCIENTIFIC & REVIEW COMMITTEE

### SCIENTIFIC CHAIRMAN

Prof. univ. dr. Sorin Mihai CÎMPEANU

### MEMBERS\*

- Alexandru BADEA - University of Agronomic Sciences and Veterinary Medicine of Bucharest, Romania
- Ioan BICA - Technical University of Civil Engineering of Bucharest, Romania
- Daniel BUCUR - „Ion Ionescu de la Brad” University of Agricultural Sciences and Veterinary Medicine of Iasi, Romania
- Stefano CASADEI - University of Perugia, Italy
- Fulvio CELICO - University of Molise, Italy
- Carmen CÎMPEANU - University of Agronomic Sciences and Veterinary Medicine of Bucharest, Romania
- Sorin Mihai CÎMPEANU - University of Agronomic Sciences and Veterinary Medicine of Bucharest, Romania
- Marcel DARJA - University of Agricultural Sciences and Veterinary Medicine of Cluj-Napoca, Romania
- Claudiu DRAGOMIR - University of Agronomic Sciences and Veterinary Medicine of Bucharest, Romania
- Eric DUCLOS-GENDREU - Spot Image, GEO-Information Services, France
- Delia DUMITRIU - Manchester Metropolitan University, United Kingdom
- Ion GIURMA - „Gheorghe Asachi” Technical University of Iasi, Romania
- Jean-Luc HORNICK - Faculté de Médecine Vétérinaire, Université de Liège, Belgium
- Ilias KYRIAZAKIS - Newcastle University - United Kingdom
- Eugeniu LUCA - University of Agronomic Sciences and Veterinary Medicine of Bucharest, Romania
- Carmen MAFTEI - Ovidius University of Constanta, Romania
- Raluca MANEA - University of Agronomic Sciences and Veterinary Medicine of Bucharest, Romania
- Florin MĂRĂCINEANU - University of Agronomic Sciences and Veterinary Medicine of Bucharest, Romania
- Sevastel MIRCEA - University of Agronomic Sciences and Veterinary Medicine of Bucharest, Romania
- Nicolae PETRESCU - Valahia University Targoviste, Romania
- Marius Ioan PISO - Romanian Space Agency, Romania
- Maria POPA - „1 Decembrie 1918” University of Alba Iulia, Romania
- Dorin Dumitru PRUNARIU - Romanian Space Agency, Romania
- Ramiro SOFRONIE - University of Agronomic Sciences and Veterinary Medicine of Bucharest, Romania
- Răzvan Ionuț TEODORESCU - University of Agronomic Sciences and Veterinary Medicine of Bucharest, Romania
- Augustina TRONAC - University of Agronomic Sciences and Veterinary Medicine of Bucharest, Romania
- Ana VÎRSTA - University of Agronomic Sciences and Veterinary Medicine of Bucharest, Romania

*\*alphabetically ordered by family name*



# CONTENTS

## ENVIRONMENTAL SCIENCE AND ENGINEERING

1	AN ASSESSMENT OF THE ENERGETIC PROPERTIES OF FUEL PELLETS MADE BY AGRICULTURAL WASTES - <b>Hasan Huseyin OZTURK, Bulent AYHAN, Kazim TURGUT</b> .....	9
2	ANALYSIS IN TERMS OF STRUCTURAL DISPLACEMENTS AND ACCELERATIONS FOR SOME TOWER BUILDINGS UNDER MODERATE MAGNITUDE EARTHQUAKES - <b>Stefan Florin BALAN, Alexandru TIGANESCU, Bogdan Felix APOSTOL</b> .....	17
3	THE USAGE OF THE FAE FIXED WING UAV FOR THE EVALUATION OF AFFECTED RAPESEED CULTURE DUE TO PEST ATTACKS - <b>Alexandra TRIF, Mihai GIDEA, Cristian CIOINEAG, Sorin Mihai CIMPEANU</b> .....	22
4	THE LIMITATION OF ANTIBACTERIAL USE OF SILVER IONS: ACTING AS SELECTIVE AGENTS FOR PROKARYOTE GENETIC RESOURCES - <b>Cristian Mihai AURORI, Daniel Severus DEZMIREAN</b> .....	28
5	STUDIES ON THE EFFECTS OF VIBRATIONS FROM INDUSTRIAL ENVIRONMENTS - <b>Claudiu-Sorin DRAGOMIR, Daniela DOBRE</b> .....	39
6	AN ENERGY EFFICIENCY PROJECT FOR A BROILERS FARM - <b>Georgi KOMITOV, Violeta RASHEVA, Georgi VALTCHEV</b> .....	45
7	NOVEL MBBR SYSTEMS BIOFILM CARRIERS AND PHYSICAL-CHEMICAL ANALYSIS - <b>Ovidiu IORDACHE, Ioana Corina MOGA, Cornelia MITRAN, Dana CIUTARU, Irina SANDULACHE, Lucia SECAREANU, Gabriel PETRESCU, Elena PERDUM</b> .....	53
8	BIO-AUGMENTATION OF POLYETHYLENE BIOFILM CARRIERS BY <i>Ceritoporus squamosus</i> WHITE ROT FUNGI - <b>Ovidiu IORDACHE, Ioana Corina MOGA, Cornelia MITRAN, Dana CIUTARU, Irina SANDULACHE, Lucia SECAREANU, Gabriel PETRESCU, Elena PERDUM</b> .....	59
9	EFFECT OF COMPOST AND VERMICOMPOST AMENDMENTS ON HEAVY METALS UPTAKE BY TOBACCO - <b>Violina ANGELOVA, Zhivko TODOROV</b> .....	65
10	THE IMPACT OF METEOROLOGICAL DROUGHT CASE STUDY - NORTHEASTERN ROMANIA - <b>Flaviana CORDUNEANU, Sorin Mihai CIMPEANU, Silviu IORDACHE, Denis-Constantin TOPA, Claudiu-Ionut PRICOP, Isabela-Elena BALAN, Daniel BUCUR</b> .....	71

## SUSTAINABLE DEVELOPMENT OF RURAL AREA

1	DEGRADATION OF VEGETAL COVER THROUGH INAPPROPRIATE GRAZING ON LANDS ARRANGED WITH DRAINAGE WORKS - <b>Minodora AILENEI (RADU), Oprea RADU, Daniel BUCUR, Razvan Ionut TEODORESCU</b> .....	79
2	EUROPEAN UNION STRATEGY AND CROSS-BORDER COLLABORATION - OPPORTUNITIES FOR CITIZENS IN THE LOWER DANUBE REGION - <b>Cristiana SIRBU</b> .....	87
3	TREND ANALYSIS IN TEMPERATURE, PRECIPITATION AND HUMIDITY: THE CASE OF MEDITERRANEAN REGION - <b>Ali YÜCEL, Atilgan ATILGAN, Hasan ÖZ</b> .....	91
4	DETERMINATION OF GEOTHERMAL ENERGY AREAS AND USAGE POSSIBILITIES IN GREENHOUSE HEATING - <b>Hasan ERTOP, Atilgan ATILGAN, Ercüment AKSOY</b> .....	99
5	DEVELOPING A WEATHER-BASED INDEX FOR CROP INSURANCE TO PROMOTE SUSTAINABLE AGRICULTURE AND MITIGATE AN AGRARIAN CRISIS, A CASE STUDY IN INDIA - <b>Vijendra BOKEN</b> .....	109

## TOPOGRAPHY AND CADASTER

1	DETERMINING STOCKPILE VOLUMES USING PHOTOGRAMMETRIC METHODS - <b>Tudor SALAGEAN, Elemer-Emanuel SUBA, Ioana Delia POP, Florica MATEI, Jutka DEAK</b> .....	114
2	SUSTAINABLE ARCHITECTURE: RESTORATION OF THE FACADES OF HISTORIC BUILDINGS USING MODERN METHODS - <b>Bogdan ERGHELEGIU, Alexandra TRIF, Raluca-Margareta MANEA</b> .....	120

## EARTH OBSERVATION AND GEOGRAPHIC INFORMATION SYSTEMS

1	INVESTIGATION OF ANIMAL ORIGIN BIOGAS POTENTIAL USING GEOGRAPHICAL INFORMATION SYSTEMS: EAST MEDITERRANEAN REGION CASE - <b>Ozan ARTUN, Burak SALTUK</b> .....	126
2	A COMPARISON OF BIOCLIMATIC FACTORS EFFECT FOR CUTANEOUS LEISHMANIASIS CURRENT STATUS BETWEEN EASTERN MEDITERRANEAN REGION AND TIGRIS BASIN OF TURKEY BY USING ECOLOGICAL NICHE MODELING - <b>Ozan ARTUN, Hakan KAVUR</b> ...	134
3	MAKING A DIGITAL DATABASE REGARDING LAND ANTI-EROSION ORGANIZATION WORKS AND ITS DISSEMINATION THROUGH THE CARRY MAP EXTENSION - <b>Maria-Olivia MOLDOVAN, Marcel DIRJA, Iulia-Diana GLIGA (ARION), Mihai VOEVOD</b> .....	142
4	RESEARCHES REGARDING THE USE OF G.I.S. TECHNOLOGIES IN MODELLING AND SPATIAL ANALYSIS OF THE VARATEC MINING COMPLEX, MARAMURES COUNTY - <b>Petruta SOLCAN, Tudor SALAGEAN, Elemer-Emanuel SUBA, Marioara ILEA</b> .....	148
5	ANALYSIS OF THE INFLUENCE OF OROGRAPHICAL FACTORS ON THE PLANIMETRIC ACCURACY OF POINTS DETERMINED USING GPS IN FORESTED AREAS - <b>Cornel Cristian TERESNEU, Maria Magdalena VASILESCU</b> .....	152
6	WEB PLATFORM SOLUTION FOR SMART FARMING MANAGEMENT - <b>Andreea CALUGARU, Petre LEU, Andreea DAMALAN, Doru MIHAI</b> .....	156
7	SHADOWS CORRECTION METHODS FOR LANDSAT SATELLITE IMAGES - <b>Bianca BADULESCU, Alexandru Marin MATACHE, Luciana VRANCUTA, Silviu MUSAT, Sevastel MIRCEA, Nicolae PETRESCU</b> .....	162
8	ADVANTAGES OF REALISTIC REPRESENTATION OF A GEOGRAPHIC AREA BY COMBINING OPTICAL AND LIDAR DATA CAPTURED WITH UAVs - <b>Gabriel POPESCU, Octavian Laurentiu BALOTA, Daniela IORDAN, Daniel ILIE</b> .....	169

## MISCELLANEOUS

1	PROTEIN SOURCES FOR ANIMAL FEED: YEAST BIOMASS OF BEER AND/OR WINE - REVIEW - <b>Corina DUMITRACHE, Florentina MATEI, Diana Iuliana BARBULESCU, Mihai FRINCUI, Valerica TUDOR, Lucian Nelutu HIRJOABA, Razvan Ionut TEODORESCU</b> .....	175
2	COMPARE OF THE TECHNICAL MEANS WHEN ADMINISTERED OF PLANT EXTRACTS FOR CONTROL OF R PESTS OF OIL SEED RAPS - <b>Dimitar KEHAYOV, Nedyalka PALAGACHEVA</b> .....	183
3	INFLUENCE OF SOME FACTORS ON THE GAS FLOW PRODUCED BY HHO GENERATOR - <b>Dimitar KEHAYOV, Georgi KOMITOV, Ivan IVANOV</b> .....	188
4	ADVANTAGES OF USING THE ELECTRO-KINETIC METHOD FOR SOIL DEPOLLUTION - <b>Maria POPA, Loredana Irena NEGOITA, Bogdan Petre ARNAUTU</b> .....	192
5	BIO-INGREDIENTS BASED ON SPENT INDUSTRIAL YEAST BIOMASS - <b>Simona-Ioana MARINESCU, Daniela Eliza MARIN, Zsuzsa JÓKAI, Márta ÜVEGES, Madalina ALBU KAYA, Vasile BUNDUC, Mihály DERNOVICS, Hajnalka HINGYI, Mihaela BEGEA, Iuliana Diana BARBULESCU</b> .....	196

## AN ASSESSMENT OF THE ENERGETIC PROPERTIES OF FUEL PELLETS MADE BY AGRICULTURAL WASTES

Hasan Huseyin OZTURK<sup>1</sup>, Bulent AYHAN<sup>2</sup>, Kazim TURGUT<sup>2</sup>

<sup>1</sup>Cukurova University, Faculty Engineering of Agricultural Machinery and Technology, 01330, Adana, Turkey

<sup>2</sup>Ministry of Agriculture and Forestry, Directorate of Agricultural Production Enterprise, Agricultural Extension and Training Center Mithat Ozsan Bulvarı Koprulu Mahallesi, 01230, Yuregir, Adana, Turkey

Corresponding author email: hhozturk@cu.edu.tr

### Abstract

*In this study, it is aimed to produce pellets for use as solid biofuel from corn production wastes. Palletization of the biomass material increases volumetric heat value, reduces transport and storage costs, improves combustion properties, reduces emissions of particulate emissions, and produces a biofuel of the same size and shape. For this purpose, corn stalks were milled with a hammer mill and pellets were produced in an automatic feed pelletizing machine. Pellets produced from corn waste; hardness resistance, water absorption resistance, moisture content, ash content, equivalent moisture content, gas emission values released in the combustion result and calorific values which are important indicators of energy content have been determined. The upper calorific value of maize pellets with an average length of 17.28 mm and a diameter of 6.26 mm was determined to be 18.11 MJ/kg. The CO<sub>2</sub>, NO and NO<sub>x</sub> emission values of pellets from corn stalks were measured as 4.7 ppm, 38 ppm and 40 ppm, respectively. The evaluation of corn waste as pelletized solid biofuel will contribute to the prevention of agricultural land damage and environmental pollution as a result of the burning of residual vegetable waste from corn production.*

**Key words:** ash content, biopellet, corn wastes, heating values.

### INTRODUCTION

Global emissions of greenhouse gases, caused by the use of fossil fuels all over the world, have led to further global warming threats and the steady decline of fossil fuel reserves has encouraged countries to be more interested in environmentally friendly, renewable energy sources. Between 1970 and 2004, CO<sub>2</sub> emissions from fossil fuel use increased by about 80% and global temperature by 0.5°C. If the air pollution continues at this level, it is predicted that the temperature will rise to 4-5°C and the sea level will rise to 2.2 m in the next 100 years (IPCC, 2011). On the other hand, estimating that energy demand across the globe will increase by about 55% between 2005 and 2030 does not justify worries about the anticipated drawbacks of global climate change, but also obliges the energy sector to reduce fossil fuel consumption. Therefore, to reduce fossil fuel consumption, the European Commission has set a goal of raising the renewable energy consumption rate, which is currently 5% in Europe, to 20% by 2020. In

Turkey as well, priority is given to strategic planning to ensure resource diversification by prioritizing domestic resources and to increase the share of renewable energy resources in energy supply. In this context, in order to reduce the external dependency rate of 73% on energy, it is aimed that the share of renewable energy resources in electric energy production in 2023 should be at least 30%.

In today's Turkey, some industries are benefiting from agricultural wastes on a small scale. Nevertheless, the private sector is not yet sufficiently interested in the biomass and solid waste-based power plants, due to the financial and technical obstacles to the use of biomass energy in Turkey, and the inadequacy of policy and market instruments. The fact that any residual vegetable waste is not evaluated and destroyed as a result of agricultural production seriously causes environmental pollution and creates economic loss. The aim of this research is to improve the use of agricultural biomass resources in Turkey by using sustainable methods and taking into account the environmental-economic-social benefits of new

technologies. In this study, it is aimed to produce pellets for use as solid biofuel from the remaining biomass material except corn in seed production. In Turkey corn production areas are treated by burning or crushing soil to remove remaining plant wastes. The incineration of corn plant wastes causes beneficial organisms in the soil and harmful environmental effects. On the other hand, the process of shredding plant wastes into the soil causes considerable energy consumption. As a result of the production of corn, the remaining palletization of biomass waste will be eliminated and the environmentally friendly, clean and renewable fuel will be produced with improved physical properties and combustion characteristics. The pelletizing process will facilitate the transport and storage of residues and at the same time reduce shipping costs. Most importantly, the evaluation of such biomass materials through palletization will provide for the economization of waste and will partially or even reduce our country's external dependency on energy.

The utilization of pellet fuel not only protects the environment, but also the best substitute for coal and natural gas. The cost of pellet fuel is less than half price of the coal, but it has the same heat as the coal, and a kilo of pellet can be burned for hours. The raw materials of biomass pellet fuel are very extensive; they can be the crop straw, wood processing waste such as wood chips, bark, etc. All of the raw material with lignin can be used to make biomass pellet fuel. For that reason, in the present study, it was aimed to pelletize biomass waste from corn stalks as solid biofuels. The pelletization of corn waste has reduced storage and transport costs and improved combustion characteristics, resulting in a cheap, quality, environmentally friendly, domestic and renewable biomass solid fuel. The physico-mechanical properties of the produced pellets and the emission values resulting from combustion are determined. Endurance resistance, hardness resistance, dehydration resistance, moisture content, ash content, equivalent moisture content, gas emission values released as a result of combustion, and thermal values which are an important indicator of energy content of the pellets produced from corn stems were identified. The higher and lower heating values (HHV and LHV) were

determined and compared to the standards used in the European Union for biomass-produced pellets.

## **MATERIALS AND METHODS**

### **Biopellets production**

The evaluation of agricultural wastes in the form of solid fuel as a source of energy is of great importance in Turkey as well as in the whole world. One of the easiest and most effective ways to generate energy from agricultural wastes is to use these wastes as solid fuel. However, the most important problem encountered in using vegetable wastes as solid fuel is the low density of vegetable wastes and the high moisture content. Low density and high moisture content also bring with it transportation and storage problems. For this reason, one of the methods to be applied in order to use vegetable wastes efficiently and easily in order to produce energy is to dry these wastes and to pellet them after grinding.

One of the effective methods for using agricultural residues as improved solid fuels is pelletizing. In recent years, palletization has become increasingly prevalent and the use of pellets has become widespread. The pellet has a small, cylindrical shape resembling animal feed. Biomass pellets are generally 6-12 mm in diameter and 10-30 mm in length. The process of bringing the material into a smaller size (about 30 mm) under pressure is called pelletizing. Pellets can be produced from materials such as wood chips, wood chips, tree bark, agricultural products, grains, nuts, almonds, walnut shells, and even paper. Biological crops such as corn cobs, beet pulp, sunflower spices, dried olives, cherry seeds and soybean can also be used in the production of pellets. The pelletizing process increases the density of the material, reduces transportation, storage and transport costs, and ensures homogeneity in size and shape can be fed automatically to the combustion systems for thermal purposes, thus enabling more efficient use of the material.

Roller presses are used in biomass pelletizing machines. Small press (approx. 30 mm) is used in the cylinder presses. For this reason, this type of press is also called pellet press. There are a number of molds arranged in thick steel

discs or holes drilled on the ring. The material is forced into the molds by means of 2 or 3 cylinders. The process flow and main components for biomass palletization is given in Figure 1. Biomass pellet production consists of following processes; raw materials, screening, drying, cyclone separation, forming granulation, cooling, screening, finished products. At the same time, each part is equipped with strict quality control system to ensure the product quality.

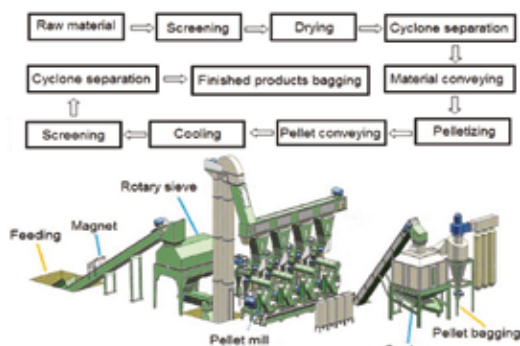


Figure 1. Pellet process flow diagram and main parts of the pellet plant (Kyriakopoulos et al., 2016)

Agricultural wastes can be used singly or as a solid fuel by mixing. In this case, when the wastes with higher quality and higher thermal value are used together with wastes with lower thermal value, the thermal value of the mixture is increased. High quality agricultural wastes, in terms of thermal value and ash content, are used as solid fuel in excess amount when they are mixed with agricultural wastes which are high in quantity and low in thermal value. Among the remaining wastes from field crop production, the thermal values of rice paddy and rice paddy are the lowest values (14.65 MJ/kg).

### Pellet material and palletization process

Approximately 200 kg corn stalks were harvested from corn grown during the first crop corn production period in 2016 and 2017 at Cukurova University Agricultural Faculty Research and Application Farm. Corn pellets using collected corn wastes were produced at a pellet production facility in the Adana Organize Industrial Zone. Corn stalks were passed through the mill and made into small powder.

Then, the powdered material was dried in the oven to reduce the humidity. The dried material was pelletized by pressing under high pressure. The pressed material was cooled and ready for use at the end of packaging.

### Determination of physical and chemical characteristics of biopellets

#### Moisture content

The moisture content of the biomass material was measured in two steps, before and after pelletizing. The moisture content of the pellets was determined according to the ASAE D245.6 standard (ASAE, 2007). For this purpose, the biomass material was stored in a drying oven at 105°C for 24 hours. Moisture contents were determined according to wet basis, taking into account the masses measured before and after drying.

#### Dehumidification resistance

The damping resistances of the pellets were determined using a conditioning test cabinet. In this test, pellet specimens of 300 g mass were analyzed at 4 different temperatures (15°C, 25°C, 35°C and 45°C) and 3 different moisture contents (50%, 65% and 80%) in the air conditioning test cabinet, depending on the temperature and humidity content, they were kept waiting for a time period of 22-68 hours.

#### Equivalent moisture content

The pellets produced were stored 21 days under normal environmental conditions and the difference between the recorded first and last masses was calculated as the equivalent moisture content.

#### Water intake resistance

Water intake (or sorption) resistance is intended to monitor the amount of water that the water immersed pellets absorb to their structure after a certain period of time and consequently the deterioration of their structure. For this purpose, the pellets were weighed and stored before the water was immersed in the water. Each pellet sample was then submerged at a depth of 25 mm into a water-filled container at a temperature of about 27°C. After a total of 30 s, the pellets were removed and the masses were again measured.

This process was repeated four times for the same pellet sample.

#### **Durability resistance**

The durability of the pellets was determined using a durability tester made in accordance with the resistance standard ASAE S269.4 (ASAE, 2007). In this test, 500 g of pellet samples were placed inside the test device and continuously stirred for 10 minutes to reduce the test device. After the test, the pellets were taken out and sieved using a sieve having a hole diameter of 5.4 mm. The masses of the pellets remaining on the sieve were weighed and recorded. The resistance of the pellet was determined to be % depending on the mass loss during the test.

#### **Compression resistance**

Pellet compression resistance or hardness is defined as the maximum load applied prior to breakage of pellet. This test is performed during transport and storage to calculate the pressures that the upper pellets apply to the underlying pellets. The hardness of the densified products is often determined by the compression resistance test. For this purpose, a manually controlled pressure tester was used. In this test, 50 randomly selected pellets were used from the pellet samples. Each pellet was placed between two plates and compressive loads were applied to the pellets by compression strength tester. The applied compressive loads were recorded on the computer and the maximum compressive force before the pellet breakage was determined as pellet hardness. Compression resistance results are given as Newton (N).

#### **Breaking resistance**

In determining the breaking (shatter) resistance, the pellets were weighed before the test and their masses were recorded. Then, the pellets were dropped 10 times from a certain height (1-1.8 m) onto a hard surface. After the dropping process, the pellets were weighed again and their masses were recorded. The shatter resistance is calculated as percent (%).

#### **Calorific value**

The upper calorific values of the produced pellets were determined using a calorimeter

according to ASTM D5865-04 standard (ASTM, 2010). For this purpose, the pellets were kept at 105°C for 24 hours to remove the moisture. In the calorific value test, samples of 1 g mass furnace samples are burned in an oxygen environment in a calorimeter bomb under standard conditions. The calorific value is determined according to the increase in the temperature of the water in the calorimetric vessel and the average actual heat capacity of the system. The combustion heat is calculated by monitoring the temperature before combustion, at the moment of combustion and after combustion, and applying thermochemical and heat exchange corrections to them.

#### **Flue gas emissions**

In order to determine the pellets produced, their combustion characteristics and their environmental effects, flue gas emissions that have been burned and formed as a result of combustion have been measured. Pellets are burned with solid fuel-burning layer. A flue gas measuring device was used to measure the flue gas emissions resulting from the combustion of the pellets. The values of O<sub>2</sub> (%), CO (ppm), CO<sub>2</sub> (%), NO (ppm), NO<sub>2</sub> (ppm) and SO<sub>2</sub> (ppm) were determined in the emission measurements.

#### **Ash content**

The ash content of the pellets was determined by thermogravimetric tester according to ASTM D5142 standard (ASTM, 2010). In order to determine the ash content, pellet samples were first dried in a drying oven at 105°C for 24 hours. The ash content was then calculated by burning samples of 2 g mass in an ash oven for 5 hours at 800°C.

## **RESULTS AND DISCUSSIONS**

#### **Physical properties of biopellets**

The physical and chemical properties of crude biofuels are different from petroleum derived fuels. Biofuels with very complex structure contain more than about 300 components. In general, crude biofuels consist of a mixture of organic acids, alcohols, aldehydes, esters, ketones, phenols, furans and lignin-derived oligomers (Xiu & Shahbazi, 2012). The

physical and thermal analyzes of the produced corn pellets were carried out in laboratories of the Department of Energy Plants of the Black Sea Agricultural Research Institute. In the following sections, the results of the analysis are given and the evaluations are carried out.

### Dimensions of biopellets

The average length of pellets produced from corn stalks (Figure 2) is 17.28 mm. The diameter of the produced pellets is measured as 6.26 mm on average. For biomass pellets, it has been reported in the European standard EN 16127 that pellet length should be 3.15-40 mm and diameter 6-8 mm. The length and diameter of pellets produced from corn stems are in line with the EU standard EN 16127 (EN, 2013).



Figure 2. Pellets made from corn stems

### Strength of biopellets

Strength resistance of the pellets produced from corn stalks was determined to be 93.82%. The durability of the produced pellets was determined to be slightly lower than the durability (> 97.5%) specified for the forest and wood waste in the EU standard EN 15210-1 (EN, 2013).

The breaking resistance and hardness of the pellets produced from corn stalks were determined to be 99.14% and 488.33 N respectively. The pellet hardness is defined as the applied maximum load before breaking the pellet. Water sorption resistance is an indication of the amount of water that the submerged pellets have absorbed into their bodies after a certain period of time and consequently the deterioration of their structure. The water sorption resistance of the corn pellets produced was determined as 76.9%

in the first minute and 120.4% in the second minute.

### Moisture content of biopellets

As the amount of water contained in biofuels increases, the thermal value decreases. If the amount of water in the fuel is excessive, it is the most important obstacle to its use as transportation fuel. According to the ASAE D245.6 standard, the moisture content of the pellets produced from corn stalks was determined to be 2.29% (ASAE, 2007). It has been determined that the moisture content of the produced corn pellets is compatible with the moisture content (% 10) specified for forest and wood waste in the EU standard EN 14775-1 (EN, 2013). In DIN 51731 standard, the pellet moisture content has been reported to be at most 12% (DIN, 1996). The moisture content of the produced corn pellets was found to be in accordance with DIN 51731 standard. The equivalent moisture content of corn pellets was determined to be 1.012% after 1 week and 1.013% after 3 weeks.

### Calorific values of biopellets

The calorific value of a fuel is the quantity of heat produced by its combustion at constant pressure and under normal (standard) conditions (i.e. to 0°C and under a pressure of 1013 mbar). The combustion process generates water vapor and certain techniques may be used to recover the quantity of heat contained in this water vapor by condensing it. Therefore, are there mainly two types of calorific values:

*Higher Calorific Value* (HCV or Gross Calorific Value-GCV, or Higher Heating Value-HHV): When 1 kg of a fuel is burnt, the heat obtained by the complete combustion after the products of the combustion are cooled down to room temperature (usually 15°C) is called *higher calorific value* of that fuel (HCV). The water of combustion is entirely condensed and that the heat contained in the water vapor is recovered.

*Lower Calorific Value* (LCV or Net Calorific Value-NCV, or Lower Heating Value-LHV): When 1 kg of a fuel is completely burned and the products of combustions are not cooled down or the heat carried away the products of combustion is not recovered and the steam produced in this process is not condensed then

the heat obtained is known as the *lower calorific value* (LCV). The products of combustion contain the water vapor and that the heat in the water vapor is not recovered. The LCV is the energy that turns on as a result of burning the fuel.

The relation between HCV and LCV is the amount of LCV can be obtained by subtracting the amount heat carried away by the combustion products especially the heat carried away by the steam. The LCV is about 8-9% lower than the HCV due to the condensation heat of the water vapor which is released as a result of combustion (Antmen, 2019).

The HCV of the pellets produced from corn stalks were determined to be 4325 cal/g (18.11 MJ/kg) using the calorimeter apparatus according to ASTM D5865-04 standard (ASAE, 2007). If the LCV of the produced corn pellets is assumed to be 8% lower than the HCV, it was calculated as 16.66 MJ/kg. It has been reported that the pellet calorific value in the EU standard (EN 14918) must be within the range of 16-19 MJ/kg for biomass pellets. The LCV of pellets produced from corn stems is suitable to the EU standard (EN 16127) (EN 2013). However, it has been reported that for the pellets the calorific value should be at least 17.5 MJ/kg in the German DIN 51731 standard. On the other hand, the LCV of the corn pellets (16.66 MJ/kg) is higher than that of industrial lignite (12.56 MJ/kg), central lignite (8.37 MJ/kg), Elbistan lignite (4.60 MJ/kg), wood (12.56 MJ/kg), animal and plant waste (9.62 MJ/kg) reported by Ozturk, 2008.

#### **Ach content of biopellets**

It is desirable that the ash content in a good fuel is low. The ash content of the corn pellets was determined to be 2.01% by thermogravimetric analyzer according to ASTM D-5142 standard (ASTM, 2010). The ash content of the produced corn pellets was determined to be in accordance with the ash content (< 3%) specified for the forest and wood waste (EN-B) in the EU standard EN 14775 (EN, 2013). On the other hand, it has been reported in the DIN 51731 standard (DIN, 1996) that the pellet ash content should be at most 1.5%. The moisture content of the corn pellets produced was found to be in accordance with DIN 51731 standard.

#### **Flue Gas Emissions for Corn Pellets**

The flue gas analysis of the produced corn pellets was carried out at the laboratories of the Energy Plant Department of the Black Sea Agricultural Research Institute. The flue gas emission results of the corn pellets are given in Table 1.

Table 1. Flue gas emission values of corn pellets

Emissions	Values
O <sub>2</sub>	16.1%
CO <sub>2</sub>	4.7%
CO	1028 ppm
NO	38 ppm
NO <sub>x</sub>	40 ppm
SO <sub>2</sub>	2 ppm

#### **Oxygen**

It is desirable that the ratio of oxygen (O<sub>2</sub>) is as low as possible in the flue gases, so as not to cause carbon monoxide (CO) formation, depending on the type of fuel and air excess coefficient. Oxygen is considered to be the ideal value for flue gas analysis for natural gas 2-3%, for liquid fuels 3-4%, for solid fuels 5-6% (Bilgin, 2001). O<sub>2</sub> value of the produced corn pellets was determined as 16.1% as a result of flue gas analysis.

#### **Carbon dioxide**

Carbon dioxide (CO<sub>2</sub>) is the least harmful gas in the emissions resulting from combustion. Depending on the fuel type, CO<sub>2</sub> is preferred to be present in the flue gases in high proportions. CO<sub>2</sub> values are accepted as suitable for flue gas analysis, 11% in natural gas, 14% for liquid fuels and 14% for solid fuels. As a natural consequence of good combustion, the high CO<sub>2</sub> demand in flue gases is considered an undesirable emission in recent years, due to the greenhouse effect caused by the atmosphere. The solution here is possible with the widespread use of low-carbon, high-hydrogen-containing fuels and the limited use of fossil fuels over time (Bilgin, 2001). The CO<sub>2</sub> value was determined as 4.7%. The CO<sub>2</sub> emissions determined for corn pellets produced are much lower than the reported values for solid, liquid and gaseous fuels. This result indicates that burning of corn pellets will result in less CO<sub>2</sub> emissions compared to other fuels. This is important for the widespread use of biofuels in order to prevent environmental pollution.

### **Carbon monoxide**

Carbon monoxide (CO) is considered to be unwanted and harmful emission in flue gases due to energy loss and pollution as a result of soot. By increasing the amount of O<sub>2</sub> supplied, the CO must be converted to CO<sub>2</sub> by completing the incomplete combustion. In the flue gas analysis, the amount of CO is considered normal up to 100 ppm (Bilgin, 2001). As a result of the flue gas analysis of the produced corn pellets, the CO value was determined to be 1028 ppm.

The main reason for the presence of CO among the combustion products is the inability to meet the fuel with oxygen. If the CO value is higher than desired, it can be said that there is not a complete combustion, in other words, the fuel does not meet with enough oxygen. CO reduces blood oxygen carrying capacity. In this case, due to local oxygen deficiency, malfunctions occur in sensitive organs and tissues such as the blood vessel walls, brain and heart.

### **Nitrogen monoxide**

During the combustion process, especially at high temperature (1200°C), the nitrogen (N) molecule in the air used with the burning reaction reacts with the radical oxygen (O<sub>2</sub>) to initiate a chain reaction with oxides and nitrogen monoxide (NO). At temperatures above 1700°C, such reactions occur more rapidly. As a result of combustion, NO and nitrogen dioxide (NO<sub>2</sub>) generally occurs in a lesser amount. NO generally occurs during combustion in air fuel mixtures near stoichiometric. Parameters that increase NO formation are gas temperature and O<sub>2</sub> concentration. NO released from the exhaust and the exhaust is rapidly converted into NO<sub>2</sub> by the ozone gas as oxides. NO<sub>2</sub> is a strong oxidant that enters the reaction to form nitrate acid. As a result of flue gas analysis of the produced corn pellets, the value of NO was determined to be 38 ppm.

NO is an odorless gas. It disrupts the functioning of the lungs, irritates the mucous membrane and has a paralyzing effect. It causes the formation of nitric acid. It is unstable in environmental conditions and it combines with O<sub>2</sub> and turns into NO<sub>2</sub>. The maximum acceptable concentration (MAC) is 9 mg/m<sup>3</sup>.

### **Nitrogen oxides**

Nitrogen oxides (NO<sub>x</sub>) are formed due to the air excess coefficient and furnace design, depending on the fuel type, and are harmful to the environment. There is no possibility to interfere with the nitrogen oxides other than the possibility of the fuel air adjustment, and it is regarded as a criterion to be taken into consideration when buying the boiler. Excessive NO<sub>x</sub> in emissions indicates excessive rise in combustion temperature. As a result of flue gas analysis of the produced corn pellets, the NO<sub>x</sub> value was determined to be 40 ppm.

Along with many nitrogen oxide compounds, the most common are NO and NO<sub>2</sub>. NO<sub>x</sub> gases are acidic gases. NO<sub>x</sub> gases can be carried at very long distances in the atmosphere with the help of wind. One of the most important gases causing air pollution is NO<sub>2</sub>. NO<sub>2</sub> is very dangerous for human health. NO<sub>2</sub> not only cause air pollution itself, but also cause ozone formation and ozone pollution, especially in summer. An alarm is issued when the concentration of NO<sub>2</sub> is higher than 400 mg/m<sup>3</sup> in one hour in the European Union Countries. Restrictions are made especially on the use of motor vehicles. When the concentration of NO<sub>2</sub> is 150 ppm (285 µg/m<sup>3</sup>) or higher, it has a lethal effect on human been. NO<sub>x</sub> combines with the neighboring hemoglobin. NO<sub>2</sub> is irritating to the lungs and causes respiratory infections. NO<sub>x</sub> also causes eye irritation, infection in the upper respiratory tract (especially in children), asthma exacerbation, and increased bronchitis. NO<sub>x</sub> negatively affects the throat and lungs. NO<sub>2</sub> is a gas with a pungent reddish-brown mixture. Even at low concentrations, it irritates the lungs and damages the tissues and mucous membrane. The MAC value for NO<sub>2</sub> is 9 mg/m<sup>3</sup>.

### **Sulfur dioxide**

Sulfur dioxide (SO<sub>2</sub>) is the most common of air pollutant emissions. The most important part of the SO<sub>2</sub> emissions is exposed to thermal power plants that burn very large quantities of sulphated solid and liquid fuels to generate electricity. SO<sub>2</sub>, which is produced by the combustion of sulfur in the fuel, is considered to be the beginning of dangerous emissions to the environment. This gas, which is not concerned with the burner and the measures to

be taken, can only be reduced in flue gases with low sulfur fuels. When natural gas is used, SO<sub>2</sub> value which is zero in the flue gas can be 150–200 ppm in the flue gas when imported coal containing 0.5% sulfur is used (Bilgin, 2001). SO<sub>2</sub>, in flue gases, at low temperatures, combines with water vapor to form sulfuric acid and causes destruction in boilers. As a result of the flue gas analysis of the produced corn pellets, the SO<sub>2</sub> value was determined to be 2 ppm.

## CONCLUSIONS

In the corn production areas of Turkey, landfill mixing processes are applied in order to remove remaining plant wastes by burning or shredding. The incineration of corn plant wastes causes beneficial organisms in the soil and harmful environmental effects. On the other hand, the process of shredding plant waste into the soil causes significant energy consumption. Clean and renewable fuels with improved physical properties and improved combustion characteristics will be produced, eliminating these problems as indicated by the pelletization of corn biomass waste. The pelletizing process will facilitate the transport and storage of residues and at the same time reduce shipping costs. Most importantly, the evaluation of such biomass materials through pelletization will provide for the economization of waste and will partially or even reduce our country's external dependency on energy. It is primarily necessary to evaluate such wastes and bring them to the national economy. One of the most important benefits that can be achieved in the medium and long term in case of widespread application of such practices is to enable the establishment of agricultural based industry which is one of the most important elements of rural development by evaluating the wastes generated as a result of the production of some agricultural products intensively cultivated in Cukurova Region as biofuels, to provide employment to people living. In the case of establishing pellet production facilities in rural areas from agricultural wastes, it will provide a useful service for rural employment and rural development. The efficient use of biomass in

Turkey is a matter of enabling new business areas to open up. In addition, because there is no carcinogenic substances and sulfur present in fossil fuels in the biomass material structure, it will contribute to the prevention of air pollution as there is very little damage to the environment.

## ACKNOWLEDGEMENTS

We would like to thank Cukurova University Scientific Research Projects (BAP) Coordination Unit for supporting this project with FBA-2015-4798 project number. We would like to thank the officials and staff of DOGAC Biomass Pellet Production Facility for biopellets made of peanut and hazelnut shells and STANDART Laboratories Ltd. for calorimetric tests of the biopellets.

## REFERENCES

- Antmen, Z. F. (2019). Exploitation of peanut and hazelnut shells as agricultural industrial wastes for solid biofuel production. *Fresenius Environmental Bulletin*, 28(3), 2340–2347.
- ASAE (2007). ASAE/ASABE D245.6 (R2017ED) Moisture relationship of plant based agricultural products. STANDARD by American Society of Agricultural and Biological Engineers, 11/01/2007.
- ASTM (2010). ASTM D5142-09 Standard test methods for proximate analysis of the analysis sample of coal and coke by instrumental procedures. Developed by Subcommittee: D05.21.
- Bilgin, A. (2001). Evaluation of flue gas analysis in boilers, examination of internal cooling losses. V. National Plumbing Engineering Congress, 617–622.
- DIN (1996). DIN 51731 Testing of solid fuels-compressed untreated wood-requirements and testing. 1996-10-01.
- EN 14961-2 (2013). Solid biofuels-fuel specifications and classes - Part 2: Wood pellets for non-industrial use. Handbook for the Certification of Wood Pellets for Heating Purposes. Version: 2 April, 2013.
- IPCC (2011). Intergovernmental Panel on Climate Change. *IPCC Expert Meeting Report*, 20-22 June 2011, Lima, Peru.
- Kyriakopoulos, G. L., Arabatzis, G., Chalikias, M. (2016). Renewables exploitation for energy production and biomass use for electricity generation. A multi-parametric literature-based review. *AIMS Energy*, 4(5), 762–803.
- Ozturk, H.H. (2008). *Energy Plants and Biofuel Production*. Hasad Publication, İstanbul, Turkey.
- Xiu, S., Shahbazi, A. (2012). Bio-oil production and upgrading research: A review. *Renewable and Sustainable Energy Reviews*, 16, 4406–4414.

## ANALYSIS IN TERMS OF STRUCTURAL DISPLACEMENTS AND ACCELERATIONS FOR SOME TOWER BUILDINGS UNDER MODERATE MAGNITUDE EARTHQUAKES

**Stefan Florin BALAN, Alexandru TIGANESCU, Bogdan Felix APOSTOL**

National Institute of Research and Development for Earth Physics, 12 Calugareni Street,  
Magurele, 077125, Ilfov, Romania

Corresponding author email: sbalan@infp.ro

### **Abstract**

*The paper presents displacements and accelerations of two tower type buildings, one near the epicenter zone, Vrancea and one South of Bucharest (~150 km from epicenter zone). Displacements and accelerations were computed from the processed recorded accelerograms. Were used 3 "Triaxial Seismic Accelerometers" on 3 levels of each building. The displacements and accelerations on the analyzed structures were a result of Vrancea medium earthquakes between 2014-2017 years with magnitudes  $M_w$  ranging from 3.8 to 5.6 and depths between ~ 41 km to 147 km. A discussion of structural response was made concerning each building (one on 12 seismic events, the other on 6 ones and both on 4 that are common). The recorded data will contribute to a better understanding of the structures responses, even subjected to medium magnitude seismic events, and to the mitigation of seismic risk for densely populated areas.*

**Key words:** tower structure, seismic records, structural displacement, building monitoring, Vrancea epicentre area.

### **INTRODUCTION**

Romania is a seismic country, subjected to strong intermediate-depth earthquakes, which affect especially its Eastern and Southern parts. The earthquakes hypocenters are located in a certain volume, and consisting of confined focal sources, in the Vrancea region. This seismogenic area is characterized of both superficial earthquakes, but also of deep ones, attaining even 200 km focal depths.

The Bucharest city is located at ~160 km epicenter distance. In the XX<sup>th</sup> century were four major earthquakes:

- 1940 November 10 with magnitude  $M_w = 7.5$ ;
- 1977 March 4, with magnitude  $M_w = 7.4$ ;
- 1986 August 30, with magnitude  $M_w = 7.1$ ;
- 1990 May 30 with magnitude  $M_w = 6.9$ .

Bucharest city was seriously affected with 600 (in the year 1940) and almost 1400 (in the year 1977) deadly casualties and many totally collapsed buildings. All these four seismic events had over 90 km focal depth (ROMPLUS Catalog, 2018).

This paper intends to evaluate and analyse the influence of the recent earthquakes (2014-2017) from Vrancea source on some buildings in the Metropolitan Bucharest area and Focsani (town in Vrancea near the

seismic source). At the same time is trying to find similar trends and differences between the responses of the buildings, given different epicentre distances, and correlations of the earthquake parameters (magnitude, depth) with building response.

After the earthquake of 1977, which had catastrophic effects on tall buildings of reinforced concrete built between the two world wars, in Bucharest, has begun a large-scale campaign to calculate the period of oscillation of various locations in the city.

We consider that the dynamic response of certain structures is strongly dependent of the ratio between the natural period of the structure and the dominant period of the emplacement site (Bratosin et al., 2017; Cioflan et al., 2018). Starting from information comprised by data bases for soils and buildings existing in Bucharest were selected two types of structures (Balan et al., 2015).

### **MATERIALS AND METHODS**

#### **The monitoring processes**

National Institute of Research and Development for Earth Physics from Magurele is conducting monitoring for 6 instrumented buildings (Since 2011).

However, the recorded earthquakes data are transmitted in real time to the National Data Centre. Therefore, the earthquakes catalogue (<http://www.infp.ro/romplus>) is continuously set up and up dated.

The input data are consisting in accelerations or velocities recordings that could be used for seismic hazard evaluation.

The structural seismic response is computed and employed for developing risk and damage maps (Marmureanu G., 2016; Marmureanu et al., 2011), more of them in near-real time. Also, they are useful as input data for design regulations.

In this paper are presented the results of the continuous monitoring with “Triaxial Seismic Accelerometers” mounted on different floors,

in order to characterize the structural behaviour of the following structures: a tower type structure (T1) in Magurele (South Bucharest city) and a tower type structure in Focsani (T2) (Figure 1).

The monitoring is achieved at building T1 with 3 seismometers placed at basement, 6<sup>th</sup> floor and 10<sup>th</sup> floor, and at building T2 with 3 seismometers placed at basement, 4<sup>th</sup> floor and 8<sup>th</sup> floor; the data being transmitted in real time to the NIEP’s National Data Centre.

The recordings are on three directions, two horizontal N-S and E-W, and one vertical, Z. The considered earthquakes in the analysis (No. 1-14) had magnitudes  $M_w$  ranging from 3.8 to 5.6 and a large variety of depths between ~ 41 km to 147 km.



Figure 1. Location map of the instrumented buildings (T1 and T2)

The instrumented structures are tower type of different design and at different epicentre site distances: T1, tower structure situated in the Southern part of Bucharest city (10 floors high), office building, of reinforced concrete with shear walls, built in 1974 and T2, tower structure in Focsani, located close to the Vrancea epicentre area, apartments and single rooms (8 floors high), of reinforced concrete frame, built in 1971.

We shall analyse and discuss the effects of magnitudes and epicentre distance on displacements induced on these buildings, by the considered seismic events (No. 1-14). From Tables 1 to 6 could be observed the

4 common recorded earthquakes (events 10-13).

## RESULTS AND DISCUSSIONS

The recorded acceleration time-histories were pre-processed: baseline corrected and filtered using a 4<sup>th</sup> order Butterworth band pass (0.2-25 Hz) filter. The limits were set for obtaining a good signal to noise ratio, and for small earthquakes where the signal was strongly affected by noise the calculus was not performed (building T1, event No. 9 of magnitude  $M_w = 3.8$ ). Having the corrected acceleration time-histories, the corresponding

velocity and displacement time-histories were obtained through time-integration, using the trapezoidal rule. For acceleration values, sampled at a small-time interval (0.01 s or 0.005 s), the integral can be approximated by the area under the plot, assuming a linear function from one point to the next one. Consequently, the velocity was integrated in the same manner to obtain the displacement.

Table 1. Maximum displacements in [mm] for building T1 at base (B), floor 6 (F6) and floor 10 (F10), direction N-S, for the corresponding earthquakes magnitudes ( $M_w$ ) and depths

No.	Depth [km]	$M_w$	Direction N-S		
			B	F6	F10
1	132.3	4.4	0.16	0.45	0.65
2	134.4	4.6	0.20	0.31	0.61
3	147.3	4.2	0.04	0.09	0.14
4	106.1	4.3	0.05	0.11	0.16
5	40.9	5.4	0.90	2.51	3.70
6	88.4	4.3	0.02	0.05	0.09
7	118.2	4.3	0.08	0.17	0.27
8	145.4	4.3	0.11	0.18	0.23
10	92.0	5.5	0.70	2.12	3.00
11	96.9	5.6	1.25	2.77	4.04
12	123.2	4.8	0.36	0.83	1.20
13	121.6	4.5	0.07	0.18	0.30

Table 2. Maximum displacements in [mm] for building T1 at base (B), floor 6 (F6) and floor 10 (F10), direction E-W, for the corresponding earthquakes magnitudes ( $M_w$ ) and depths

No.	Depth [km]	$M_w$	Direction E-W		
			B	F6	F10
1	132.3	4.4	0.12	0.28	0.44
2	134.4	4.6	0.25	0.57	0.86
3	147.3	4.2	0.07	0.12	0.20
4	106.1	4.3	0.05	0.09	0.14
5	40.9	5.4	1.56	1.95	2.85
6	88.4	4.3	0.04	0.08	0.12
7	118.2	4.3	0.09	0.22	0.34
8	145.4	4.3	0.33	0.53	0.75
10	92.0	5.5	1.69	3.25	4.78
11	96.9	5.6	1.95	3.95	5.52
12	123.2	4.8	0.23	0.50	0.73
13	121.6	4.5	0.05	0.12	0.15

Table 3. Maximum displacements in [mm] for building T1 at base (B), floor 6 (F6) and floor 10 (F10), direction Z, for the corresponding earthquakes magnitudes ( $M_w$ ) and depths

No.	Depth [km]	$M_w$	Direction Z		
			B	F6	F10
1	132.3	4.4	0.06	0.07	0.05
2	134.4	4.6	0.06	0.08	0.08
3	147.3	4.2	0.01	0.02	0.02
4	106.1	4.3	0.04	0.04	0.04
5	40.9	5.4	0.59	0.59	0.61
6	88.4	4.3	0.02	0.02	0.02
7	118.2	4.3	0.03	0.04	0.06
8	145.4	4.3	0.06	0.08	0.10
10	92.0	5.5	0.42	0.46	0.42
11	96.9	5.6	0.46	0.60	0.44
12	123.2	4.8	0.10	0.15	0.10
13	121.6	4.5	0.02	0.03	0.02

From the displacement time-histories, the maximum values were extracted and represented in Tables 1-6, for buildings T1 and T2. The same analysis was conducted in order to compute maximum values for accelerations at the same levels.

Table 4. Maximum displacements in [mm] for building T2 at base (B), floor 6 (F6) and floor 10 (F10), direction N-S, for the corresponding earthquakes magnitudes ( $M_w$ ) and depths

No.	Depth [km]	$M_w$	Direction N-S		
			B	F4	F8
9	65.0	3.8	0.04	0.09	0.13
10	92.0	5.5	5.44	12.08	12.42
11	96.9	5.6	2.86	4.30	3.51
12	123.2	4.8	0.10	0.27	0.55
13	121.6	4.5	0.17	0.26	0.37
14	131.0	4.6	0.34	0.54	0.55

Table 5. Maximum displacements in [mm] for building T2 at base (B), floor 6 (F6) and floor 10 (F10), direction E-W, for the corresponding earthquakes magnitudes ( $M_w$ ) and depths

No.	Depth [km]	$M_w$	Direction E-W		
			B	F4	F8
9	65.0	3.8	0.02	0.07	0.11
10	92.0	5.5	7.28	11.10	18.74
11	96.9	5.6	3.02	4.21	6.66
12	123.2	4.8	0.19	0.28	0.49
13	121.6	4.5	0.09	0.18	0.35
14	131.0	4.6	0.32	0.75	1.23

Table 6. Maximum displacements in [mm] for building T2 at base (B), floor 6 (F6) and floor 10 (F10), direction Z, for the corresponding earthquakes magnitudes ( $M_w$ ) and depths

No.	Depth [km]	$M_w$	Direction Z		
			B	F4	F8
9	65.0	3.8	0.03	0.04	0.05
10	92.0	5.5	1.59	1.57	1.70
11	96.9	5.6	0.71	0.72	0.77
12	123.2	4.8	0.07	0.08	0.10
13	121.6	4.5	0.06	0.06	0.08
14	131.0	4.6	0.06	0.08	0.07

Regarding the structural responses, in order to highlight the impact of the earthquakes on the built environment, acceleration response spectra at the basement of buildings are calculated for two strongest earthquakes, and spectral ratio (top/base) for three, respectively two strongest seism's (Figures 2 and 3). There was achieved an analysis regarding the influence of the magnitude for the considered earthquakes on maximum displacements of buildings T1 and T2 (Tables 1 to 6). The analysis is made for building T1 at basement, floors 6 and 10 and for building T2, at basement, floors 4 and 8.

For building T1 the largest maximum displacements are observed at floor no. 9 for the following three seismic events: 5,  $M_w = 5.4$ , depth = 40.9 km (direction N-S = 3.70 mm, direction E-W = 2.85 mm), event 10,  $M_w$

= 5.5, depth = 92 km (direction N-S = 3.00 mm, direction E-W = 4.78 mm) and event 11,  $M_w = 5.6$ , depth = 96.9 km (direction N-S = 4.04 mm, direction E-W = 5.52 mm).

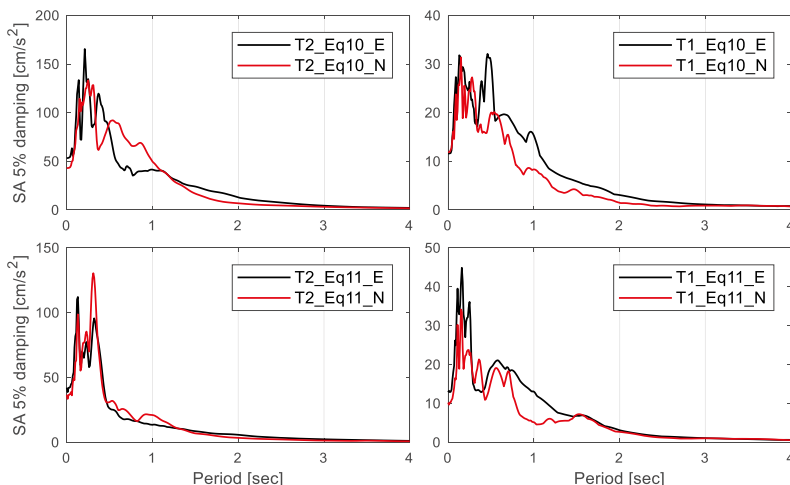


Figure 2. Acceleration response spectra at basement of buildings T1 and T2 on horizontal directions (N-S and E-W) due to earthquakes 10 and 11

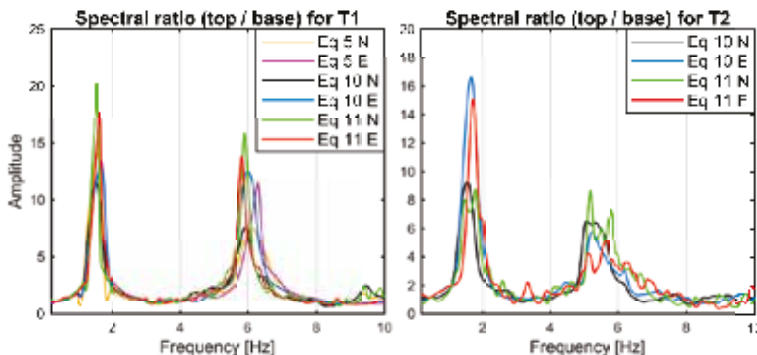


Figure 3. Spectral ratio for building T1 (left), for earthquakes 5, 10 and 11, and for building T2 (right), for earthquakes 10 and 11, on two horizontal components

These were the greatest seismic events recorded at building T1. In general, could be observed an increasing tendency of displacements with magnitudes, and a less influence or correlation of the focal depths. The values for the vertical displacements have an approximately similar behaviour on all the monitored floors.

At building T2, near the epicentre, is observed that the greatest maximum displacements (at level no. 8) are by far also

for the strongest events: 10,  $M_w = 5.5$ , depth = 92 km (direction N-S = 12.42 mm, direction E-W = 18.74 mm) and event 11,  $M_w = 5.6$ , depth = 96.9 km (direction N-S = 3.51 mm, direction E-W = 6.66 mm).

As regarding the influence of the epicentre distance, by comparing the maximum displacements on the upper floors of the recorded largest earthquakes at both tower-type buildings, it is observed that larger horizontal and vertical displacements are on

building T2 near the Vrancea epicentre, for almost all seismic events. The exception for this general tendency could be attributed either to inherent recording errors, or to the seismogenic particularities of the Vrancea active focal region or even to the type of soils beneath the buildings.

The analysis of the acceleration response spectra (Figure 2) from earthquakes no. 10 and 11 exhibits that the significant amplitudes of spectral acceleration (5% damping) for T1 are in the range of periods 0-1 s, while for T2 is in the range of 0-0.5 s. One shall keep in mind that the corresponding accelerations does not exceed  $160 \text{ cm/s}^2$  in T2 and  $50 \text{ cm/s}^2$  in T1, therefore was no danger regarding structural damage.

For building T1, the spectral ratio was computed for three earthquakes with magnitudes  $M_w$  larger than 5 (no. 5, 10 and 11), and the results show a good consistency for the peaks, despite different focal depths. Their mean value for the fundamental period is 0.63 seconds (1.59 Hz, Figure 3, left).

For the building T2, a larger dispersion of the results regarding the second peaks was observed (Figure 3, right). However, the mean value for the fundamental periods is 0.61 seconds (1.64 Hz), and compared to T1 building, which is 2 stories higher, the two fundamental periods are close (0.61 and 0.63 seconds). This could be explained by the fact that the two structural systems are different, shear walls and frames, and by the fact that T1 was retrofitted after the 1977 earthquake.

## CONCLUSIONS

The buildings are not identical and stand on very different grounds type, both in densely populated regions. All these recordings and observations have their importance because could represent a checking possibility for the earthquake engineer in modelling the structural analysis. At the far away building from the source, T1, is observed the direct influence of magnitude over maximum displacements. In the near from source, at building T2 is observed the depths of around 90 km and magnitude over 5 giving maximum displacements. However, for the both buildings the magnitude influence

appears to be much decisive. The largest displacements are, as expected, at the top floors on all directions.

Therefore, many parameters could affect the structural response of a building, such as: focal depth, magnitude range, epicentre distance.

These types of analyses contribute to a better understanding of the behaviour of the structures when subjected to earthquakes. The seismic monitoring of buildings can give also a rapid damage assessment after a strong seismic event, based on the level of accelerations the buildings experienced, therefore mitigating the seismic risk for densely populated areas in Romania. The results are aiming to contribute to a better understanding of the structures responses, even subjected to medium magnitude seismic events and to the mitigation of seismic risk for densely populated areas in Romania.

## ACKNOWLEDGEMENTS

This paper was carried out within Nucleu Program MULTIRISC, supported by MCI, project no. PN19080102.

## REFERENCES

- Balan, S. F., and Apostol, B. F. (2015). Mitigation of seismic risk considering soil-structure interaction analysis for Bucharest Metropolis. *15<sup>th</sup> International Multidisciplinary Scientific GeoConferences, SGEM 2015*, Bulgaria, 903–910.
- Bratosin, D., Apostol, B. F., and Balan, S. F. (2017). Avoidance strategy for soil-structure resonance by considering nonlinear behavior of the site materials. *Rom. J. Phys.*, 62(5-6), 808.
- Cioflan, C. O., Apostol, B. F., Radulian, M., Ionescu, C., and Balan, S. F. (2018). Practical insights on seismic risk evaluation from site-structure dynamic behaviour perspective for Bucharest urban area. *Rom. J. Phys.*, 63(7-8), 811.
- Marmureanu, G. (2016). *Certainties/Uncertainties in Vrancea Hazard and Seismic Risk Evaluation*. Romanian Academy Printing House, Bucharest.
- Marmureanu, G., Cioflan, C. O., and Marmureanu, A. (2011). Intensity seismic hazard map of Romania by probabilistic and (neo)deterministic approaches, linear and nonlinear analyses. *Romanian Reports in Physics*, 63(1), 226–239.
- ROMPLUS (2018). *Earthquake Catalog*. National Institute for Earth Physics.

## THE USAGE OF THE FAE FIXED WING UAV FOR THE EVALUATION OF AFFECTED RAPESEED CULTURE DUE TO PEST ATTACKS

Alexandra TRIF<sup>1</sup>, Mihai GIDEA<sup>1</sup>, Cristian CIOINEAG<sup>2</sup>, Sorin Mihai CIMPEANU<sup>1</sup>

<sup>1</sup>University of Agronomic Sciences and Veterinary Medicine of Bucharest, 59 Marasti Blvd, District 1, Bucharest, Romania

<sup>2</sup>Probstdorfer Saatzzucht, 20 Siriului Street, District 1, Bucharest, Romania

Corresponding author email: trif\_alexandra@yahoo.com

### Abstract

*The paper aims to evaluate the potential of using aerial images captured from FAE Fixed Wing UAV in order to determine the density of plants and areas affected by pests. Based on the unsupervised classification of the orthophoto map obtained with the help of UAV, the re-sowing plan of the affected areas with a spring culture was created. For this purpose, we use professional equipment to gather images, GPS RTK to provide advanced precision, as well as software such as, Agisoft to compose the orthophoto, ArcMap for georeferencing the orthophoto map and LeoWorks to process and classify the resulting images.*

*The utilized method has allowed for a way to obtain an estimate of the degree of destruction of the rapeseed culture and to facilitate making the optimal decision with the help of a sowing plan. The usage of this method offsets the losses due to pest attacks.*

**Key words:** *drones for agriculture, sowing plan, pixel classification.*

### INTRODUCTION

Plant density is a key factor influencing crop functioning with consequences on many aspects including yield, water and fertilizer requirements as well as susceptibility to pathogens (Xiuliang Jin et al., 2017).

Determination of the plant number per hectare represents an important index to assess plant density as well as field emergence (Gnädinger F. & Schmidhalter U., 2017).

The current methods used are based on visual plant counting in the fields over a predefined sampling area. They are repetitious, time consuming and prone to human errors. Further, the soil conditions, particularly in case of rainfall or frost, may limit the time slots when walking in the field is possible without damaging the crop (Xiuliang Jin et al., 2017).

Most studies on plant density estimation are using ground level non-contact measurements, mainly focusing on relatively large plants such as maize that are further regularly spaced. Most techniques are based on plant identification using RGB images (Jia et al., 1991; Nakarmi & Tang, 2012; Nakarmi & Tang, 2014; Shrestha & Steward, 2003; Shrestha & Steward, 2005;

Tang & Tian, 2008a; Tang & Tian, 2008b), or LiDAR systems (Shi et al., 2015).

For many applications, UAV-based airborne methods offer the possibility for cost-efficient data collection with the desired spatial and temporal resolutions (Ejia H. et al., 2013; Trif A. et al., 2018).

Due to the lack of precipitation from 30 August to 10 September 2017, agricultural crops have suffered, as it is the period of their growth and accumulation of the soil water reserve. Therefore, the lack of water has led to a slowdown in the development of the rapeseed culture located in Dichiseni, Calarasi County and after the hectic days developed the black flea of rape (*Phyllotreta atra*), which attacked in a very short time 40 hectares, the plants that were poorly developed. Therefore, a diagnosis has been made on the land to estimate the damage for taking a decision on this sole.

### MATERIALS AND METHODS

The parcel with the area of 132.46 ha was sown with rapeseed (Pedro hybrid) with a density of 55 germinal grains/sqm.

In order to acquire the aerial images, the FAE 1718 FIXED WING (Figure 1) and the Agisoft

software for the composing of the orthophoto map were used.



Figure 1. UAV FAE 1718 Fixed Wing  
(Source: <http://fae-drones.com/FAE-1718-FIXED-WING-47.html>)

FAE 1718 Fixed Wing is an automated drone-based machine for fast and accurate data acquisition, covering extensive areas (over 500 ha) and large distances. This is used for precision farming or to collect supporting data for territorial and environmental planning.

Following the flight, 558 images were obtained. The flight altitude was 149 m, the ground resolution was 3.5 cm/px, and the target area was 140 ha.

The Trimble RTK L1 + L2 GNSS receiver was used to determine the coordinates of the control points for a better accuracy in georeferencing of the orthophoto map.

Image classification was performed in the LeoWorks 4.2 specialized software to determine the plant density.

## RESULTS AND DISCUSSIONS

Figure 2 shows the orthophoto plan obtained from the flight in RGB format. It was subjected to the pixel classification process which uses the supervised classification method.

Within this method, several samples were selected from each class that needs to be represented.

The entire classification process and an exemplary workflow in the LeoWorks processing software can be seen in Figures 2 and 3.

The first sequence in the program shows the selection of samples and the creation of density classes according to the *in situ* measurements. The second shows the result obtained following the supervised classification.

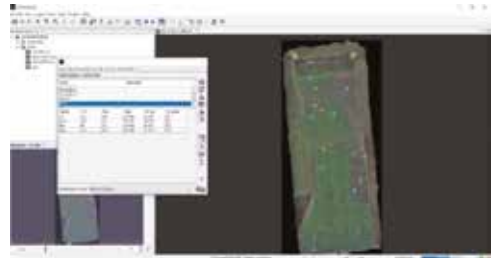


Figure 2. Defining the samples in each class for supervised classification

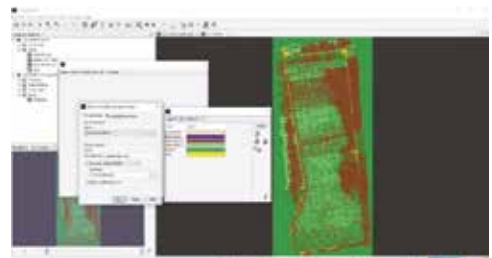


Figure 3. Sharing the classes obtained from the image classification

The next step was to define the areas with different densities according to the classification and the field measurements (Figure 4).

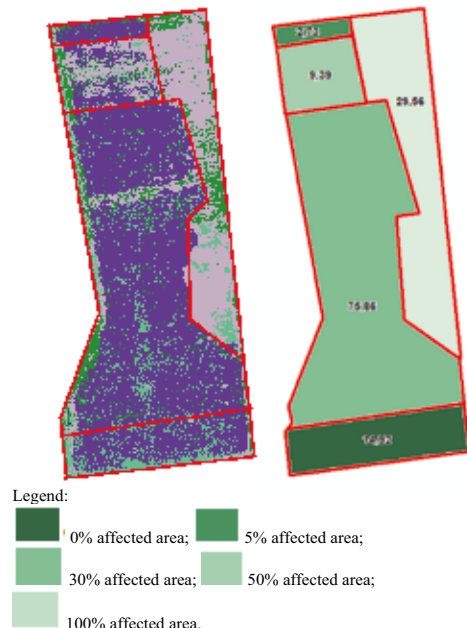


Figure 4. Classifying the pixels of plants and affected areas

Figure 5 shows the values (in meters) of the corresponding sides of the determined areas in order to obtain the sowing plan of the affected areas. This is useful to the farmer for the field work.



Figure 5. Area delimitation/Determination of different density areas

Using GIS tools, the affected areas were delineated to highlight areas with different densities as:

- an area of 14.92 ha with a density of 55 plants/sqm normally developed in 4-6 leaf phenophase has been delineated (I);
- an area of 2.73 ha with a density of 50 plants/sqm (II);
- an area of 75.86 ha with a density of 45 plants/sqm (III);
- an area of 9.39 ha with a density of 15 plants/sqm (IV);
- an area of 29.56 ha with a density of less than 5 plants/sqm (V).

It is possible to observe: 100% of the 29.56 ha being attacked by flea beetles, 50% for the 9.39 ha area, 30% for 75.86 ha area and 5% for the 2.73 ha area. For the 14.92 ha area there was no recorded attack by flea beetles.

The area affected by the flea attack, determined based on the orthophoto plan, obtained by the drone had a 29.56 ha Density V surface and a 9.39 ha Density IV surface which together represents a non-uniform yield of the crop.

Therefore, the area with the surface of 38.95 ha was re-sowed.

Following the analysis, the sowing lines were drawn according to the seeding-machine with a width of 6 m.

Figure 6 represents the re-sowing plan according to the density of plants obtained from the entire pixel classification study. This method of pixel classification is a fast method with high accuracy as Trif A. et al (2016) said, when comparing other modern methods of assessing the damage suffered by rapeseed crops. Those methods were the digitization on the image, and the method in which a GPS is used resulting in the affected areas being determined in the field.

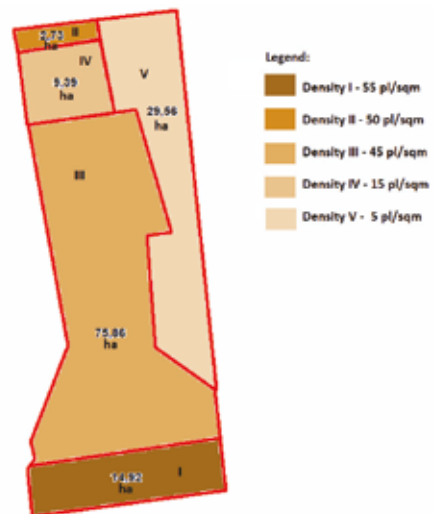


Figure 6. Density of plants

The sowing process was carried out in March 2018 according to the drawings represented in Figure 5. The marginal lines of the 38.95 hectares plot were followed, thus facilitating the work of the mechanizer, which reduces the fuel consumption, the number of passes and overlaps of the sowing operation of the new cultures.

This decision was also taken after the determination of economic efficiency and the profit rate for each identified density area.

An overview of the vegetation state of the plot cultivated with rapeseed and peas can be seen in Figure 7.

The 38.95 ha land was seeded with 92 germinal grains per square meter of peas and 82 beans during sunrise. The plants grew on 4 to 5 levels with an average of 3 grains in the pod with a mass of 100 grains.



Figure 7. Overhead image taken with DJI Phantom 3 Professional

The obtained yield from the area with density I was 2300 kg/ha, 2100 kg/ha from the area with density II, and 1900 kg/ha from the area with density III planted with rapeseed (Table 1). The obtained yield from the areas with density IV and V cultivated with peas was 1800 kg/ha. (Table 1). Thus, the obtained yield for each density area can be seen below:

Table 1. Obtained yield (rapeseed and peas)

Class	Rapeseed				Peas
	Surface ha	Density pl/sqm	Yield kg/ha	Total Yield tons	Yield kg/ha
I	14.92	55	2300	34.31	-
II	2.73	50	2100	5.73	-
III	75.86	45	1900	144.13	-
IV	9.39	15	-	-	1800
V	29.56	5	-	-	-
<b>Total</b>	<b>132.46</b>		<b>1969</b>	<b>184.17</b>	<b>70.11</b>

The plant density was between 55 plants/sqm and 5 plants/sqm, so the last two classes were not considered as viable to maintain the rapeseed culture.

According to Table 1, a yield of 184.17 tons of rapeseed was estimated for the surface of 93.51 ha, and 70.11 tons of peas for the surface of 38.95 ha after replanting.

Table 2 shows the costs in lei (Romanian currency) per hectare. Costs include the mechanical work, materials including the seeds,

plant protection products, the scanning service with drones, harvesting and transportation. They are between 0.93 and 1.13 lei/kg for rapeseed and 1.05 lei/kg for peas. Thus, a production price was obtained for each density class.

Table 2. Costs

Class	Costs lei/ha	Yield kg/ha	Production price lei/kg
I*	2143	2300	0.93
II*	2143	2100	1.02
III*	2143	1900	1.13
IV**	1897	1800	1.05
V**	1897	1800	1.05

\*rapeseed; \*\*peas

If the rapeseed crop was maintained on the 9.39 ha and 29.56 ha surfaces with 5 and 15 plants per square meter, no profit would have been obtained on these areas; The production price would have reached 10.72 lei/kg, compared to the selling price of 1.5 lei/kg (Table 3).

Table 3. Costs

Class	Costs lei/ha	Yield kg/ha	Production price lei/kg
I	2143	2300	0.93
II	2143	2100	1.02
III	2143	1900	1.13
IV	2143	650	3.30
V	2143	200	10.72

Table 4 shows the sale prices for rapeseed and peas, the incomes per hectare for each surface with different density, and the total incomes for each surface.

Table 4. Income

Class	Yield kg/ha	Selling Price lei/ha	Income lei/ha	Total Income
I	2300	1.5	3450	51474
II	2100	1.5	3150	8599,5
III	1900	1.5	2850	216201
IV	1800	1.5	2700	25353
V	1800	1.5	2700	79812

Income ranged between 2850 lei and 3450 lei per hectare for rapeseed and 2700 lei per hectare for peas. There is a difference of 600 lei per hectare between the two classes of density: 3450 lei per hectare for the first class with 55 plants/sqm, and the third class with 45 plants/sqm.

In Table 5 the profit per hectare was also determined for each different density class. Thus, it can be seen that the profit rate of the density zone I differs by 28 percent compared to the density zone III. Also, the profit rate of the area with density III is smaller than the IV and V zones by 9.3 percent.

Table 5. Economic efficiency

Class	Costs lei/ha	Income lei/ha	Profit lei/ha	Total Profit	Profit Rate %
I	2143	3450	1307	19500	61.0
II	2143	3150	1007	2749	47.0
III	2143	2850	707	53633	33.0
IV	1897	2700	803	7540	42.3
V	1897	2700	803	23736	42.3

With the help of this method, the profit rate has increased to 42.33%, which is a difference of 9.3% compared to the class III, 45 plants/sqm. If the rapeseed culture had been maintained on the surfaces IV and V the profit rate would have had negative values in case 2, so it would not have been rented. In case 1, the profit rate is even higher than the third (Figure 8).



Figure 8. Economic efficiency Case 1 and Case 2

## ACKNOWLEDGEMENTS

This research work was carried out with the support of the University of Agronomic Sciences and Veterinary Medicine of

Bucharest, Faculty of Land Reclamation and Environmental Engineering and S.C. FAE Drones S.R.L. We also want to give thanks to the Chief Executive Officer Dr. Doru Epure for all his support and to the entire team of Probstdorfer Saatzucht Romania S.R.L.

## CONCLUSIONS

In this paper, we presented a procedure that was developed to determine the density of plants and to obtain the re-sowing plan using an UAV. It has been verified successfully by the analysis of both indoor and outdoor measurements that different classes of densities can be determined using an orthophoto plan correlated with in situ measurements.

An UAV can be used successfully to make a diagnosis of the land with the purpose of determining the affected area and making a decision about whether to re-seed or not.

In the present case it was possible to divide the land according to the obtained plans, so that the affected area was re-seeded with peas, which is a spring culture.

This modern method involves the use of drones in taking pictures and determining the density of plants based on the pixel classification. By using this method, the profit rate for the area of 38.95 ha increased to 42.33%.

The plans delivered to the farmer were used for the compilation of the APIA (Agricultural Payments and Intervention Agency) file, and to schedule the working data in the field, for reusing the calamity areas.

The use of UAVs provides time- and cost-saving data for further processing and allows for flexible and weather-independent data collection. (Gnädinger F. & Schmidhalter U., 2017)

## REFERENCES

- Gnädinger, F., Schmidhalter, U. (2017). Digital Counts of Maize Plants by Unmanned Aerial Vehicles (UAVs). *Remote Sensing*, 9, 544, doi:10.3390/rs9060544.
- Jia, J., Krutz, G. W., Gibson, H. W. (1991). Corn plant locating by image processing, *Fibers' 91*, Boston, MA, *Int. Soc. Opt. Photon.* 246–253.
- Nakarmi, A. D., Tang, L. (2012). Automatic inter-plant spacing sensing at early growth stages using a 3D vision sensor. *Comput. Electron. Agric.*, 82, 23–31.

- Nakarmi, A. D., Tang, L. (2014). Within-row spacing sensing of maize plants using 3D computer vision. *Biosyst. Eng.*, 125, 54–64.
- Shi, Y., Wang, N., Taylor, R. K., Raun, W. R. (2015). Improvement of a ground-LiDAR-based corn plant population and spacing measurement system. *Comput. Electron. Agric.*, 112, 92–101.
- Shrestha, D. S., Steward, B. L. (2003). Automatic corn plant population measurement using machine vision. *Trans. ASAE*, 46, 559.
- Shrestha, D. S., Steward, B. L. (2005). Shape and size analysis of corn plant canopies for plant population and spacing sensing. *Appl. Eng. Agric.*, 21(2), 295–303.
- Tang, L., Tian L. F. (2008a). Plant identification in mosaicked crop row images for automatic emerged corn plant spacing measurement. *Trans. ASABE*, 51, 2181–2191.
- Tang, L., Tian L. F. (2008b). Real-time crop row image reconstruction for automatic emerged corn plant spacing measurement. *Trans. ASABE*, 51, 1079–1087.
- Trif, A., Gidea, M., Penescu, A. (2016). Evaluation of the modern methods of assessing the damage suffered by rapeseed crops at the end of winter. *AgroLife Scientific Journal*, 5(2), ISSN 2285-5718; ISSN CD-ROM 2285-5726; ISSN ONLINE 2286-0126; ISSN-L 2285-5718.
- Trif, A., Gidea, M., Ergehegiu, B., Boasca, A., Cimpeanu, S. M. (2018). Research into the utilization of aerial imaging for evaluating the state of vegetation. SciendoDOI: 10.2478/alife-2018-0061.
- Xiuliang, Jin, Shouyang, Liu, Frédéric, Baret, Matthieu, Hemerlé, Alexis, Comar (2017). Estimates of plant density of wheat crops at emergence from very low altitude UAV imagery. *Remote Sensing of Environment*, 198, September 1, 105–11.

## THE LIMITATION OF ANTIBACTERIAL USE OF SILVER IONS: ACTING AS SELECTIVE AGENTS FOR PROKARYOTE GENETIC RESOURCES

Cristian Mihai AURORI, Daniel Severus DEZMIREAN

University of Agricultural Sciences and Veterinary Medicine Cluj-Napoca,  
3-5 Calea Manastur Street, 400372, Cluj-Napoca, Romania

Corresponding author email: caurori@yahoo.com

### **Abstract**

*Silver cations are the building blocks of silver based antimicrobial traditional therapies, which are known and used by man for centuries. However, when facing heavy metals, bacterial genetic plasticity can induce the development of adaptive mechanisms required for survival under such major microbe-associated stressors. Whether they act as part of the natural environment, polluted industrial sites or medical antimicrobial protocols, silver ions are systematically exerting a selection pressure on bacterial communities. Thus, sublethal doses of silver ions stimulate inter-bacterial genetic material exchange and the expression of chromosome or plasmid located genes, which encode proteins with biochemical capabilities to counteract their harmful effects. Depending on Gram stain corresponding traits, species and strains, bacteria interact with silver ions at both cellular envelope and internal structure levels. The continued spread of using silver-based materials in the recent years offered opportunities to discover novel antimicrobial strategies but equally induced an increase in bacterial resistance and adaptation against this chemical element.*

**Key words:** bacteria, gene, Gram stain, silver ions, resistance.

### **INTRODUCTION**

Silver has been used for centuries as a hygiene catalyst in human society all over the world (Hobman & Crossman, 2014; Randall et al., 2015). Silver ions were the building blocks of traditional antimicrobial employment of silver even before any biochemical trait would have been found to explain their action. The heavy metal ions, as major microbial stressors, gave the opportunity to many bacterial species to develop adaptive mechanisms necessary for their survival in environments containing elements such as  $Cd^{2+}$ ,  $Hg^{2+}$ ,  $Co^{2+}$ ,  $Ni^{2+}$ ,  $Cu^{2+}$ ,  $Zn^{2+}$  or  $Ag^+$  (Babu et al., 2011). These evolutionary traits could be considered valuable since they constitute a resource for bioremediation in case of the far too many contaminated industrial, urban and health care associated sites occurring nowadays all around the globe.

As would be the case in other antibacterial agents, a major drawback in the extensive use of silver proved to be the increased microbial resistance encountered in various species and strains. The popularity of silver associated materials in human activity induced nowadays a significant environmental pollution (Kedziora et al., 2018).

Silver based compounds are increasingly used in various fields such as clinical healthcare and general hygiene sectors) agriculture and industry (Gupta et al., 2001). The growing popularity of silver antibacterial use in products such as wound dressings, textiles, catheters, or washing machines, gave way to significantly increased chances for selection of adapted bacterial populations than would have been the case several decades ago (Sutterlin et al., 2014). Thus, silver's clinical utility can be compromised in a manner very similar to nowadays occurrence of antibiotic resistance (Randall et al., 2015). Constant bacterial adaptation against antibiotics is still rising in recent years. Thus, in 2007 alone about 25000 patients died in Europe due to antibacterial "therapeutic failure", about two thirds of the cases involving Gram-negative species (Sutterlin et al., 2014). Bacterial enzymes such as extended-spectrum beta-lactamases (ESBLs) have been spread not only in hospitals or human communities but in ecological niches sometimes even lacking human activities (Sutterlin et al., 2014). As a defence against harmful compounds, silver resistance genes were found even to be placed on antibiotics associated plasmids, thus giving the possibility for this chemical element to exert a selective

pressure for antibiotics resistance as well (Sutterlin et al., 2014). The recent years recoderd an increasing number of reports signaling the isolation of silver resistant bacterial strains in silver contaminated environments or healthcare associated locations (Chabert et al., 2017).

In modern and recent times, the progress in life science confirmed the antibacterial role of silver, further spreading its use in activities requiring sterile environments. Sources report silver as being effective against more than 650 pathogens (Salomoni et al., 2017). Both environmental and clinical sources made possible the isolation of silver resistant strains from various species such as: *Escherichia coli*, *Salmonella typhimurium*, *Pseudomonas stutzeri*, *Enterobacter cloacae*, *Klebsiella pneumoniae*, *Acinetobacter baumannii* (Li et al., 1997), *Pseudomonas aeruginosa* (Muller & Merrett, 2014), *Staphylococcus aureus* (Loh et al., 2009; Sobisch et al., 2019), *Bacillus subtilis*, *Bacillus cereus* (Kroeger et al., 2015) or *Enterococcus* sp. (Sobisch et al., 2019).

However, silver remains a major antibacterial actor, including due to its plausible enhancing effect of antibiotics (Barras et al., 2018). In order to preserve its remarkable potential against pathogens a sustained worldwide monitoring strategy should be employed in order to quantify bacterial silver resistance traits and their perspective to spread among microbial communities.

## **MECHANISMS OF IONIC SILVER ANTIBACTERIAL ACTIVITY**

Despite its importance in health care and other scientific or practical domains, the complete spectrum of interactions between ionic silver and bacterial biochemistry is yet to be fully understood (Saulou-Berion et al., 2015). Among the proposed models, most likely the basis of silver action relies on its affinity towards electron-donating groups such as thiols, imidazoles, indoles, amides, carboxylates, and hydroxyls (Saulou-Berion et al., 2015), in a similar manner to other heavy metals such as copper ions, engaged in amino acid binding via imidazole, thiolate or thioether functional groups (Rubino et al., 2011).

Most data suggest that at low concentration, silver ions act at the membrane level, which is the main entrance gate and the place of several fundamental processes such as the respiratory chain and transmembrane transport system (Holt & Bard, 2005). Additionally, at higher concentration silver penetrates further into the bacterial cell acting at cytoplasm level as well (Holt & Bard, 2005). Experimental procedures showed that silver ions enter bacterial cell within 30 minutes after exposure and subsequently bind to intracellular components (Yamanaka et al., 2005; Kedziora et al., 2018). Data gathered by Yamanaka et al. (2005) suggested that at least in *E. coli*, silver toxicity is primarily exerted at cytoplasm level, before the onset of membrane damage. Thus, silver ions were found to pass via ion channels without disrupting the membrane, subsequently inducing ribosome denaturation, with negative effects on proteins engaged in ATP synthesis. Compromising the ATP associated pathways was hypothesized to result in subsequent cellular failure to maintain the membrane structural integrity with the final cellular disruption as a possible outcome.

Under certain Ag<sup>+</sup> treatment circumstances, the successful maintenance of cellular metabolism and physiology has been reported, but at the expense of the growth and viability loss, condition that suggested an “active but non-culturable state” under silver stress condition (Kedziora et al., 2018).

Several mechanisms have been identified in case of silver induced antibacterial activity (Saulou-Berion et al., 2015; Kedziora et al., 2018): (1) structural damage in the cell envelope; (2) interactions with intracellular molecules such as proteins and nucleic acids; (3) generation of reactive oxygen species.

## **EFFECTS OF SILVER IONS ON BACTERIAL CELL ENVELOPE**

Bacterial plasma membrane is fundamental to prokaryote metabolism as a location of essential reactions (e.g. respiratory chain events, protein transport and secretion, biosynthesis of lipids) (Bondarenko et al., 2018). Under ionic silver treatment, membrane disruption leading to cellular lysis, cytoplasm leakage and separation of plasma membrane from the cell

wall has been observed in both Gram-positive and Gram-negative species (Kedziora et al., 2018). The destabilization of the bacterial phospholipid bilayer is mostly induced via  $K^+$  ion loss and ATP level decrease (Saulou-Berion et al., 2015), the latter being a consequence of the impairment of respiratory chain enzymes, thus decoupling ATP synthesis from respiration. Experimental studies confirmed an increased permeability of the cell envelope structures under silver ion stress (Barras et al., 2018). As revealed by transmission electron microscopy the cell envelope seems to be affected by silver ions via expansion of the periplasmic space, probably due to the detachment of the inner membrane from the peptidoglycan layers (Barras et al., 2018). The thicker cell wall and its negative charge seem to confer to Gram-positive bacteria a passive advantage by blocking and attracting the silver ions, thus acting like a filter and limiting their access into the cytoplasm (Dakal et al., 2016). In Gram-negative species such as *Vibrio cholerae* changes in the pH gradient occurred on inside-out membrane vesicles under ionic silver treatment, by a presumable proton leakage, induced by changes in membrane proteins or phospholipid bilayer (Barras et al., 2018; Bondarenko et al., 2018). Silver was found to induce the shortening of cell membrane fatty-acyl chains, process that has been correlated with the down-regulation of *fadL* gene, engaged in fatty acid transport and lipid A synthesis/modification-associated *lpxA/arnA* genes (Saulou-Berion et al., 2015). The increasingly altered secondary structure of proteins in the presence of ionic silver was correlated with *hfg* peptidase and *dnaJ* chaperone upregulation, as well as the regulation of transpeptidase genes *ycfS* and *ycbB* (Saulou-Berion et al., 2015). Both YcfS and YcbB are L, D-transpeptidases which are known in *E. coli* to have the following functions: YcbB forms the peptidoglycan crosslinks and YcfS has the role of anchoring the Braun's lipoprotein to peptidoglycan (Hugonnet et al., 2016). As enzymes engaged in the structural integrity of the cell wall, their regulation under these conditions identify also the cell membrane as being a key target for  $Ag^+$  (Saulou-Berion et al., 2015).

## INTERACTIONS BETWEEN IONIC SILVER AND PROTEINS

Whether part of cell envelope or cytoplasm, the proteins, through their specific amino acid sequence are actively engaged in interactions with heavy metals, including silver cations. Ionic silver was found to inhibit several fundamental cellular processes involving proteins, such as cellular respiration and proton motive force (Hobman and Crossman, 2014). At high concentration, the inhibitory activity of silver ions was targeted against proteins by compromising their  $\alpha$ -helix conformation (Saulou-Berion et al., 2015). Recent studies found that this would not be always the case, at least in biochemical pathways engaged in silver toxicity control. Thus, silver ions interact positively with proteins engaged in their binding, as starting and consolidating mediators in their function-associated  $\alpha$ -helix sequences (Asiani et al., 2016; Chabert et al., 2017).

The  $Ag^+$  interactions with the thiol groups were also found to be often engaged in ionic silver antibacterial toxicity (Kedziora et al., 2018). The sulfhydryl group, as part of cysteine residues, links the silver ions to metalloprotein activity alteration, recent studies confirming silver as acting on the-S cluster containing proteins, which can be members of the respiratory chain, or could belong to the dehydratase group such as would be the case with fumarase A (Barras et al., 2018). The most common Fe-S clusters are mostly coordinated to proteins by cysteine residues (Ayala-Castro et al., 2008). Fumarase A can be reactivated under incubation with  $Fe^{2+}$  and thiols (Reaney et al., 1993). As previously mentioned, besides thiol, other electron-donating groups interacting with  $Ag^+$  are carboxylates, hydroxyls, amides, imidazoles, or indoles, all being involved in membrane or cytoplasmic protein-associated reactions as well (Saulou-Berion et al., 2015).

Silver ions were found to have an affinity towards the S2 ribosomal protein, by compromising its structure and inhibiting subsequent protein biosynthesis (Kedziora et al., 2018). Yamanaka et al. (2005) found with high probability a significant decrease in the 30S ribosomal subunit protein S2, together with succinyl-CoA synthetase and MalK

maltose transporter under ionic silver treatment. Both succinyl-CoA synthetase and MalK are engaged in ATP associated functions, such as synthesis (Phillips et al., 2009) and binding/transport (Schneider et al., 1995), their reduced titer reflecting an inhibition in ATP activity.

## INTERACTION OF IONIC SILVER WITH NUCLEIC ACIDS

Although sometimes mentioned as a major target for silver toxicity (Greulich et al., 2012; Finley et al., 2015), the nucleic acids could play a secondary role in this process. Thus, due to the localization of bacterial genome in the cell core, usually surrounded by proteins, nucleic acids seem not to get often into contact with silver ions as previously considered (McQuillan and Shaw, 2014). Since cytoplasmic proteins interact more frequently with the heavy metal ions, experimental results at sub-inhibitory silver concentrations showed no evidence for significant nucleic acid damage (McQuillan and Shaw, 2014).

When interaction with nucleic acids does occur, silver binds mainly to pyrimidine bases, inducing DNA condensation and subsequent inhibition of replication (Kedziora et al., 2018). Indeed, microscopic studies showed DNA condensation in silver treated bacteria and at high concentration silver ions seem to interact with adenine and guanine, usually having a higher affinity for the latter and generally leading to an increasing risk of pyrimidine dimerization (Barras et al., 2018). Thus, DNA lesions can affect the bacterial chromosome replication (Saulou-Berion et al., 2015) under specific concentrations.

## REACTIVE OXYGEN SPECIES (ROS) GENERATION

Silver cations associated increase in ROS is mainly induced by the inhibition of main respiratory chain proteins such as cytochrome b (Kedziora et al., 2018). Accumulation of reactive oxygen species induces itself protein damage or nucleic acid breakage, in addition to the more direct interaction of silver ions with these molecular structures. In silver treated *E. coli*, oxidative stress-related genes, together with metal ion/general stress genes were up-

regulated on the expense of generally growth associated heredity units, which were down-regulated under ionic silver challenge (Saulou-Berion et al., 2015).

Experimental data showed that a significant number of silver induced *E. coli* and *Staphylococcus aureus* bacterial deaths in reporter strains expressing a specific response to super oxide radicals, were due to ROS-mediated activity (Park et al., 2009). These studies revealed a major generation of some of the superoxide radicals, but without the induction of H<sub>2</sub>O<sub>2</sub>. The limiting effect of ionic silver on hydrogen peroxide was also observed in multi-species co-culture experiments engaging pyocyanin synthesized by *Pseudomonas aeruginosa*. Thus, by adding Ag<sup>+</sup> to the medium, microbial induced hydrogen peroxide accumulation has been significantly inhibited (Muller, 2018).

## SILVER ASSOCIATED RESISTANCE MECHANISMS

Many bacterial species and strains can withstand against toxic concentrations of heavy metal ions in polluted environments. This resistance is often encoded on plasmid genes, but their location on bacterial chromosome is not uncommon either (Li et al., 1997; Gupta et al., 2001; Randall et al., 2015).

The bacteriostatic or bactericidal effect of silver ions is often species and strain-dependent. Thus, by testing several tens of clinical isolates from several bacterial species, the minimal inhibitory concentrations were found to be around 200-300 μM Ag<sup>+</sup> for most of them excepting one *Enterobacter cloacae* and one *Klebsiella pneumoniae* strain which required significantly higher MIC values, of 5,500 μM Ag<sup>+</sup> (Finley et al., 2015).

In most cases environmental bacterial communities are not represented by single species, which means a constant biological interaction with complex and often unpredictable consequences. This fact constitutes a more elaborate level of dealing with environmental conditions, by enabling sensitive species or strains to benefit from better adapted populations in order to overcome adverse conditions. *Pseudomonas aeruginosa* has the ability to reduce the Ag<sup>+</sup> ion to nontoxic Ag<sup>0</sup>

through pyocyanin biosynthesis, a redox-active toxin with broad-spectrum antimicrobial activity (Muller, 2018) via super oxide and hydrogen peroxide synthesis (Hall et al., 2016). Pyocyanin is a metabolite usually engaged in reduction of molecular oxygen and  $Fe^{3+}$  ions (Muller and Merrett, 2014) and was also found to be a reductant of  $Ag^+$  to  $Ag^0$  form. *E. coli* and *S. aureus* strains, usually unable to reduce ionic silver were capable to do it in the presence of pyocyanin, if cultured in the presence of this toxin-producing *Pseudomonas aeruginosa* strain. This result was considered to suggest that both oxygen and silver compete as electron acceptors for pyocyanin-associated reactions (Muller, 2018).

Often, bacterial silver resistance requires heavy metal exposure to induce gene expression. Sutterlin et al. (2014) found that none of the confirmed *sil* gene carrier bacteria were showing silver resistance phenotype before the  $Ag^+$  treatment, but *in vitro* resistance has been easily subsequently induced. By using sub-inhibitory concentrations of silver ions, a selection of silver resistant *E. coli* strains was possible after only 6 days of treatment (Randall et al., 2015; Kedziora et al., 2018).

The antibacterial effect of silver ions can be dependent on cellular or environmental conditions. Thus, silver cations can be neutralized following interactions with proteins such as albumin or by turning them into insoluble precipitates such as  $AgCl$  (Kedziora et al., 2018).

Bacteria can deal with ionic silver by reducing it via nanoparticle synthesis. *Bacillus* strain CS11 exposed to  $AgNO_3$  at room temperature induced various sized silver particles within 24 hours (Siddiqi et al., 2018). Pyocyanin producing *Pseudomonas aeruginosa* strain neutralized 95% of the silver ions in a matter of minutes by reducing them to  $Ag^0$  based nanoparticles (Muller & Merrett, 2014).

Mechanisms regarding silver ion uptake into the bacterial cell differ between Gram-positive and Gram-negative species, due to the structural differences in the bacterial envelope (Kedziora et al., 2018). The relative differences in silver resistance between Gram-positive and Gram-negative species are sustained by contradictory information available in the literature. Thus, according to some authors, *S.*

*aureus* still can be regarded as a target of the biocidal effects of silver due to its inner membrane high vulnerability (Randall et al., 2015), while others reveal at least a slightly higher staphylococcal resistance than *E. coli* during a comparative study between the two species. The higher resistance of *S. aureus* was hypothesized as being induced by its thicker cell wall structure, at least in case of using silver acetate as ion source (Greulich et al., 2012; Saulou-Berion et al., 2015).

Generally, two mechanisms are identified in bacterial defence against heavy metal challenge, one endogenous and one exogenous (Randall et al., 2015; Kedziora et al., 2018): the endogenous mechanism (via mutations in the own genome) involve features such as the loss of uptake-associated protein functions of the outer membrane porins (ex. OmpF or OmpF/C). In *E. coli*, endogenous resistance against silver was induced by two-point mutations in *ompR* and *cusS* genes which resulted in both loss of OmpC/F porins and depression of the CusCFBA efflux transporter system (Randall et al., 2015). The final effect of both mutations was a reduced intracellular accumulation of silver.

The exogenous mechanism (induced by horizontally acquired genetic material) involves the presence or the increase of plasmid genetic activity such as that related to *sil* operon associated efflux mechanisms, by both periplasmic sequestration and active efflux of the silver ions in the extracellular environment (Randall et al., 2015).

## RESISTANCE AGAINST SILVER IONS IN GRAM-NEGATIVE BACTERIA

In Gram-negative bacteria such as *E. coli*, the main gateway for ionic silver uptake are the major outer membrane proteins (OMPs) (McQuillan and Shaw, 2014) such as OmpF porin and OmpC (its homolog) (Kedziora et al., 2018). OmpF is a trimeric beta-barrel transmembranar protein, each monomer consisting in sixteen hydrogen bonded antiparalel beta strands (Kedziora et al., 2018). The strands form a cylindrical channel engaged in ion and molecule (such as drugs) transporting activity through the cellular outer membrane (Kedziora et al., 2018). As it has

been previously specified, mutations at porin genes group level can induce silver resistance. Experimental data showed that bacterial strains lacking expression of *ompF* or *ompF/ompC* genes were significantly more resistant against silver treatment (Randall et al., 2015; Kedziora et al., 2018) by impaired outer membrane permeability. Additionally, the exposure to silver in species such as *E. coli* induced itself the loss of function of the *OmpF/OmpC* transcription factor *OmpR* (Kedziora et al., 2018). A reduced expression of *ompF* gene under silver treatment was observed in *Salmonella typhimurium* as well (Kedziora et al., 2018). These results show not only the mechanisms involved in bacterial silver uptake, but also the selective pressure made on the microbial high plasticity in genetic response by this chemical element.

A genotype-dependent response is suggested by similar studies, but showing no differences in culture reaction to silver regardless of the *OmpF/OmpC* status in the bacterial outer membrane (Kedziora et al., 2018) which could be explained by alternative pathways engaged in overcoming silver toxicity.

The *Salmonella* associated plasmid pMG101 is the most representative example of horizontally acquired silver resistance in Gram-negative bacteria. It contains the 14.2 kb *sil* operon, which gathers 9 ORFs (open reading frames) divided in three transcription units (Silver, 2003; Gupta et al., 2001; Randall et al., 2015), identified as *sil-PGABFCRSE* (Asiani et al., 2016). Out of these, seven seem to be structural genes (*silE*, *C*, *F*, *B*, *A*, *ORF105(G)* and *silP*) and the other two (*silR* and *silS*) are considered to encode a membrane sensor and responder grouped as a transcriptional regulatory system (Silver, 2003; Asiani et al., 2016).

The *SilE* protein has been found to have a silver binding role at periplasm level (Silver, 2003; Randall et al., 2015; Asiani et al., 2016) together with *SilF* protein. The two active efflux systems are the resistance-nodulation-division (RND)-type efflux transporter *SilCFBA* and the presumed P-type ATPase inner membrane transporter *SilP* (Silver, 2003; Randall et al., 2015; Asiani et al., 2016). The same genes were identified on at least 5 plasmids belonging to the 19 incompatibility group H (Silver, 2003; Finley et al., 2015).

Several species/taxonomic groups have been identified until now to carry *sil* genes, including *Salmonella* sp., *E. coli*, *Enterobacter* sp., *Acinetobacter* sp., *Pseudomonas* sp., *Klebsiella* sp. and methicillin-resistant coagulase-negative staphylococci (Finley et al., 2015).

Close homologues for *silA*, *B*, *C*, *F* and *silR*, *S* from the *Salmonella* plasmid were found to be clustered on the *E. coli* K-12 and O157: H7 chromosomes (Gupta et al., 2001; Silver, 2003). These *E. coli* genome-associated genes constitute the former *agr* group, currently named *cus* (from copper and silver resistance), a 6 gene cluster grouped into *CusCFBA* and *CusR/S* systems (Silver, 2003; Holt and Bard, 2005; Randall et al., 2015). The original NCTC 86 *E. coli* strain, described by Theodor Escherich in 1885, has been recently sequenced and found to contain a nine ORF chromosomal 36 kb *sil* locus (ROD36) (Dunne et al., 2017).

The *CusCFBA* transporter was described first as a copper efflux system and later shown to be involved in silver binding and externalization as well. The *cus* operon, similarly to its *sil* plasmid counterpart includes genes coding for a sensor kinase (*CusS*), a periplasmic efflux system (*CusBCA*) and a periplasmic silver binding protein (*CusF*) (Finley et al., 2015). The amino acid sequence of the two systems has an 80% identity (Finley et al., 2015; Chabert et al., 2017).

*SilE* has no homologue ORF in the copper efflux pump (Chabert et al., 2017) and according to Gupta et al. (2001), this is an indication of a later addition of the gene to the plasmid system. Interestingly, in a study regarding the screening for 3 *sil* genes in *S. aureus*, *silE* was the only one identified, in a relatively small fraction (6%) of the analyzed strains (Loh et al., 2009), its presence together with its particular feature in Gram-negative bacteria suggesting a special evolutionary and selection pathway of this gene among microorganisms.

*SilE* protein has a primary sequence of 143 amino acids, including an N-terminal short (20 aa) signal peptide that is cleaved after reaching the periplasm (Chabert et al., 2017). Previous studies involving various experimental conditions reported the *SilE* protein as being able to bind between 5 and 38 Ag<sup>+</sup> (Asiani et

al., 2016). Experiments of Asiani et al. (2016) on SilE binding activity showed the protein as shifting between two forms: a disordered protein as apo-SilE, which, upon binding  $\text{Ag}^+$  ions, turns into a holo-SilE with a highly  $\alpha$ -helical secondary structure. SilE-metal complexes showed a binding efficiency for up to 8  $\text{Ag}^+$  ions but also an affinity for divalent cations, bonded in a lower number of atoms per molecule:  $\text{Cu}^{2+}$  (up to six ions),  $\text{Zn}^{2+}$  (up to five) and  $\text{Ni}^{2+}$  (up to two). The silver binding capacity of the SilE protein confirmed the decisive role of histidine and methionine residues within specific sequence motifs in  $\text{Ag}^+$  binding. Single and double mutations made on histidine (to alanine) and methionine (to leucine) confirmed the two amino acid dependent silver binding capacity of SilE and also the silver binding dependence of the holo-SilE structure. Thus, the study of Asiani et al. (2016) suggest that during subsequent binding/accumulation of silver ions, the SilE molecule increase its folding status to a maximum, reached after binding six  $\text{Ag}^+$ . Additional two ions were found to be possibly attached to the fully folded form of the protein in some cases. An additional indication that the binding and folding processes are linked was that in the case of  $\text{Cu}^{2+}$ ,  $\text{Zn}^{2+}$  and  $\text{Ni}^{2+}$  treatments, lower binding yields induced a lower folding degree of the molecule as well. This mechanism of gradual molecular conformation during the cation accumulation process was suggested by the authors as a clear indicator of SilE protein as firstly being dependent on  $\text{Ag}^+$  binding before subsequent resistance mechanisms against heavy metal toxicity to be initiated.

Based on SilE amino acid sequence, Chabert et al. (2017) tested the binding activity of the histidine and methionine associated sequences, grouped in nine  $\text{MX}_2\text{H}$  or  $\text{HX}_n\text{M}$  ( $n = 1, 2$ ) motifs. Their results showed that all of them can coordinate a silver cation, thus suggesting an up to 9  $\text{Ag}^+$  ion binding efficiency by the protein. If these shorter peptides are grouped and looked at as larger motifs, the authors identified two, namely H80-M90 and M108-M121 sequences as essential for the successful silver coordinated  $\alpha$ -helix folding.

Besides these resistance gene mediated responses, several other pathways are

influenced by the presence of ionic silver in the proximity of bacteria. In *E. coli*, 258 genes, representing 5.8% of the genome were differentially expressed under silver nitrate treatment, with a total of 220 up-regulated and 38 down-regulated (McQuillan & Shaw, 2014). A full transcriptome profile made by the authors showed a significant activity of the Heat Shock Response (HSR) gene group under these conditions. Since the main reaction of heat shock proteins against environmental pressure is to facilitate protein folding and to be engaged in protein rescue or degradation of denatured/misfolded polypeptides (Roncarati & Scarlato, 2017), a massive protein degradation/impairment must have been induced by the silver nitrate treatment.

From the Heat Shock Response gene group, several families were strongly up-regulated under silver stress, especially those related to polypeptide binding and stabilization, protein folding, synthesis of proteolytic enzymes (especially those engaged in breakdown of insoluble protein aggregates or denatured polypeptides), heat shock locus proteins and heat stress associated genes. Essential protein folding chaperone genes such as *groL* and *dnaK* were up-regulated by more than 9 and 19 times respectively and *ipaA*, engaged in denatured polypeptide binding and stabilization, had an expression ratio of over 180 (McQuillan & Shaw, 2014). Other gene groups, mostly iron and copper associated, such as Fur regulon, iron-sulphur cluster assembly complex, sulphate transport/assimilation and copper homeostasis were significantly up-regulated as well. Among the Fur regulon associated genes, generally essential in iron acquisition (Tsolis et al., 1995), positively regulated were those engaged in enterobactin siderophore synthesis,  $\text{Fe}^{3+}$  associated membrane ligand and uptake, and those associated to ferric citrate and ferrichrome uptake. The sulphate transport and assimilation associated genes included those engaged in cysteine biosynthesis.

## RESISTANCE AGAINST SILVER IONS IN GRAM-POSITIVE BACTERIA

As already mentioned, resistance against silver ions in Gram-positive species often takes place differently than in their Gram-negative

counterparts, mainly due to their cell envelope structural distinction (Kedziora et al., 2018; Greulich et al., 2012; Saulou-Berion et al., 2015). The major differences in the bacterial envelope structures between the two groups already suggest differences in influx/efflux mechanisms occurring at silver intake and its subsequent expulsion outside the cell. The lack of outer membrane, the less defined periplasmic space in Gram-positive bacteria, along with the significantly thicker peptidoglycan layer in the cell envelope suggests a more passive way to overcome environmental toxicity. The differences between Gram-positive and Gram-negative species fluctuate from slightly higher resistance (Greulich et al., 2012) to 32 times higher minimal bactericidal concentration for Gram-positive bacteria (Kedziora et al., 2018).

More than one and half decade ago in *Enterococcus hirae* genes for both copper and silver resistance were identified coding for either uptake or efflux associated mechanisms (Holt and Bard, 2005). At least one of them proved to be a copper efflux ATPase, found to pump outside the cell  $\text{Ag}^+$  as well (Li et al., 1997). Some data suggest that in Gram-positive species, some of the most common silver ion binding sites seem to be the phosphate groups in teichoic acid and carboxyl groups in the glutamic acid (Kedziora et al., 2018).

The occurrence of *sil* genes seem to be significantly lower in species such as *Staphylococcus aureus*, though being present and expressed in some strains. Thus, studies regarding *S. aureus* revealed no evidence of silver resistance in 876 strains taken from clinical isolates (Randall et al., 2015). Also, unlike in Gram-negative species such as *E. coli*, *S. aureus* showed no reduction in silver susceptibility even during extended culture maintenance of 42 days under *in vitro* silver treatment.

On the other hand, studies performed on methicillin resistant *S. aureus* and MR coagulase negative staphylococci isolated from humans and other mammals revealed the presence of *silE* gene in 2 out of 33 tested MRSA strains and in one out of 8 MR-CNS isolates (*Staphylococcus sciuri*) (Loh et al., 2009). These findings show that even bacterial species with statistically low occurrence of *sil* genes can carry resistance against silver

treatment via this pathway. Gram-positive species such as *S. aureus* and *Bacillus subtilis* were already shown to possess a periplasmic space between the peptidoglycan layer and the plasma membrane (Zuber et al., 2006). Interestingly, the presence of a gene encoding a periplasm associated protein in a Gram-positive species suggest that additional details could be revealed in the future about the role of this binding molecule in microbes, with or without the engagement of the other members of the *sil* gene group. Extra-chromosomal transfer between Gram-negative and Gram-positive bacteria do occur (Dakal et al., 2016) and, if accurate, the finding of *silE* in *S. aureus* could reveal new aspects regarding the functional features of this protein in bacterial biochemistry.

Usually encoded by the *sil* operon in Gram-negative species, the SilE protein is still considered to have unconfirmed details regarding its exact function of silver resistance excepting its binding activity (Chabert et al., 2017). Unlike the other members of the group *silRS* and *silCFBAGP*, *silE* is a separate transcriptional unit, controlled by its own promoter (Asiani et al., 2016). As mentioned before, SilE has the ability to bind not only silver ions, but copper, zinc and nickel as well. Matias and Beveridge, cited by Zuber et al. (2006) showed that *B. subtilis* and *S. aureus* have a periplasmic space, defined as the inner wall zone, which they suggested as containing low density compounds with high affinity for heavy metal stains, which in fact could constitute a fundamental defense environment against silver ions and other similarly toxic metals. According to some authors (Randall et al., cited by Kedziora et al., 2018) in staphylococci, the most important harmful effect of  $\text{Ag}^+$  ions seems to be located in the inner membrane.

In the literature, extensive studies regarding Gram-negative silver resistance describe a highly specialized capacity to overcome silver biocidal effect. However, experimental data suggest that at least in some cases, Gram-positive species have a higher potential to withstand silver contaminated environments (Kedziora et al., 2018; Sobisch et al., 2019). Among the surviving bacteria on stainless steel control versus silver or silver/ruthenium coated

surfaces on the International Space Station, Gram-positive species belonging to genera such as *Staphylococcus*, *Bacillus* and *Enterococcus* proved to be the most successful (Sobisch et al., 2019).

A *Bacillus cereus* transcriptome analysis made by Babu et al. (2011) showed a strong bacterial genetic response against silver treatment. Thus, high concentration (1 mM) of silver nitrate induced the up-regulation of about 10% (524) out of the 5234 genes in *Bacillus cereus* ATCC 14579. Most of them were related to DNA replication, nutrient transporter, chaperones and membrane protein groups. Genes linked to proteins engaged in carbohydrates, aminoacids, drugs and antibiotics synthesis, transcription, DNA replication, repair and recombination, inorganic ions, cell envelope and membrane synthesis were upgraded under silver stress also. Among the transport and membrane associated processes, mostly efflux and drug resistance and osmoprotectant transporter protein synthesis genes were preferentially activated as well. Other genes, such as those associated with chemotaxis and flagellar proteins were down-regulated by the silver ions, suggesting a significant inhibition of the bacterial motility under silver nitrate treatment. Gram-positive bacteria such as *Bacillus cereus* have a large number of drug transporter coding genes, which possibly compensate for the lower occurrence of silver associated specific resistance genes and/or plasmids (Kroeger et al., 2015). Thus, the ATCC 14579 strain was found to contain 93 drug transporter annotated genes, representing about 1.7% of its the genome, which is significantly higher than 32 and 37 corresponding genes from *B. subtilis* and *E. coli*, respectively (totalizing 0.8 and 0.9% of their protein associated genes) (Kroeger et al., 2015). The high number of transporters associated genes in *Bacillus cereus* group was explained by its soil associated ecological niche, an environment characterized by a high variability regarding nutrients and sustained exposure to harmful chemicals (Hassan et al., 2017).

## CONCLUSIONS

Gram-negative bacteria were found to acquire by horizontal gene transfer or by mutation

highly effective genetic traits which enable them to survive an ionic silver treated/contaminated environment. These gene response mechanisms are made via cation binding and sequestration in the periplasm or by expulsion of the toxic metal outside the bacterial cell by efflux pump systems. Generally, Gram-positive species show a higher passive resistance against toxic silver due to their specific cell envelope and are engaged in a significant metabolic and repair, transporter and overall molecular protective systems traceable by transcriptome analysis.

The increased employment of silver in current modern society, visible mostly in industrial, agricultural, general hygiene or healthcare associated sectors induced a major selection pressure on microbial communities. The response is today obvious, species and strains proved to possess the resources to overcome silver toxicity in a manner similar to antibiotics resistance. This process is to be taken into consideration, especially because these genetic traits can be transferred horizontally between species that share the same ecological niche or can be selected by the bacterial remarkably high mutation rate. Last but not least silver associated resistant features are already available without being phenotypically proven until silver stressors act as catalysts to induce subsequent resistance pathways.

## ACKNOWLEDGEMENTS

Financial support for this study was granted by the Ministry of National Education (MEN-UEFISCDI), project PN-III-P4-ID-PCE-2016-0637, no. 162/2017.

## REFERENCES

- Asiani, K. R., Williams, H., Bird, L., Jenner, M., Searle, M. S., Hobman, J. L., Scott, D. J., Soultanas, P. (2016). SilE is an intrinsically disordered periplasmic "molecular sponge" involved in bacterial silver resistance. *Molecular Microbiology*, 101(5), 731–742, doi: 10.1111/mmi.13399.
- Ayala-Castro, C., Saini, A., Outten, F. W. (2008). Fe-S cluster assembly pathways in bacteria. *Microbiology and Molecular Biology Reviews*, 110–125, doi: 10.1128/MMBR.00034-07.
- Babu, M. M. G., Sridhar J., Gunasekaran, P. (2011). Global transcriptome analysis of *Bacillus cereus* ATCC 14579 in response to silver nitrate stress.

- Journal of Nanobiotechnology*, 9: 49, <http://www.jnanobiotechnology.com/content/9/1/49>.
- Barras, F., Aussel, L., Ezratty, B. (2018). Silver and antibiotic, new facts to an old story. *Antibiotics*, 7(79), doi: 10.3390/antibiotics7030079.
- Bondarenko, O. M., Sihtmäe, M., Kuzmičiova, J., Rageliene, L., Kahru, A., Daugelavičius, R. (2018). Bacterial plasma membrane is the main cellular target of silver nanoparticles in *Escherichia coli* and *Pseudomonas aeruginosa*. *International Journal of Nanomedicine*, 13, 6779–6790, doi: 10.1101/322727.
- Chabert, V., Hologne, M., Seneque, O., Crochet, A., Walker, O., Fromm, K. M. (2017). Model peptide studies of Ag<sup>+</sup> binding sites from the silver resistance protein SilE. *Chemical Communications*, 53(45), 6105–6108.
- Dakal, T. C., Kumar, A., Majumdar, R. S., Yadav, V. (2016). Mechanistic basis of antimicrobial actions of silver nanoparticles. *Frontiers in Microbiology*, 7, 1831, doi: 10.3389/fmicb.2016.01831.
- Dunne, K. A., Chaudhuri, R. R., Rossiter, A. E., Beriotto, I., Browning, D. F., Squire, D.,... Henderson, I. R. (2017). Sequencing a piece of history: complete genome sequence of the original *Escherichia coli* strain. *Microbial Genomics*, 3, doi: 10.1099/mgen.0.000106.
- Finley, P. J., Norton, R., Austin, C., Mitchell, A., Zank, S., Durham, P. (2015). Unprecedented silver resistance in clinically isolated Enterobacteriaceae: major implications for burn and wound management. *Antimicrobial Agents and Chemotherapy*, 59, 4734–4741, doi: 10.1128/AAC.00026-15.
- Greulich, C., Braun, D., Peetsch, A., Diendorf, J., Siebers, B., Epple, M., Koller, M. (2012). The toxic effect of silver ions and silver nanoparticles towards bacteria and human cells occurs in the same concentration range. *RSC Advances*, 2, 6981–6987.
- Gupta, A., Phung, L.T., Taylor, D.E., Silver, S. (2001). Diversity of silver resistance genes in IncH incompatibility group plasmids. *Microbiology*, 147, 3393–3402.
- Hassan, K. A., Fagerlund, A., Elbourne, L. D. H., Voros, A., Kroeger, J. K., Simm, R. (2017). The putative drug efflux systems of the *Bacillus cereus* group. *PLoS ONE* 12 (5): e0176188. Retrieved January 23, 2019, from <https://doi.org/10.1371/journal.pone.0176188>.
- Hall, S., McDermott, C., Anoopkumar-Dukie, S., McFarland, A. J., Forbes, A., Perkins, A. V.,... Grant, G. D. (2016). Cellular effects of pyocyanin, a secreted virulence factor of *Pseudomonas aeruginosa*. *Toxins*, 8, 236, doi: 10.3390/toxins8080236.
- Holt, K.B., Bard, A.J. (2005). Interaction of silver (I) ions with the respiratory chain of *Escherichia coli*: an electrochemical and scanning electrochemical microscopy study of the antimicrobial mechanism of micromolar Ag<sup>+</sup>. *Biochemistry*, 44, 13214–13223.
- Hobman, J. L., Crossman, L. C. (2015). Bacterial antimicrobial metal ion resistance. *Journal of Medical Microbiology*, 64, 471–497, doi: 10.1099/jmm.0.023036-0.
- Hugonnet, J. E., Mengin-Lecreulx, D., Monton, A., den Blaauwen, T., Carbonnelle, E., Veckerle, C.,... Arthur, M. (2016). Factors essential for L, D-transpeptidase mediated peptidoglycan cross-linking and β-lactam resistance in *Escherichia coli*. *ELife*, 5: e19469, doi: 10.7554/eLife.19469.
- Kedziora, A., Speruda, M., Krzyzewska, E., Rybka, J., Łukowiak, A., Bugla-Płoskonska, G. (2018). Similarities and differences between silver ions and silver in nanoforms as antibacterial agents. *International Journal of Molecular Sciences*, 19, 444, doi: 10.3390/ijms19020444.
- Kroeger, J. K., Hassan, K., Voros, A., Simm, R., Saidijam, M., Bettaney, K. E.,... Kolsto, A. B. (2015). *Bacillus cereus* efflux protein BC3310 - a multidrug transporter of the unknown major facilitator family, UMF-2. *Frontiers in Microbiology*, 6, 1063, doi: 10.3389/fmicb.2015.
- Li, X. Z., Nikaido, H., Williams, K. E. (1997). Silver-resistant mutants of *Escherichia coli* display active efflux of Ag<sup>+</sup> and are deficient in porins. *Journal of Bacteriology*, 179(19), 6127–6132.
- Loh, J. V., Percival, S. L., Woods, E. J., Williams, N. J., Cochrane, C. A. (2009). Silver resistance in MRSA isolated from wound and nasal sources in humans and animals. *International Wound Journal*, 6, 32–38.
- McQuillan J. S., Shaw A. M. (2014). Differential gene regulation in the Ag nanoparticle and Ag<sup>+</sup>-induced silver stress response in *Escherichia coli*: A full transcriptomic profile. *Nanotoxicology*, 8(supl.1), 177–184, doi: 10.3109/17435390.2013.870243.
- Muller, M. (2018). Bacterial silver resistance gained by cooperative interspecies redox behavior. *Antimicrobial Agents Chemotherapy*, 62(8), e00672-18. <https://doi.org/10.1128/AAC>.
- Muller, M., Merrett, N. D. (2014). Pyocyanin production by *Pseudomonas aeruginosa* confers resistance to ionic silver. *Antimicrobial Agents and Chemotherapy*, 58(9), 5492–5499.
- Park, H. J., Kim, J. Y., Lee, J. H., Hahn, J. S., Gu, M. B., Yoon, J. (2009). Silver-ion-mediated reactive oxygen species generation affecting bactericidal activity. *Water Research*, 43(4), 1027–1023.
- Phillips, D., Aponte, A. M., French, S. A., Chess, D. J., Balaban, R. S. (2009). Succinyl-CoA synthetase is a phosphate target for the activation of mitochondrial metabolism. *Biochemistry*, 48(30), 7140–7149. doi: 10.1021/bi900725c.
- Randall, C. P., Gupta, A., Jackson, N., Busse D., O'Neill, A. J. (2015). Silver resistance in Gram-negative bacteria: a dissection of endogenous and exogenous mechanisms. *Journal of Antimicrobial Chemotherapy*, 70, 1037–1046. doi: 10.1093/jac/dku523.
- Reaney, S. K., Bungard, S. J., Guest, J. R. (1993). Molecular and enzymological evidence for two classes of fumarase in *Bacillus stearothermophilus* (var. *non-diastaticus*). *Journal of General Microbiology*, 139, 403–416.
- Roncarati, D., Scarlato, V. (2017). Regulation of heat-shock genes in bacteria: from signal sensing to gene expression output. *FEMS Microbiology Reviews*, fux015, 41, 549–574, doi: 10.1093/femsre/fux015.
- Rubino, J. T., Chenkin, M. P., Keller, M., Riggs-Gelasco, P., Franz, K. J. (2011). A comparison of methionine,

- histidine and cysteine in copper (I)-binding peptides reveals differences relevant to copper uptake by organisms in diverse environments. *Metallomics*, 3, 61–73.
- Salomoni, R., Léo, P., Montemor, A. F., Rinaldi, B. G., Rodrigues, M. F. A. (2017). Antibacterial effect of silver nanoparticles in *Pseudomonas aeruginosa*. *Nanotechnology, Science and Applications*, 10, 115–121, doi: 10.2147/NSA.S133415.
- Saulou-Bérion, C., Gonzalez, I., Enjalbert, B., Audinot, J. N., Fourquaux, I., Jamme, F.,... Girbal, L. (2015). *Escherichia coli* under ionic silver stress: an integrative approach to explore transcriptional, physiological and biochemical responses. *PLoS One*, 10(12): e0145748. doi: 10.1371/journal.pone.0145748.
- Schneider, E., Linde, M., Tebbe, S. (1995). Functional purification of a bacterial atp-binding cassette transporter protein (MaIK) from the cytoplasmic fraction of an overproducing strain. *Protein Expression and Purification*, 6, 10–14, doi:10.1006/prep.1995.1002.
- Siddiqi, K. S., Husen, A., Rao, R. A. K. (2018). A review on biosynthesis of silver nanoparticles and their biocidal properties. *Journal of Nanobiotechnology*, 16(1), 14, doi: 10.1186/s12951-018-0334-5.
- Silver, S. (2003). Bacterial silver resistance: molecular biology and uses and misuses of silver compounds. *FEMS Microbiology Reviews*, 27, 341–353, doi:10.1016/S0168-6445(03)00047-0.
- Sobisch, L.Y., Rogowski, K.M., Fuchs, J., Schmieder, W., Vaishampayan, A., Oles, P., Novikova, N., Grohmann, E. (2019). Biofilm forming antibiotic resistant gram-positive pathogens isolated from surfaces on the international space station. *Frontiers in Microbiology*, 10, 543, doi: 10.3389/fmicb.2019.00543.
- Soloz, M., Mermoud, M., Abicht, H., Mancini, S. (2011). Responses of lactic acid bacteria to heavy metal stress. doi: 10.1007/978-0-387-92771-8\_9. In book: *Stress Responses of Lactic Acid Bacteria*. Springer-Verlag New York Inc.
- Sütterlin, S., Edquist, P., Sandegren, L., Adler, M., Tängdén, T., Drobni, M., Olsen, B., Melhus, A. (2014). Silver resistance genes are overrepresented among *Escherichia coli* isolates with CTX-M production. *Applied and Environmental Microbiology* 80(22), 6863–6869, doi: 10.1128/AEM.01803-14.
- Tsolis, R. M., Baumler A. J., Stojiljkovic, I., Hefron, F. (1995). Fur regulon of *Salmonella typhimurium*: identification of new iron-regulated genes. *Journal of Bacteriology*, 177(16), 4628–4637.
- Yamanaka, M., Hara, K., Kudo, J. (2005). Bactericidal actions of a silver ion solution on *Escherichia coli*, studied by energy-filtering transmission electron microscopy and proteomic analysis. *Applied and Environmental Microbiology*, 7589–7593, doi: 10.1128/AEM.71.11.
- Zuber, B., Haenni, M., Ribeiro, T., Minning, K., Lopes, F., Morellion, P., Dubochet, J. (2006). Granular layer in the periplasmic space of gram-positive bacteria and fine structures of *Enterococcus gallinarum* and *Streptococcus gordonii* septa revealed by cryo-electron microscopy of vitreous sections. *Journal of Bacteriology*, 188(18), 6652–6660, doi: 10.1128/JB.00391-06.

## STUDIES ON THE EFFECTS OF VIBRATIONS FROM INDUSTRIAL ENVIRONMENTS

Claudiu-Sorin DRAGOMIR<sup>1,3</sup>, Daniela DOBRE<sup>2,3</sup>

<sup>1</sup>University of Agronomic Sciences and Veterinary Medicine of Bucharest, 59 Marasti Blvd,  
District 1, Bucharest, Romania

<sup>2</sup>Technical University of Civil Engineering Bucharest, 122-124 Lacul Tei Avenue,  
District 2, Bucharest, Romania

<sup>3</sup>National Institute of Research and Development URBAN-INCERC, 266 Pantelimon Street,  
District 2, Bucharest, Romania

Corresponding author email: dragomircs@gmail.com

### Abstract

*Vibrations caused by some industrial sources (forges, presses etc.) are transmitted to the ground, generating different surface waves, with significant effects on building foundations, as well as some effects on buildings and their occupants. The structural dynamic response to this type of vibration also depends on the phenomenon of structure-soil interaction and the phenomenon of attenuation/amplification of vibrations. The principle of the applied method consists in determining the actual values of the characteristic parameters from the recorded vibrations in-situ /in building, in order to verify the fulfilment of the velocity criteria which are correlated with certain degrees of damage. In view of the means of controlling vibrations (at source, by transmission and in remote buildings) with physical or on human perception effects, the made assessments will determine whether the prevailing frequency produced by industrial equipment, within the monitored activities, is finds itself in the area of adjacent buildings' frequencies, with possible effects on the comfort of the inhabitants. The article aims to present comparatively the results obtained from the some instrumented sites.*

**Key words:** damages, industrial vibrations, velocities.

### INTRODUCTION

Vibrations caused by some industrial sources (forges, presses for forging large and heavy parts, loading/unloading ramps and silos platforms, activities specific to the mineral industry/cement plant/co-incineration of waste in the cement plant etc.) are transmitted to the ground, generating different continuous, impulsive or intermittent waves, with significant effects on building foundations, as well as some effects on buildings and their occupants. The dynamic response of buildings to vibrational forces is an important concern and often involves adopting measures to reduce the level of vibrations transmitted through the soil and to prevent their propagation to adjacent buildings. Determination of the vibration level is generally based on direct measurements and there are some technical codes that make references to structural vibrations (C 125 – 2013, DIN 4150-3/1999, STAS 12025/2-94). These codes set limits for normal use of residential and social-cultural buildings

subjected to vibrations produced by equipment located inside or outside buildings (admissible vibration level, admissible values for the internal equivalent vibration level - equally physiological effect curves, curves to appreciate material degradation). The structural dynamic response also depends, in this case, on the phenomenon of soil-structure interaction, the approach being relatively similar to the propagation of seismic waves, not surface type (Dobre, 2012) and the phenomenon of attenuation/amplification of vibrations (from source to the foundations of neighboring buildings, then to the top of the building) (Dragomir, 2011).

### MATERIALS AND METHODS

The principle of the applied method is based on the determination of the actual values of the characteristic parameters (displacement, velocity, acceleration) from the vibrations recorded in a site/building, in order to verify the fulfilment of the velocity criteria (in

particular). The velocity criteria, as defined in various norms or studies, generally refer to buildings with structures designed in accordance with technical standards. Limits allowed for the normal functioning of residential and social-cultural buildings subjected to vibrations produced by equipment located inside or outside buildings (admissible vibration levels, allowable values for the internal vibration equivalent level - curves of equal physiological effect, curves for appreciate material degradation).

## RESULTS AND DISCUSSIONS

In view of the means of controlling vibration (at source, by transmission and in remote buildings) with physical effects or at the level of human perception, the assessments made will determine whether the predominant frequency of industrial equipment or activities generating oscillations in the monitored activities are in the area of adjacent building frequencies, with possible effects on the comfort of the inhabitants. The article aims to present comparatively the results obtained from some instrumented locations.

**Case study 1:** Determining the level of vibrations produced by an industrial activity (forging press)

Records made to determine the vibration level produced by a 12 000t forging press have been sequential and performed with GMS Plus, GeoSIG multichannel stations. The position of the seismic sensors was the following: a sensor inside the hall, in the same line as the large tonnage press and the outer sensor, and a sensor located outside the hall on the sidewalk (the eastern side) (Figure 1).



Figure 1. Position of seismic sensors. The outside sensor

The velocity variation on the three directions highlights predominant values in the z-direction at the sensor near the press (Figure 2) and with comparative values in the y and z directions, smaller than the press, in most of the records, to the external sensor (Figure 3).

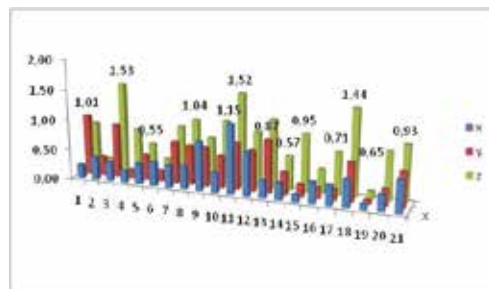


Figure 2. Variation of velocity at the sensor near the press

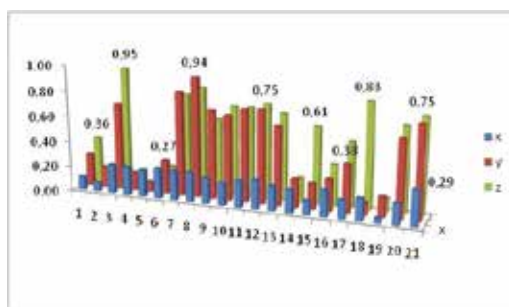


Figure 3. Velocity variation at outer sensor (eastern side)

Also, Tables 1 and 2 show the maximum/minimum values of accelerations and velocities outside the industrial hall (east side), these values being of interest. There is a distribution of the frequency values near the forging press and from the outside sensor, in directions x and y (inside of industrial hall – black; east side/outside of industrial hall - grey) (Figure 4):

- in the direction of x, the predominant field [9.2...10.89] Hz - near the press, [8.79...9.59] Hz - at the eastern side, with point values of 5 Hz and 12 Hz in both locations;
- in the direction of y, the predominant field [8.54...11.50] Hz - near the press, [9.47...11.25] Hz - at the eastern side, with point values of 12 Hz in both locations.

Table 1. Maximum/minimum acceleration values

Acceleration [mm/s <sup>2</sup> ] (outside - east side)	Forging press at work/direction			The forging press removed from work/direction		
	x	y	z	x	y	z
Maximum	17.99	56.80	48.44	3.46	6.46	5.66
Minimum	1.45	4.51	4.57	0.20	0.33	0.32

Table 2. Maximum/minimum velocity values

Velocity [mm/s] (outside - east side)	Forging press at work/direction			The forging press removed from work/direction		
	x	y	z	x	y	z
Maximum	0.29	0.94	0.95	0.053	0.095	0.11
Minimum	0.04	0.08	0.11	0.005	0.009	0.02

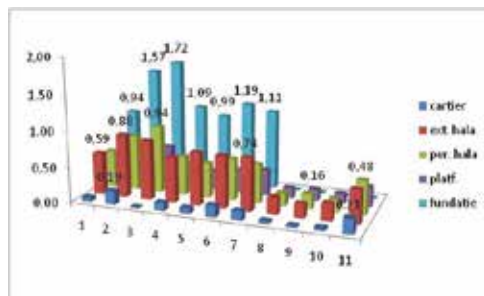


Figure 5. Velocity values recorded in 2014

From the figure above, it can be seen that at a velocity of 0.19 mm/s ... 0.21 mm/s, from the point of view of human comfort, vibrations are not perceived, or are easily perceived, according to the technical codes mentioned at the beginning, or, for example, BS 5228-2: 2009, where the following vibration levels (velocities) are associated with the corresponding effects on human comfort, as follows:

- 0.14 mm/s at low frequencies, vibrations are not perceived;
- 0.3 mm/s vibrations can be easily perceived;
- 1 mm/s sensations appear, but vibrations are tolerated if they are explained to those who feel them;
- 10 mm/s the vibrations are intolerable.

**Conclusion 1:** After processing all data, the degree of attenuation of the vibration level from the press to the eastern side is obtained; the recorded velocities are not exceeding the permissible value and the recorded values in the outside are lower. Regarding admissible values, the admissible velocity was considered 8 mm/s.

**Case study 2:** Determining the level of vibrations produced by industrial activity (loading/unloading ramps and silo platforms) within the Monsanto Sinesti agricultural complex

In the program of micro vibration measurements in the ramp hall, four series of records were made using the GMS Plus stations (4 x 1 internal triaxial sensor – 4 x 3 channels) (Figure 6).

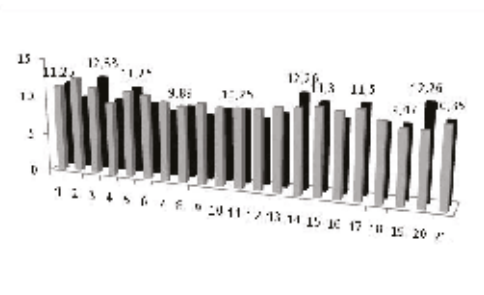
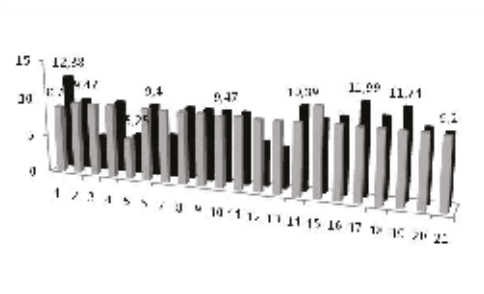


Figure 4. Frequency values, in the direction of x and y (4 ... 13 Hz)

According to the 2014 study, we can compare the recorded velocities with a 12-channel GeoDAS station equipped with four triaxial sensors (placed as follows: on the foundation of 12000 tf; on the slab/at the edge of the hall; outside the hall to the eastern side; outside to the road, at a distance of 1-5 m) and a 3-channel GeoDAS station equipped with 1 triaxial sensor (3 axial sensors, respectively) (located on the ground in the area of blocks with height regime P + 4 and P + 5), which are shown in Figure 5.

The recordings were made with auto-trigger at a pre-set date for synchronization of records from all sensors.

Measurements have been made in several different situations, as follows:

- I: corresponds to the situation where the ramps and the download zone are not loaded (static regime);
- II: corresponds to the situation where the ramps and the download area are not loaded, but the two unloading equipment are in operation (dynamic regime);
- III: corresponds to the situation where the ramps and the download zone are loaded at maximum capacity, but the unloading equipment is not in operation (static regime);
- IV: corresponds to the situation when the ramps and the download zone are loaded and operate at maximum capacity (dynamic regime).

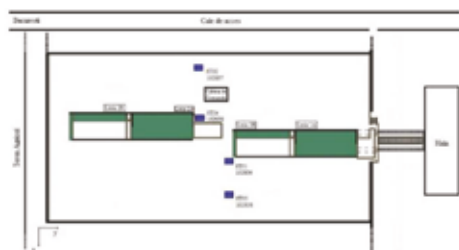


Figure 6. Location of GeoSIG acquisition system consisting of 4 GMSPlus stations. Line 1B

In Figure 7, the velocity variation on the two directions reveals predominant values in the direction x, in situation II (dynamic regime), and predominant in the y direction in the situation IV (dynamic regime), and in Tables 3 and 4 the max/min values of accelerations and velocities are presented.

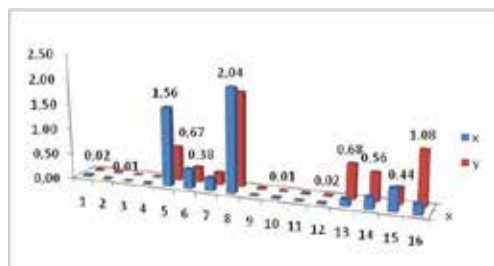


Figure 7. Predominant velocity values in the dynamic regime

A distribution of the frequency values is presented in both directions, with the predominant values: in situation I (static regime) - 13.5 Hz; in situation II (dynamic regime) - 8 Hz; in situation III (static regime) - 19.7 Hz; in situation IV (dynamic regime) - 7.9 Hz (Figure 8).

*Conclusion 2:* For the present study, the permissible velocity was considered 12 mm/s, not exceeding, and from the point of view of human comfort it is not taken into account, the area of the agricultural complex being quite far from the inhabited area.

Table 3. Maximum/minimum acceleration values

A m/ s <sup>2</sup>	Situation I		Situation II		Situation III		Situation IV	
	x	y	x	x	y	y	x	y
ma	0.58	0.34	28.9	20.1	0.24	0.32	8.4	20.7
x	4	6	4	4	5	2	3	3
min	0.20	0.24	3.99	7.89	0.17	0.20	3.5	7.87
	3	0			2	2	9	7.87

Table 4. Maximum/minimum velocity values

V mm /s	Situation I		Situation II		Situation III		Situation IV	
	x	y	x	x	y	y	x	y
max	0.03	0.02	2.03	1.86	0.01	0.01	0.44	1.07
	90	0	9	0	0	9	3	7
min	0.00	0.00	0.25	0.22	0.00	0.00	0.14	0.32
	53	47	8	8	49	64	2	4

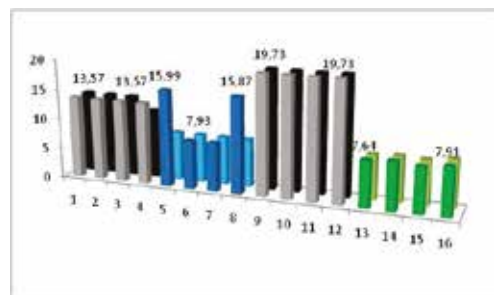


Figure 8. Predominant frequency value in dynamic regime: 8 Hz

**Case study 3:** Determining the level of vibrations produced by industrial activity (activities specific to the mineral industry/cement plant/co-incineration of waste in the cement plant etc.) within the CRH Cyclone Building, located in Hoghiz, Brasov

The vibrations were determined in four distinct points (established in agreement with the designer), in three directions (two horizontal and one vertical), in the state of technological operation of the cyclone tower building, which will allow the designer to identify the real level of vibrations, amplitudes and frequencies to correlate with the potential damage to some floors and/or other structural elements (at each measuring point, a sequence of 5 records of about 90 seconds). The four triaxial sensors of the GeoSIG, Kinometrics multi-channel acquisition system were placed vertically on the building (1st floor, 3rd floor, 5th floor, 6th floor terrace) (Figure 9). The orientation of the sensors placed on the vertical of the building was done as follows: the direction x - the direction of the rotating furnace; direction y - direction perpendicular to x direction; direction z - vertical direction of the building.

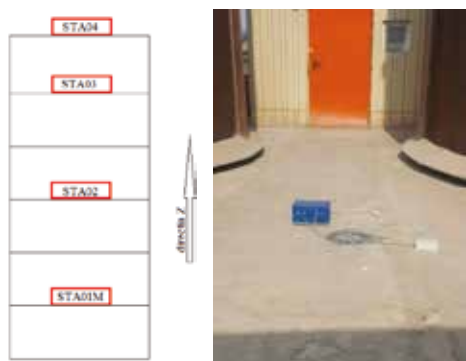


Figure 9. Location of the GeoSIG acquisition system consisting of 4 GMSPlus stations. Sensor on the 6<sup>th</sup> floor

In Figures 10-13, the velocity variation on the three directions reveals predominant values in the z direction at the lower level and increasing in direction x to the last level (6<sup>th</sup> floor).

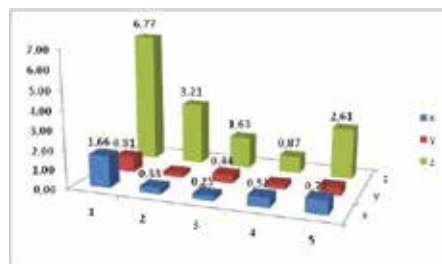


Figure 10. Velocities at the level 1

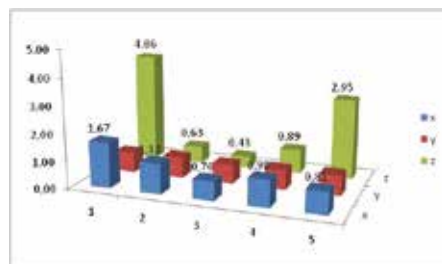


Figure 11. Velocities at the level 3

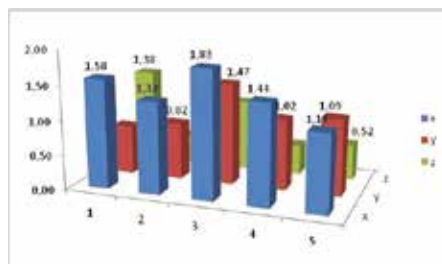


Figure 12. Velocities at the level 5

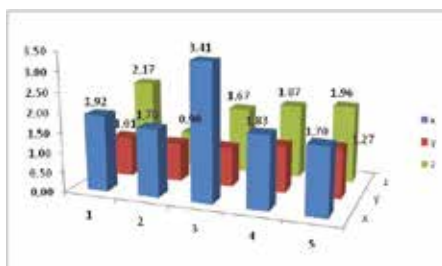


Figure 13. Velocities at the level 6

In Tables 5 and 6 the maximum/minimum values of accelerations and velocities are shown.

Table 5. Maximum/minimum acceleration values

Acceleration [mm/s <sup>2</sup> ]	dir x	dir y	dir z
maximum	92	78.1	570
minimum	13.45	11.54	32.21

Table 6. Maximum / minimum velocity values

Velocity [mm/s]	dir x	dir y	dir z
maximum	3.412	1.466	6.77
minimum	0.2541	0.222	0.4255

On the upper floor, the frequency values: 1.1 Hz- x direction; 1.4 Hz- y direction; 5 Hz- z direction (Figure 14).

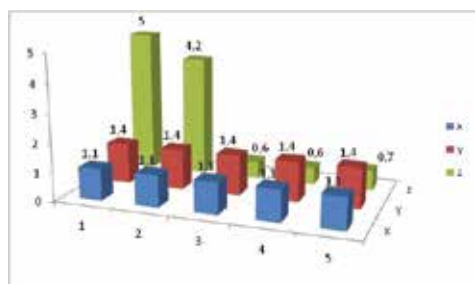


Figure 14. Frequency values on the upper floor (0.6 ... 5 Hz)

**Conclusion 3:** The recorded velocity values, at the level of the four floors, are below the lower limit of 12 mm/s and from the point of view of human comfort it is not taken into account, the area of the industrial complex being quite far from the inhabited area.

## CONCLUSIONS

The normative provisions quite generally specify some admissible limits for vibrations produced in industrial activities. However, the level of vibrations recorded, the nature of the possible vibration source and the specificity of measured vibrations (correlated with the study

of Fourier spectra), their secondary effects, with a great variability of the combinations between them, and the impossibility of establishing a general cause and effect relationship applicable, etc. have not been the subject of advanced long-term studies. This paper seeks to clarify some theoretical and practical aspects that improve the level of understanding and the degree of involvement in taking measures to mitigate the effects on adjacent buildings and neighboring people. Excessive vibrations generally create discomfort (sometimes with health damage) rather than effects on structural safety, and tolerance to these vibrations decreases as exposure time increases.

In the first presented case study, the comfort limits were not exceeded, but at a careful analysis it can be determined to what extent the applied criteria could be overcome as a result of the industrial activities carried out.

## ACKNOWLEDGEMENTS

This paper is based on results obtained in Programme: “Research for the development of an instrumental detection system for structural damage caused by seismic or non-seismic sources PN 18-35 01 01”.

## REFERENCES

- C 125 (2013). Acoustics code in constructions and urban areas (Part IV and Chapter 4.2).
- DIN 4150-3 (1999). Vibration in buildings - Effects of vibrations on structures.
- STAS 12025/2-94. Acoustics in constructions- Effects of vibrations on buildings or on building parts.
- Dobre, D. (2012). The soil-structure interaction in the seismic conditions of Vrancea, Romania, Proceedings 15<sup>th</sup> World Civil Earthquake Engineering in Lisbon, Portugal.
- Dragomir, C. S. (2011). *Raspunsul seismic al cladirilor civile iregulare*. Ed. Noua.

## AN ENERGY EFFICIENCY PROJECT FOR A BROILERS FARM

Georgi KOMITOV<sup>1</sup>, Violeta RASHEVA<sup>2</sup>, Georgi VALTCHEV<sup>2</sup>

<sup>1</sup>Agricultural University of Plovdiv, 12 Mendeleev Blvd, Plovdiv, Bulgaria

<sup>2</sup>University of Food Technology of Plovdiv, 26 Maritza Avenue, Plovdiv, Bulgaria

Corresponding author email: gkomitov@abv.bg

### Abstract

*Improving energy efficiency and reducing greenhouse gases is a central issue of the Europe energy strategy. The challenge of significant reduction in energy consumption is high. It can only be achieved if we all work together and share good experiences and practices. Recently in the livestock sector is highly relevant topic of the requirements for the breeding conditions of farm animals. These conditions are necessary for industrial methods of production and for poultry farming. They define health, ensure productivity and preserve the reproductive performance of farmed animals. The accumulation of products obtained in the process of birds breeding (heat, moisture, waste gases, etc.) in the premises may have a negative impact on the health of the birds. Correct determination of these products will result in the exact sizing of the ventilation and heating installations of poultry farms. This article identifies the incoming and outgoing heat flows from a broiler farm and proposes a methodology for determining the amount of energy required for heating the farm by providing the necessary zoo technical parameters for broilers breeding. The methodology has been developed on the basis of European and national regulations in the field of energy efficiency and in the field of veterinary medical requirements for livestock premises. The proposed methodology could be used for designing of heating and ventilation installations of poultry farms operating under different conditions.*

**Key words:** agrarian buildings, microclimate, energy balance, energy consumption, poultry farming.

### INTRODUCTION

Europe's energy policy is part of the EU's overall economic policy. Three are the reference points of the energy policy: limiting climate change, encourage-vane for creating growth and jobs and limiting the EU's dependence on imports of natural gas and petroleum products.

European policy is aimed at ensuring the security of energy supplies and the introduction of an integrated approach to energy efficiency. Energy saving is the most direct and economically effective way to address these energy challenges (Rasheva V., 2011; <http://www.seea.government.bg/>).

That's why EU countries have agreed on a new 2030 Framework for climate and energy, including EU-wide targets and policy objectives for the period between 2020 and 2030. These targets aim to help the EU achieve a more competitive secure and sustainable energy system and to meet its long-term 2050 greenhouse gas reductions target.

The strategy sends a strong signal to the market, encouraging private investment in new low-carbon technologies and plants

(<https://ec.europa.eu/energy/en/topics/energy-strategy-and-energy-union/2030-energy-strategy>).

That's why the Bulgarian national policy follows the priorities of European policy on sustainable energy development (Law of energetics, 2018; Law on energy efficiency, 2016; Regulation № E- RD-04-05, 2016; Regulation № E-RD-04-1, 2016; Regulation № E-RD-04-2, 2016; Regulation № RD-16-932, 2009). The main activities to improve energy efficiency are aimed at reducing the cost of production, transmission and distribution of energy, as well as in its final consumption.

Extensively current in the livestock sphere is recently the subject of the requirements for the conditions for rearing livestock. The agrarian buildings are one of the most important elements of modern technology used in agriculture. By properly designing of them largely depend on energy expenditure, the creation of suitable zoohygiene conditions for the cultivation of animals and their health and productivity, as well as the final economic results of production (Dinev D., 1999).

Managing the production environment is achieved by creating a good microclimate for

the animals. It is necessary that the premises and conditions in them meet the physiological requirements of the animals kept (Hristev Hg., 2008).

A microclimate means the sum of the physical, chemical and biological properties of the air environment in a given room. The microclimate is determined by external climatic conditions, bird breeding technology, the type, shape and construction of the buildings. The factors of climate are: temperature, humidity, gas composition, movement of air masses, lighting, etc. (Spasov M., 1975).

The heating balance of the poultry farm is necessary to maintain these vital requirements. It is also in the design of the heating installation to take account of the specific conditions in keeping the birds in such a way as to meet the volume of production.

**The purpose of this paper** is to determine the proper amount of heat for heating the farm for industrial rearing of broiler chickens on the basis of normative documents in the field of energy efficiency.

## MATERIALS AND METHODS

The heat balance of the poultry farm (Figure 1) includes all the heat inflows and heat losses of the poultry farm.

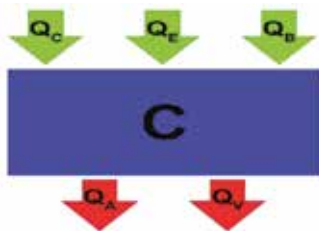


Figure 1. Heat exchange model of poultry farm:  
C - premises of poultry farm;  $Q_C$  - heat released from the poultry;  $Q_E$  - heat delivered by electric power;  $Q_B$  - heat released from the poultry bed;  $Q_A$  - thermal losses from heat transfer;  $Q_V$  - heat losses from ventilation

The object of research is a modern building for industrial broilers grow thing.

In the EU and in our country act the veterinary medicine requirements and requirements to animal buildings and requirements for the protection and humanitarian regards by growthing of farm animals, that provide optimal values and tolerances of the parameters

of temperature-humidity regime and air quality in agricultural holdings (Regulation № 26, 2008; Regulation № 44, 2006). According to these requirements, the minimum bird density in the room should not exceed 33 kg/m<sup>2</sup>. The intensity of the light in the rooms shall be at least 20 lux, measured at the bird's eye level, with at least 80% of the area illuminated. The concentration of ammonia (NH<sub>3</sub>) should not exceed 20 ppm and the concentration of carbon dioxide (CO<sub>2</sub>) should not exceed 3000 ppm measured at bird level.

The internal room temperature should not exceed the outside temperature by more than 3°C when the outside shade temperature is above 30°C. When measured for 48 hours, the average relative humidity in the room shall not exceed 70% when the outside temperature is below 10°C.

In other publications (Broileri, 2009; Dinkova V., 2013) are presented more specific data on the microclimate in the premises broiler management skills: in room should be supported with temperature-30-32°C in the first 3 days. At the end of the first week the temperature at the level of the chickens should be with 30°C. In the after next week, it decrease by 2°C to 20°C, and is kept at the end of cultivation in the range of 18°C to 20°C. The relative air humidity is optimal in the range 60-70%. Ventilation must maintain an air velocity of 0.2 to 0.3 m/s.

The starting point for determining the heat flows imported or taken from the bird breeding building is the technical reference. It includes the following basic parameters:

1. Heated building - a poultry farm for 10 000 broilers. From them, 1000 broilers are with mass 0.2 kg, 4000 are with mass 1 kg, 3000 are with mass 2 kg and 2000 are with mass 3 kg. The rearing of birds is floor with separate broilers by mass;
2. The building is on the one floor with a total built up area of 564 m<sup>2</sup> and a heated area of 564 m<sup>2</sup>;
3. The dimensions of the building are: height 2.7 m, width 12 m and length 47 m;
4. The built-up volume of the building is equal to the heated volume and is equal to 1522.8 m<sup>3</sup>;
5. The walls and the roof are made of sandwich panels and the floor is made of reinforced concrete, located on land;

6. The yindows are with double glazed and structural considerations they are height 0.9 m, situated bilaterally along the entire length of the building. The area of windows is 84.6 m<sup>2</sup>;

7. The poultry farm is located in the region of city Plovdiv. The average temperature of the outside air with the longer duration during the heating season is 2°C;

8. Room temperature and air humidity are respectively - 25°C and 70%.

Calculations made based on Regulation № 7, 2004.

## RESULTS AND DISCUSSIONS

Initially, a check is made on the compliance of the area required for broiler breeding (equation 1):

$$A_n = N/a_n = 556 \text{ m}^2 \quad (1)$$

where:

- $a_n$  is number of broilers/m<sup>2</sup>; by hygienic norms  $a_n = 18$ ;
- $N$  - number of broilers in the poultry farm.

In the shown in Figure 1 model of the heat balance in the poultry farm, the heat input is represented by: the heat emitted by the birds  $Q_C$ , heat delivered by electric power  $Q_E$  and heat released from the poultry bed  $Q_B$ .

The separated heat from birds can be obvious and hidden. It is obvious this heat, which is expressed in the increase of the air temperature. Hidden heat is needed to evaporate moisture from birds. In this case, the total released heat from the birds is expressed as a sum of the other two. The heat flow value separated from the birds is derived from equation (2) (Spasov M., 1975):

$$Q_C = \Sigma q_C \cdot N = 77.085 \text{ kW} \quad (2)$$

where:

- $q_C$  is the heat flow separated from one bird depending on its mass (W);
- $N$  - number of birds.

The heat flow separated by one broiler is plotted by (Hristev Hg., 2008) and depends on the bird mass (Table 1).

Heat flow from electric light are taken into account for summer mode only when sunlight

coincides with lighting. Heat flux, separated by the electrical power is only from light in the room for growing broiler chickens. It is the installed power for lighting and is determined by the dependence (equation 3) (Spasov M., 1975):

$$Q_E = nL \cdot N_L = 1.06 \text{ Kw} \quad (3)$$

where:

- $N_L$  the power from - one illuminant (W);
- $n_L$  - the calculated numbers of illuminants.

Table 1. Heat flow separated from broilers  $Q_C$

№	Mass of bird, kg	$q_C$ for one bird, $\times 10^{-4}$ W	Number of birds	$q_C$ for batch birds, kW	Heat separated from birds, kW
1	0,2	8.34	1000	0.83	42.11
2	1	27.8	4000	11.12	
3	2	54.77	3000	16.43	
4	3	68.67	2000	13.73	

For the poultry farm under consideration are selected energy-saving lamps of the brand "OSRAM" with power 20 W and light flow of 1300 lm. The number of illuminants is determined according to equation (4) and the required luminous flux for broiler breeding is related to the luminous flux of a luminaire (equation 5):

$$n_L = S_n/S_L = 52.3 \approx 53 \quad (4)$$

where:

- $S_L$  is light flow of one illuminate (lm);
- $S_n$  - necessary light flow (lm).

The necessary light flow  $S_n$  is evaluated from dependence (equation 5):

$$S_n = F_L \cdot S_C = 68100 \text{ lm} \quad (5)$$

where:

- $F_L$  is the total illuminated area of the luminaires (m<sup>2</sup>). It includes areas of all walls, floor and roof;
- $S_C$  - the necessary illumination for broiler breeding. According to the hygiene requirements for the breeding

of birds the required illumination is  $S_C = 50 \text{ lx}$ .

According to the requirements of the assignment the height of the building is 2.7 m and the windows are on the long side and are 0.9 m high. Then the illuminated area of the illuminates is  $F_L = 1362 \text{ m}^2$  and is presented in Table 2.

As mentioned, birds are growing on bed with straw. Bed due to processes of decay heat is evolved. This heat can be defined in the equation 6 (Spasov M., 1975):

$$Q_B = A_n \cdot Q_B = 0.42 \text{ kW} \quad (6)$$

where:

- $Q_B$  is heat separate from  $1 \text{ m}^2$  bed ( $\text{Wm}^{-2}$ ). According to the data on the straw bed and the selected internal room temperature it is  $0.744 \text{ Wm}^{-2}$  (Hristev Hg., 2008);
- $A_n$  - floor area ( $\text{m}^2$ ). In this case it is  $564 \text{ m}^2$ .

Table 2. Total illuminated area of the poultry farm

No	Name	Dimensions, m	Area, $\text{m}^2$	Total illuminated area, $\text{m}^2$
1	Wall	47x1.8	84.6	1362
2	Wall	12x2.7	32.4	
3	Wall	47x1.8	84.6	
4	Wall	12x2.7	32.4	
5	Floor	47x12	564	
6	Roof	47x12	564	

The sum of the incoming heat flows in the poultry rearing can be given by dependence (equation 7), and the results for the poultry farm under consideration are given in Table 3.

$$Q_I = Q_C + Q_B + Q_E \quad (7)$$

Table 3. Inflow heat power of the poultry farm

No	Heat energy	Quantity, kW	Total heat flow, kW
1	Heat flow separate from birds, $Q_C$	42.11	43.59
2	Heat flow from electric power, $Q_E$	1.06	
3	Heat flow from bed, $Q_B$	0.42	

During the heating period heat losses from heat transfer through the external enclosures of the building  $Q_A$  depend on the thermal properties of these elements.

The outer walls of the building are made of sandwich panels with a thickness of 0.15 m. The area of the outer walls is  $212.40 \text{ m}^2$ , and the area of the windows is  $0.15 \text{ W}(\text{m}^2\text{K})^{-1}$  (Monoroof\_Agro\_Metecno\_Bulgaria\_BG).

The area of the windows is  $84.6 \text{ m}^2$ . The joinery is aluminium with double glazing and interrupted thermal insulation. The coefficient of heat transmission of the windows is  $1.7 \text{ W}(\text{m}^2\text{K})^{-1}$ .

The roof of the building is a warm roof without air space. The ceiling is made of 10 cm thick roof sandwich panels. The area of roof is  $564 \text{ m}^2$ , and its perimeter is 172 m. The coefficient of heat transmission of the roof is  $0.21 \text{ W/m}^2\text{K}$  (Monoroof\_Agro\_Metecno\_Bulgaria\_BG).

The floor slab is reinforced concrete with a thickness of 0.16 m and is located on the ground. The individual layers of the floor slab with their respective parameters are presented in Table 4. The floor area is  $564 \text{ m}^2$  and its perimeter is 172 m. The coefficient of heat transfer from the heated area to the outside air is determined according to Regulation No 7, 2004. The spatial characteristic of floor B' is determined by equation (8):

$$B' = A/(0.5P) = 6.56 \text{ m} \quad (8)$$

where:

- $A$  is floor area ( $\text{m}^2$ );
- $P$  - floor perimeter (m).

The equivalent thickness of the floor  $d_t$  is determined by the equation (9):

$$d_t = w + \lambda \cdot (R_{si} + R_f + R_{se}) = 4.342 \text{ m} \quad (9)$$

where:

- $w$  is the thickness of the overhead part of the vertical wall above the level of the terrain (m);
- $\lambda$  is the coefficient of thermal conductivity of the Earth. Assume that  $\lambda = 2 \text{ W}(\text{m}^2\text{K})^{-1}$ ;
- $R_{si}$  - heat transfer resistance from the inner surface,  $R_{si} = 0.17 \text{ m}^2\text{KW}^{-1}$ ;

- $R_f$  - heat conductivity coefficient of the floor plate (Table 4),  $R_f = \sum(\delta_i/\lambda_i) = 1.881 \text{ m}^2\text{KW}^{-1}$ ;
- $R_{se}$  - thermal resistance of the outer surface,  $R_{se} = 0.04 \text{ m}^2\text{KW}^{-1}$ .

Table 4. Evaluating of floor heat transfer coefficient

Floor layers	Layer thickness, $\delta_i$	Coefficient of thermal conductivity, $\lambda_i$	Layer resistance $R_i$
-	m	$\text{W}(\text{m}^2\text{K})^{-1}$	$\text{m}^2\text{KW}^{-1}$
Straw bed	0.10	0.07	1.429
Concrete slab	0.16	1.63	0.098
Rubble	0.2	1.1	0.182
Thick finger	0.2	1.16	0.172

At  $d_t < B'$  the heat transfer coefficient through floor is evaluating with dependence (equation 10):

$$U = [(2\lambda)/(\pi B' + d_t)] \ln(\pi B'/d_t + 1) = 0.28 \text{ W}(\text{m}^2\text{K})^{-1} \quad (10)$$

The coefficient of heat transfer through heat transfer is determined by the  $H_{tr}$  equation (11):

$$H_{tr} = H_D + H_g + H_U + H_A \quad (11)$$

where:

- $H_D$  is the coefficient of heat transfer by heat transfer through the enclosing elements, bordering the outside air ( $\text{WK}^{-1}$ );
- $H_g$  - coefficient of heat transfer by heat transfer through the Earth in the stationary regime ( $\text{WK}^{-1}$ );
- $H_U$  - coefficient of heat transfer through heat transfer through the elements, bordering on non-heated or non-cooled areas ( $\text{WK}^{-1}$ );
- $H_A$  - coefficient of heat transfer by heat transfer through the elements, bordering clinging buildings ( $\text{WK}^{-1}$ ).

The coefficient of heat transfer by heat transfer through the enclosing structures bordering the outside air,  $H_D$  is given by the formula 12:

$$H_D = \sum_i(U_i \cdot A_i) + \sum_k(l_k \cdot \psi_k) + \sum_j \chi_j \quad (12)$$

where:

- $i, j, k$  are numbers of element, of linear heated bridge and of point heated bridge;
- $U_i$  - coefficient of heat transfer of  $i$ -th enclosing element, bordering the outside air [ $\text{W}(\text{m}^2\text{K})^{-1}$ ];
- $A_i$  - the surface area of the  $i$ -th enclosing element ( $\text{m}^2$ );
- $l_k$  - the length of the  $k$ -th linear thermal bridge (m);
- $\psi_k$  - linear coefficient of  $k$ -th linear thermal bridge [ $\text{W}(\text{mK})^{-1}$ ];
- $\chi_j$  - coefficient of heat transfer in thermal  $j$ -point bridge ( $\text{WK}^{-1}$ ).

The coefficient of heat transfer through heat transfer through the enclosing walls adjacent to the outside air  $H_{D1}$  is determined by equation 13. The impact of thermal bridges has been taken into account when calculating the heat transfer coefficient through the walls. For this reason, the second and third member of the equation are ignored.

$$H_{D1} = U_w A_w = 0.15 * 212.40 = 31.86 \text{ WK}^{-1} \quad (13)$$

The heat transfer coefficient by heat transfer through the windows  $H_{D2}$  is determined according to equation 14.

$$H_{D2} = UA = 1.7 * 84.6 = 143.82 \text{ WK}^{-1} \quad (14)$$

The coefficient of heat transfer by heat transfer through the roof  $H_{D3}$  is calculated by equation (15):

$$H_{D3} = UA = 0.21 * 564 = 118.44 \text{ WK}^{-1} \quad (15)$$

The coefficient of heat transfer through the floor plate is  $H_g$  is calculated by equation (16).

$$H_g = UA = 0.28 * 564 = 157.92 \text{ WK}^{-1} \quad (16)$$

Therefore, the coefficient of heat transfer through heat transfer calculated in (11) is:

$$H_{tr} = H_{D1} + H_{D2} + H_{D3} + H_g = 452.04 \text{ WK}^{-1}$$

Heat transfer heat losses are calculated by  $Q_{tr}$  for the duration of the heating for each area and for each month in a formula 17 and are shown in the Table 5.

$$Q_{tr} = 1/1000 * [(H_{tr} + \Phi_g) * (\theta_{i,H} - \theta_e)] * t \quad (17)$$

where:

- $H_{tr}$  - coefficient of heat transfer in the surrounding area elements when temperature difference 1 K,  $WK^{-1}$ ;
- $\Phi_g$  - heat flow through the Earth at temperature difference 1 K, caused by the thermal inertia of the Earth,  $WK^{-1}$ ;
- $\theta_{i,H}$  - zone temperature in winter mode ( $^{\circ}C$ ). Middle volume temperature of internal air is  $25^{\circ}C$ ;
- $\theta_e$  - the average monthly value of the ambient temperature ( $^{\circ}C$ );
- $t$  - months duration (h).

Heat losses from heat transfer through the building envelope are reduced by heat gains from sunshine through transparent enclosures.

Table 5. Heat losses from heat transfer

Month	Days	$\theta_{i,H}$	$\theta_e$	$\theta_{i,H}-\theta_e$	Htr	Qtr
	numbers	$^{\circ}C$	$^{\circ}C$	K	$WK^{-1}$	kWh
1	31	25	0.2	24.8	452.04	8340.680
2	28	25	1.8	23.2	452.04	7047.484
3	31	25	6.9	18.1	452.04	6087.351
4	6	25	12.4	12.6	452.04	820.181
10	8	25	12.8	12.2	452.04	1058.858
11	30	25	7.4	17.6	452.04	5728.251
12	31	25	1.9	23.1	452.04	7768.940
Total						36851.747

Heat flow  $\Phi_{sol,k}$  of sunshine through the building enclosing element k is given by the equation (18):

$$\Phi_{sol,k} = F_{sh,ob,k} * A_{sol,k} * I_{sol,k} - F_{r,k} * \Phi_{r,k}, W \quad (18)$$

where:

- $F_{sh,ob,k}$  is the shading of the host solar energy from external causes;
- $A_{sol,k}$  - effective area of the host solar energy surface (m);
- $I_{sol,k}$  - middle daily intensity of sunshine on the host surface ( $Wm^{-2}$ );
- $F_{r,k}$  - angular coefficient between element k and heaven, there are values as follows  $F_r=1$  horizontal surface,  $F_r = 0.5$  for no shading vertical surface;
- $\Phi_{r,k}$  - heat flow as a result of the elements k to heaven (W).

The effective receiving surface of a transparent envelope (for example a window)  $A_{sol}$  is determined by the formula (19) and the values obtained are shown in Table 6.

$$A_{sol} = F_{sh,gl} * g_{gl} * (1-F_F) * A_{w,p} \quad (19)$$

where:

- $F_{sh,gl}$  is the shading factor (from moving shadows);
- $g_{gl}$  - the total throughput of the transparent part of the element;
- $F_F$  - the frame factor of the element k (the part occupying the frame);
- $A_{w,p}$  - the total area of element k ( $m^2$ ).

When the sun's rays do not fall perpendicular to the surface, the value of  $g_{gl}$  is determined by formula (20):

$$g_{gl} = F_W * g_{gl,n}, \quad (20)$$

where:

- $F_W$  is the correction factor for no perpendicular radiation.  $F_W = 0.90$ ;
- $g_{gl,n}$  - the actual ratio of total solar energy transmittance at normal radiation, account of Regulation № 7, 2004.

Table 6. Effective host surface of transparent enclosing element

$A_{w,p}$	$1-F_F$	$F_{sh,gl}$	$g_{gl,n}$	$F_W$	$A_{sol}$
84.6	0.85	1	0.75	0.9	48.54

Needed energy for heating for each month of the heating period and for each area of the building is calculated according to equation (21):

$$Q_A = Q_{H,Ht} - \eta_{H,gn} * Q_{H,gn} \quad (21)$$

where:

- $Q_A$  is needed energy for heating zone (kW);
- $Q_{H,Ht}$  - full heat losses of the month (kWh);
- $Q_{H,gn}$  - heat gains in the area for months (are presented in Table 7) (kWh);
- $\eta_{H,gn}$  - dimensionless factor of utilization of heat gains in the area for months.

Table 7. Heat gains in the area

Month	Days, numbers	A <sub>sol,k</sub> m <sup>2</sup>	I <sub>sol,k</sub> kWm <sup>-2</sup>	Coefficient 24/1000	Q <sub>H,gn</sub> kWh
1	31	48.54	63.55	0.024	2295.029
2	28	48.54	75.13	0.024	2450.656
3	31	48.54	83.43	0.024	3012.971
4	6	48.54	90.30	0.024	631.175
10	8	48.54	80.35	0.024	748.836
11	30	48.54	60.75	0.024	2123.140
12	31	48.54	51.50	0.024	1859.859
Total					13121.67

$Q_A = 36851.747 - 0.5 \cdot 13121.67 = 30290.912$  kWh for the year.

It is necessary to turn the energy power through division and of the heated days of the year (they are 165) and for a period of 24-hour security. Thus, heat losses from the poultry farm result in  $Q_A = 2.78$  kW.

In determining the heat losses from ventilation  $Q_V$ , it is necessary to determine the amount of air taken in CO<sub>2</sub> and moisture. After, setting for subsequent calculations into the greater value.

To determine the amount of respiration required depending on the maximum allowable amount of carbon dioxide, a dependence (22) is used:

$$V_{CO_2} = \Sigma CO_2 / (k_{max} - k_a) = 8688.88 \text{ m}^3 \text{h}^{-1} \quad (22)$$

where:

- $\Sigma CO_2$  is quantity CO<sub>2</sub>, accumulated in the premises as a result of metabolic processes in organisms of the birds. The calculated value of CO<sub>2</sub> is 38593 (g.h<sup>-1</sup>),  
 $k_{max}$  - maximum permissible concentration of CO<sub>2</sub> in the room. According to hygienic norms it is 3 lm<sup>-3</sup> (Hristev Hg., 2008);
- $k_a$  - CO<sub>2</sub> content in the ambient air. It is constant and equal to 0.3 lm<sup>-3</sup>.

The value of the carbon dioxide of the birds is determined by the subject (2), provided that the  $q_C$  is replaced by the concentration of CO<sub>2</sub>, separated from a bird  $k_{CO_2}$ . The value varies between: for 0.2 kg - 2.7 l.h<sup>-1</sup>; for 1 kg - 1.31 l.h<sup>-1</sup>; for 2 kg - 2.74 l.h<sup>-1</sup>; for 3 kg - 3.65 l.h<sup>-1</sup> (Hristev Hg., 2008).

Determination of the necessary quantity of air in order to maintain a certain relative humidity

shall be carried out in the relation (23) (Spasov M., 1975):

$$V_W = W / (d_i - d_0) = 3665.89 \text{ m}^3 \text{h} \quad (23)$$

where:

- W is separated moisture from the birds. The computed value of the moisture, separated from broiler chickens is 47400 g.h<sup>-1</sup>;
- $d_i$  - moisture content of the air in the room at a temperature of 25°C and a relative humidity of 70% ( $d_i = 9.55 \text{ g. m}^{-3}$ ) (Kimenov G., 1995);
- $d_a$  - the moisture content of the ambient air at a temperature of 20°C and a relative humidity of 85% ( $d_a = 4.74 \text{ g. m}^{-3}$ ) (Kimenov G., 1995).

The separated moisture in the rearing of broiler chickens is determined in dependence (2), as in the formula instead of using the  $q_C$  separated moisture from a broiler  $w_C$ . The value varies between 0.2 kg - 1.1 g.h<sup>-1</sup>, for 1 kg - 3.2 g.h<sup>-1</sup>, for 2 kg - 6.1 g.h<sup>-1</sup> and for 3 kg - 7.6 g.h<sup>-1</sup> (Hristev Hg., 2008).

Of dependencies (22) and (23) shows that the air quantity depending on the maximum level of carbon dioxide ( $V_{CO_2}$ ) is greater than the air required for the maintenance of a specific relative humidity ( $V_W$ ). As mentioned in the calculations, the higher value is taken and the required amount of heat for ventilation is determined by the dependence (24) (Spasov M., 1975):

$$Q_V = V_{CO_2} * C_P * (\theta_{i,H} - \theta_e) = 84.13 \text{ kW} \quad (24)$$

where:

- $C_P$  is the specific heat capacity of the air and is 1 kJ (kg.K)<sup>-1</sup> (Kimenov G., 1995).

The heat losses from the farm can be expressed with formula (25). Heat flow consumed to overcome the losses of heat transfer and ventilation is:

$$Q_{EX} = Q_A + Q_V = 86.91 \text{ kW} \quad (25)$$

According to the heat balance (Figure 1) its necessary energy for heating on the farm can be expressed by the subject (26):

$$Q = Q_{EX} - Q_I = 86.91 - 43.59 = 43.32 \text{ kW} \quad (26)$$

## CONCLUSIONS

It is developed a methodology to determine the necessary quantity of thermal energy for heating poultry farm, in providing the necessary zootechnical parameters for growing birds.

The calculations are made on the basis of European and national normative documents in the field of energy efficiency, so that power consumption and consequently CO<sub>2</sub> emissions allocated to be minimized.

The methodology may be used in the design of poultry farms with parameters other than those specified in the publication.

## REFERENCES

- Broileri (2009). Rakovodstvo, Ross. <http://pt.aviagen.com/assets/Uploads/Ross-Broiler-Manual-bg.pdf>.
- Dinev, D., Delchev, N. (1999). Tehnologhno projektirane na agrarni sgradi. Universe, Stara Zagora.
- Dinkova, V. (2013). Ventilation, cooling and heating of ANIMAL farms, Agro biotechnika, year I, broi 3. <http://agrobio.elmedia.net/bg/2013-3/editorials/>
- Hristev, Hg. (2008). Rakovodstvo za uprazhnenia po zoothigiena. AU-Plovdiv. <https://ec.europa.eu/energy/en/topics/energy-strategy-and-energy-union/2030-energy-strategy> <http://www.seea.government.bg/>
- Kimenov, G. (1995). Termodinamichni I toplofizichni svoistva na veshtestvata. Spravochnik, Tehnika, Sofia.
- Spasov, M., Grozev, G. (1975). Ventilatsia I otopenie v zhivotnovadni fermi. Zemizdat, Sofia.
- Law of energetics, 2018. <https://www.me.government.bg/bg/library/zakon-za-energetikata-256-c25-m258-1.html>.
- Law on energy efficiency (2016). [http://www.seea.government.bg/documents/ZEE\\_30.12.2016.pdf](http://www.seea.government.bg/documents/ZEE_30.12.2016.pdf).
- Monorooft\_Agro\_Metecno\_Bulgaria\_BG. <https://metecno.bg/index.php/bg/products-and-services/pur-roof-panels/monorooft-agro>.
- Rasheva, V. (2011). *Energy technological analyses of industrial systems*. Academic Publishing House of UFT, Plovdiv (in Bulgarian).
- Regulation № E-RD-04-1 of 22.01.2016 on energy efficiency audits, certification and assessment of energy savings of buildings.
- Regulation № E-RD-04-2 from 22.01.2016 on the indicators for energy consumption and energy performance of buildings.
- Regulation № E-RD-04-05 of September 8, 2016 for the determination of energy consumption indicators, energy performance of enterprises, industrial systems and external lighting systems, as well as for setting the terms and conditions for conducting energy efficiency audits and preparation of energy savings assessment.
- Regulation № RD-16-932 of 23 October 2009 on terms and conditions for carrying out the verification of energy efficiency for hot water boilers and air conditioning installations under article 27, al. 1 and article 28, al.1 of the law on energy efficiency and for establishing, maintenance and use of the basis data about them.
- Regulation № 7 of 2004 on Energy Efficiency of Buildings.
- Regulation № 26 of 05.08.2008 laying down minimum welfare and protection requirements for broiler breeding. Ministry of Agriculture and Food.
- Regulation № 44 of 20 April 2006 for veterinary medical requirements for animal sites.

## NOVEL MBBR SYSTEMS BIOFILM CARRIERS AND PHYSICAL-CHEMICAL ANALYSIS

Ovidiu IORDACHE<sup>1</sup>, Ioana Corina MOGA<sup>2</sup>, Cornelia MITRAN<sup>1,3</sup>, Dana CIUTARU<sup>1</sup>,  
Irina SANDULACHE<sup>1</sup>, Lucia SECAREANU<sup>1</sup>, Gabriel PETRESCU<sup>2</sup>, Elena PERDUM<sup>1</sup>

<sup>1</sup>National R&D Institute for Textile and Leather (INCDTP), 16 Lucretiu Patrascanu Street,  
District 3, Bucharest, Romania

<sup>2</sup>DFR Systems L.L.C., 46 Drumul Taberei Street, District 6, Bucharest

<sup>3</sup>Politehnica University of Bucharest, 313 Splaiul Independentei, District 6, Bucharest

Corresponding author email: iordachevidiu.g@gmail.com

### Abstract

*Moving Bed Biofilm Reactors systems (MBBRs) have lately emerged as highly effective tools for treatment of wastewaters originating from various industrial sectors. System performance within the MBBRs is highly dependent on the carriers used, regarding efficiency in wastewater treatment (BOD/COD removal, heavy metal content reduction, nitrification and denitrification processes, various recalcitrant compounds removal etc.). Novel carrier structures have been obtained (patents pending), based on a mix of polyethylene with inorganic and organic compounds. Morphology analyses were carried out by Scanning Electron Microscopy, for assessment of internal surface structure, which will serve as an immobilization substrate for future bio-functionalization experiments. Chromatographic profile was assessed by Headspace Gas Chromatography, in order to identify Volatile Organic Compounds from the developed structures. The carried out analyses will serve as a starting point for future augmentation of the carriers with microbial strains.*

**Key words:** MBBRs, reactors, wastewater treatment.

### INTRODUCTION

Moving Bed Biofilm Reactors systems (MBBRs) technology utilizes free-moving biofilm carriers, which represents a future evolution of the activated sludge process that allows a greater pollutant removal degree in smaller systems (i.e., bioreactors) (Puigagut et al., 2007). The biofilm grows protected within small plastic carriers, which are carefully designed with high internal surface area. These biofilm carriers are suspended and mixed throughout the water phase. The wastewater treatment with bio-media consists in adding biofilm carriers (small cylindrical shaped polyethylene carrier elements with specific density) in aerated or anaerobic basins to support biofilm growth (Chao et al., 2015). MBBR technology is widely involved in advanced wastewater treatment solutions for the industrial and municipal markets. This solution is used for the removal of organic substances, nitrification and denitrification, BOD and COD reduction etc., in highly polluted effluents (Pulicharla et al., 2017). The

wastewater treatment based on MBBR systems allows a self-regulating biofilm formation inside the polymeric structures, which is stable in extreme parameters conditions (treated water organic load), it is an easy to run process, without need of sludge backflow, in order to achieve a good treatment efficiency (Jing et al., 2009; Moga et al., 2011). Microbial biofilms have the advantages of allowing environmental changes and presence of toxic chemicals inside the treatment tank (through several cellular bioaccumulation and biosorption mechanisms of pollutants) (Babel et al., 2003; Miriazimi et al., 2015; Kratochvil & Volesky, 1998).

Key parameters that define efficient carriers inside an MBBR system take into account performance, stability in time, 3D structure, wear resistance, composition etc.

In this paper, a new generation of carriers has been tested, which consists of a mix of polyethylene with inorganic and organic compounds (patent pending). Physical-chemical analyses were carried out on the new generation of carriers: Scanning Electron Microscopy (SEM) for assessment of surface

morphology; GC-Headspace analysis, for study of volatile compounds from the samples.

## MATERIALS AND METHODS

### HDPE carriers and SEM analysis

Four new HDPE based carriers were subjected to morphological analysis. The newly developed carriers are based on a mix consisting of HDPE and inorganic and organic compounds, in various ratios. Sample notations are as follows: 1F, 2F, 3F and 4F.

SEM analysis was performed on a Quanta 200, Fei (Netherlands) electron microscope, GSED detector, Low Vacuum mode, spot beam size of 4.0, 20 kV filament voltage, with image acquisition at 27.2 seconds. Samples were visualized without metallic coating, on both the surface of the structures, and the interior (internal spacers). Sample acquisition was carried out at magnification levels of 5000x and 1000x.

### GC-Headspace analysis

GC analysis was carried out on an Agilent Technologies 6890N GC with 7694E Headspace (Agilent Technologies) and 5973N MS detector. Samples were cut in small pieces, weighted to approximately same mass (1F = 0.9460 g; 2F = 0.9720 g; 3F = 0.9280 g; 4F = 9850 g), and placed in Headspace vials.

Headspace parameters were set as follows: vial temperature: 140°C; Loop temperature: 135°C; Transfer line temperature: 130°C; Stirring: Stop; Balance equilibration time: 120 min; Pressurization time: 2 min; Loop filling time: 3 min; Loop Balancing Time: 2 min. Following GC method was used: Capillary column: DB-35MS (J&W)®, length: 35 m, inner diameter 0.25 mm; Layer thickness: 0.25 µm; Injection system: splitless; Injector temperature: 300°C; Constant flow: 1.2 ml/min; Carrier gas: Helium; Temperature schedule: 50°C (1 min) at 290°C with 10°C/min, 290°C (10 min); Injection volume: 2.0 µl; Auxiliary: 300°C; MS detector: scan mode.; Scanning range: 50-450 amu.

## RESULTS AND DISCUSSIONS

SEM analysis was used as a pre-screening tool in order to assess the surface morphology of the

newly developed samples. The carriers will be further used, in future experiments, for bio-augmentation with various microbial strains, and knowledge about the surface morphology can prove useful, when selecting the strain (based on enzymatic activity and battery of specific enzymes). SEM images are showcased in Figures 1 to 4, for the four samples (1F, 2F, 3F and 4F), for the external and internal surface (500x and 1000x).

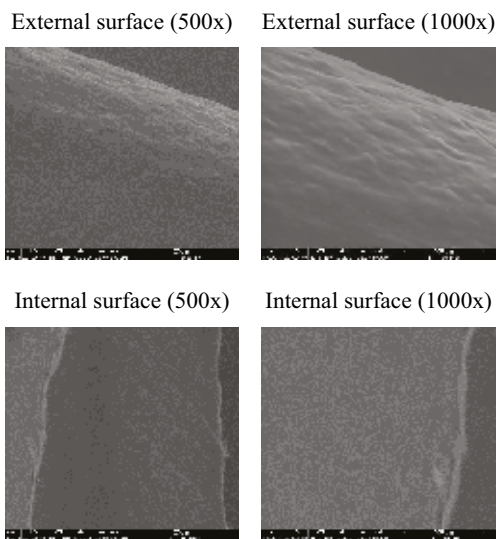


Figure 1. SEM analysis for 1F carrier

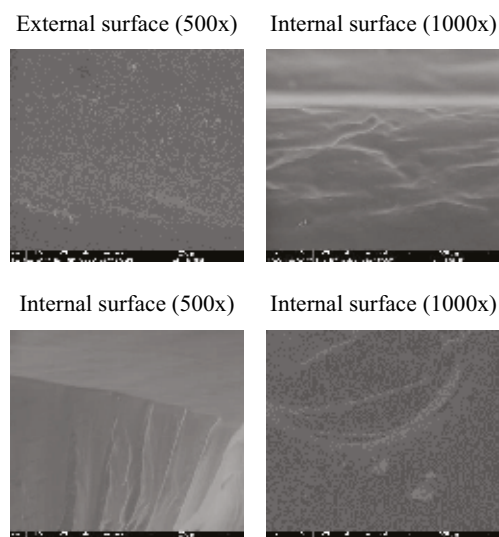


Figure 2. SEM analysis for 2F carrier

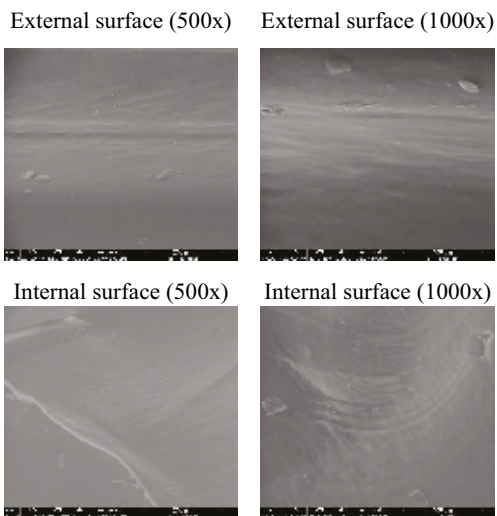


Figure 3. SEM analysis for 3F carrier

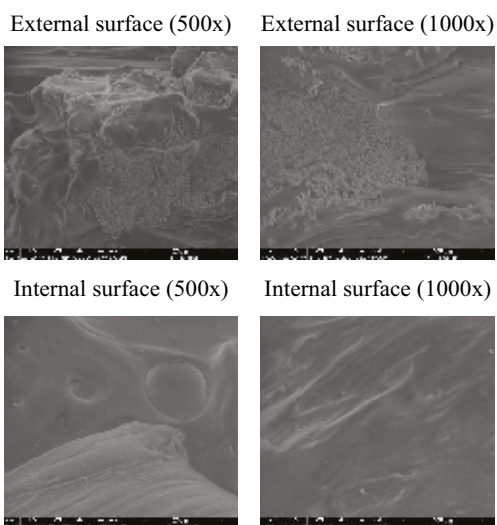


Figure 4. SEM analysis for 4F carrier

SEM analysis revealed different surface morphologies of the carriers, from sample to sample.

Therefore, it can be observed that surface rugosity increases from sample 1F to sample 4F, with sample 4F having the most rugose surface, while sample 1F has a plain-smooth looking surface.

Gas Chromatography analysis was carried out on each sample (Figures 5 to 8), in order to assess the main volatile compounds present in each sample. This can contribute to building a

knowledge base that could prove useful to better understand the behaviour of the newly developed carriers in various conditions.

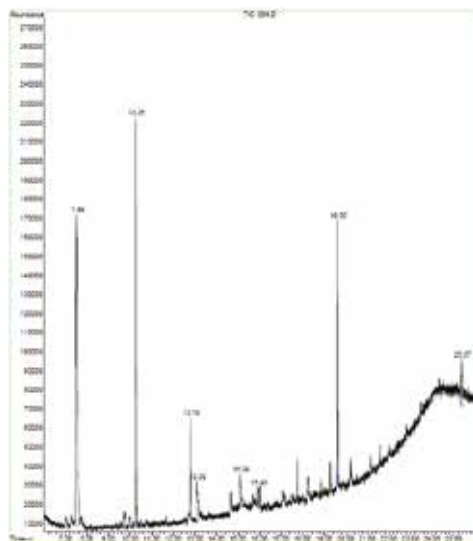


Figure 5. GC chromatogram for 1F carrier

Following compounds were assessed in 1F sample: 1-Decene; 1-Tetradecanol; Tetradecyl trichloro acetate; 2,6-Di-tert-butylphenol; Benzyl oleate; 2-tert-Butyl-4-(2-phenylpropan-2-yl) phenol; Ethyl stearate; p-Xylenolphthalein (Table 1).

Table 1. Sample 1F compounds

Rt.	CAS	Name	Area
7.488	112-41-4	1-Decene	715334
10.254	112-72-1	1-Tetradecanol	397588
12.788	74339-52-9	Tetradecyl trichloro acetate	86066
13.085	5875-45-6	2,6-Di-tert-butylphenol	971170
15.094	55130-16-0	benzyl oleate	56278
15.926	56187-92-9	2-tert-Butyl-4-(2-phenylpropan-2-yl) phenol	44334
19.617	111-61-5	Ethyl stearate	216783
25.372	50984-88-8	p-Xylenolphthalein	69848

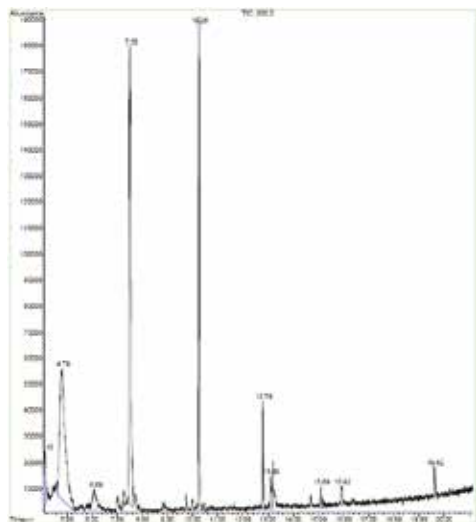


Figure 6. GC chromatogram for 2F carrier

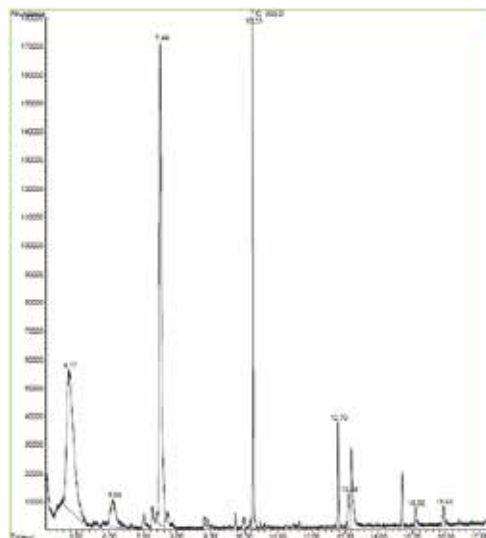


Figure 7. GC chromatogram for 3F carrier

Following compounds were assessed in 2F sample: 4,4'-Dichlorodiphenyl sulfone (DCDPS); 1-Decene; 2-Butyloctanol; 1-Tetradecanol; 1-Hexadecene; 2,6-Di-tert-butylphenol; 7-(Z)-Hexadecane; 2-tert-Butyl-4-(2-phenylpropan-2-yl) phenol; Ethyl stearate (Table 2).

Table 2. Sample 2F compounds

Rt.	CAS	Name	Area
4.118	80-07-9	4,4'-Dichlorodiphenyl sulfone (DCDPS)	96275
4.787	872-05-9	1-Decene	781144
6.089	3913-02-8	2-Butyloctanol	77097
7.497	112-41-4	1-Decene	763939
10.254	112-72-1	1-Tetradecanol	352165
12.788	629-73-2	1-Hexadecene	65223
13.085	5875-45-6	2,6-Di-tert-butylphenol	54442
15.089	35507-09-6	7-(Z)-HEXADECANE	31672
15.917	56187-92-9	2-tert-Butyl-4-(2-phenylpropan-2-yl) phenol	23068
19.622	111-61-5	Ethyl stearate	23643

Following compounds were assessed in 3F sample: 1-Decene; 2-Butyloctanol; 1-Tetradecanol; 1-Hexadecene; 2,6-Di-tert-butylphenol; Eicosane; 1,5-Diphenyl-1H-1,2,4-triazole-3(2H)-thione (Table 3).

Table 3. Sample 3F compounds

Rt.	CAS	Name	Area
4.769	872-05-9	1-Decene	717238
6.089	3913-02-8	2-Butyloctanol	112187
7.493	112-41-4	1-Decene	731741
10.254	112-72-1	1-Tetradecanol	333366
12.788	629-73-2	1-Hexadecene	60157
13.090	5875-45-6	2,6-Di-tert-butylphenol	49967
15.094	74685-33-9	Eicosane	23186
15.926	5055-74-3	1,5-Diphenyl-1H-1,2,4-triazole-3(2H)-thione	21285

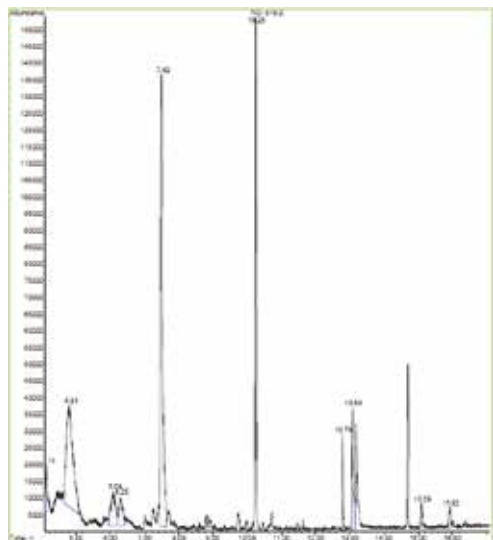


Figure 8. GC chromatogram for 4F carrier

Following compounds were assessed in 4F sample: 4,4'-Dichlorodiphenyl sulfone (DCDPS); 1-Decene; 2-Butyloctanol; 5-methyl furfural; 1-Tetradecene; 1-Hexadecene; 2,6-Di-tert-butylphenol; Eicosane; 1,5-Diphenyl-1H-1,2,4-triazole-3(2H)-thione (Table 4).

Table 4. Sample 4F compounds

Rt.	CAS	Name	Area
4.131	80-07-9	4,4'-Dichlorodiphenyl sulfone (DCDPS)	45225
4.806	872-05-9	1-Decene	405661
6.089	3913-02-8	2-Butyloctanol	96121
6.284	620-02-0	5-methyl furfural	63686
7.488	112-41-4	1-Decene	603158
10.249	1120-36-1	1-Tetradecene	275861
12.788	629-73-2	1-Hexadecene	49887
13.076	5875-45-6	2,6-Di-tert-butylphenol	118058
15.094	74685-33-9	Eicosane	18905
15.921	5055-74-3	1,5-Diphenyl-1H-1,2,4-triazole-3(2H)-thione	19402

Overlapped chromatograms of samples 1F, 2F, 3F and 4F are showcased in Figure 9.

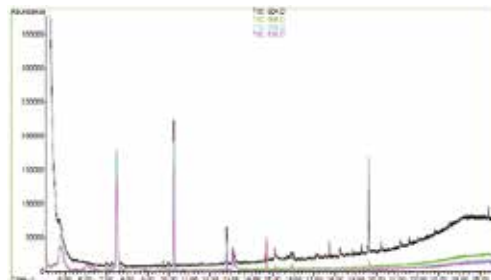


Figure 9. Overlapped chromatograms (sample 1F=804.D; sample 2F=806.D; sample 3F=808.D; sample 4F=810.D)

Polyethylene, whether high density (HDPE) or low density (LDPE) is essentially a very long hydrocarbon molecule. Pyrolysis of PE produces shorter hydrocarbons, mostly normal alkanes, alkenes and dienes, which may be analysed by gas chromatography.

4,4'-Dichlorodiphenyl sulfone (DCDPS) is an organic compound with the formula  $(C_6H_4)_2SO_2$ . Classified as a sulfone (Sime et Abrahams, 1960), this white solid is most commonly used as a precursor to polymers that are rigid and temperature-resistant such as PES or Udel™.

Besides many uses of 1-decene, it can be used in the manufacture of C11 plasticizer alcohols. 1-Decene and Eicosane was also found in samples of Polyethylene (Hermabessiere et al., 2018) and High-Density Polyethylene (Sarker et al., 2011).

Previous studies (Kato, 1967) showed that volatile compounds were produced through the radicals formed by the scission of glycosidic linkages of cellulose and oxidized cellulose. Chromatographic method for the identification of cellulose degradation compounds highlighted presence of acetaldehyde, furan, propionaldehyde, acrolein, acetone, diacetyl, furfural and 5-methyl furfural.

Other compounds that were analysed in the fur samples: 1-Tetradecene, is often found as a semi-volatile emission compound, in agricultural plastics (Linak et al., 1989); 2,6-Di-tert-butylphenol is an alkylated phenol, its derivatives being used industrially as stabilizers for hydrocarbon-based products (plastics

included) (Fiege et al., 2002); 7-(Z)-Hexadecane and 7-(Z)-Hexadecene compounds have been often found in various resin films structures (Niimura and Miyakoshi, 2003); 2-tert-Butyl-4-(2-phenylpropan-2-yl)phenol is a compound with wide usage as an additive for plastics.

## CONCLUSIONS

Within the current paper, four newly developed carriers based on a mix of HDPE and inorganic and organic compounds where morphologically characterized along with the assessment of their chromatographic profiles. Scanning Electron Microscopy allowed assessment of specific surface morphology which will prove useful in future experiments, in order to see modifications of the surfaces, after bioaugmentation of microbial strains (due to enzymatic activity). Chromatography analyses allowed identification of volatile compounds originating from the newly developed carriers, based on a mix of HDPE with organic and inorganic compounds. This allowed building up of knowledge base regarding carriers used in MBBR system for industrial wastewaters treatment.

## ACKNOWLEDGEMENTS

This work was supported by a grant of the Romanian National Authority for Scientific Research and Innovation, CCCDI – UEFISCDI, project number COFUND-MANUNET III-FUNCELL, within PNCDI III. Publication is funded by the Ministry of Research and Innovation within Program 1 - Development of the national RD system, Subprogram 1.2 - Institutional Performance - RDI excellence funding projects, Contract no. 6PFE/ 16.10.2018.

## REFERENCES

Babel, S., Kurniawan, T. A. (2003). Low-cost adsorbents for heavy metals uptake from contaminated water: a review. *J. Hazard. Mat.*, 97, 219–243.  
Chao, Li, Zhen, Zhang, Yi, Li, Jiashun, Cao (2015). Study on dyeing wastewater treatment at high temperature by MBBR and the thermotolerant mechanism based on its microbial analysis. *Process Biochemistry*, 50(11), November 2015, 1934–1941.

Fiege Helmut, Heinz-Werner Voges, Toshikazu Hamamoto, Sumio Umemura, Tadao Iwata, Hisaya Miki, Yasuhiro Fujita, Hans-Josef Buysch, Dorothea Garbe, Wilfried Paulus (2002). Phenol Derivatives. In *Ullmann's Encyclopedia of Industrial Chemistry*. Wiley-VCH, Weinheim.  
Hermabessiere, L., Himber, C., Boricaud, B., Kazourb, M., Amara, R., Cassone, A. L., Laurentie, M., Paulpont, I., Soudant, P., Dehaut, A., Duflos, G. (2018). Optimization, performance and application of a Pyrolysis-GC/MS method for the identification of microplastics, *Analytical and Bioanalytical Chemistry*.  
Jing, J. Y., Feng, J., Li, W. Y. (2009). Carrier effects on oxygen mass transfer behavior in a moving bed biofilm reactor. *Asia-Pacific Journal of Chemical Engineering*, 4, 618–623.  
Katō, Kunio (1967). Pyrolysis of Cellulose. *Agricultural and Biological Chemistry*, 31(6), 657–663.  
Kratochvil, D., Volesky, B. (1998). Advances in the biosorption of heavy metals. *Trends in Biotechnol.*, 16, 291–300.  
Linak, W. P., Ryan, J. V., Perry, E., Williams, R. W., DeMarini, D. M. (1989). Chemical and biological characterization of products of incomplete combustion from the simulated field burning of agricultural plastic. *JAPCA*, 1989 Jun, 39(6), 836–46.  
Mirazimi, S. M. J., Abbasalipour, Z., Rashchi, F. (2015). Vanadium removal from LD converter slag using bacteria and fungi. *Journal of Environmental Management*, Volume 153, 15 April 2015, 144–151.  
Moga, I. C., Năsăribă-Grecescu, B., Robescu, D. (2011). Oxydation of Biodegradable Compounds inside a MBBR Reactor. Proceedings of 5th International Conference on Energy and Environment - CIEM, Bucharest.  
Niimura, Noriyasu, Miyakoshi, Tetsuo (2003). Characterization of Natural Resin Films and Identification of Ancient Coating. *J. Mass Spectrom. Soc. Jpn.*, 51(4), 439.  
Puigagut, J., Villaseñor, J., Salas, J. J., Bécares, E., García, J. (2007). Subsurface-flow constructed wetlands in Spain for the sanitation of small communities: a comparative study. *Ecol. Eng.*, 30, 312–319.  
Rama Pulicharla, Satinder Kaur Brar, Tarek Rouissi, Serge Auger, Patrick Drogui, Mausam Verma, Rao Y. Surampalli (2017). Degradation of chlortetracycline in wastewater sludge by ultrasonication, Fenton oxidation, and ferro-sonication. *Ultrasonics Sonochemistry*, 34, January 2017, 332–342.  
Sarker Moinuddin, Mohammad Mamunor Rashid, and Mohammed Molla (2011). Abundant High-Density Polyethylene (HDPE-2) Turns into Fuel by Using of HZSM-5 Catalyst. *Journal of Fundamentals of Renewable Energy and Applications*, 1.  
Sime, J. G., Abrahams, S. C. (1960). The crystal and molecular structure of 4,4'-dichlorodiphenyl sulphone. *Acta Crystallographica*, 13.

## BIO-AUGMENTATION OF POLYETHYLENE BIOFILM CARRIERS BY *Cerioporus squamosus* WHITE ROT FUNGI

Ovidiu IORDACHE<sup>1</sup>, Ioana Corina MOGA<sup>2</sup>, Cornelia MITRAN<sup>1,3</sup>, Dana CIUTARU<sup>1</sup>,  
Irina SANDULACHE<sup>1</sup>, Lucia SECAREANU<sup>1</sup>, Gabriel PETRESCU<sup>2</sup>, Elena PERDUM<sup>1</sup>

<sup>1</sup>National R&D Institute for Textile and Leather (INCDTP), 16 Lucretiu Patrascanu Street,  
District 3, Bucharest, Romania

<sup>2</sup>DFR Systems L.L.C., 46 Drumul Taberei Street, District 6, Bucharest

<sup>3</sup>Politehnica University of Bucharest, 313 Splaiul Independentei, District 6, Bucharest

Corresponding author email: iordachevidiu.g@gmail.com

### Abstract

*Fungi have been widely used in industrial wastewater treatment, as real alternative to conventional treatment methods. Specific filamentous fungi (FF) have been used for sludge treatment, bioflocculation, SS concentration reduction, degradation and removal of certain toxic compounds etc. Very few research works exploited the use of fungi augmented carriers inside MBBR systems. Present work explored the bio-augmentation experiments of four polyethylene based carriers with strain of Cerioporus squamosus (syn. Polyporus squamosus), a basidiomycete bracket fungus. Bio-augmentation was carried out in various conditions (varying certain process parameters) in order to facilitate growth of strain inside the carriers' structure, which were composed of a mix of polyethylene with inorganic and organic compounds, especially designed in order to allow microbial growth inside the carriers' internal space.*

**Key words:** fungi, MBBR, reactors, wastewater treatment.

### INTRODUCTION

HDPE carriers are the heart of a Moving Bed Biofilm Reactor (MBBR) system for treating of industrial wastewater. This system offers a real efficient alternative to traditional methods of wastewater treatment (with activated sludge) (Kruszelnicka et al., 2018). MBBR processes can be successfully used in industrial application, being characterized by quality improvement in BOD and nitrogen removal, limited footprint of the installation, modularity (for future scaling of the plant), minimization of process complexity in terms of operator input, fast recovery from process upsets. Currently, several compositions carriers are being used in the modern MBBR systems: polypropylene (PP), low-density polyethylene-polypropylene (LDPE-PP), and polyurethane foam-polypropylene (PUF-PP) (Sonwani et al., 2019).

The biological wastewater treatment process consists of a transfer of materials from the water to the living cells and vice versa (Adrados et al., 2014). Pollutants from the wastewater pass to the mass of microorganisms, following interfacial contact

or adsorption-desorption processes. The adsorbed compounds are trained in enzymatic reactions that take place in multiple stages (Wesenberg et al., 2003; Nilsson et al., 2006). Between the enzyme molecules and the nutrient substrate, reactive complexes are formed which in a later stage decompose, releasing the product or reaction products and the regenerated enzyme that can resume the reactions (Zottia et al., 2014).

The present paper explored the bio-augmentation of four newly developed prototypes of carriers (made of a mix of HDPE, organic and inorganic compounds) with *Cerioporus squamosus* strain which was already successfully tested by the team in residual concentration reduction of some pollutants in samples of textile industry originated wastewater (Iordache et al., 2015; Iordache et al., 2016). *Cerioporus squamosus* is a basidiomycete, with a particular importance in natural ecosystems, being able to degrade a wide range of cellulosic substrates. No studies have been highlighted so far with forced bio-augmentation of wastewater treatment carriers with *Cerioporus squamosus* strain. More than that, the study aimed the treatment of the

carriers using two methods: dynamic treatment method and static treatment method.

## MATERIALS AND METHODS

### Carriers bio-augmentation

In the present study, *Cerrioporus squamosus* (of Basidiomycota Phylum) strain was used for bioaugmentation of newly developed HDPE carriers used in MBBR systems for wastewater treatment. The carriers are made of a mix consisting of HDPE and inorganic and organic compounds, in various ratios (patent pending). *Cerrioporus squamosus* is a basidiomycete bracket fungus, belonging to a group of fungi that form fruiting bodies with pores or tubes on the underside. Fresh starter strain was grown in Czapek nutritive broth, for 14 days at 28°C. The bioaugmentation experiments were run by two methods, one in dynamic conditions, and one in static conditions. For dynamic conditions treatment, the HDPE carriers were put in 250 ml Erlenmeyer flasks, counting 20 carriers/flask (Figure 1), and autoclaved for 15' at 121°C.

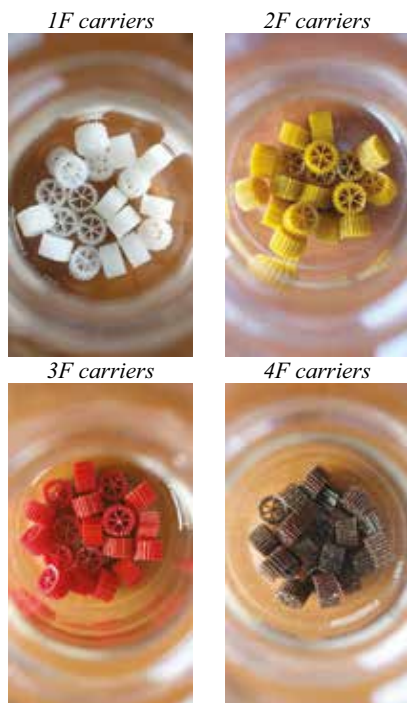


Figure 1. Pre-autoclaving carriers

Furthermore, Czapek nutritive broth was autoclaved at 121°C for 15 minutes, and poured, in sterile conditions, over the carriers, and brought to sign at 200 ml. From starter culture, 1mL was inoculated in each flask (Figure 2).

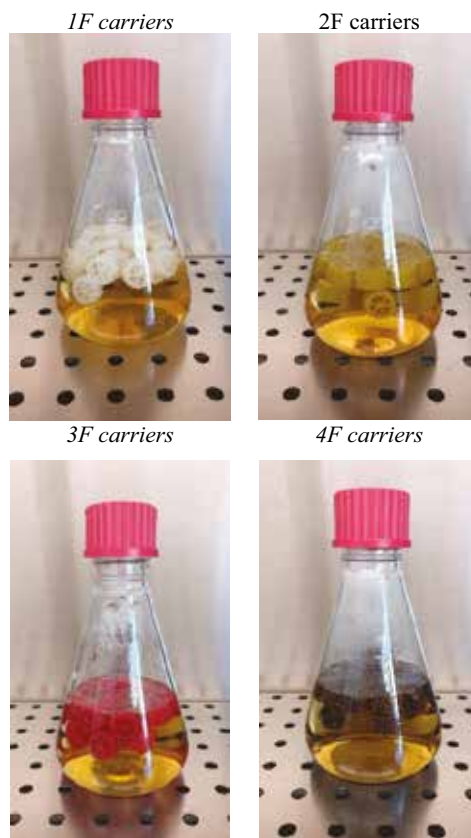


Figure 2. Inoculated flasks containing carriers and Czapek broth

After inoculation, flasks were incubated for 7 days, at 28°C, at 140 rpm, in an SIF6000R incubated shaker, from Medline Scientific.

For bioaugmentation of the carriers in static conditions, six carriers were placed in sterile Petri dishes, over which pre-inoculated Czapek broth was poured in a volume of 20 ml (Figure 3).

The samples were incubated for the same period of time as the samples treated in dynamic conditions, for 7 days, at 28°C.

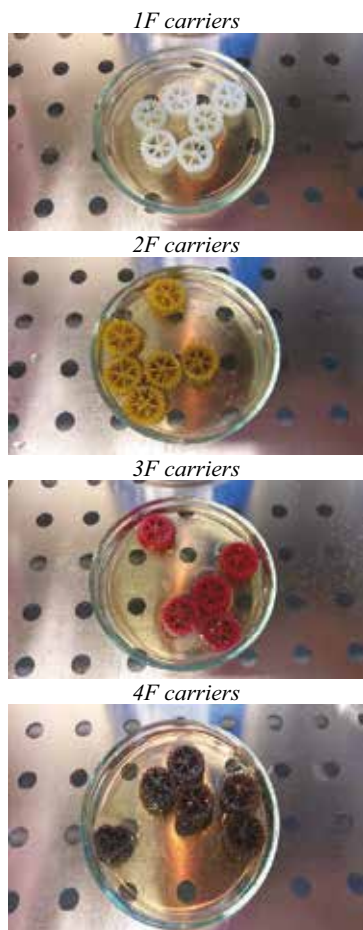


Figure 3. Inoculated Petri dishes containing carriers and Czapek broth

### Optical microscopy analysis

Optical microscopy analysis was carried out on an Olympus SZX7 stereomicroscope, with 7: 1 zoom ratio, built-in electrostatic discharge protection, and advanced Galilean optical system for highly resolved images. Analyses were carried out at a magnification level of 0.67x, on both sets of the carriers (treated in dynamic and static conditions) in order to highlight the presence of the strain on the surface of the carrier, and in the internal spacers.

## RESULTS AND DISCUSSIONS

Present research work explored to bio-augmentation activity of a new generation of HDPE based carriers (patent pending) with *Cerioporus squamosus* strain. The work repre-

sents a novelty in this field, as not only *Cerioporus squamosus* gained little attention in treatment of industrial wastewater, but no studies have been found about bio-augmentation with this specific strain of carriers used in MBBR systems.

Bio-augmentation experiments were run on four types of carriers in both dynamic and static conditions. Results varied greatly not only from treatment method to treatment method, but also from carrier to carrier.

In dynamic conditions, after incubation at 28°C for 7 days (140 rpm), no microbial biomass could be observed neither in the external spacers or the internal ones (Figure 4).

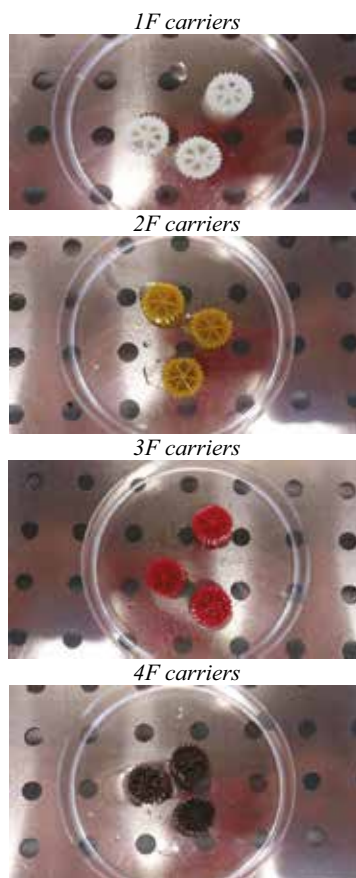


Figure 4. Photographs of post-incubation in dynamic conditions carriers

For exact assessment of presence of biomass in the external and internal spacers, the carriers were analysed under a stereomicroscope (magnification level 0.67x – Figure 5).

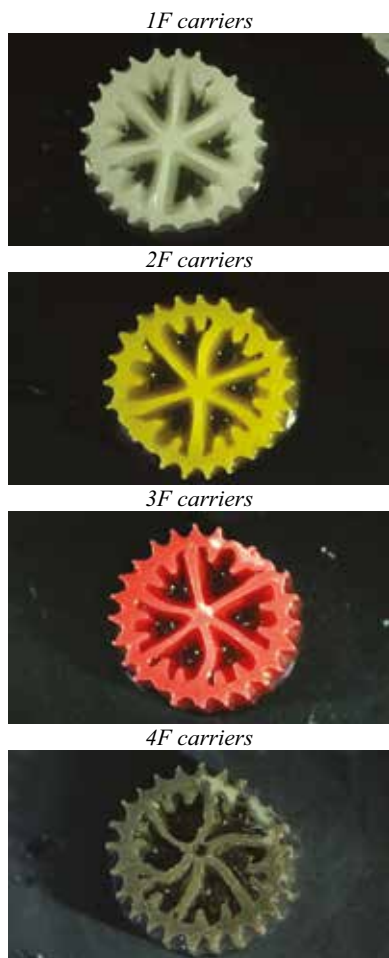


Figure 5. Stereomicroscopy of post-incubation in dynamic conditions carriers

Images show no growth of microbial biomass in dynamic conditions. White zones can be observed on 3F (red carriers) and 4F (brown carriers), belonging to the mix compounds. Lack of microbial biomass growth can be caused by several factors, such as: short timespan of the incubation process – usual bacterial biofilm formation in MBBR systems take around 40 days, which is a longer period of time than 7 days used in this experiment; agitation rate – a higher agitation rate can work against mechanical attachment of biomass on the carriers, leading to both short contact time and easy wash of the already attached biomass; nutrients depletion – in order for new biomass to grow in the external and external spacers, the

nutrients depletion rate must be high enough so it can “force” the strain to access the carriers as nutritive substrate. This parameter is tightly influenced by process timespan, as a short-lived process won’t allow both proper microbial development and nutrients depletion. Future experiments will be concentrated on longer processes timespan and lower agitation rate. The carriers bio-augmented in static conditions yielded far better results, the method allowing the strain to colonize both external and internal spacers (Figure 6).

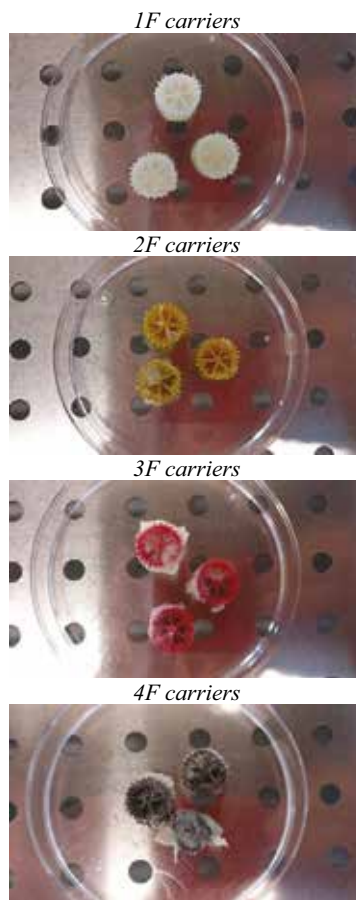


Figure 6. Photographs of post-incubation in static conditions carriers

Carriers’ treatment in static conditions revealed very good colonization efficiency of *Ceriporus squamosus* strain, with good surface coverage for carriers 1F and 2F and very good for 3F and 4F.

Furthermore, microscopy analysis was carried out on the bio-augmented carriers, for assessment of developed biomass (Figure 7).

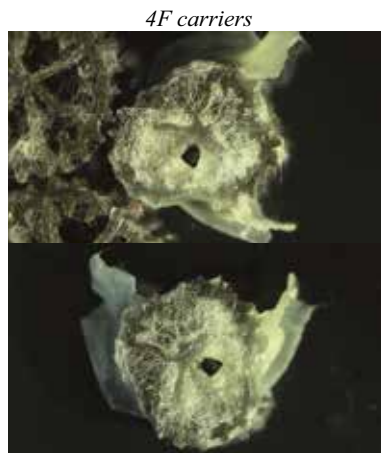
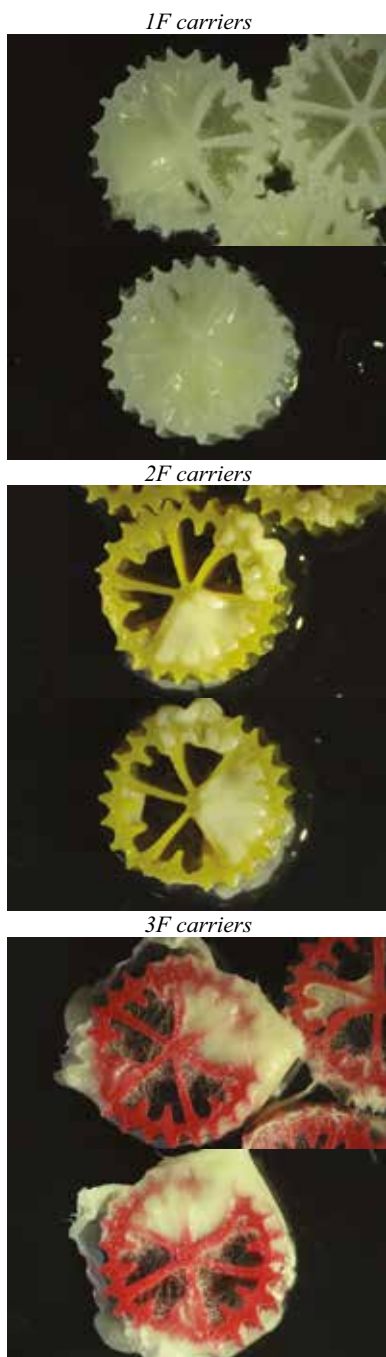


Figure 7. Stereomicroscopy of post-incubation in static conditions carriers

Analyses showed good development on all carriers, with very good development on 3F and 4F carriers. Colonization on 4F carriers was very good, with significant biomass quantity developed on both internal spacers, but also on the exterior of the carriers.

Even though the two methods differ by nature, key differentiators are: significantly lower nutritive broth volume - this allowed faster nutrients depletion, and therefore, faster access of the carriers to the strain, thus leading to good colonization; static contact conditions - this allowed uninterrupted contact between the strain and the carriers, without possibility of being “washed”, like was the case in dynamic conditions treatment.

## CONCLUSIONS

The experiments carried out within current research paper explored the potential of bio-augmentation of four new generation carriers (for use in MBBR systems) with Basidiomycota strain, *Cerioporus squamosus*. Two treatment methods were tested, one in dynamic conditions and one in static conditions, for a treatment timespan of 7 days. Even though this is a very short time period for biomass formation on the carriers, when compared to regular timespan of approximately 40 days in regular MBBRs (for formation of bacterial biofilm), the results were more than promising, with static treatment conditions rendering far better results when compared to

dynamic ones. The best results were obtained on 3F and 4F carriers, with very good development of *Cerrioporus squamosus* strain, on both external and internal carriers' spacers. Future work will focus on bio-augmentation of the carriers in dynamic conditions, as this will mimic closely the real in-situ implementation (as similar to MBBR systems). A personalized programme will be aimed, in order to allow proper microbial development on the carriers, that will mix both static treatment conditions and dynamic treatment conditions.

## ACKNOWLEDGEMENTS

This work was supported by a grant of the Romanian National Authority for Scientific Research and Innovation, CCCDI – UEFISCDI, project number COFUND-MANUNET III-FUNCELL, within PNCDI III. Publication is funded by the Ministry of Research and Innovation within Program 1 - Development of the national RD system, Subprogram 1.2 - Institutional Performance - RDI excellence funding projects, Contract no. 6PFE/ 16.10.2018.

## REFERENCES

- Adrados, B., Sánchez, O., Arias, C. A., Becares, E., Garrid, L., Mas, J., Brix, H., Morató, J. (2014). Microbial communities from different types of natural wastewater treatment systems: Vertical and horizontal flow constructed wetlands and biofilters, *Water Research*, 55, 15 May 2014, 304–312.
- Iordache, O., Cornea, C. P., Diguta, C., Dumitrescu, I., Ferdes, M. (2015). Discolouring and Bioremediation of Synthetic Textile Dyes by Wastewater Microbial Isolates. *Scientific Bulletin. Series F. Biotechnologies*, Volume 19, University of Agronomic Sciences and Veterinary Medicine, Faculty of Biotechnologies.
- Iordache O., Popa, G., Dumitrescu, I., Rodino, S., Matei, A., Cornea, C. P., Diguta, C., Varzaru, E., Ionescu, I. (2016). Evaluation of decolorisation abilities of some textile dyes by fungal isolates. *Industria Textila*, 67(3), 181. National Research & Development Institute for Textiles and Leather-INCOTEX.
- Kruszelnicka Izabela, Dobrochna Ginter Kramarczyk, Przemysław Poszwa, Tomasz Stręk (2018). Influence of MBBR carriers' geometry on its flow characteristics. *Chemical Engineering and Processing - Process Intensification*, 130, August 2018, 34–139.
- Nilsson, I., Moller, A., Mattiasson, B., Rubindamayugi, M. S. T., Welander, U. (2006). Decolorization of synthetic and real textile wastewater by the use of white-Rot fungi. *Enzyme and Microbial Technology*, 38, 94–100.
- Sonwani, R. K., Swain, G., Giri, B. S., Singh, R. S., Rai, B. N. (2019). A novel comparative study of modified carriers in moving bed biofilm reactor for the treatment of wastewater: Process optimization and kinetic study. *Bioresour Technol*, Jun 2019, 281, 335–342. doi: 10.1016/j.biortech.2019.02.121. Epub 2019 Feb 27.
- Wesenberg, D., Kyriakides, I., Agathos, S. N. (2003). White-Rot fungi and their enzymes for the treatment of industrial dye effluents. *Biotechnol. Adv.*, 22(1-2), 161–87.
- Zottia, M., Di Piazza, S., Roccotiello, E., Lucchetti, G., Mariotti, M.G., Marescotti, P. (2014). Microfungi in highly copper-contaminated soils from an abandoned Fe–Cu sulphide mine: Growth responses, tolerance and bioaccumulation. *Chemosphere*, 117, December 2014, 471–476.

## EFFECT OF COMPOST AND VERMICOMPOST AMENDMENTS ON HEAVY METALS UPTAKE BY TOBACCO

Violina ANGELOVA, Zhivko TODOROV

Agricultural University of Plovdiv, 12 Mendeleev Blvd, Plovdiv, Bulgaria

Corresponding author email: vileriz@abv.bg

### Abstract

*A comparative research regarding the impact of organic amendments on the uptake of heavy metals within Oriental tobacco Krumovgrad 90 has been carried out. Experiments have been implemented in controlled conditions. The soil used in this experiment was sampled from the vicinity of KCM – Plovdiv. The pot experiment was a randomized complete block design containing five treatments and three replications (15 pots). The treatments consisted of a control (no organic ameliorants) and compost, and vermicompost amendments (added at 2.5% and 5%, recalculated based on dry soil weight). Heavy metals were measured in roots, stems and leaves of tobacco. The photosynthetic and transpiration rates were measured during treatment using an LCA-4 portable photosynthesis system. Amendments favour the growth and development of tobacco and increased photosynthesis and transpiration intensity. Amendments dose not lead to effective immobilization of Cd, Zn and Cu phytoaccessible forms in soil. The effect of the amendments used for the reduction of the Cd and Zn content in tobacco is negligible. The use of vermicompost can result in a reduction of Pb content in tobacco leaves to 30-40%.*

**Key words:** heavy metals, organic amendments, Oriental Tobacco, photosynthesis and transpiration rate.

### INTRODUCTION

Tobacco is a major agricultural crop for many countries, including Bulgaria. It is known that tobacco is a plant which, compared to other agricultural crops, accumulates higher amounts of heavy metals, even when grown on unpolluted soils (Tso, 1972). The content of metals in tobacco varies widely and depends on a number of factors such as soil type and pH, the use of metal-containing pesticides and fertilizers and others (Adamu et al., 1989; Bell et al., 1992; Khan et al., 1992). Some of the metals such as Fe, Mn, Zn and Cu are important micro elements for plant growth and yield. Other metals, such as Pb, Cd, Ni and Cr, are not relevant to plant development but can cause serious health and environmental problems. Cd content in tobacco ranges from 0.5 mg/kg to 3.5 mg/kg (Golia et al., 2007). Tso (1972) reports a Cd concentration in tobacco leaves reaching 11.6 mg/kg. These are much higher values than most cultures containing Cd (which is below 0.05 mg/kg). Pb content in tobacco leaves varies widely from 0 to 200 mg/kg depending largely on the soil characteristics, type and variety of tobacco, as well as its place of cultivation (Tso, 1972).

Besides from the soil, Pb pollution can also be done by aerosol route.

Addition of organic matter amendments, such as compost, fertilizers and wastes, is a common practice for immobilization of heavy metals and soil amelioration of contaminated soils (Clemente et al., 2005). Organic amendments have the ability to improve the physical, chemical and biological properties of soil by: (i) raising the pH; (ii) increasing the content of organic matter; (iii) adding nutrients that are essential for plant growth; (iv) increasing the capacity for holding water; and (v) modifying the bioavailability of heavy metals (Walker et al., 2003; Walker et al., 2004; Angelova et al., 2013). Using organic fertilizers can improve biological activities and physicochemical properties of crop growth environment. Also, organic fertilizers can neutralize or decrease the soil acidity and supply some micronutrients such as zinc, and copper. Organic fertilizers could advance in weight of single tobacco leaf and yield. Fertilizer efficiency was required to induce rapid growth, improve leaf maturation and ripe, as well as leaf combustibility. It was believed that biological organic-inorganic mixed fertilizer could advance in growth, quality and output of tobacco (Hu, 2004). The

increasing application of organic fertilizers obviously improved soil capacity of supplying nutrients, thus enhancing the release of N, P, and K, providing enough K for tobacco (Cao et al., 2004). Noticeably, organic fertilizer could also improve resistance of tobacco plant in order to reduce diseases (Li, 2008).

The main objective of this article is to conduct a systematic comparative study to determine: (i) the influence of compost and vermicompost on the amount of Pb, Cu, Zn and Cd phytoaccessible forms, and (ii) to compare the effect of the selected amendments on the growth parameters, physiological status of Oriental tobacco and accumulation of Pb, Cd, Zn and Cu in Oriental tobacco when grown on highly contaminated soils.

## MATERIALS AND METHODS

The soils were collected from the surface soil horizon (0-20 cm) of sites located at 0.1 km from the source of pollution (KCM - Plovdiv, Non-Ferrous Metal Plant). The studied soils are slightly sandy loam and are characterized by alkaline reaction (7.7), average content of carbonate (7.3%) and humus (2.2%).

Soil properties are a precondition for low to medium mobility of the metals, as confirmed by the results for DTPA-extracted Pb, Cd, Zn and Cu (low mobility for Pb, Zn and Cu, and medium for Cd).

The total content of Pb, Cd, Zn and Cu is very high and significantly exceeds the permissible concentrations (Table 1).

Table 1. Total content and DTPA - extractable (mg/kg) mobile forms of Pb, Cd, Zn and Cu in soil

Element	DTPA-extractable	Total content	DTPA - extractable/total content, %	MPC*
Pb	401.3	10293	3.8	80
Cd	65.5	174.7	37.5	2,5
Zn	260.1	11795	2.2	340
Cu	45.3	629.6	7.2	280

\*MPC - maximum permissible concentrations

Organic soil amendments were tested in the study. A major consideration when choosing them was the requirement not to pollute the soil further and to favour soil fertility. Compost and vermicompost obtained from the processing of natural fertilizer and other organic waste from the California worm were selected.

Characteristics of soils and organic amendments are shown in Table 2.

Table 2. Characterization of the soil and the organic amendments used in the experiment

Parameter	Soil	Compost	Vermicompost
pH	7.7	7.5	7.8
EC, dS/m	0.3	0.2	2.2
Organic matter, %	2.2	53.8	34.9
N Kjeldal, %	0.23	1.81	1.96
Pseudo total P, mg/kg	2961	1005	1009
Pseudo total K, mg/kg	5882	2452	5684
Pseudo total Ca, mg/kg	31029	420	893
Pseudo total Mg, mg/kg	11495	168	410
Pseudo total Pb, mg/kg	10293	10.5	26.0
Pseudo total Zn, mg/kg	11795	93.2	191.8
Pseudo total Cd, mg/kg	174.7	0.47	0.43
Pseudo total Cu, mg/kg	629.6	30.3	53.0

After the soils sieving through a 2 cm<sup>2</sup> mesh sieve, organic soil amendments (compost and vermicompost) were added at 2.5% and 5% (recalculated based on dry soil weight) and gently hand-mixed with the soil. The total amount of mix used in all variants was 9 kg. All treatments were performed in three replications. Additionally, three test pots were prepared for the control samples (no amendments).

Oriental tobacco plants (Krumovgrad 90) were used as test plants. When the plants had developed three pairs of leaves, they were transferred to the pots, where they were left to grow in a climate chamber for 67 days, with regular watering and random rotation of pots position. All plants were grown successfully, with some of the plants reaching blooming phase (control sample and variants with vermicompost - 2.5 and 5%). Tobacco plants were harvested and the content of Pb, Cu, Zn and Cd in different parts - roots, stems and leaves was determined. Since Pb, Zn and Cd were accumulated less in the leaves of the lower belt compared to the leaves of the middle and upper belt (Lugon-Moulin et al., 2004), only the leaves from the lower belt were analyzed. The plant samples were dried at 60°C.

The photosynthetic and transpiration rates were measured during treatment using an LCA-4 (ADC, England) portable photosynthesis system.

The content of heavy metals in Oriental tobacco leaves was determined by the method of dry mineralization. The pseudo total content of metals in the soil was determined in

accordance with ISO 11466. The mobile forms were extracted by a solution of 0.005 M DTPA and 0.1 M TEA (pH 7.3) (ISO 14870). The quantitative measurements were carried out with inductively coupled plasma emission spectrometry (ICP) (Jobin Yvon Emission - JY 38 S, France).

## RESULTS AND DISCUSSIONS

The Table 3 shows the amounts of mobile forms of DTPA-extracted Pb, Cd, Zn and Cu in the control sample from anthropogenically contaminated soil used in the experiment and their changes in 6 weeks after the addition of organic soil amendments.

Table 3. Impact of soil organic amendments on the amount of DTPA-extractable mobile forms of Pb, Cd, Zn and Cu

Element	Control	Compost		Vermicompost	
		2.5%	5.0%	2.5%	5.0%
Pb	401.3	452.0	453.6	446.5	432.5
Cd	65.5	64.2	64.6	62.3	66.9
Zn	260.1	262.4	255.8	298.5	278.6
Cu	45.5	41.3	43.7	45.2	47.4

The results presented in the table shows that the influence of soil amendments on the mobile forms of Pb, Cd, Zn and Cu is diversely and relatively poorly expressed, with up to 15% deviations from the control sample. The addition of compost and vermicompost resulted in an increase of mobile Pb by 13%. Adding compost practically does not affect the amount of mobile Zn, and the biofertilizer leads to an increase in the amount of mobile Pb by 13%. The quantities of Cd and Cu remained practically unchanged.

After harvesting, the mass and height of the plants were measured (data are not shown). The results shown that the amount of fresh (dry) biomass as well as the height of the plants are influenced by the type and amount of the amendments used. Adding vermicompost leads to their more intense growth, and this effect is more visible in 5.0% vermicompost. In practice, the addition of 2.5% and 5% compost does not have a significant effect on plant growth.

Greater biomass and differences in tobacco development (the earlier flowering of variants

with the addition of 2.5% and 5% vermicompost) may be due to the improvement of soil physical characteristics favouring better root development and greater absorption of macro and microelements compared to the control sample. The photosynthetic response of the plants to the effect of heavy metals was thoroughly analyzed by determining the parameters of *leaf gas exchange*, including photosynthesis rate, transpiration intensity and stomata conductivity. The results are presented in Table 4.

Table 4. Influence of organic soil amendments on the rate of photosynthesis ( $\mu\text{mol}(\text{CO}_2) \cdot \text{m}^{-2} \cdot \text{s}^{-1}$ ), the transpiration intensity ( $\text{mmol}(\text{H}_2\text{O}) \cdot \text{m}^{-2} \cdot \text{s}^{-1}$ ) and stomata activity ( $\text{mol} \cdot \text{m}^{-2} \cdot \text{s}^{-1}$ )

Treatment	Parameters		
	Photosynthesis rate, $\mu\text{mol}(\text{CO}_2) \cdot \text{m}^{-2} \cdot \text{s}^{-1}$	Transpiration, $\text{Mmol}(\text{H}_2\text{O}) \cdot \text{m}^{-2} \cdot \text{s}^{-1}$	Stomata conductivity $\text{mol} \cdot \text{m}^{-2} \cdot \text{s}^{-1}$
Control	5-6	2.7-2.9	0.07-0.08
2.5% Compost	3-4	3.0-3.5	0.07-0.09
5% Compost	6-7	3.6-4.0	0.10-0.12
2.5% Vermi compost	8-10	4.0-5.2	0.16-0.18
5% Vermi compost	10-14	4.0-5.3	0.17-0.19

The results shows that changes in the physiological status of the plants are observed depending on the type and amount of organic additive used. The increase in the photosynthesis rate in plants after the addition of vermicompost compared to the control sample is visible, with the experiment of 5% vermicompost reaching 50-60%. Reverse but less obvious is the tendency for tobacco after the addition of 2.5% compost, where the photosynthesis rate reduction reaches 30%.

On the other hand, the addition of compost and vermicompost results in an increase in transpiration intensity and in the stomata conductivity compared to the control sample, with this increase being more pronounced with 5% compost and 5% vermicompost.

The influence of organic amendments on the accumulation and distribution of Pb, Zn, Cu and Cd in the plants tested are presented in Table 5. The change in heavy metal content is also presented in comparison with the control sample (%).

A major route for the entry of heavy metals in plants is the root system. Once they have entered the roots, they can be stored or moved to the stems. As can be seen from the data presented in Figure 1, the major portion of Pb, Zn and Cu is retained by the tobacco roots, and a smaller portion of them moves to the stems and leaves. In cadmium case, however, the main portion is accumulated in the leaves. These trends are observed both in the control sample and in the cultivated plants after the addition of organic amendments.

The Cd content in tobacco leaves is higher than the root system and the stems, which is also consistent with the results of other authors (Mench et al., 1989; Keller et al., 2003; Angelova et al., 2006). Their higher accumulation in tobacco leaves is probably due to the absorption of heavy metals from the soil through the root system of the plant and their movement through the conductive system. This is consistent with the results of Yeargan et al. (1992) and Angelova et al. (2006), who found that tobacco has an extraordinary ability to digest Cd in comparison with other plants when grown on highly Cd-contaminated soils. Our results are significantly higher than the data on Cd content in leaf tobacco (Lugon-Moulin et al., 2004) reported in literature. According to Mench et al. (1994) and Sappin-Didier and Gomez (1994), the Cd content in tobacco ranges from 40 to 120 mg/kg depending on the soil characteristics.

Cd content in Oriental tobacco leaves reaches 261.8 mg/kg in the control sample and is significantly higher than the concentrations considered being critical for plant growth - 5 to 10 mg/kg (Kabata Pendias, 2001). The visible symptoms caused by the increased Cd content in plants such as growth inhibition, root system damage, leaf chlorosis, reddish-brown colour at the edges were not observed.

The Pb content in tobacco leaves reaches 92.3 mg/kg in the control sample and is lower than the concentrations considered to be critical for plant growth - 30 to 300 mg/kg (Kabata Pendias, 2001). The visible symptoms caused by the increased Pb content occurring in dark green leaves, deformation of old leaves, dark brown and short roots in tobacco were not observed.

The Zn content in tobacco leaf reaches 304.6 mg/kg in the control sample and is below the critical concentrations for plants - 100-400 mg/kg (Kabata Pendias, 2001). Symptoms of zinc toxicity, such as chlorosis and leaf-edge necrosis, interveinal chlorosis on young leaves, inhibition of plant growth as a whole, root damage, were not observed as well.

Cu content in tobacco leaves reaches 22.4 mg/kg in the control sample and is lower than the concentrations considered to be critical for plant growth - 30 mg/kg (Kabata Pendias, 2001).

The distribution of heavy metals in Oriental tobacco organs has a selective character which decreases in order: Pb - roots > stems > leaves, Cd - leaves > stems > roots, Zn and Cu - roots > leaves > stems (Figure 1).

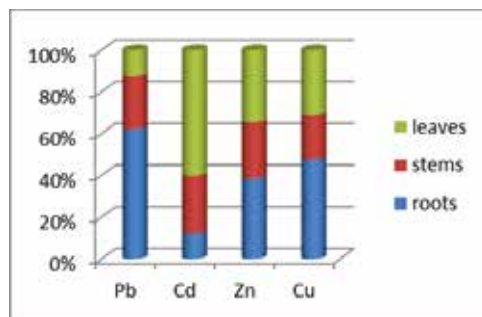


Figure 1. Distribution of Pb, Cd, Zn and Cu (%) in the Oriental tobacco organs

Our results show that the absorption of Pb, Zn and Cd from tobacco is not one-sided and depends on soil amendments and treatment (type and norm).

The addition of 2.5% and 5% compost results in a decrease in Pb content in tobacco stems and leaves; this decrease being more pronounced with 5% compost. Adding vermicompost also leads to a decrease in Pb content in stems and leaves compared to the control sample, this decrease being more pronounced with a 2.5% additive. The influence of the organic amendments used on the accumulation of Pb in tobacco roots is more complex and substantially dependent on their quantity. While in the addition of 2.5% compost and vermicompost, the reduction in Pb content is relatively high (16.2% and 10.5%), in 5.0% amendments the reduction is

significantly lower and is 10.0% and 7.7%, respectively. The probable cause for this is the much stronger root system in the second case. The trends in the change of Cd and Zn content in tobacco organs are quite complicated and controversial. The content of both elements in the root system increases in all variants of the experiments. A similar but less pronounced trend is observed for cadmium in stems and leaves. The exception is only the case of using a 5.0% vermicompost additive in which the Cd content in the stems decreases by 7.9% and it's in contradiction with the results of Chlopecka and Adriano (1997) who found that amendments the soil are low, probably because the high Cd content in the leaves remains close to that of the control sample. The reason is probably the amount of biomass. The result obtained reveals the number of added

enhancers is not sufficient to immobilize the Cd amount.

The increase in Zn content in leaves compared to the control sample is higher, as in the experiment with 5.0% vermicompost and it reaches 50%. Reverse but less pronounced is the trend in stems where the reduction in Zn content is from 4.4 to 24.4%.

The addition of 2.5% and 5.0% compost results in a decrease in the copper content in tobacco stems and leaves, this decrease being more pronounced with 5.0% compost.

The increase in copper content in leaves compared to the control sample is higher, as in the experiment with 5.0% vermicompost it reaches 57%. Reverse but less pronounced is the trend in stems where the reduction in copper content is 10% to 31%.

Table 5. Influence of organic amendments on the accumulation of Pb, Zn, Cu and Cd (mg/kg) in the Oriental tobacco

Element	Plant part	Control	Compost	Change	Compost	Change	Vermicompost	Change	Vermicompost	Change
			2.5%	%	5.0%	%	2.5%	%	5.0%	%
Pb	Roots	475.8	398.5	-16.2	430.2	-10.0	425.9	-10.5	439.2	-7.7
	Stems	195.3	149.4	-23.5	120.2	-38.5	125.9	-35.5	144.9	-25.8
	Leaves	92.3	87.1	-5.6	65.6	-28.9	52.1	-43.6	59.5	-35.5
Cd	Roots	59.2	75.1	+26.9	85.0	+43.6	132.4	+123.6	63.5	+7.3
	Stems	121.3	137.8	+13.6	142.4	+17.4	125.8	+3.7	111.7	-7.9
	Leaves	261.8	303.1	+15.8	266.5	+1.8	285.9	+9.2	260.1	-0.6
Zn	Roots	340.7	348.8	+2.4	468.8	+37.6	569.5	+67.2	431.9	+26.8
	Stems	240.4	201.9	-16.0	187.1	-24.4	229.8	-4.4	197.9	-17.7
	Leaves	304.6	408.3	+34.0	327.7	+7.6	316.8	+4.0	460.0	+51.0
Cu	Roots	34.5	32.3	-6.4	47.3	+37.1	53.8	+55.9	37.7	+9.3
	Stems	15.5	12.3	-20.6	10.7	-31.0	12.8	-17.4	14.0	-9.7
	Leaves	22.4	22.8	+1.8	17.0	-24.1	25.9	+15.6	35.1	+56.7

## CONCLUSIONS

On the basis of the results obtained, the following conclusions can be drawn:

1. Tobacco is a crop tolerant to heavy metals and it develops normally when grown on soils contaminated with heavy metals. The distribution of heavy metals in Oriental tobacco organs has a selective character which decreases in order: Pb - roots> stems> leaves, Cd - leaves> stems> roots, Zn and Cu - roots> leaves> stems.
2. Organic ameliorants influences the amount of fresh (dry) biomass as well as the height of the plants. The addition of 5% vermicompost leads to tobacco plants more intense growth. The addition of 2.5% and 5% compost in practice does not have a significant effect on plant growth.
3. Organic ameliorants influences tobacco physiological status. The addition of compost and vermicompost leads to increased photosynthesis rate, transpiration intensity and in the stomata conductivity.
4. The use of organic amendments does not lead to effective immobilization of Cu, Zn and Cd phytoaccessible forms in heavily polluted soil. This contradicts the results of other authors who worked with slightly or moderately contaminated soils. Explaining

this contradiction requires the accumulation and analysis of more experimental results.

5. The effect of the compost and vermicompost used for the reduction of the Cd and Zn in tobacco is negligible. The use of vermicompost can result in a reduction in Pb content in tobacco leaves to 30-40%.

## ACKNOWLEDGEMENTS

The financial support by the Bulgarian National Science Fund Project DFNI H04/9 is greatly appreciated.

## REFERENCES

- Adamu, C. A., Mulchi, C. L., Bell, P. F. (1989). Relationships between soil pH, clay, organic matter and CEC [cation exchange capacity] and heavy metal concentrations in soils and tobacco. *Tob. Sci.*, 33, 96–100.
- Angelova, V., Ivanov, K., Dospatliev, K. (2006). Uptake of Fe, Mn, Zn, Cu, Pb and Cd from Virginia tobacco. *Ecology and Future*, 2, 3–9.
- Angelova, V. R., Akova, V. I., Artinova, N. S., Ivanov, K. I. (2013). The effect of organic amendments on soil chemical characteristics. *Bulgarian Journal of Agricultural Science*, vol. 19(5), 958–971.
- Bell, P. F., Mulchi, C. Z., Chaney, R. (1992). Microelement concentration in Maryland air-cured tobacco. *Commun. Soil Sci. Plant anal.*, 23(13-14), 1617–1628.
- Cao, P. Y., Lu, S. J., Zhang, W. S. (2004). Advances in soil organic matter contents and vermicomposts application in tobacco growing areas. *Acta Tabacaria Sinica*, 10(6), 40–42.
- Chlopecka, A., Adriano, D. C. (1997). Influence of zeolite, apatite and Fe-oxide on Cd and Pb uptake by crops. *Sci. Tot. Environ.*, 207, 195–206.
- Clemente, R., Walker, D. J., Bernal, M. P. (2005). Uptake of heavy metals and As by *Brassica juncea* grown in a contaminated soil in Aznaco'llar (Spain). The effect of soil amendments. *Environmental Pollution*, 138, 46–58.
- Golia, E. E., Dimirkou, A., Mitsios, I. K. (2007). Accumulation of metals on tobacco leaves (primings) grown in an agricultural area in relation to soil. *Bull Environ Contam Toxicol.*, 79 (2), 158–162.
- Hu, Z. (2004). Effect of bio-organic compound vermicompost on improvement of tobacco quality. *Chinese Agricultural Science Bulletin*, 20(3), 157–158.
- ISO 11466 (1995). Soil Quality- Extraction of trace elements soluble in aqua regia.
- ISO 14870 (2001). Soil Quality- Extraction of trace elements by buffered DTPA solution.
- Jones, J., Wolf, Jr., Mills, H. (1991). *Plant Analysis Handbook*. Micro – Macro Publishing, Ins.
- Kabata-Pendias, A. (2001). *Trace Elements in Soils and Plants*, 3rd ed. CRC Press LLC, Boca Raton.
- Keller, C., Hammer, D., Kayser, A., Richner, W., Brodbeck, M., Sennhauser, M. (2003). Root development and phytoextraction efficiency: comparison of different species. *Plant Soil*, 249, 67–81.
- Khan, M. A., Mulchi, C., McKee, C. G. (1992). Influence of pH and soils on the bioaccumulation of trace elements in Maryland tobacco. *Tob. Sci.*, 36, 53–56.
- Li, C. X. (2007). Effect of EM bio-organic vermicompost on tea garden. *J. Tea Business.*, 29(2), 65–66.
- Lugon-Moulin, N., Zhang, M., Gadani, F., Rossi, L., Koller, D., Krauss, M., Wagner, G. L. (2004). Critical review of the science and options for reducing cadmium in tobacco (*Nicotiana tabacum* L.) and other plants. *Adv. Agron.*, 83, 111–180.
- Mench, M. J., Didier, V. L., Loëffler, M., Gomez, A., Masson, P. (1994). A mimicked *in situ* remediation study of metal contaminated soils with emphasis on cadmium and lead. *J. Environ. Qual.*, 23, 58–63.
- Mench, M. J., Tancogne, J., Gomez, A., Juste, C. (1989). Cadmium bioavailability to *Nicotiana tabacum* L., *Nicotiana rustica* L., and *Zea mays* L. grown in soil amended or not amended with cadmium nitrate. *Biol. Fert. Soils*, 8, 48–53.
- Sappin-Didier, V., Mench, M., Gomez, A., Lambrot, C. (1997). Use of inorganic amendments for reducing metal bioavailability to ryegrass and tobacco in contaminated soils. In *Remediation of Soils Contaminated with Metals*. Eds. I. K. Iskandar and D. C. Adriano. (pp. 85–98). Science Reviews, Northwood.
- Tso, T. C. (1972). *Physiology and Biochemistry of Tobacco Plants*, 393.
- Walker, D. J., Clemente, R., and Bernal, D. J. (2004). Contrasting effects of manure and compost on soil pH, heavy metal availability and growth of *Chenopodium album* L. in a soil contaminated by pyritic mine waste. *Chemosphere*, 57, 215–224.
- Walker, D. J., Clemente, R., and Bernal, M. P. (2003). The effects of soil amendments on heavy metal bioavailability in two contaminated Mediterranean soils. *Environmental Pollution*, 122, 303–312.
- Yeagan, R., Maiti, I. B., Nielsen, M. T., Hunt, A. G., Wagner, G. J. (1992). Tissue partitioning of cadmium in transgenic tobacco seedlings and field grown plants expressing the mouse metallothionein I gene. *Transgenic Res.*, 1, 261–267.

## THE IMPACT OF METEOROLOGICAL DROUGHT CASE STUDY - NORTHEASTERN ROMANIA

Flaviana CORDUNEANU<sup>1</sup>, Sorin Mihai CIMPEANU<sup>2</sup>, Silviu IORDACHE<sup>3</sup>,  
Denis-Constantin TOPA<sup>1</sup>, Claudiu-Ionut PRICOP<sup>4</sup>, Isabela-Elena BALAN<sup>4</sup>,  
Daniel BUCUR<sup>1</sup>

<sup>1</sup>University of Agricultural Sciences and Veterinary Medicine of Iasi, 3 Mihail Sadoveanu Alley,  
Iasi, Romania

<sup>2</sup>University of Agronomic Sciences and Veterinary Medicine of Bucharest, 59 Marasti Blvd,  
District 1, Bucharest, Romania

<sup>3</sup>National College Emil Racovita of Iasi, 4 Nicolina Alley, Iasi, Romania

<sup>4</sup>Water Basin Administration Prut -Barlada, 10 Theodor Vascauteanu Street, Iasi, Romania

Corresponding author email: dbucur@uaiasi.ro

### Abstract

Prut River basin is located in the south-eastern Europe, in a temperate climate of transition with significant variations of the precipitation regime. This study proposes a spatial and temporal analysis of drought in northeastern Romania, in the area drained by Prut River and its tributaries, between hydrological sections Oroftiana and Gorban, to emphasize its impact on a region where water resources need to be managed efficiently. Excessively dry months, with a frequency over 20% and excessively rainy ones placed between 18.08% and 21.69, lead to the frequent occurrence of drought. According to Topor aridity index a 67.60% frequency was obtained and most of the years have proven to be moderate-dry. Between 1997 and 2013 the multiannual average values and the number of the extreme months have grown. The territorial variation of their weight, proved an increased torrentiality in the region delimited by the Botosani, Stefanesti-Stanca and Cotnari sections. UNESCO aridity index between 0.6 and 0.8 claim that this region is the second in terms of aridness intensity from Romania even if they belong to the wet class. Water has been a major limiting factor in the region as a result of the steadily decreasing amount due to the pollution and its insufficient reserves according to the riparian communities' requirements.

**Key words:** correlation, drought, evapotranspiration, indices, shortage.

### INTRODUCTION

Prut River between Oroftiana (the point of entry of the river into the country) and Gorban (south-eastern extremity of Iasi County) has a length of 241 km and drains an area of 8020 km<sup>2</sup>, divided as follows: 4469 km<sup>2</sup> in Botosani county and 3551 km<sup>2</sup> in Iasi (Figure 1).

In the analyzed region the main climatic elements are: central and southern of Moldavian Plain is crossed by 9°C isotherm, but values may exceed 9.5°C at altitudes below 120 m.

As the altitude increases, temperature drops below 8°C to over 350 m (7.5 at Harlau).

Moldavian Plain is crossed by 500 mm isohyet in center and east, however in the high hills frame from west and south and in north may approach 560 mm (Oroftiana, Harlau - Figure 2).

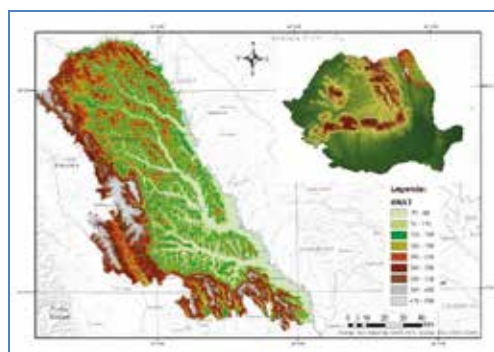


Figure 1. Hypsometric map - Prut River catchment area between Oroftiana and Gorban

Maximum values are recorded in the summer (June and July) and reach a 39-45% frequency, spring follows with 21.5 to 25.6% and in autumn the frequency is between 18.3% and 22%.

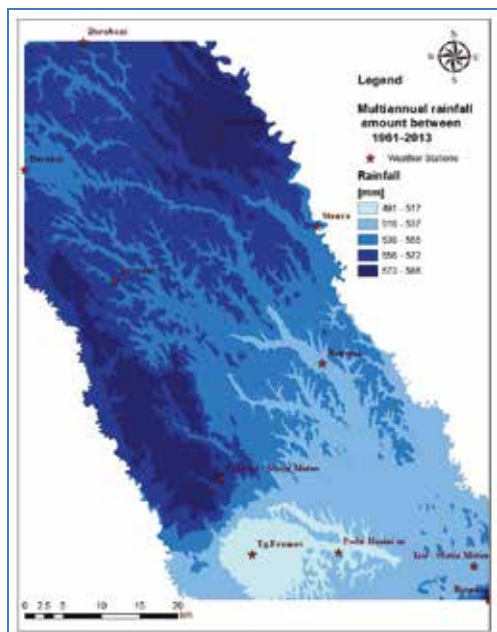


Figure 2. Multiannual rainfall amount between 1961-2013

In the winter values are within the range 12.3% to 15.9%.

Hydro-climatic risks study is based on a set of empirical and statistical analysis of involved variables closely related with the components of natural setting: geology and geomorphology of the region, biological, climatic and pedological conditions, to which was added the increased influence of human activities.

Drought is defined as the period and state of water deficit caused by negative difference between water intakes and outputs from the system, which causes reversible or irreversible imbalances and malfunctions (Stanga I.C., 2009).

Drought and the phenomena generated by it (aridization, desertification) are based, in addition to the natural and anthropogenic causes, which have a negative effect on the water balance, also on changes that arise in the general circulation of the atmosphere inflicted by the manifestation of the greenhouse effect, the irrational land use, deforestation, etc.

## MATERIALS AND METHODS

For the study of drought was used a large amount of data recorded by the National

Meteorological Administration and Water Basin Administration Prut-Barlad. Discrete continuous variables had been processed and the established range (1961-2013) was considered optimum for the statistical analysis.

The rainfall characterization of a month was based on Hellmann's criterion. The framing is based on the percentage deviations of the monthly precipitation quantities from the multiannual average of the period (Romanescu et al., 2014).

Under this criterion were assessed:

- normal month (NM) – when the rainfall varies between +10% and -10% compared to the multiannual average amount;

- moderately rainy month (MRM) - when varies between +10.1% and +20%;

- rainy month (RM) - when varies between +20.1% and +30%;

- very rainy month (VRM) - when varies between +30.1% and +50%;

- extremely rainy month (ERM) - when varies with more than +50%;

- moderately dry month (MDM) - when varies between 10.1% and -20%;

- dry month (DM) - when varies between -20.1% and -30%;

- very dry month (VDM) - when varies between -30.1% and -50%;

- extremely dry month (EDM) - when varies with more than -50% (Topor, 1964).

Topor aridity index ( $T_{AI}$ ) was obtained from the equation 1:

$$T_{AI} = \frac{N + 2R}{N + 2D} \quad (1)$$

where:

- N - number of normal months;
- R - number of rainy months;
- D - number of dry months;

$T_{AI} < 0.33$  - exceptionally dry year;

$0.33 < T_{AI} < 0.41$  - excessively dry year;

$0.41 < T_{AI} < 0.71$  - very dry year;

$0.71 < T_{AI} < 0.85$  - dry year;

$0.85 < T_{AI} < 1.0$  - less dry year;

$1.0 < T_{AI} < 1.18$  - normal year;

$1.18 < T_{AI}$  - rainy year (Apostol L., 2000).

Annual values of De Martonne aridity index were obtained from:  $I_{DM-a} = R / (T_a + 10)$ , where: R = sum of annual rainfall and  $T_a =$

average annual temperature. The value of 10°C is added to the denominator to generate positive results. Monthly values were calculated as follows:  $I_{DM-monthly\ \alpha} = r + 12 / (t_{\alpha} + 10)$ , where  $r$  and  $t_{\alpha}$  define monthly values of rainfall and average temperature.

Potential evapotranspiration ( $ET_0$ ) is a commonly used variable in climatic and hydrological studies which count in the soil balance of water or the moisture requirements of agricultural crops; brings geographic information about the sort of landscape and the type / class of soil.

Standard method, Penman-Monteith, which has substituted other empirical methods to reckon  $ET_0$ , is precise and close to direct determinations, in lysimeters, because it uses most of the factors that influence the potential evapotranspiration (Monteith J.L., 1965). The six meteorological stations to which this study refers, did not record the entire climate data set required in the estimation of  $ET_0$ , which is why very significant correlations have been used. They have been set between the average monthly temperature and the potential evapotranspiration obtained through the standard method ( $ET_0 - PM$ ). The value of the determination coefficient ( $R^2$ ) is very high, according to the equation 2, Paltineanu et al. (2007):

$$ET_0 - PM = 0.0048 * T_{\alpha}^2 + 0.0678 * T_{\alpha} + 0.4888 \quad (R^2 = 0.93 \dots) \quad (2)$$

Compared to  $I_{DM-\alpha}$ , this difference between annual precipitation and reference evapotranspiration values ( $ET_0 - PM$ ) is called annual climate (or hydrological) water deficit. It is calculated as a difference between two variables that characterize the essence of the natural landscape presents absolute values (mm), not relative, percentages from  $ET_0$ . UNESCO 1979 aridity index ( $I_{R/\Delta T_3}$ ) is obtained from the annual or monthly report of rainfall and  $ET_0 - PM$ , even if potential evapotranspiration was obtained by means of the correlation. The desert climate, characterized by lower values than 0.03 and those in 0.03-0.20 class (arid climate) of  $I_{R/\Delta T_3}$  does not exist in Romania. The eastern part of the Danube Delta, the Black Sea coast,

Dobrogea and northeastern of Baragan are the areas with the lowest values, but they belong to the semi-arid class. The southeastern part of Moldavian Plateau and a narrow strip of the Danube meadow are framed by the 0.65 mm isoline (Paltineanu et al., 2007).

## RESULTS AND DISCUSSIONS

In northeastern Romania predominates excessively dry months (with a frequency over 20%, the maximum value of 24.37% was obtained for Barnova weather station) and excessively rainy ones whose frequency is between 18.08% and 21.69% (Figure 3).

Thus, explains the high frequency of droughts in the analyzed region, where the temperate – continental climate has excessive influences.

Tormentality increases in the region from north to south, as a consequence of the high frequency of pluviometric extremes. In Iasi county the frequency of extremely dry months is higher than in Botosani, but the significant values calculated for the extremely rainy months belong to the Botosani (19.81%) and Stefanesti (21.69%) meteorological stations, the latter highlights local climate elements as is placed in the proximity of Stanca-Costesti reservoir.

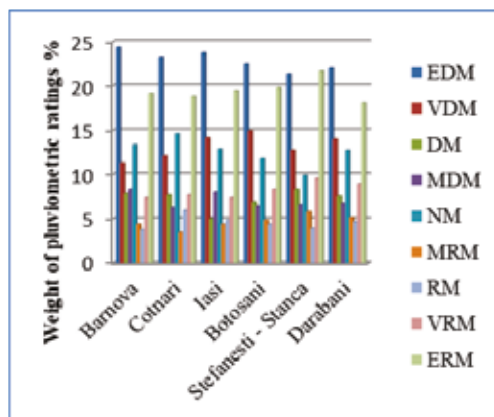


Figure 3. The weight of the pluviometric ratings at the meteorological stations in northeastern Romania, during 1961-2013 (according to Hellmann's criterion) (%)

As in previous research (Corduneanu et al., 2016) where Topor aridity index was used, drought frequency reached 67.60% and most of the years were moderate-dry. Temporal variability, a defining feature of the temperate -

continental climate is supported by the fact that the exceptionally dry years frequency in the entire region was between 3.77 and 9.43%.  $T_{A_i}$  smallest value of 0.09 was recorded at Cotnari meteorological station in 1967.

A study that highlighted the drought and relied on Topor aridity index (Minea I., Stanga I.C., 2004) shows that the trend of climate aridization spatially varies from the mountain area to the Moldavian Plain, here having pronounced character as a consequence of the

continental - eastern influences. In Iasi and Botosani counties, the frequency of the dry years oscillates between 75.47% at the Barnova meteorological station and 62.26% at Stefanesti-Stanca. Statistics of extreme values indicate that 2000 was exceptionally dry throughout the studied region just like 1986, when the intensity of the drought diminished in narrow areas, in Iasi had an excessive character.

Table 1. Multiannual average values of  $T_{A_i}$  in northeastern Romania

The analysed period	Weather stations					
	Darabani	Botosani	Stefanesti-Stanca	Cotnari	Iasi	Barnova
1961-1978	0.891	0.941	0.858	0.809	0.853	0.822
1979-1996	0.790	0.830	1.016	0.904	0.897	0.757
<b>1997-2013</b>	<b>1.034</b>	<b>0.943</b>	<b>1.145</b>	<b>1.127</b>	<b>0.953</b>	<b>1.006</b>

Between 1961 and 1978 the drought was moderate (Table 1) while in the middle period, the phenomenon has become stronger,  $T_{A_i} < 0.84$  south of Iasi county (Barnova -  $T_{A_i} = 0.757$ ), as well as in the northern half of the studied region (Botosani -  $T_{A_i} = 0.830$ , Darabani -  $T_{A_i} = 0.790$ ). In the last interval the mean values of the Topor aridity index and the number of the extreme months, from the pluviometric point of view, are growing (EMD+ERM).

The territorial variation of their weight, which is between 43.13 and 50.49% indicates an increased torrentiality in the region delimited

by the Botosani, Stefanesti-Stanca and Cotnari meteorological stations.

In the last years (1997-2013) the mean of the aridity index changes very little from a spatial point of view, it is maintained quite high at Stefanesti-Stanca and Cotnari (Table 2). Fact explained by the pluviometric extremes growth, the highest multiannual average of the Topor aridity index (Cotnari -  $T_{A_i} = 1,127$ ) was obtained from values ranging between 0.2 (extreme drought) and 3.8 (value corresponding to 2010 which was very rainy).

Table 2. Weight of the extreme months from the pluviometric point of view (EDM+ERM) in northeastern Romania (%)

The analyzed period	Weather stations					
	Darabani	Botosani	Stefanesti - Stanca	Cotnari	Iasi	Barnova
1961-1978	39.81	42.59	42.12	41.20	35.18	41.20
1979-1996	40.27	41.20	37.96	42.12	39.35	46.75
1997-2013	41.17	43.13	50.49	43.13	42.64	42.64

The territorial distribution of the De Martonne aridity index  $I_{DM-\pi}$  shows that northeastern Romania is characterized by values between 20 and 30 mm/°C (Paltineanu et al., 2007), dry areas with values between 15 and 20 mm/°C are highlighted in the southeastern extremity (Baragan or the South of the Romanian Plain).

In Iasi county, values of  $I_{DM-\pi}$  lower than 20 (semiarid climate, after De Martonne 1926) were calculated for 2000 (15.92 mm/°C – Iasi, 19.27 mm/°C – Barnova and 19.29 mm/°C – Cotnari), also for 2011 (Iasi – 17.76 mm/°C), when this value was exceeded at Cotnari – 20.42 mm/°C and Barnova – 21.19 mm/°C.

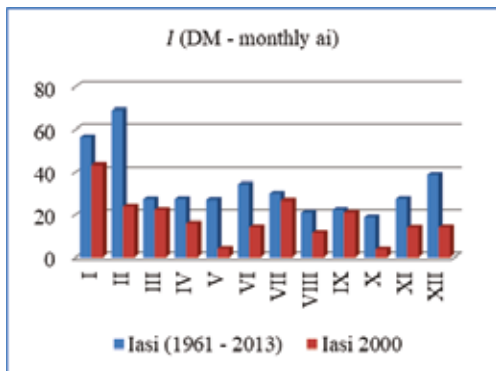


Figure 4. De Martonne monthly aridity index - Iasi meteorological station

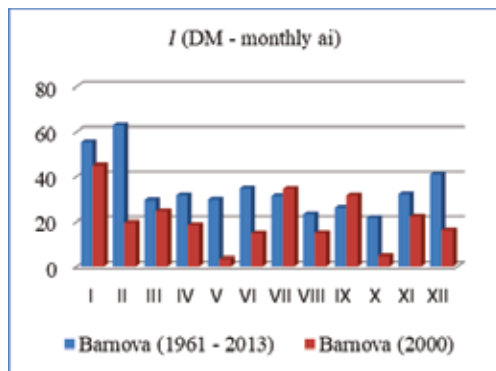


Figure 6. De Martonne monthly aridity index - Barnova meteorological station

At Iasi (Figure 4) monthly multiannual values vary between 18.7 and 34.3 mm/°C, showing a downward trend since August  $I_{DM-monthly ai} = 20.9$  mm/°C (in September - 22.36 mm/°C, and in October - 18.7 mm/°C). At the other two meteorological stations, the values are in the range of 20 - 30 mm/°C (Figures 5 and 6), except the related ones of June (36.6 at Cotnari and 34.9 at Barnova) and July (34.1 and 31.3, respectively). During 2000 year  $I_{DM-monthly ai}$  is below the multiannual values, with the exception of the one calculated for July at Cotnari (41.02 mm/°C > 34.1 mm/°C) and Barnova (34.7 mm/°C > 31.3 mm/°C).

In May, Moldavian Plain is crossed by the isoline of de 30 mm/°C (Paltineanu et al., 2007) but a trend of aridization of the climate has been identified, due to average monthly temperature increase and the decrease of rainfall amount. De Martonne aridity index is in the 0-5 mm/°C class (very dry and arid climate) at Iasi and Barnova, respectively 5-15 mm/°C (semiarid) at Cotnari in May 2000. Similar values (between 5.13 and 7.44 mm/°C), therefore severe climatic conditions, can be observed in Botosani county at the same period (Figures 7, 8 and 9).

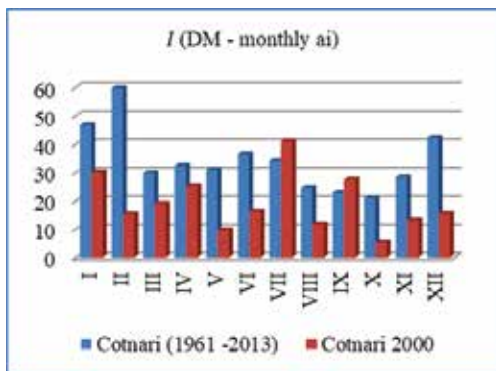


Figure 5. De Martonne monthly aridity index - Cotnari meteorological station

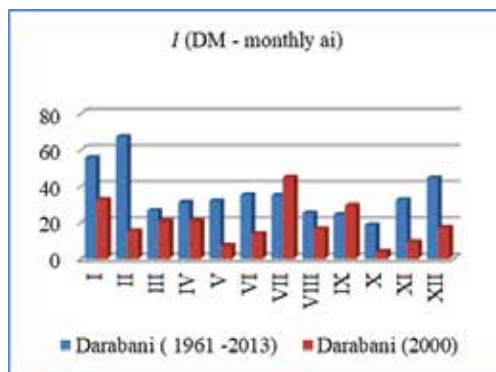


Figure 7. De Martonne monthly aridity index - Darabani meteorological station

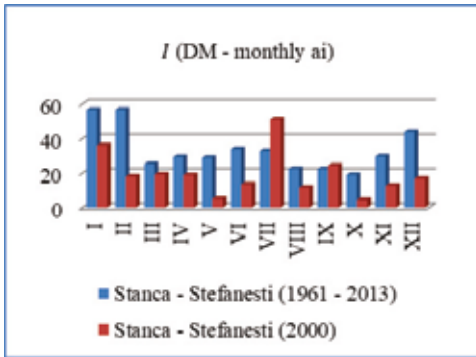


Figure 8. De Martonne monthly aridity index - Stanca-Stefanesti meteorological station

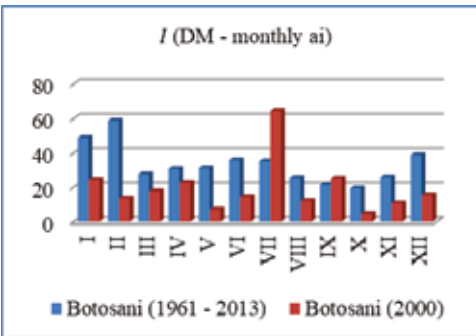


Figure 9. De Martonne monthly aridity index – Botosani meteorological station

Northeast Romania, with values of  $I_{R/\Delta T_0}$  between 0.6 and 0.8 is the second in terms of aridness intensity.

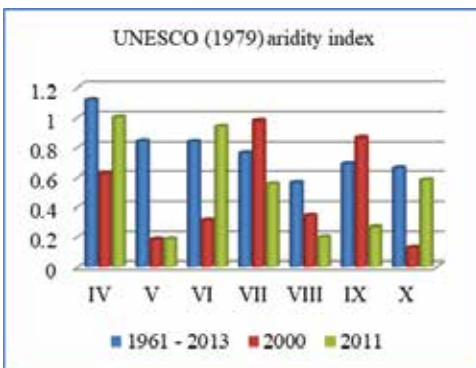


Figure 10. Monthly/multiannual values of  $I_{R/\Delta T_0}$  calculated with  $\Delta T_0 - PM$  (mm/mm) at Darabani meteorological station

After UNESCO classification, these belong to the wet class. In the north part (Figures 10, 11 and 12) the vegetation period of 2011 and 2000 was characterized by monthly values of the UNESCO (1979) aridity index lower than multiannual ones.

In this interval June made an exception  $I_{R/\Delta T_0} = 0.939 (> 0.838)$ . Both in 2011 and in 2000, the values corresponding to May  $I_{R/\Delta T_0} = 0.182$ ,  $I_{R/\Delta T_0} = 0.183$ , respectively, emphasize severe climatic conditions.

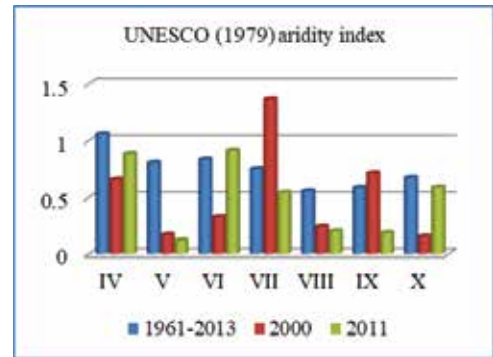


Figure 11. Monthly/multiannual values of  $I_{R/\Delta T_0}$  calculated with  $\Delta T_0 - PM$  (mm/mm) at Botosani meteorological station

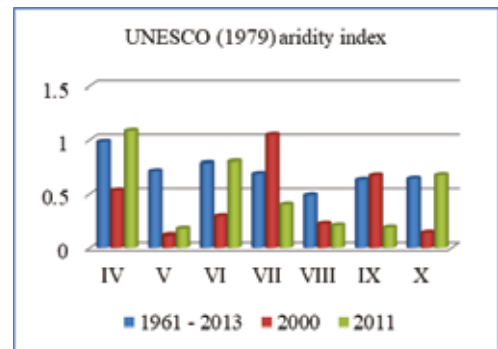


Figure 12. Monthly / multiannual values of  $I_{R/\Delta T_0}$  calculated with  $\Delta T_0 - PM$  (mm/mm) at Stanca-Stefanesti meteorological station

It can be observed that in 2000, May values are descending to the south  $I_{R/\Delta T_0} < 0.20$ , ranging from 0.096 to 0.083 at the Iasi and Barnova weather stations. Aridity extends over wide areas in May 2011, the indicators are

maintained in the same gap, less in the south of the region: at Iasi  $I_{R/ET_0}$  was 0.343, while at higher altitudes, at Barnova,  $I_{R/ET_0}$  reached 0.525 (Figures 13, 14 and 15).

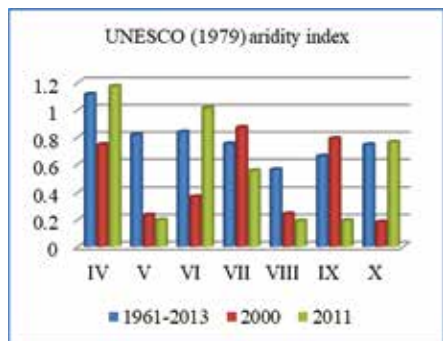


Figure 13. Monthly/multiannual values of  $I_{R/ET_0}$  calculated with  $P-T_0-PM$  (mm/mm) at Cotnari meteorological station

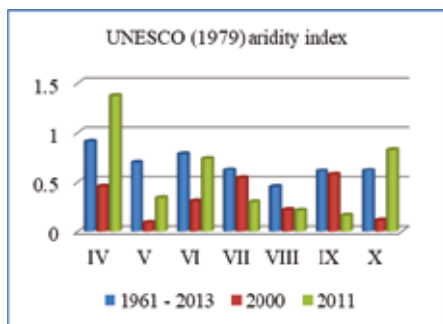


Figure 14. Monthly/multiannual values of  $I_{R/ET_0}$  calculated with  $P-T_0-PM$  (mm/mm) at Iasi meteorological station

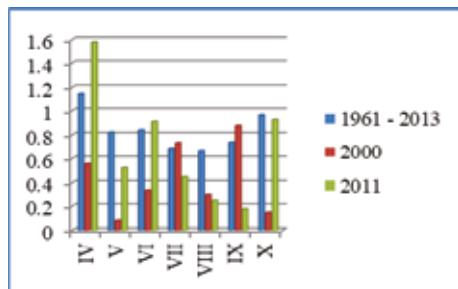


Figure 15. Monthly / multiannual values of  $I_{R/ET_0}$  calculated with  $P-T_0-PM$  (mm/mm) at Barnova meteorological station

Table 3. UNESCO (1979) aridity index - annual/multiannual values for northeastern Romania (mm/mm)

The analyzed period	Weather stations					
	Darabani	Botosani	Stefanesti-Stanca	Cotnari	Iasi	Barnova
1961-2013	0.972	0.927	0.892	0.964	0.850	0.967
2000	0.641	0.674	0.598	0.627	0.498	0.628
2011	0.597	0.565	0.535	0.633	0.536	0.670

Moldavian Plain is characterized by multi-annual values ranging from 0.85 and 1 (0.972 at Darabani meteorological station, 0.967 at Barnova) specific to the high hills that shape it in the north and southwest. 2011 was characterized by values ranging from 0.535 to 0.633 dry climate **under** wet conditions where  $I_{R/ET_0} = 0.670$  value influenced extensive areas with forest from the region.

Analyzing the annual water deficit, Paltineanu shows that the annual values between -200 to -300 mm cover the southern and central part of Moldavian Plateau, they descend to the north, ranging from -200 to -100 mm. For Barnova meteorological station, the multiannual value of this indicator is -109.4 mm, years with a deficit greater than -200 mm are: 1986 (-246.13 mm), 2000 (-232.2 mm) and 2011 (-203.2 mm). In the lower area of the county, in Iasi, the annual climate water deficit has a value of -149.55 mm between 1961 and 2013, significant values of -339 mm (2000), -310 mm (2011) and -304 mm (1994), are explained through the influence of the urban landscape on evapotranspiration and through the reduced amounts of rainfall. At Cotnari, multiannual value of this parameter is -110.45 mm and in the dry years 1986, 2000 and 2011 there were obtained -258.41mm, -236.10 mm, -234.91 mm respectively.

In Botosani County, the annual water deficit increases in the NW-SE direction and is between -114.98 at the Darabani and -127.81 at Botosani meteorological station. In the vicinity of Stanca-Costesti reservoir, the multi-annual average water deficit has the highest value, -155.038, consequence of the increased evapotranspiration values at the level of the cuvette.

## CONCLUSIONS

Northeastern Romania, Prut basin delimited by Oroftiana and Gorban, is influenced by a pluviometric regime with large monthly variations, specific to the transitional temperate continental climate. Excessively dry months, with a frequency over 20% and excessively rainy ones whose frequency is between 18.08% and 21.69%, lead to the frequent occurrence of the drought.

From the values of Topor aridity index a 67.60% frequency of droughts was obtained, most of them are moderate-dry years. Between 1997 and 2013 the multiannual average values of Topor aridity index and the number of the extreme months, from the pluviometric point of view, have grown. The territorial variation of their weight, proved an increased torrentiality in the region delimited by the Botosani, Stefanesti-Stanca and Cotnari sections.

The territorial distribution of the De Martonne aridity index stressed that northeastern Romania is characterized by values between 20 and 30 mm/°C, but in 2000 and 2011 were considerably lower. Values of UNESCO aridity index between 0.6 and 0.8 claim that this region is the second in terms of aridness intensity even if they belong to the wet class.

In the last years water has been a major limiting factor of the environment as a result of the steadily decreasing amount due to the pollution and its insufficient reserves according to the society requirements.

## ACKNOWLEDGEMENTS

This work was co-financed from Competitiveness Operational Program (COP) 2014-2020,

under the project number 4/AXA1/1.2.3. G/05.06.2018, SMIS2014+ code 119611, with the title “Establishing and implementing knowledge transfer partnerships between the Institute of Research for Agriculture and Environment - Iasi and agricultural economic environment”.

## REFERENCES

- Corduneanu, F., Vintu, V., Balan, I., Crenganis, L., Bucur, D. (2016). Impact of drought on water resources in north-eastern Romania, Case study - Prut River. *Environmental Engineering and Management Journal*, Iasi, 15(6), 213–1222.
- Minea, I., Stanga, I. C. (2004). *Evaluarea perioadelor secetoase în Campia Moldovei. IC.DMP.1* (pp. 131–142), „Gh. Asachi” Tehnical University Iasi, Edit. Performantica.
- Monteith, J. L. (1965). Evaporation and the environment, in the state and movement of water in living organisms. XIX<sup>th</sup> Symposium Soc. For Exp. Biol., Swansea, Cambridge University Press: 205–234.
- Paltineanu, Cr., Mihailescu, Fl. I., Secoleanu, I., Dragota, C., Vaseniuc, F. (2007). *Ariditatea, seceta, evapotranspiratia si cerintele de apa ale culturilor agricole în Romania*. Editura Ovidius University Press, Constanta.
- Paltineanu, Cr., Chimu, E. (2007). Relationships between De Martonne aridity index and water requirements of some representative crops: A case study from Romania. *International Agrophysics*, 21(10).
- Romanescu, Ghe., Zaharia, C., Paun, E., Machidon, O., Paraschiv, V. (2014). Depletion of watercourses in north-eastern Romania. Case study: The Mileitin River. *Carpathian Journal of Earth and Environmental Sciences*, 9(1), 209–220.
- Stanga, C.I. (2009). Quantifier la sécheresse. Durée, intensité, fréquence. *Scientific Annals, Geography Series*, “Al. I. Cuza” University Iasi.

## DEGRADATION OF VEGETAL COVER THROUGH INAPPROPRIATE GRAZING ON LANDS ARRANGED WITH DRAINAGE WORKS

Minodora AILENEI (RADU)<sup>1</sup>, Oprea RADU<sup>1</sup>, Daniel BUCUR<sup>1</sup>,  
Razvan Ionut TEODORESCU<sup>2</sup>

<sup>1</sup>University of Agricultural Sciences and Veterinary Medicine of Iasi, 3 Mihail Sadoveanu Alley, Iasi, Romania

<sup>2</sup>University of Agronomic Sciences and Veterinary Medicine of Bucharest, 59 Marasti Blvd, District 1, Bucharest, Romania

Corresponding author email: aminodora2004@yahoo.com

### Abstract

*The improvement of the conditions of plant growth and development and raising the productive capacity of soils following the application of hydro and agropedoameliorative works, allowed the cultivation of large areas of land with grazing and hay fields and the possibility of cultivating a wide range of agricultural plants. This paper presents a study carried out on a surface arranged with drainage works with the current use of grazing field and exploited as arable between 1978 and 1992. Repeated and uncontrolled passing of the animals over the channel network through unarranged areas led to the acceleration of the bank erosion and the strong clogging of the channels with negative influence on the functional efficiency of the drainage network. The non-rational grazing, both on the overwet soil and over the periods affected by water deficiency, caused the destruction of the vegetal cover. The prolongation of humidity excess and water stagnation in microdepressions formed on the drained surface favoured the installation of low-quality hygrophilous vegetation.*

**Key words:** clogging channel, drainage works, inadequate grazing, vegetal cover.

### INTRODUCTION

Soil resources, together with the other environmental components, are directly or indirectly involved in all the aspects of the development process, and play an important role in the economic power of any country, at all levels of development (Rauta C. et al., 1998).

Increasing food demand in direct proportion to population growth has imposed either the expansion of cultivated areas or the modernization and intensification of agriculture.

The problem of increasing the productive potential of the soil lies mainly in regions where it is very low, namely in areas either with shortage of humidity or those with excess, regions in which, unfortunately, it is recorded in most cases severe shortage of food.

Excessive humidity is one of the major soil fertilities limiting factors, as it is able to diminish considerably and sometimes even completely destroy the productive capacity of the land.

The grassland is the major resource of the biosphere that sustains the life of around one

billion people around the world. With the development of agriculture and means of production, human intervention in natural grasslands ecosystems has progressively increased (Schnyder H. et al., 2010).

In Romania, grasslands cover about 33% of the agricultural area (Statistical Yearbook, 2017) and form the basis of a strong growing sector of ruminants and are an essential element of sustainable farming systems that meet the demands of healthy and high-quality food.

The quantity and quality of feed is largely influenced by soil nutrients and the amount of precipitation and their distribution. The creation of anaerobic conditions in wet soils leads to the production of toxic gases such as hydrogen sulphide and carbon dioxide that drastically affect the growth of roots (Van Der Woude B.J. et al., 1994).

By the roots of grasslands feeding plants, which act as a binder in the presence of organic matter, the process of destroying the granular soil structure is stopped, in most cases leading to their improvement (Mocanu V. et al., 2013; Marusca T. et al., 2013; Simtea N. et al., 1990).

## MATERIALS AND METHODS

The investigations were carried out in the middle part of Moldova watershed, Suceava County, located in the NE of the Oriental Carpathians and NV of the Moldavian Plateau. The watershed of Moldova River is framed by the meridians  $25^{\circ}08'37''$  -  $26^{\circ}58'35''$  East longitude and the parallel  $46^{\circ}55'37''$  -  $47^{\circ}43'38''$  Northern latitude.

The studied area is crossed by the  $8.2^{\circ}\text{C}$  isotherm. The medium annual rainfall is 625.6 mm. The precipitations are characterized by an uneven distribution for months and seasons, and by large amounts recorded in 24 hours and 1-5 consecutive days.

Natural conditions favour the appearance and maintenance of excess moisture in the soil and the water stagnation on the surface of land. The flood plain of Moldova river and the terraces with width of 1.5 km, small slopes ranging from 1-5%, with flat areas and many microdepressions, facilitate the moisture excess in the soil and water stagnation on the land (Moca V. et al., 1977).

In order to increase the productive capacity of the lands, the surface and subsurface drainage system Rotopanesti-Radaseni-Fantana Mare was laid out, between 1978 and 1980, with an area of 5527 ha of which 1806 ha with underground drainage works (Figure 1).

The studied area is located in the north-eastern part of the Rotopanesti-Radaseni-Fantana Mare drainage system and is lengthwise crossed by the main collector Somuzel (Figure 2).

The land laid out with underground drainage works is relatively flat and has been exploited as arable from the setting up (1980) until 1992. Since then, the studied area went to the use prior to the layout, namely the grassland one.

In order to reveal the degradation of the vegetal cover, observations were made on the laid-out surface and on the channel network, and topographical measurements were made on which transverse and longitudinal profiles were made.

The process of identifying grassland areas affected by excess humidity was conducted through observations on the floral composition.

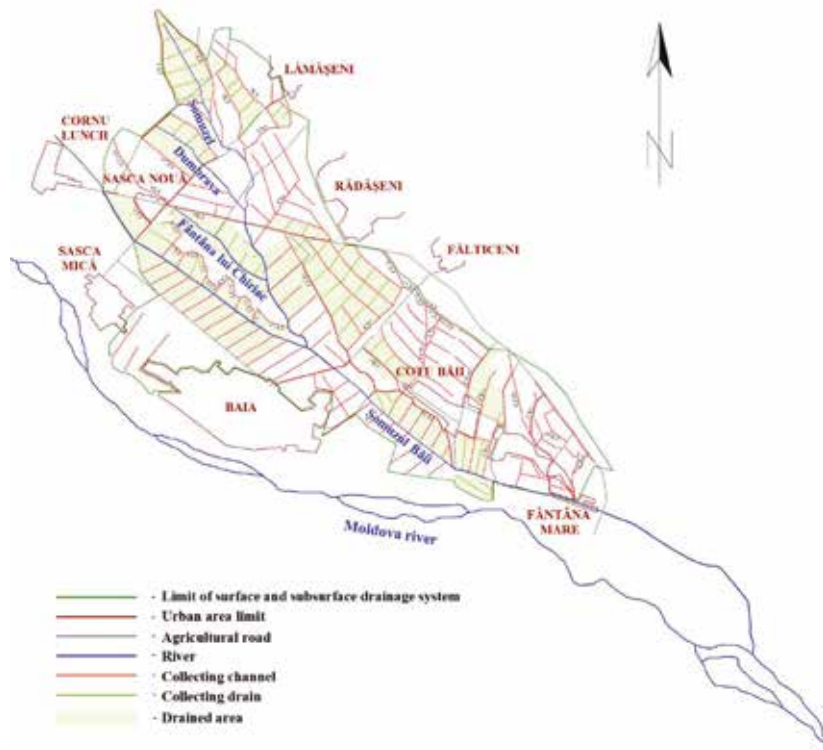


Figure 1. Surface and subsurface drainage system Rotopanesti-Radaseni-Fantana Mare

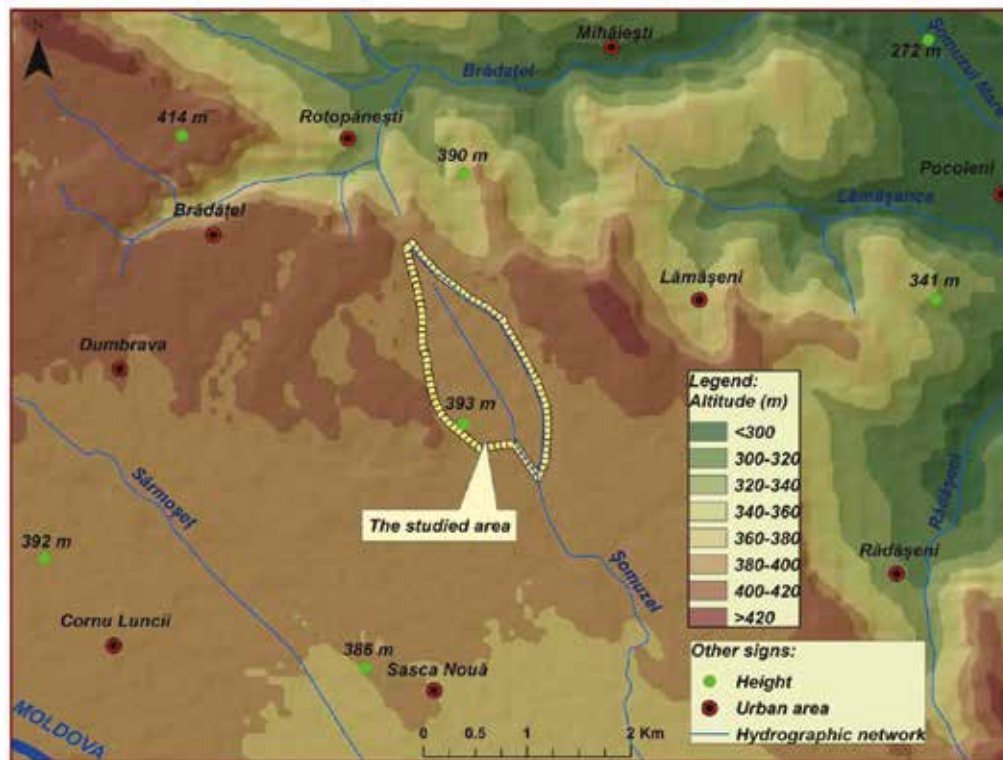


Figure 2. Location of the studied area

## RESULTS AND DISCUSSIONS

Rational grazing on laid-out areas with draining works requires the observance of grazing rules related to the optimal beginning of grazing and the layout of special constructions.

On the passing of the drained surface from arable use to pasture use, no layout was made for the animals crossing the Somuzel collector channel and the two belt channels, protecting the drained surface by intercepting leaks in the higher boundary areas.

Successive crossings and grazing on the channel section with moist soil accelerated shore erosion and clogging the drainage network (Figure 3).

The clogging of belt channels of approximately 75% does no longer ensure the interception and transport of water coming from the higher perimeter areas. In the spring, on the melting of

snow and over periods of abundant precipitations fallen within 1-5 consecutive days, the accumulated waters overflow, flooding the drained surfaces (Figure 4).

The clogging of the Somuzel collector channel has led to the clogging of the discharge outlet of the collector drains and their decommissioning (Figure 5). The repetitive and uncontrolled passage of animals over the channel network through unscheduled places led to clogging on the sections and the creation of back slopes that favoured water stagnation and sedimentation of alluvium.

The layout of a dam on the Somuzel collector channel for the accumulation of water for watering the animals accelerates the erosion and clogging of the channel and favours the prolongation of the excess moisture in the adjacent area (Figure 6).

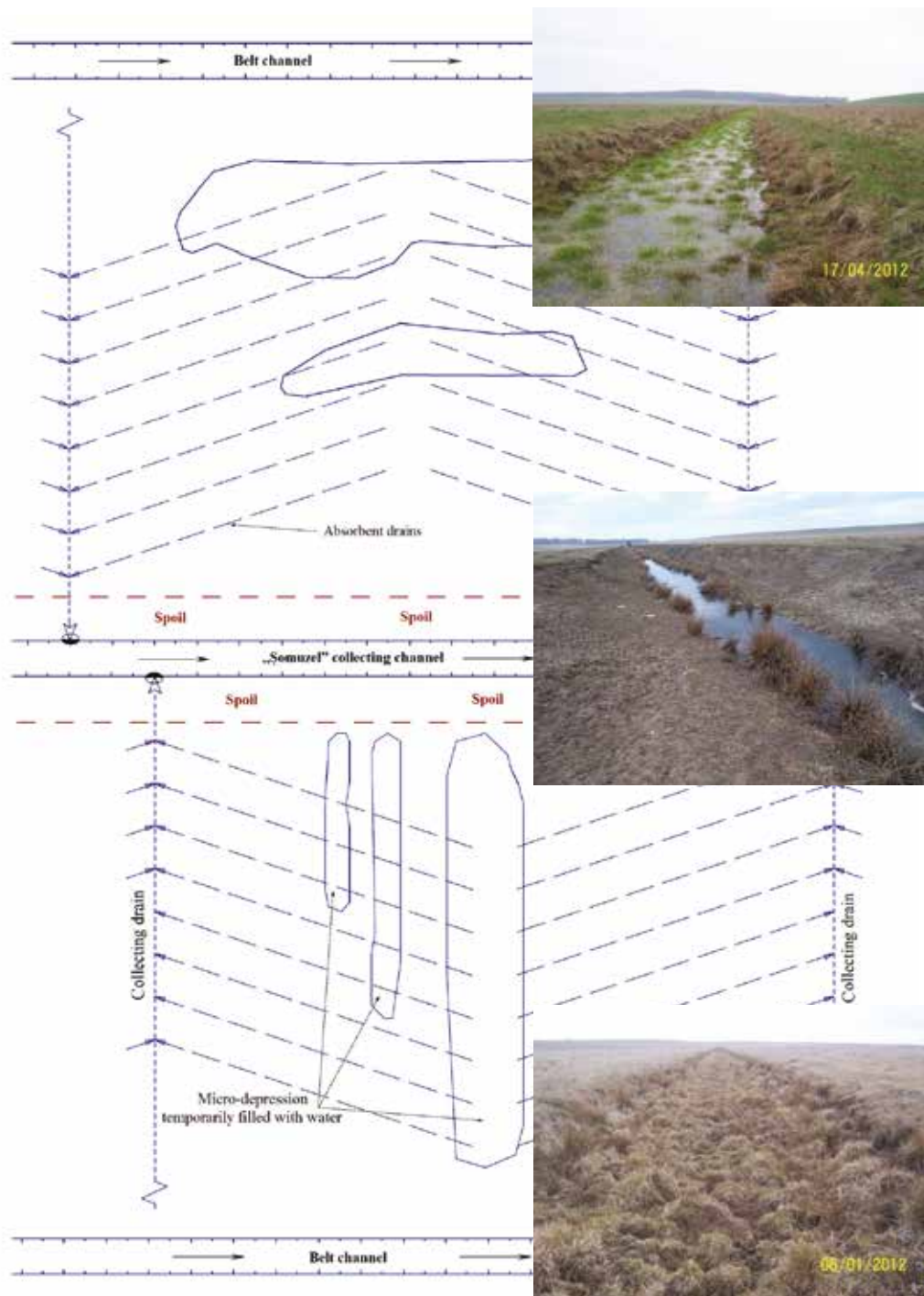


Figure 3. Draining layout scheme and current channel state



Figure 4. Water overflow on the drained surface



Figure 5. Drain holes to clogged



Figure 6. Arranging watering holes on the Somuzel collecting channel

The decommissioning of the drainage network through the clogging of the discharge outlets favoured water stagnation in the micro-depressions formed on the drained surface (Figure 7). These microdepressions formed during the exploitation period as arable land have expanded due to the stagnation of the water for a long time, the settling of the surface planted and the soil's kneading by animals

during grazing. The gradual increase in water stagnation is due to greater susceptibility of soils to softening with excess moisture. The flat lands situated at the base of the slopes between the two ring channels are most affected by the spring rains that coincide with the melting of snow. The water cannot leak to the surface of the soil and the drainage does not

occur due to the discharge outlets of the destroyed and clogged collector drains.

Water stagnation is also favored by the landfill sites resulted from the excavation of the

channels that have been leveled along the canals over a width of about 20 m, the resulting platforms having a height of up to 0.50 m (Figure 8).



Figure 7. Water stagnation in microdepressions



Figure 8. Landfill sites modelling along channels

According to the Methodological Norms for the application of the provisions of Government Emergency Ordinance no. 34/2013 on the organization, management and exploitation of permanent grasslands and amendment and supplement of the Land Fund Law no. 18/1991, article 6, paragraph 1 - the introduction of animals into grasslands is allowed only during the grazing period provided for in the pastoral arrangement, and paragraph 2 stipulates that: "grazing is forbidden in the case of excess humidity of the grassland" (Vintu V. et al., 2017).

In the early phase of vegetation, the plants on the grazing fields have special organoleptic (taste, odour) attributes that increase the appetite of the animals and thus increase the degree of consumption of grass that can reach

85-95%. If grazing starts too early, when plants that are too young and the soil that is too wet destroy the celery layer, the soil is struck and soil air is getting worse. Pits and heaps are also formed (Figure 9), and young plants with reduced foliar surface use for their restoration reserve substances accumulated in the organs in the soil, which lead to their exhaustion.

Excessive grazing when soil is moist makes the vegetable cover be destroyed by clogging.

The wetter soil becomes, the lower the ability to withstand compaction and subsidence is, causing the asphyxiation of plants.

In addition, in areas whose celery layer is kneaded, over periods with shortage of water the vegetation suffers from the poorly developed root system and excessive grazing destroys the vegetal cover.



Figure 9. Destroyed vegetational cover

As a result of inadequate grazing in periods of the moist soil but also when the soil is dry, the clogging of the channel network and the discharge outlets of the collector drains, water stagnation in microdepressions, the interference of the surface water leakage by landfills deposited along the channels, the use of drainage channels as water troughs, the studied permanent grazing fields have made important changes in the floral composition of the vegetational cover.

Thus, valuable, more demanding species of water, air, and soil have disappeared from large areas and have been replaced by hydrophilic

species with very low fodder value: *Carex caryophylla*, *Carex praecox*, *Juncus trifidus*, *Juncus effusus*, *Agrostis stolonifera*, *Ranunculus repens*, *Ranunculus acris*, *Ranunculus sceleratus*, *Glyceria maxima*, *Glyceria frutans*, *Galega officinalis* and *Trifolium fragiferum* (Figure 10).

The degradation of the grazing field is manifested both by destroying the vegetational cover and by changing its floral composition. The well finished and good-quality vegetational cover is only found in the higher areas, including the landfill area, unaffected by the presence of excess moisture.



Figure 10. Hydrophilic vegetation

Due to the inappropriate operation of the draining network, water from snow melting stagnates by up to 15-20 days longer, which has a negative effect on the growth of the grass cover. Excessive grazing until late autumn with sheep and the delay of spring plant growth does not allow the restoration of the vegetational cover.

Repeating this cycle year after year has led to the degradation of large grazing fields. For the restoration of the vegetational cover, it is necessary to start grazing later, to interrupt the grazing by at least 3-4 weeks before the first frost and to perform the rehabilitation works of the draining network.

## CONCLUSIONS

Repeated crossing of animals through unscheduled places, grazing and watering on the channel section accelerate shore erosion and clogging of the drainage network.

The clogging of channels and obstruction of discharge outlets leads to the decommissioning of drainage network, stagnation of water in microdepressions and prolongation of excess moisture, changing the floral composition of pastures by replacing valuable species with low-quality hydrophilic species.

Grazing over periods of moist soil causes the soil to knead and compact, and the vegetal cover is destroyed by clogging, causing asphyxiation of the plants. In addition, over periods with water scarcity, vegetation in the areas with kneaded soil suffers from the poorly developed root system.

The degradation of the vegetal cover due to soil kneading by grazing depends on factors such as soil physical properties, soil moisture content, animal number and size, grazing duration and grazing field coverage.

The measures necessary for the recovery of the grasslands with the destroyed vegetal cover consist in the rehabilitation of the draining systems, the upturning of the grazing fields and the sowing and the elaboration of a grazing arrangement. The widespread application of such large-scale measures is unlikely due to the lack of support and financial resources. In this situation, the authors recommend concentrating the efforts of local authorities to facilitate the leakage of water to the surface by making trenches, the unclogging of discharge outlets of collecting drains, banning grazing in moist soil areas and the interruption of grazing by at least 3-4 weeks before the first frost.

## ACKNOWLEDGEMENTS

This work was co-financed from Competitiveness Operational Program (COP) 2014 -

2020, under the project number 4/AXA1/1.2.3. G/05.06.2018, SMIS2014+ code 119611, with the title "Establishing and implementing knowledge transfer partnerships between the Institute of Research for Agriculture and Environment - Iasi and agricultural economic environment".

## REFERENCES

- Marusca, T., Pop, O. G. (2013). *Gospodaria durabila a pajistilor din zona rurala montana*. Editura Universitatii Transilvania, Brasov.
- Moca, V., Vaisman, I., Vieru, I., Nitu, T. (1977). Cercetari privind punerea in valoare prin lucrari de drenaj-desecare a solurilor cu exces de umiditate din depresiunea Baia-Sasca (Bazinul raului Moldova). *Publicatiile Societatii Nationale Romane pentru Stiinta Solului*, Craiova, România, vol. 16 C, 241-251.
- Mocanu, V., Hermenean, I. (2013). *Mecanizarea lucrarilor agricole pe pajisti. Tehnologii, masini si echipamente*. Editura Universitatii Transilvania din Brasov.
- Rauta, C., Carstea, St., Tuhai, A. (1998). Elemente fundamentale ale strategiei dezvoltarii agriculturii durabile. Bucuresti, 52-57.
- Schnyder, H., Taube, F., Isselstein, J. (2010). Foreword of Grassland in a changing world. European Grassland Federation, Kiel, Germany.
- Simtea, N., Cardasol, V., Craciun, St., Boldea, Gh. (1990). *Reinsamantarea si suprainsamantarea pajistilor*. Intreprinderea Poligrafica, Deva.
- Van Der Woude, B. J., Pegtel, D. M., Bakker, J. P. (1994). Nutrient limitation after long-term nitrogen fertilizer application in cut grasslands. *Journal of Applied Ecology*, 31(3) (Aug., 1994), 405-412. Published by: British Ecological Society DOI: 10.2307/2404438, <https://www.jstor.org/stable/2404438>
- Vintu, V., Samuil, C., Stavarache, M. (2017). *Cultura pajistilor si a plantelor furajere. Indrumator de lucrari practice*. Editura „Ion Ionescu de la Brad” Iasi, 152-156. ISBN: 978-973-147-265-2.
- \*\*\*2013 – Ordonanta de Urgenta a Guvernului Romaniei nr. 34/2013 privind organizarea, administrarea si exploatarea pajistilor permanente si pentru modificarea si completarea Legii fondului funciar nr. 18/1991

## EUROPEAN UNION STRATEGY AND CROSS-BORDER COLLABORATION - OPPORTUNITIES FOR CITIZENS IN THE LOWER DANUBE REGION

Cristiana SIRBU

University of Agronomic Sciences and Veterinary Medicine of Bucharest,  
59 Marasti Blvd, District 1, Bucharest, Romania

Corresponding author email: [cris\\_sirbu@yahoo.com](mailto:cris_sirbu@yahoo.com)

### Abstract

*2018, a year of multiple significance like: the celebration of the 100th anniversary of the proclamation of the Union of Bessarabia with Romania, the 8th anniversary of adoption of the European Union Strategy for the Danube Region, and the completion of ten years since Romania and Austria launched the initiative to set up a European strategy dedicated to the development of the Danube macro-region, it is necessary to highlight the opportunities that this strategy can bring, as well as the importance of cross-border cooperation between neighboring countries. The paper presents the opportunities for the Danube area and for our country as well, opportunities that can be brought by a good cross-border collaboration and respecting the principles of the European Union Strategy for the Danube Region.*

**Key words:** cross-border collaboration, Danube Region, development, European Union Strategy, opportunities.

### INTRODUCTION

The year 2018 has a triple significance, first of all, the celebration of the 100th anniversary of the proclamation of the Union of Bessarabia with Romania, and the 8th anniversary of the adoption in December 2010 of the European Union Strategy for the Danube Region, as well as the fact that Romania will take over the SUERD Presidency from November 2018 to October 2019.



Figure 1. The area covered by the EU Strategy for the Danube Region stretches from the Black Forest (Germany) to the Black Sea

We also can add ten years since Romania and Austria (June 2008) launched the initiative to set up a European strategy dedicated to the development of the Danube macro-region, one of the successful projects promoted by our country at the level The European Union.

### MATERIALS AND METHODS

The Danube, the second largest river in Europe, traverses approximately 2850 km, linking the Black Forest to the Black Sea, crossing ten countries and having tributaries of four more.

Following the example of the EU Strategy for the Baltic Sea Region, the first such macro-regional approach, the EU Strategy for the Danube Region was based on the efforts of stakeholders in the region, allowing them to create a region where all 115 million inhabitants would enjoy security, prosperity and equal opportunities.

The EU Strategy for the Danube Region is a model of regional cooperation at European level.

More than one third of EU citizens live and work in the border regions of Europe.

Borders have a direct and indirect impact on their lives.

European territorial cooperation plays an important role in removing obstacles and fostering cross-border cooperation.

Although relatively few of them have a budget, Interreg projects have represented countless concrete achievements for citizens in different areas, including:

- border security;
- transport;
- education;
- energy;
- health;
- training or job creation;
- agriculture.

Over 2014-2020, more than € 10 billion will be invested in cooperation between regions, of which about € 6.6 billion will be directed to border regions. This should ensure maximum impact and better use of investment.

The current socio-economic context of the Danube region is the result of a multitude of factors including:

- demographic factors;
- education and training levels;
- salary and unemployment levels;
- general level of economic activity and economic structure by sectors;
- activity level and SME promotion;
- local fiscal framework;
- foreign investment, including investment in agriculture, etc.

For Romania, the consolidation of Danube cooperation remains a priority given that the potential for sustainable development of the region is considerable and we want to contribute to transforming the Danube into a backbone of the European space as part of the Rhin-Main-Danube axis.

The problems we face are numerous and the dimensions of regional cooperation are multiple:

- transport;
- energy;
- tourism;
- agriculture;
- environment.

The economic and social development of the Danube region must be sustainable and comply with the environmental acquis.

Romania supports this approach as it manages most of the Danube Delta reservation.

Climate change, the need to protect localities against natural disasters and national parks in the Danube region are extremely important aspects to be addressed in the current strategy. The projects under this strategy can be supported financially by developing strong synergies between different EU policies:

- cohesion;
- transport;
- tourism;
- agriculture;
- fishing;
- social and economic development;
- energy;
- environment;
- neighbourhood and enlargement policy.

Delta's population has a lifestyle unchanged for centuries. Discrete human implantation has allowed the survival of stunning ecosystems in the Delta.

The large water spell explains the small number of inhabitants. Fisheries are a constant human activity in the region. Renewal of reed and poppy crops is another branch of human activity. Some people have crops, others livestock husbandry.

Navigation on the Danube branches and canal transport is another concern for locals. Agriculture remains a vital sector for the Danube region, which includes 5.07 million hectares of agricultural land - tillable land, pastures, meadows and orchards, accounting for 34.5% of the total agricultural area at national level.



Figure 2. Fishing in the Danube Delta

Of the agricultural land area, over half are indigestible and drained agricultural land. As regards the use of agricultural land, the largest share is the tillable land, followed by natural meadows. The vineyards and orchards occupy insignificant areas, which are usually located in

the village hearts, on the private plots of the inhabitants.

Regarding the structure of agricultural crops, we can see the share of straw cereals, corn and flax, the other crops (oil flax, vegetables and fodder on their own farm) occupying a smaller surface area.

*Cultivated melons and fodder plants.* The agricultural land on the coast, the shores of the shore and the delta in free floods are occupied with pastures and small arable land, traditionally exploited by the local population, most of which are livestock breeders and small producers of cereals, vegetables and fodder.

In the development regions that comprise the counties of the Danube region, namely the:

- South-East,
- South-Muntenia,
- South-West Oltenia,

regions where agriculture, hunting and fish farming have a higher share in regional gross domestic product than the share of agriculture in Romania's gross domestic product.

Supporting the sustainable development of fisheries areas and improving the quality of life in these areas, creating opportunities for alternative income for fishermen, developing specific infrastructure, training qualified personnel, providing endowment with specific exploitation and processing equipment, and encouraging partnerships to be set up are important actions in the new Strategy.

## RESULTS AND DISCUSSIONS

The multifunctional role of agriculture in ensuring food security, employment in rural areas, ensuring a fair standard of living for farmers and mitigating the effects of climate change is strongly emphasized.

The European Union Strategy for the Danube Region sets the foundations of the European agricultural model, characterized by viable exploitation structures close to the market, along with rural development and environmental protection.

It is desirable to create sustainable and competitive communities through the use of resource efficiency, promoting profitable initiatives and opportunities offered by the development and horizontal cross-flows on the Danube-Black Sea corridor by:

- improving the planning, development and coordination of cross-border transport systems in order to ensure better connections to the TEN-T network;
- increasing safety on inland waterways and maritime transport;
- improving the sustainable use of natural resources and heritage;
- improving the sustainable management of ecosystems in the border area;
- improving risk management in the common border area;
- encouraging cross-border integration in terms of employment and labour mobility;
- cooperation has increased the capacity and efficiency of public institutions in the context of cross-border cooperation.

The Cross-Border Cooperation Program between Romania and Bulgaria for the period 2014-2020 comprises seven counties in eight districts in Bulgaria and Romania, which are mostly composed of municipalities.

In the cross-border cooperation area, a new, flexible and improved transport system with intermodal connections is needed.

The Ecological Initiative and Sustainable Development Group is a partner in the cross-border cooperation project between Romania and Bulgaria on Priority Area 1: A Well-Connected Region, "Investigation of opportunities for reducing the TEN-T network use within the cross-border region Romania-Bulgaria through optimization of the freight and passenger transport and the development of a joint mechanism for support of the intermodal connections".

The total budget of the project is 1428765.75 euro, of which the ERDF 1214450.87 euro, the contribution from the state budget (Romania and Bulgaria) of 185739.54 euro and the own contribution of the beneficiary of 28575.32 euro.

## CONCLUSIONS

The project addresses the issues of accessibility, efficiency, ecology and safety of the CBC transport system, improving the planning, development and coordination of cross-border transport systems for a better

connection to the TEN-T network. This is done by investing in a joint study, planning and adoption of strategic documents on optimizing the transport system through improved intermodal interconnections in the CBC area.

The main objective of the project is to significantly improve the planning, development and coordination of CBC transport systems for a better connection with the TEN-T network in the CBC area.

The documents elaborated within the project will be presented and handed over to all interested parties - public authorities to change transport planning and policy, transport professionals, businesses and the non-governmental sector.

Smart, faster, safer and greener intelligence transport and communications are essential conditions for economic development.

#### **ACKNOWLEDGEMENTS**

This research was conducted by the University of Craiova - Faculty of Mechanics, SC IPA SA, M&A Expert Contab SRL and The Ecological Initiative and Sustainable Development Group for the Preliminary study on the current state of the European Union strategy and cross-border cooperation on opportunities for citizens in the

Lower Danube Region, Project INTERREG V-A Romania Bulgaria Programme “Investigation of opportunities for reducing the TEN-T network use within the cross-border region Romania-Bulgaria through optimization of the freight and passenger transport and the development of a joint mechanism for support of the intermodal connections”.

#### **REFERENCES**

- Centre for Road Engineering and Computer Science - The National Road Traffic Management Company Romanian Ministry of Transport, Statistical data, 2014-2019.
- Interreg V-A Romania-Bulgaria Programme, Application form Directorate for Driving and Vehicle Registration, Statistics Data, 2014-2019.
- University of Craiova, The Ecological Initiative and Sustainable Development Group, Preliminary study on the current state of the European Union strategy and cross-border cooperation on opportunities for citizens in the Lower Danube Region, Project INTERREG V-A Romania-Bulgaria Programme “Investigation of opportunities for reducing the TEN-T network use within the cross-border region Romania-Bulgaria through optimization of the freight and passenger transport and the development of a joint mechanism for support of the intermodal connections”, 2016-2019.

## TREND ANALYSIS IN TEMPERATURE, PRECIPITATION AND HUMIDITY: THE CASE OF MEDITERRANEAN REGION

Ali YÜCEL<sup>1</sup>, Atilgan ATILGAN<sup>2</sup>, Hasan ÖZ<sup>2</sup>

<sup>1</sup>Osmaniye Korkut Ata University, Osmaniye Vocational School, 80000, Osmaniye, Turkey

<sup>2</sup>Isparta University of Applied Sciences, Faculty of Agricultural Sciences and Technologies, Agricultural Structures and Irrigation, 32260, Isparta, Turkey

Corresponding author email: atilganatilgan@isparta.edu.tr

### Abstract

*Temperature and precipitation values are important parameters of climate change. Therefore, studies on meteorological data are important and such studies are increasing. The Mediterranean region, where agriculture has been intensified as a study area, has been selected. Long-term temperature, precipitation and humidity values of the provinces in the study area were used as material. The measurement range of meteorological data covers the period between 1950 and 2018. Linear regression analysis (LRA) and Spearman trend test (STT) were applied to determine climatic changes in these values. According to the results of linear regression analysis and Spearman trend test, it is determined that the most changes in long-term daily temperatures are in Isparta, Mersin, Burdur, Adana, Antalya, Kahramanmaraş and Osmaniye provinces. The provinces with relative humidity changes were determined as Isparta, Burdur, Mersin, Adana and Antalya. As a result, these and similar studies have shown that it can play an important role in the planning of agricultural crop cultivation areas.*

**Key words:** Mediterranean, precipitation, temperature, trend analysis.

### INTRODUCTION

Water and energy are critical parameters for agricultural activities. The regular application of water related activities in agriculture can be possible only by way of sufficient rainfall (Ülke & Özkoca, 2018).

The demand for water in our day is rapidly increasing with increasing population and accordingly the efforts to increase agricultural products and industrialization (Bahadır, 2011; Saplıoğlu & Çoban, 2013).

The changes and differences that take place in the atmosphere brought about changes in temperature and rainfall which make up the main elements of climate.

While the variations in climate are reflected differently in different regions of the world, different scientific communities are carrying out studies on this issue (Bahadır, 2011).

The changes in climate may emerge as significant changes in average temperatures in different regions of the world but they also include changes in rainfall. It is stated that the increases and decreases in the amount of rainfall are proofs of climate change. Rainfall is indicated to be a factor of climate system that

changes the most subject to time and location (Karabulut et al., 2008).

Changes in climate have an impact on many sectors and hence they also affect the agriculture and food sectors. Dependence on nature is inevitable for agricultural activities no matter how developed technology becomes since they are carried out in and subject to nature (Bayraç & Doğan, 2016). Rainfall and temperature are especially indicated as climate parameters with an influence on agriculture (Demir et al., 2017). Since agriculture is an economic activity, changes in production due to climate change are important for the country as well as for international commerce. Agriculture is affected by the climate but is also considered as a field of activity that causes climate change. Agricultural activities such as irrigation, soil tillage, fertilization, use of pesticides and misuse of agricultural lands, energy consumption, animal-based production all increase the release of greenhouse gases to the atmosphere. Therefore, it is stated that the greenhouse gases released as a result of such activities result in global warming and climate changes (Başoğlu, 2014; Bayraç & Doğan, 2016).

It is estimated that more intensive and longer draughts will take place in our country with the increase of global warming. Hence, both water resources and agricultural activities subject to rainfall may be affected adversely (Ülke & Özkoca, 2018). Studies carried out until today on climate factors report that temperatures have increased, especially in recent years while rainfall is decreasing (Demir et al., 2017). Many researchers carry out trend analyses especially on rainfall and temperature and emphasize issues of global warming and climate change (Türkeş et al., 2002; Karabulut et al., 2008; Karabulut, 2012; Bahadır, 2011; Demir et al., 2017; Yüce & Ercan, 2017; Ülke & Özkoca, 2018).

The purpose of this study was to evaluate using Linear Regression Analysis and Spearman Trend Test the long-term temperature, rainfall and humidity values recorded at meteorological stations in different cities in the Mediterranean

Region for determining the changes in these parameters.

## MATERIALS AND METHODS

In the study, the Mediterranean Region, where agricultural activities especially greenhouses production are carried out intensively, is determined as a research area. There is a total of 8 provinces in the region and the data obtained from the General Directorate of State Meteorological Affairs of these provinces were used. These data; long term daily maximum ( $T_{MAX}$ ), average ( $T_{AVE}$ ), minimum ( $T_{MIN}$ ) temperature values, daily maximum ( $P_{MAX}$ , mm), average ( $P_{AVE}$ , mm), annual total ( $P_T$ , mm) precipitation values and maximum ( $RH_{MAX}$ , %), average ( $RH_{AVE}$ , %), minimum ( $RH_{MIN}$ , %) relative humidity values were used as material. Some features of the meteorological stations of the provinces in the Mediterranean region are given in Table 1.

Table 1. Some features of meteorological stations

Meteorological stations	Period duration (years) (n)	Height (H, m)	Latitude-North (E, °)	Longitude-East (B, °)
Adana	1950-2018 (69)	23	37°0041'	35°3443'
Antakya (Hatay)	1950-2018 (69)	104	36°2048'	36°1513'
Antalya	1950-2018 (69)	64	36°9063'	30°7990'
Burdur	1950-2018 (69)	957	37°7220'	30°2940'
Isparta	1950-2018 (69)	997	37°7848'	30°5679'
Kahramanmaraş	1959-2018 (60)	572	37°5760'	36°9150'
Mersin	1950-2018 (69)	7	36°7808'	34°6031'
Osmaniye	1986-2018 (33)	94	37°1021'	36°2539'

Researchers have developed various parametric and non-parametric methods in order to determine whether the trend changes occurring during the observation period (temperature, precipitation, etc.) are in the direction of increasing or decreasing. In this study, parametric LRA and nonparametric STT which is the most widely used trend method are preferred.

**Linear Regression Analysis (LRA).** It is called as the method that presents the causal relationship between two variables as dependent variables and independent variables with a linear model (Helsel and Hirsch, 1993; Hamdi et al., 2009; Shammugasundram, 2012). The following is expressed by simple equality:

$$Y = a + bX \quad (1)$$

Where: Y is the dependent variable, X is the independent variable, whereas a and b are equation regression coefficients (Haan, 1977; Sneyers, 1990; Kundzewicz and Rodson, 2000; Xu, 2002; Önöz & Bayazit, 2003).

**Spearman Trend Test (STT).** It is one of the nonparametric trend tests. It is a quick and simple test used to determine whether there is an important trend between the values of the observations. Calculated in the following equations (Sneyers, 1990; Helsel & Hirsch, 1993):

$$R_{sp} = 1 - \frac{6 * \sum_{i=1}^n D_i^2}{(n^3 - n)} \quad (2)$$

$$r = R_{sp} * \sqrt{\frac{n-2}{n}} \quad (3)$$

Where:

- n total observation order,
- i chronological rank number,
- $D_i$  difference between rank (Kendall, 1975; Sneyers, 1990; Gauthier, 2001).

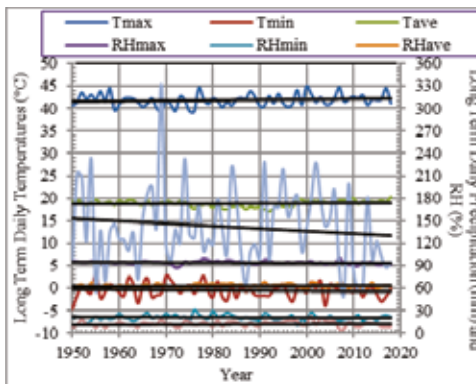
## RESULTS AND DISCUSSIONS

Parametric and non-parametric trend methods were preferred for determining the increase or decrease trends over time for the values of

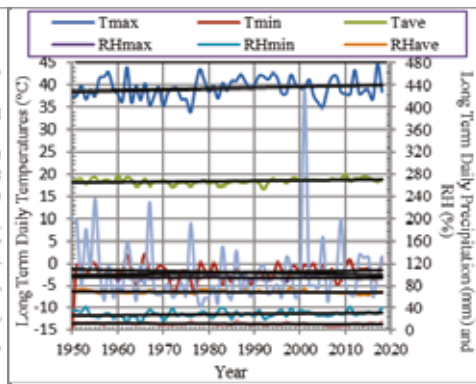
temperature ( $T_{MAX}$ ,  $T_{MIN}$  and  $T_{AVE}$ ), rainfall ( $P_{MAX}$ ,  $P_{AVE}$ ,  $P_T$ ) and relative humidity ( $RH_{AVE}$ ,  $RH_{MAX}$ ,  $RH_{MIN}$ ) used as meteorological variables in the study.

Figure 1 shows the graphic depiction for the meteorological variables for which a trend is determined in the cities as a result of the evaluations carried out according to LRA. Long term annual total rainfall variable trend in the studying area is presented in Figure 2.

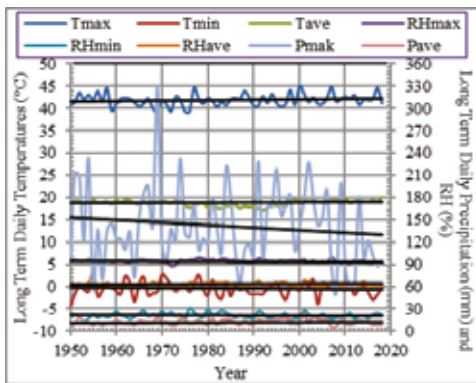
Adana



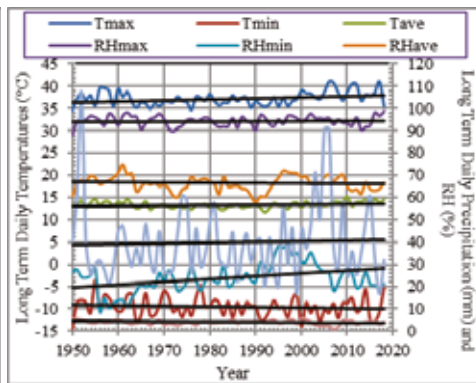
Antakya



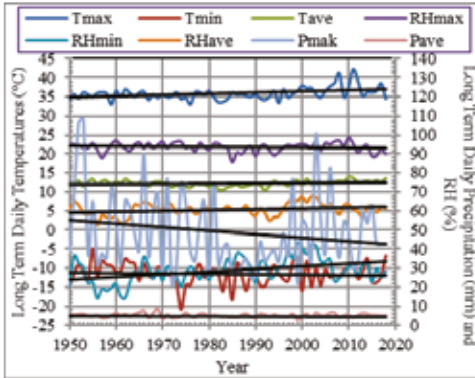
Antalya



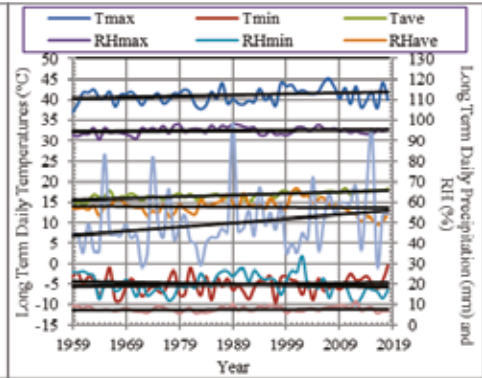
Burdur



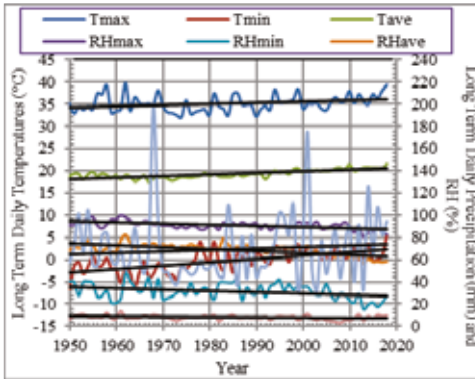
**Isparta**



**Kahramanmaraş**



**Mersin**



**Osmaniye**

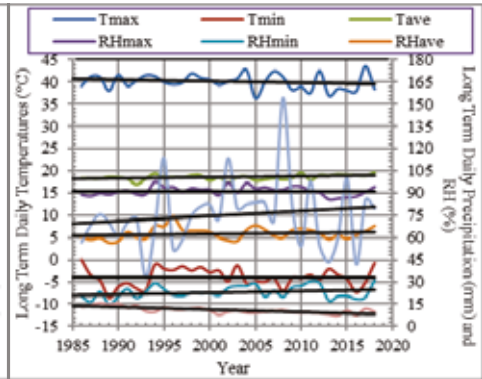


Figure 1. Trend Changes of Long-Term Meteorological Variables

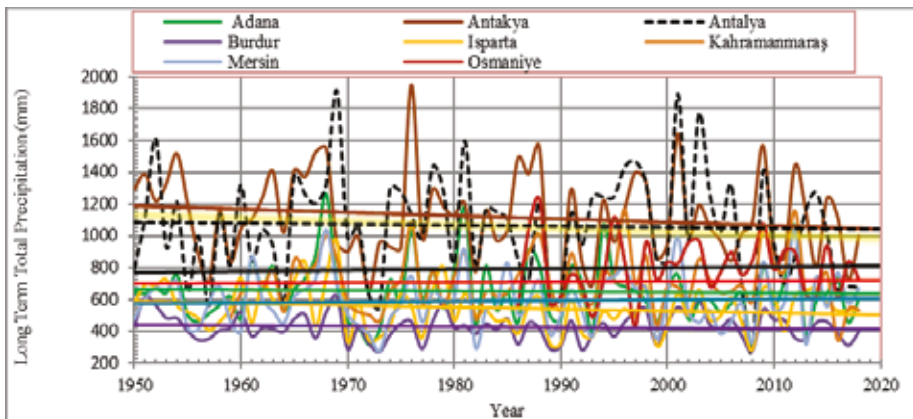


Figure 2. Long Term Annual Total Rainfall Variable Trend in Studying Area

Changes in the temperature values in the provinces respectively;  $T_{MAX}$  values in Mersin, Burdur,  $T_{MIN}$  values in Mersin, Adana,  $T_{AVE}$  values in Adana, Antalya, Kahramanmaras, Mersin and Osmaniye provinces have been determined to increase trends. It was found that  $RH_{MAX}$  values decreased in Mersin,  $RH_{MIN}$  values increased in Isparta, Burdur provinces and Mersin, Adana provinces decreased,  $RH_{AVE}$  values increased in Isparta, Antalya provinces and decrease in Mersin. In terms of  $P_{AVE}$  values, there are trends in the decreasing of Antakya, Osmaniye and Mersin provinces. It is stated that greenhouse gases released to the atmosphere are the fundamental causes of climate change (Bayraç & Doğan, 2016). Energy production and the burning of fossil fuels for heating purposes, industry, transportation, changes in land use, waste management and agricultural activities are among the primary activities that result in the increase of greenhouse gas emissions which cause global warming (Başoğlu, 2014; Bayraç & Doğan, 2016). It is put forth in general that human activities are the underlying factors for climate change (Black & Weisel, 2010; Başoğlu & Telatar, 2013; Başoğlu, 2014). It has been determined in general that there are trends for increasing temperature and

decreasing rainfall in the study region. Başoğlu (2014) indicates that the first impacts of climate change appear with increasing temperatures and changes in rainfall regime. It is stated that excessive changes in these climate factors will result in the frequency and intensity of climate based natural disasters such as droughts, floods and storms thereby leading to economic losses. Since the agricultural sector is especially related with climate and weather conditions, researchers put forth that the impact of climate change on agriculture is much greater in comparison with other sectors (Bazzaz & Sombroek, 1996; Başoğlu & Telatar, 2013). Whereas Türkeş (1996) carried out a study on rainfall as a result of which it was presented that the annual rainfall values for our country have a tendency to decrease. Demir et al. (2017) indicates that temperatures are increasing in recent years and that rainfall amount continues to decrease. Therefore, it was determined in this study that there are trends related with temperature and rainfall. It was also observed that the aforementioned changes in temperature and rainfall specified in the literature are in accordance with the findings of the present study. Linear regression analysis and statistical features are given in Table 2.

Table 2. Linear regression analysis results and statistical features

Meteorological Stations/Variables	Equation coefficients		r	s	t	p ( $\leq 0.05$ )
	a	b				
<b>Daily Maximum Temperature (<math>T_{MAX}</math>, °C)</b>						
Adana	59.81	-0.01	0.104	1.92858	-0.86	0.394
Antakya	3.05	0.01828	0.158	2.29993	1.31	0.193
Antalya	21.18	0.01043	0.154	1.35644	1.27	0.208
Burdur	-10.41	0.024	0.301	1.53869	2.58	0.012
Isparta	-28.29	0.03233	0.379	1.50968	3.54	0.001
Kahramanmaraş	-9.34	0.02533	0.234	1.85151	1.84	0.072
Mersin	-13.4	0.02449	0.260	1.83697	2.21	0.031
Osmaniye	120.0	-0.03994	0.218	1.75691	-1.24	0.223
<b>Daily Minimum Temperature (<math>T_{MIN}</math>, °C)</b>						
Adana	-45.37	0.02191	0.238	1.80734	201	0.049
Antakya	-34.66	0.01634	0.140	2.33737	1.16	0.252
Antalya	12.99	-0.006803	0.086	1.58938	-0.71	0.481
Burdur	18.60	-0.01421	0.126	2.26288	-1.04	0.303
Isparta	7.68	-0.0097	0.069	2.84573	-0.56	0.575
Kahramanmaraş	-29.29	0.01217	0.096	2.21985	0.74	0.465
Mersin	-156.0	0.07849	0.637	1.91866	6.77	0.0001
Osmaniye	0.36	-0.00211	0.010	2.12075	-0.05	0.957
<b>Daily Average Temperature (<math>T_{AVE}</math>, °C)</b>						
Adana	1.898	0.008753	0.344	0.482678	3.0	0.004
Antakya	2.249	0.008121	0.263	0.602270	2.23	0.029
Antalya	12.29	0.003265	0.098	0.671290	0.8	0.424

Burdur	-0.14	0.006777	0.191	0.702700	1.6	0.115
Isparta	-2.67	0.007524	0.198	0.753857	1.65	0.103
Kahramanmaraş	-60.57	0.03884	0.700	0.698962	7.54	0.0001
Mersin	-50.74	0.03528	0.749	0.631523	9.24	0.0001
Osmaniye	-27.8	0.02319	0.373	0.567276	2.24	0.033
Daily Maximum Relative Humidity (RH <sub>MAX</sub> , %)						
Adana	83.64	0.00543	0.047	2.33732	0.38	0.702
Antakya	113.00	-0.0097	0.087	2.24875	-0.71	0.478
Antalya	129.50	-0.01776	0.158	2.25059	-1.31	0.196
Burdur	83.64	0.00543	0.047	2.33732	0.38	0.702
Isparta	117.4	-0.01189	0.095	2.50234	-0.79	0.434
Kahramanmaraş	59.02	0.01801	0.184	1.68995	1.43	0.158
Mersin	299.0	-0.1049	0.564	3.10876	-5.58	0.0001
Osmaniye	109.3	-0.00896	0.027	3.26442	-0.15	0.882
Daily Minimum Relative Humidity (RH <sub>MIN</sub> , %)						
Adana	176.40	-0.07668	0.279	5.34149	-2.37	0.020
Antakya	-92.41	0.06056	0.198	6.05830	1.65	0.103
Antalya	43.68	-0.01102	0.058	3.79923	-0.48	0.633
Burdur	-232.7	0.1293	0.397	6.04955	3.54	0.001
Isparta	-247.8	0.1393	0.427	5.96686	3.86	0.0001
Kahramanmaraş	113.5	-0.04697	0.168	4.84917	-1.3	0.199
Mersin	286.6	-0.1286	0.354	6.87459	-3.1	0.003
Osmaniye	-207.1	0.115	0.258	4.23036	1.49	0.147
Daily Average Relative Humidity (RH <sub>AVE</sub> , %)						
Adana	93.21	-0.01351	0.079	3.42272	-0.65	0.516
Antakya	116.20	-0.02388	0.157	3.03359	-1.30	0.197
Antalya	56.00	0.00371	0.028	2.60707	2.59	0.012
Burdur	93.21	-0.01351	0.079	3.42272	-0.65	0.516
Isparta	-33.77	0.04769	0.290	3.18743	2.48	0.016
Kahramanmaraş	91.67	-0.01702	0.082	3.65713	-0.62	0.535
Mersin	412.9	-0.1733	0.672	3.85777	-7.43	0.0001
Osmaniye	-88.2	0.07539	0.179	4.07798	1.01	0.320
Daily Maximum Precipitation (P <sub>MAX</sub> , mm)						
Adana	62.4	0.0023	0.032	27.0197	0.01	0.989
Antakya	427.7	-0.1634	0.054	61.6534	-0.44	0.663
Antalya	824.9	-0.3447	0.130	52.9635	-1.08	0.286
Burdur	-25.3	0.0329	0.039	17.1942	0.32	0.752
Isparta	414.7	-0.1843	0.183	20.049	-1.52	0.133
Kahramanmaraş	-358.2	0.2052	0.245	14.3395	1.90	0.060
Mersin	-189.0	0.1303	0.086	30.4455	0.71	0.481
Osmaniye	-613.2	0.3438	0.143	23.3561	0.81	0.427
Daily Average Precipitation (P <sub>AVE</sub> , mm)						
Adana	-50.68	0.0294	0.334	1.67883	2.90	0.005
Antakya	79.55	-0.03432	0.089	2.36911	-2.40	0.019
Antalya	-9.35	0.01074	0.063	3.45219	0.51	0.608
Burdur	20.69	-0.008411	0.185	0.903605	-1.54	0.128
Isparta	5.99	-0.000537	0.010	1.03995	-0.09	0.932
Kahramanmaraş	-5.56	0.00672	0.087	1.3632	0.66	0.511
Mersin	64.31	-0.02847	0.283	1.95061	-2.41	0.018
Osmaniye	353.6	-0.1712	0.745	1.50662	-6.22	0.0001
Yearly Average Precipitation (P <sub>T</sub> , mm)						
Adana	1584.0	-0.471	0.050	191.047	-0.41	0.685
Antakya	5361.0	-2.138	0.156	273.545	-1.29	0.200
Antalya	2418.0	-0.682	0.041	332.291	-0.34	0.735
Burdur	1186.0	-0.384	0.092	84.444	-0.75	0.455
Isparta	2864.0	-1.169	0.170	137.273	-1.41	0.163
Kahramanmaraş	123.0	0.296	0.030	177.059	0.22	0.823
Mersin	-368.0	0.484	0.057	170.791	0.47	0.641
Osmaniye	-301.0	0.550	0.028	186.387	0.16	0.873

When the values obtained are examined in Table 2, it can be observed that there are statistically significant increases in daily  $T_{MAX}$  values in the cities of Burdur ( $0.024^{\circ}\text{C year}^{-1}$ ), Isparta ( $0.03233^{\circ}\text{C year}^{-1}$ ) and Mersin ( $0.02449^{\circ}\text{C year}^{-1}$ ), in  $T_{MIN}$  values in the cities of Adana ( $0.02191^{\circ}\text{C year}^{-1}$ ) and Mersin ( $0.07849^{\circ}\text{C year}^{-1}$ ), and in  $T_{AVE}$  values in the cities of Adana, ( $0.008753^{\circ}\text{C year}^{-1}$ ) Antakya ( $0.08121^{\circ}\text{C year}^{-1}$ ), Kahramanmaraş ( $0.03884^{\circ}\text{C year}^{-1}$ ), Mersin ( $0.03528^{\circ}\text{C year}^{-1}$ ) and Osmaniye ( $0.02319^{\circ}\text{C year}^{-1}$ ). Whereas it was determined that there was a statistically significant increase trend in the daily  $RH_{MAX}$  values in Mersin, daily  $RH_{MIN}$  values in Adana, Mersin, Burdur, Isparta and  $RH_{AVE}$  values in Antalya, Isparta, Mersin. The decreases in daily  $P_{AVE}$  values were observed to be statistically significant in the cities of Antakya ( $-0.03432 \text{ mm year}^{-1}$ ), Mersin ( $-0.02847 \text{ mm year}^{-1}$ ) and Osmaniye ( $-0.1721 \text{ mm year}^{-1}$ ); while the increase trend in the city of Adana ( $0.0294 \text{ mm year}^{-1}$ ) was observed to be statistically significant.

Since in general the increase in temperature and decrease in rainfall are emphasized in this and other similar studies, we also tried to emphasize the values related with temperature and decrease in rainfall.

It was determined upon examining Figure 3 prepared for the Spearman trend test that there was an increase trend for  $T_{MAX}$  values in the cities of Mersin, Isparta, Burdur; an increase trend for  $T_{MIN}$  values in the city of Mersin and an increase trend for  $T_{AVE}$  values in the cities of Mersin, Kahramanmaraş, Adana, Antakya, Osmaniye.  $RH_{MAX}$  values were observed to decrease in the city of,  $RH_{MIN}$  values were observed to increase in the city of Isparta and decrease in the cities of Mersin, Adana, while  $RH_{AVE}$  values were observed to increase in the city of Isparta and decrease in the city of Mersin. With regard to rainfall, Spearman trend test put forth that there were significant trends for  $P_{AVE}$  values to increase in the cities of Adana, Kahramanmaraş and decrease in the cities of Osmaniye, Antakya.

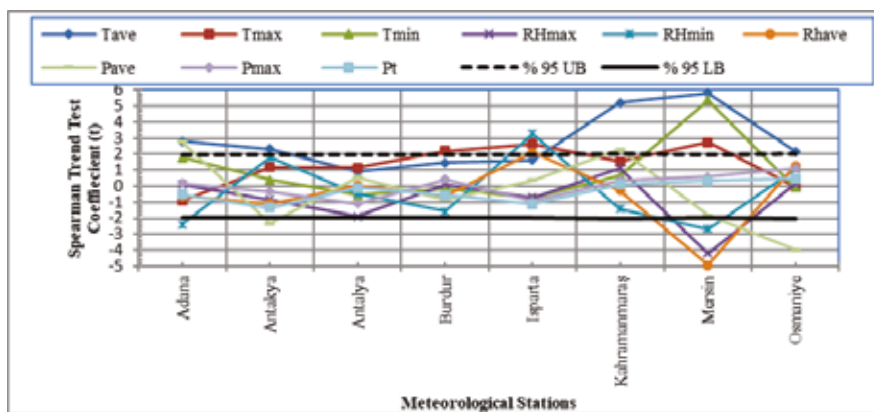


Figure 3. Results of Spearman Trend Test

## CONCLUSIONS

The changes in the long-term temperature, rainfall and humidity values acquired from meteorological stations of the cities included in the study area were evaluated via LRA and STT. Therefore, it was determined that there were increasing and decreasing trends in the daily values for  $T_{MAX}$ ,  $T_{MIN}$ ,  $T_{AVE}$ ,  $P_{AVE}$ ,  $RH_{MAX}$ ,  $RH_{MIN}$  and  $RH_{AVE}$  which were statistically significant.

High increases in temperature and decreases in rainfall as well as the changes in proportional humidity are indications that the climate of our region will be more arid in the coming years. When it is taken into consideration that intensive agricultural activities are carried out in the Mediterranean Region, it can easily be stated that there is an urgent need to replace all irrigation methods with pressurized irrigation methods. Because, the increase in temperature as well as the decrease in rainfall will further

increase the demands for our water resources. Moreover, it was also concluded that the changes in our water resources should also be examined and evaluated in addition to the changes in climate parameters. In this manner, water resource use can be planned more properly.

## ACKNOWLEDGEMENTS

The authors would like to thank the General Directorate of State Meteorology of the Ministry of Agriculture and Forestry for their assistance in data collection.

## REFERENCES

- Bahadır, M. (2011). North-South Directional Temperature and Precipitation Change Forecasts in the Reflection of Climate change in the Climatic Zones of Turkey. *Akademik Bakış Journal*, 26,1–18 (In Turkish).
- Başoğlu, A. (2014). The Economic Effects of Global Climate Change. *Karadeniz Teknik University Sosyal Bilimler Journal*, 7, 175–196 (In Turkish).
- Başoğlu, A., Telatar, O. M. (2013). The Impact of Climate Change: An Econometric Analysis on Agriculture. *Karadeniz Teknik University Sosyal Bilimler Journal*, 6, 7–25 (In Turkish).
- Bayraç, H. N., Doğan, E. (2016). Impacts of Climate Change on Agriculture Sector in Turkey. *Eskişehir Osmangazi University İİBF Journal*, 11(1), 23–48 (In Turkish).
- Bazzaz, F., Sombroek, W. (1996). *Global Climate Change and Agricultural Production*. Published 1996 by John Wiley & Sons Ltd, Baffins Lane, Chichester, West Sussex PO19 1UD, England
- Black, B. C., Weisel, G. J. (2010). *Historical Guides to Controversial Issues in America: Global Warming*. 1st. Ed., California: Greenwood.
- Demir, A. D., Demir, Y., Şahin, Ü., Meral, R. (2017). Trend Analyses of Temperature and Precipitation and Effect on Agricultural in Bingol Province. *Türk Tarımve Doğa Bilimleri Dergisi* 4(3), 284–291 (In Turkish).
- Gauthier, T. D. (2001). Detecting Trends Using Spearman's Rank Correlation Coefficient. *Environmental Forensics*, 2, 350–362.
- Haan, C. T. (1977). *Statistical Methods in Hydrology*. Iowa State University Press, Ames, USA.
- Hamdi, M. R., Abu-Allaban, M., Al-Shayeb, A., Jaber, M., Momani, N. M. (2009). Climate Change in Jordan: A Comprehensive Examination Approach. *American Journal of Environmental Sciences*, 5(1), 58–68.
- Helsel, D. R., Hirsch, R. M. (1993). *Statistical Methods in Water Resources*. *Studies in Environmental Sciences*, 49, Elsevier USA.
- Karabulut, M., Sarıyıldız, F., Korkmaz, H., Gürbüz, M. (2008). Gökşun'da Yağışve Sıcaklıkların Trend Analizleri, 100. *Yılında Gökşun Sempozyumu*, 419–434 (In Turkish).
- Karabulut, M. (2012). Analysis of Extreme Maximum and Minimum Heats at the East Mediterranean. *KSU J. Nat. Sci.*, Special Issue, 37–44 (In Turkish).
- Kendall, M. G. (1975). *Rank Correlation Methods*. Charles Griffin, London.
- Kundzewicz, Z. W., Rodson, A. (2000). Detecting Trend and Other Changes in Hydrological Data, World Climate Program-Water, WCDMP-45, WMO/TD-No: 1013, 64–82.
- Önöz, B., Bayazit, M. (2003). The Power of Statistical Tests for Trend Detection. *Turkish Journal of Engineering and Environmental Sciences*, 27, 247–251.
- Saplıgölu, K., Çoban, E. (2013). Trend Analysis of Precipitation Series Black Sea Region, II. *Ulusal Hidroloji Kongresi*, 26 -27 Eylül 2013, 500–512, Isparta.
- Shammugasundram, S. (2012). Statistical Analysis to Detect Climate Change and Its Implication on Water Resources. School of Engineering and Science, Faculty of Health, Engineering and Science, Victoria University, Australia.
- Sneyers, R. (1990). On the Statistical Analysis of Series of Observations, WMO Technical Note 143, WMO No: 415, TP-103, Geneva, World Meteorological Organization, pp:192.
- Türkeş, M. (1996). Spatial and Temporal Analysis of Annual Rainfall Variations. In *Turkey, International Journal of Climatology*, 16, 1057–1076.
- Türkeş, M., Sümer, U. M., Demir, İ. (2002). Türkiye'nin Günlük Ortalama, Maksimumve Minimum Hava Sıcaklıkları İle Sıcaklık Genişliğindeki Eğilimlerle Değişimler, Prof. Dr. Sırrı ERİNÇ Anısına Klimatoloji Çalıştayı 2002 Bildiriler Kitabı, 89–106 (In Turkish).
- Ülke, A., Özkoca, T. (2018). Trend Analyses of Temperature Data of Sinop, Ordu and Samsun Provinces. *GÜFBED/GUSTIJ*, 8(2), 455–463.
- Xu, C. (2002). *Textbook of Hydrological Models*, Edition 2002. Uppsala University, Department of Earth Sciences Hydrology, Uppsala, Sweden.
- Yüce, M. İ., Ercan, B. (2017). Monthly Temperature and Precipitation Trend Analysis of Kilis Province. IX. *Ulusal Hidroloji Kongresi*, 04-06 Ekim 2017.

## DETERMINATION OF GEOTHERMAL ENERGY AREAS AND USAGE POSSIBILITIES IN GREENHOUSE HEATING

Hasan ERTOP<sup>1</sup>, Atilgan ATILGAN<sup>1</sup>, Ercüment AKSOY<sup>2</sup>

<sup>1</sup>Isparta University of Applied Sciences, Faculty of Agricultural Sciences and Technologies,  
32260, Isparta, Turkey

<sup>2</sup>Akdeniz University, Vocational School of Technologies Sciences, 07058, Antalya, Turkey

Corresponding author email: atilganatilgan@isparta.edu.tr

### Abstract

*In this study, the determination of geothermal energy in the Aegean region and determination of the use of geothermal energy in greenhouse cultivation were investigated. The results were compared with the related literature. Heating of greenhouses with geothermal energy sources will help to increase our greenhouse areas by providing economic cultivation opportunities if technical and environmental precautions are taken. For the data on thermal areas and active faults for Denizli, Aydın and Afyonkarahisar provinces where geothermal resources are used, the data of the General Directorate of Mineral Research and Exploration was used. The geothermal energy potential map of the provinces has been tried to be obtained from these data. From these maps, the locations of the greenhouses and geothermal energy heating greenhouses were compared. The development of greenhouses making use of geothermal energy in Turkey will provide significant contributions to greenhouse cultivation in all regions and especially in the Aegean Region. In conclusion, we are of the opinion that the maps drawn during this study will shed light to producers who are considering the use of geothermal energy for their greenhouses in the study area.*

**Key words:** energy, geothermal, greenhouse, heating.

### INTRODUCTION

Greenhouses are structures that enable economic growth of culture plants in periods when the climate conditions are not suited for open field plant growth (Sevgican et al., 2000). Greenhouses should be warmed in cold weather in order to obtain quality high yield from greenhouses. However, heating costs have a significant impact on production cost. Sustainability in greenhouses can be obtained by increasing energy efficiency. The increase of energy efficiency can be possible by using renewable energy resources that do not generate any waste instead of fossil-based energy resources (Zaimoğlu, 2017).

For this purpose, the use of renewable energy sources such as biomass, wind, sun, hydraulics, geothermal energy is important for heating greenhouses as well as the use of waste heat energy of industrial establishments (Yıldız, 2010; Çaylı et al., 2014). It is an important requirement with high priority to make use of natural energy resources instead of fossil-based energy sources for decreasing heating costs as well as for preserving the energy assets and

preventing environmental pollution. Hence, research and development studies for the design of geothermal energy heating systems for greenhouses have gained importance in recent years (Yıldız, 2010).

Greenhouse cultivation is carried out mostly along the Mediterranean coastline in Turkey due to various climate advantages. However, greenhouse cultivation has recently gained importance in areas with geothermal resources and the modern greenhouses established in these locations have started to produce high quality yield (Zaimoğlu, 2017).

Geothermal energy can be defined as hot water and vapor that contains higher amounts of molten minerals, salts and gases in comparison with the normal ground and surface waters formed by the heat accumulated at various depths of the earth's crust with temperatures that are above the regional atmospheric average temperature values (Çetin, 2014).

It has been calculated that the total geothermal capacity of the already existing geothermal well and resources in Turkey is about 8000 MWt with a potential of up to 60000 MWt (Çerçioğlu & Şahin, 2016). According to the South Aegean

Development Agency (2011), 6% of the current geothermal energy applications are used for power generation, 67% for residential heating, 9% for thermal facility heating and 18% for greenhouse heating. Accordingly, it is observed that the use of geothermal sources in our country is focused mostly on heating residences and greenhouses. Greenhouse heating was 50 hectares in 2002 while it increased by 686% reaching 393.1 hectares in 2015 (Anonymous, 2016).

Greenhouse cultivation areas have increased rapidly along the Mediterranean and Aegean coasts due to the suitable climate conditions in these regions. Whereas greenhouse cultivation could not develop in other regions with low average temperatures due to the requirement of high heating costs. However, geothermal sources decreased the heating costs thereby making it possible to carry out greenhouse cultivation activities in regions with low average temperature values. The applications carried out have put forth that greenhouses heated with geothermal energy are much more economic in comparison with greenhouses

heated by liquid and gas fuels (Milivojevic and Martinovic, 2003).

The purpose of the present study was to determine the extent to which greenhouses heated by geothermal energy make use of tectonic fault lines based on the geothermal energy maps of the cities of Denizli, Afyonkarahisar and Aydın where there are geothermal sources and greenhouse cultivation activities are carried out. It is considered that the study will be an important source for establishments that are planning to use geothermal energy for greenhouse heating.

## MATERIALS AND METHODS

The study covers Afyonkarahisar, Denizli and Aydın provinces in the Aegean Region. The selection of these provinces in the Aegean Region as a study area has been considered to be rich in terms of geothermal resources and effective implementation of greenhouse activities.

The location of the research area in the Qgis program is given in Figure 1.



Figure 1. Location of the study area

To create digital maps especially thermal areas, fault lines and lake surface were included in the study.

The data of thermal areas and active faults were taken from the General Directorate of Mineral Research and Exploration.

Data of General Directorate of State Hydraulic Works is used for the lake areas. Thermal fields data type “point”, Fault lines data “line” and

Lake surface data “land” data were created in the open source Qgis program used in Geographical Information Systems (Ulazia et al., 2017). Map images are created for Aydın, Afyonkarahisar and Denizli provinces of the geothermal active fault lines by using Qgis program.

The stages of the study area in the provinces in the Qgis program are given in Figure 2.

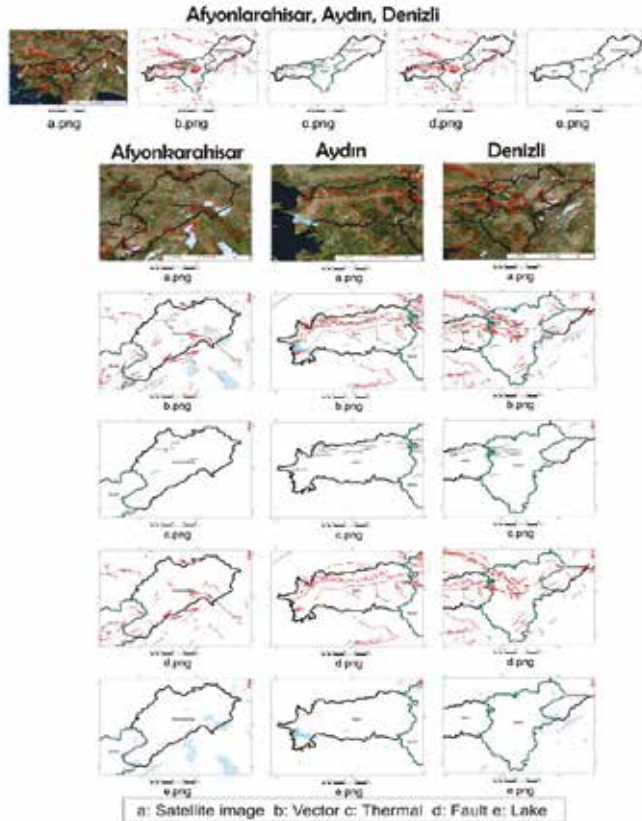


Figure 2. The stages of study area in the provinces of the Qgis program

Separate numerical maps are generated from the obtained data. Then, in the geographic information system software, these digital maps are combined. The coordinates of the greenhouses heated by geothermal energy are taken from the Provincial Directorates of Agriculture and Forestry. In determining the number of greenhouses, 5 greenhouses with approximately 10% of the greenhouses heated by geothermal energy were taken as basis for each province in the study area.

These greenhouses were randomly selected before the maps were created and also the ease of access was taken into account. The locations of the greenhouses heated by geothermal energy were determined in the coordinate plane of Aydın, Afyonkarahisar and Denizli provinces. Using the open-source Qgis program, maps of the 5 greenhouses selected for each province to the fault lines were created. From these maps, the distance of greenhouses in each province to the fault line was taken into consideration.

The selected greenhouses were considered to have the same product design and same physical characteristics and have the same initial investment and operating costs. It has been tried to determine which greenhouses have the highest and lowest geothermal heating potential.

## RESULTS AND DISCUSSIONS

Maps were prepared making use of the fault lines present in the study area due to its tectonic structure as well as the potential for the heating of the greenhouses via the geothermal energy in the region.

Figure 3 shows the positions of the fault lines of the cities of Aydın, Denizli and Afyonkarahisar as well as the greenhouses heated using geothermal energy.

It was determined upon examining Figure 3 that the fault lines in the city of Aydın continue along the northern side of the city passing over to the city of Denizli to combine with the fault lines in northwest Manisa thereby forming the fault lines in the city of Denizli.

While it was determined that the fault lines in the city of Afyonkarahisar are located in some local regions and that they do not overlap with other fault lines. Figure 4 illustrates the geothermal energy potential for the city of Aydın.

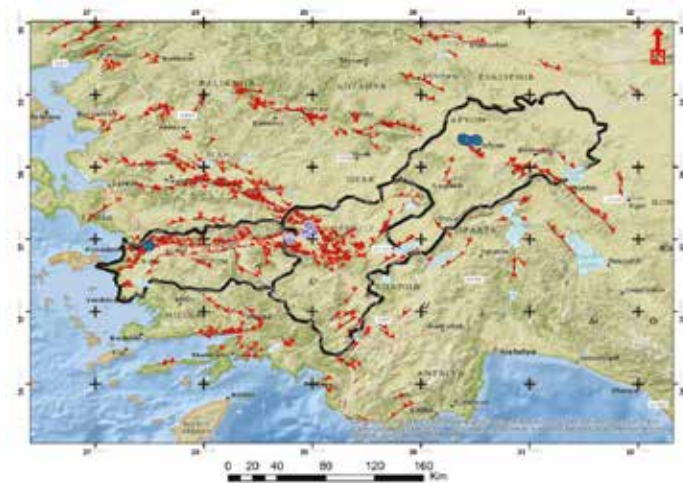


Figure 3. Location of geothermal energy heated greenhouses in the study area to fault line

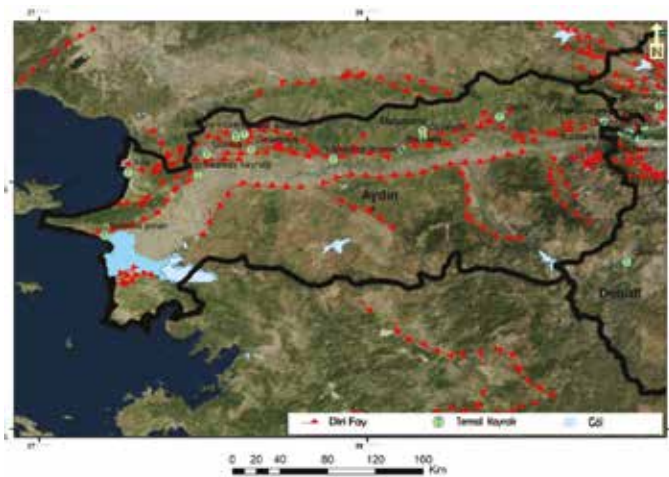


Figure 4. Geothermal energy potential map of Aydın province

It is observed that the active fault lines in the city of Aydın are concentrated in the norther part of the city and that the fault line stretches along the east-west line. It can be seen that the fault lines in the north intersect with north-south extension fault lines. It was determined that the fault lines in the city of Aydın are concentrated in thermal regions such as Bozköylücası, Ömerbeyli, Yılmazköy, Sazlıköy, İmamköy, Gümüş, Güvendik, Salavatlıand Malgaçemir. The geothermal

energy required for heating the greenhouses can be provided in these thermal regions while it is also considered that these areas will be suited for selling the produced foods due to the proximity of these thermal regions to the city of İzmir.

Table 1 shows the distances from the fault line of the five greenhouses heated via geothermal energy selected in the city of Aydın while Figure 5 depicts the locations of these greenhouses with respect to the fault line.

Table 1. Distances from fault line of the selected green houses in Aydın province

Greenhouse Number	Distance to Fault Line (km)
1	0.45
2	0.23
3	0.76
4	0.46
5	0.24

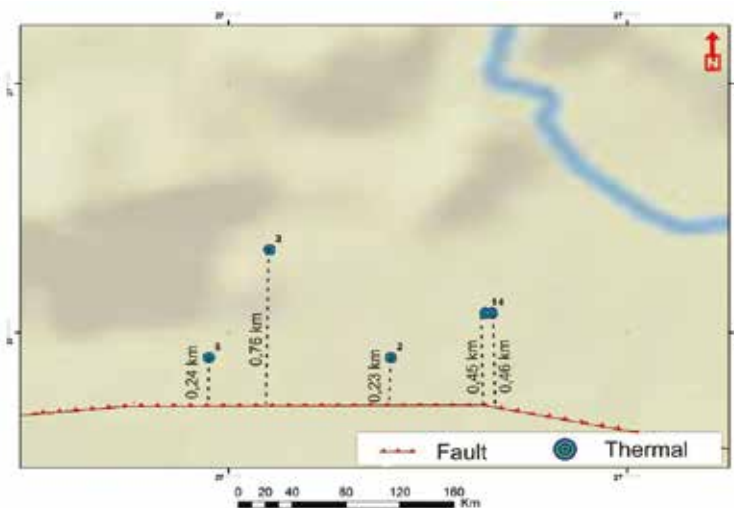


Figure 5. The location of selected greenhouses in Aydın province to fault line

It can be observed when Figure 5 is examined that the five greenhouses selected make use of the same fault line. The greenhouses heated using the geothermal energy in this fault line are observed to be as close to the fault line as possible. These greenhouses are in the Sazlıköy region. It was determined that the fault lines in the city of Aydın are concentrated more in Bozköylücası, Ömerbeyli, Gümüş regions as well as Güvendik, Salavatlıand Malgaçemir. It will be possible to make use of more than one fault line in case the geothermally heated greenhouses are located in these regions.

Therefore, it was concluded that a greenhouse that will be established in these regions will benefit from more than one fault line thereby having a higher heating potential in comparison with the greenhouses in Sazlıköy.

According to Tatar et al. (2006), two methods are used for the heating of greenhouses using geothermal energy. The first is to circulate the geothermal hot water inside the greenhouse by way of heating pipes and then mixing it with ground water via re-injection method, while the second is to pass the geothermal water through a heat exchanger system thereby resulting in an

exchange of heat between the geothermal water and domestic water after which the heated domestic water is circulated inside the greenhouse by way of pipes. Heating efficiency may decrease in case of corrosion that may develop when geothermal energy is used for heating. Yıldız (2010) reported that the fluids in the geothermal sources of the city of Aydın generally have high chlorine content and that the chlorine content of the geothermal fluids in the region vary between 16-2750 mg/l and

hence corrosion issues should be taken into consideration when making use of fluids with high chlorine content. It was concluded when the problems that may develop during the transmission of the geothermal fluid as well as the distances to the fault line were considered that greenhouses numbered 2 and 5 had the highest heating efficiency while greenhouse 3 had the lowest efficiency. Geothermal energy potential map for the city of Denizli is shown in Figure 6.

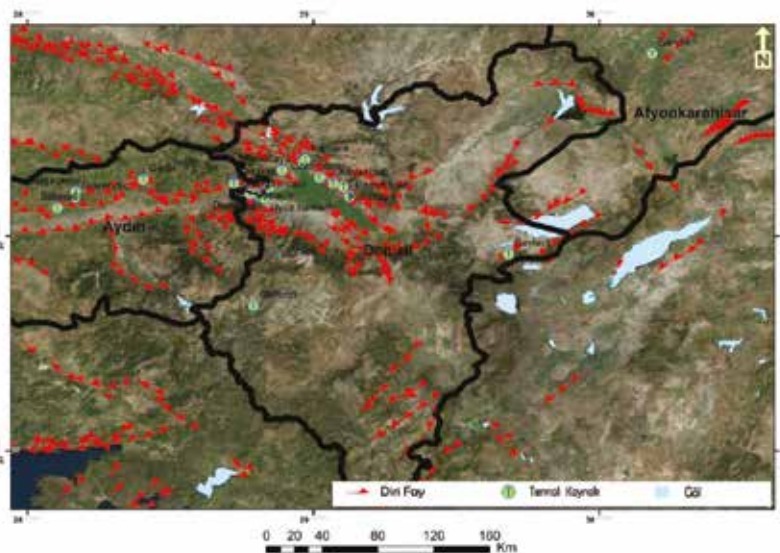


Figure 6. Geothermal energy potential map of Denizli province

It was observed that the active fault lines in the city of Denizli are concentrated to the northwest section of the city. It was also observed that the fault lines concentrated in this region are extensions of the fault lines in the cities of Aydın and Manisa and that these extensions intersect in the city of Denizli. In addition, it was also determined that the fault lines in the city of Denizli are concentrated in regions such as Bölmekaya, Ortakçı, Babacık, Kamara, Gölemezli, Kavakbaşı, Pamukkale and

Karahayıt. It was concluded that these regions may be more suited in comparison with other parts of the city due to various advantages such as the high probability of acquiring geothermal energy as well as the supply and transportation of geothermal energy. Table 2 presents the distances to the fault lines of the greenhouses in the city of Denizli heated via geothermal energy while Figure 7 shows the locations of these greenhouses with respect to the fault line.

Table 2. Distance from the fault line of the selected green houses in Denizli province

Greenhouse Number	Distance to Fault Line (km)
1	1.80
2	0.23
3	1.98-2.26
4	0.90
5	2.22

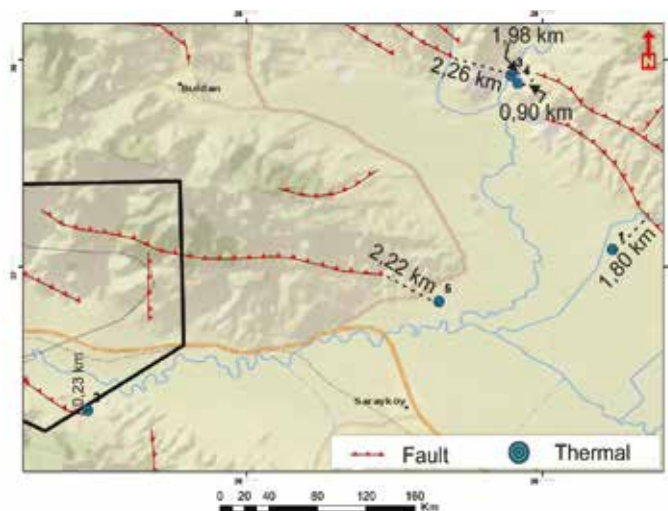


Figure 7. Location of selected greenhouses in Denizli Province to fault line

It was determined when Figure 7 was examined that the five selected greenhouses are not on the same fault line. It was also observed that the fault lines in the city are concentrated more in Bölmekeaya, Ortakçı, Babacık thermal regions as well as Kamara, Gölemezli, Kavakbaşı, Pamukkale, Karahayıt thermal regions.

It was concluded that Greenhouse number 2 has the highest heating potential due to its location inside the Babacık thermal region in the city of Denizli and its proximity to the fault line from where geothermal energy will be provided in comparison with other greenhouses. It was observed that the greenhouse numbered 5 in the study area is located outside the thermal regions and that it was farthest away from the fault line among all the other greenhouses. Even though there was no numerical difference between the distances to the nearest fault lines of greenhouses numbered 5 and 3, it was determined that the greenhouse numbered 5 had the lowest heating potential since greenhouse numbered 3 can benefit from 2 fault lines.

Ataman (2007) reported that the minerals contained in the geothermal fluid result in water

and soil pollution. While Akova (2008) set forth that chemical waste material in geothermal fluid such as mercury, arsenic, lead, lithium, ammoniac may cause environmental issues. It is necessary to carry out proper recycling procedures in order to prevent these harmful substances in geothermal fluids from polluting the environment. The fluid that cools during the flow of the generated hot water should be mixed with ground water by way of re-injection wells. When the probability is considered for having an insufficient number of re-injection wells in areas where the greenhouse is located, the cooled fluid should be recirculated back to the fault line from where hot fluid was obtained.

The costs that will incur during this cycle along with the environmental pollution that will occur in case of a leakage should be evaluated. It can be assumed that the greenhouse numbered 2 is more suited than the other greenhouses due to its proximity to the fault line as well as its economic advantages.

The geothermal energy potential map for the city of Afyonkarahisar is given in Figure 8.

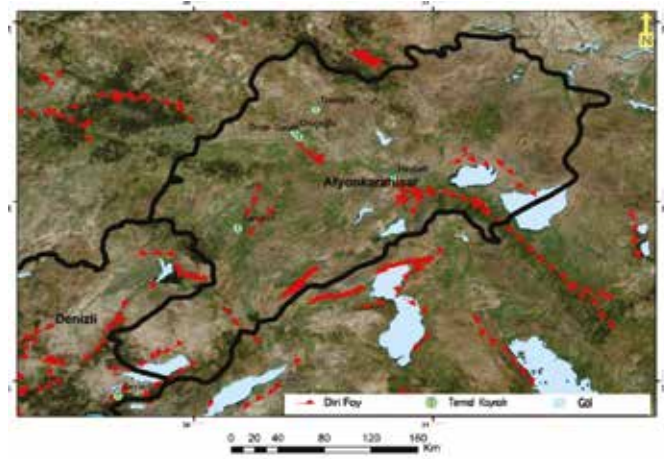


Figure 8. Geothermal energy potential map of Afyonkarahisar province

It was determined that the fault lines in the city of Afyonkarahisar are not concentrated in a specific region as was the case for the cities of Aydin and Denizli and that it has a smaller number of fault lines.

In addition, it was concluded that the greenhouses that will be established in the Heybeli thermal region in the city of Afyonkarahisar will be more suited for

geothermal energy heating due to the fact that the active fault lines are concentrated in this region and that there is a greater number of natural water springs. The distances between the fault line and the greenhouses heated via geothermal energy in the city of Afyonkarahisar are given in Table 3 while the positions of these greenhouses with regard to the fault line are shown in Figure 9.

Table 3. Distance from the fault line of the selected greenhouses in Afyonkarahisar province

Greenhouse Number	Distance to Fault Line (km)
1	3.80
2	8.90
3	1.76
4	2.67
5	8.25

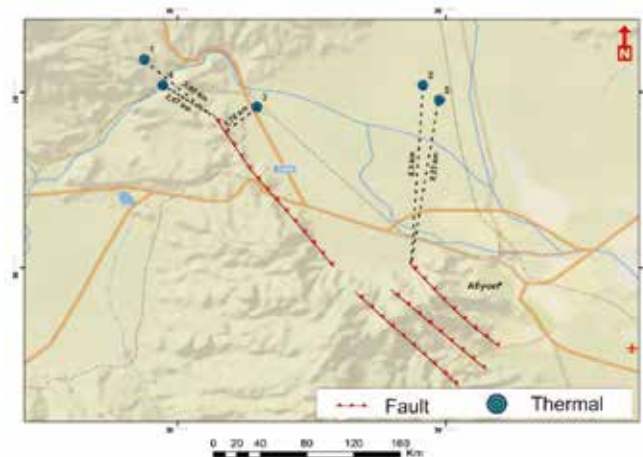


Figure 9. The location of selected greenhouses in Afyonkarahisar province to fault line

It was determined that the five greenhouses selected in the city of Afyonkarahisar are not on the same fault line. It was observed that the greenhouses are located in the thermal regions of Ömer, Geçekand Oruçoğlu and that they have different distances to the fault line.

While greenhouses numbered 1, 3 and 4 are located on the same fault line; greenhouses numbered 2 and 5 also make use of the same fault line. It was observed that there is a greater number of fault lines in the Heybeli thermal region of Afyonkarahisar when compared with the fault lines in the thermal regions of Ömer, Geçekand Oruçoğlu. It was concluded that in case the greenhouses heated with geothermal energy are established in the Heybeli thermal region, they will benefit more from the fault line in comparison with the greenhouses in the thermal regions of Ömer, Geçekand Oruçoğlu thereby resulting in a higher heating potential.

Satman (2001) suggested that the hydrological conditions in the region where the water used

for geothermal energy is re-injected should be determined properly. It was also put forth that in case the re-injected water does not directly flow to the geothermal region it may spread out thereby leading to pollution issues.

The geothermal energy used for heating the greenhouses in the city of Afyonkarahisar may have adverse impacts on the water sources in case it is not re-injected properly.

Greenhouse numbered 3 was observed to be the best among the greenhouses selected in the city of Afyonkarahisar, while it was also observed that the greenhouse numbered 2 had the lowest heating potential.

Çetin (2014) reported that there is a temperature loss of about 0.1-0.3°C/km when geothermal fluid is transported by way of specially insulated pipes. This loss was determined as 0.2°C/km on average and the temperature loss that may occur in the greenhouses in the study area were calculated as in Table 4.

Table 4. Heat loss during heat conduction in selected greenhouses

Province	Greenhouse Number	Distance to Fault Line (km)	Total Temperature Loss (°C)
Aydın	1	0.45	0.09
	2	0.23	0.046
	3	0.76	0.152
	4	0.46	0.092
	5	0.24	0.048
Denizli	1	1.80	0.36
	2	0.23	0.046
	3	1.98-2.26	0.396-0.452
	4	0.90	0.18
	5	2.22	0.444
Afyonkarahisar	1	3.80	0.76
	2	8.90	0.178
	3	1.76	0.352
	4	2.67	0.534
	5	8.25	1.65

According to Table 4, temperature losses will increase with increasing distances subject to the locations of the selected greenhouses.

It can be stated based on these results that greenhouses numbered 2 and 3 have the highest and lowest heating potential in the city of Aydın, while greenhouses numbered 2 and 5 in the city of Denizli and greenhouses numbered 3 and 2 in the city of Afyonkarahisar have the highest and lowest heating potentials respectively.

## CONCLUSIONS

Thermal maps were prepared and evaluated for determining the geothermal energy potentials of the selected sample greenhouses from each city in the study area. Factors such as distance, transportation losses and environmental factors have been effective in the determination of the geothermal energy potentials of these greenhouses. It was observed that the greenhouses numbered 2 and 5 in the city of

Aydın, greenhouse numbered 2 in the city of Denizli and greenhouse numbered 3 in the city of Afyonkarahisar had the best heating potential.

When it is taken into consideration that the Aegean Region is rich in geothermal energy sources and that greenhouse cultivation activities are carried out effectively, the use of geothermal energy for greenhouse heating can reduce heating costs significantly which is an important factor that increases the costs involved in greenhouse cultivation. The development of greenhouses making use of geothermal energy in Turkey will provide significant contributions to greenhouse cultivation in all regions and especially in the Aegean Region. In conclusion, we are of the opinion that the maps drawn during this study will shed light to producers who are considering the use of geothermal energy for their greenhouses in the study area.

## REFERENCES

- Akova, İ. (2008). *Renewable Energy Sources*. Nobel Yayınevi. Ankara (In Turkish).
- Anonymous (2016). [www.enerji.gov.tr/tr-TR/Sayfalar/Jeotermal](http://www.enerji.gov.tr/tr-TR/Sayfalar/Jeotermal) (In Turkish).
- Ataman, A. R. (2007). Renewable Energy Sources in Turkey. Ankara University, Social Sciences Institute, Master Thesis, 325 p. (In Turkish).
- Çaylı, A., Boyacı, S., Üstün, S., Akyüz, A. (2014). Determination of Maximum Heating Load in Greenhouses for Kahramanmaraş Region. 12. *Ulusal Kültürteknik Sempozyumu*, 21-23 Mayıs, Tekirdağ (In Turkish).
- Çerçioğlu, M., Şahin, H. (2016). The Utility Of Geothermal Energy For Heating Greenhouses In Simav. The *Journal of Academic Social Science Studies: International Journal of Social Science*, 47(1), 459–475 (In Turkish).
- Çetin, A. (2014). Ülkemizin Jeotermal Enerji Kapasitesi ve Yapılabilecekler, GÖNDER Geleceği Önemseyenler Derneği (In Turkish).
- Milivojevic, M., Martinovic, M. (2003). Utilization of geothermal energy in Serbia. Proceedings of the *International Geothermal Conference*, IGC-2003, September 2003, Session 10 (p. 37), Reykjavik.
- Satman, A. (2001). The Nature of Geothermal Energy. V. Ulusal Tesisat Mühendisliği Kongresive Sergisi, Jeotermal Enerji Semineri, İzmir, 3-6 Ekim (In Turkish).
- Sevgican, A., Tüzel, Y., Gül, A., Eltez, R. Z. (2000). Greenhouse Vegetable Growing in Turkey. V. *Türkiye Ziraat Teknik Kongresi*, 17-21 Ocak, Ankara, 679–707 (In Turkish).
- South Aegean Development Agency. TR32 Level 2 Region (Aydın, Denizli, Muğla) Geothermal Resources and Geothermal Power Plants Research Report. 27 p. (In Turkish).
- Tatar, O., Coşkun, M., ve Çaylı, İ., 2006. Use of Geothermal Resources in Greenhouse. *Jeotermal Kaynakların Değerlendirilmesi Sempozyumu*, İzmir (In Turkish).
- Ulazia, A., Urresti, A., Antxustegi, M. M., GonzalesAlriols, M., Campos-Celador, A., Ibarra-Berastegi, G. (2017). Using Open Software To Teach Resource Assessment of Solar Thermal And Geothermal Energy. *3rd International Conference on Higher Education Advances*, HEAd'17 Universitat Politècnica de València, 2017 DOI: <http://dx.doi.org/10.4995/HEAd17.2017.561>.
- Yıldız, M. (2010). A Research On Utilization Of Geothermal Energy Sources For Greenhouse Heating In Aydın Province. Çukurova University Institute Of Natural And Applied Sciences Department Of Agricultural Machinery, Master Thesis, 93 p. (In Turkish).
- Zaimoğlu, Z. (2017). Modeling of Heat Requirements for Agricultural Greenhouse in Different Climate Regions. *Journal of the Faculty of Engineering and Architecture*, 32(4), 79–86 (In Turkish).

## DEVELOPING A WEATHER-BASED INDEX FOR CROP INSURANCE TO PROMOTE SUSTAINABLE AGRICULTURE AND MITIGATE AN AGRARIAN CRISIS, A CASE STUDY IN INDIA

Vijendra BOKEN

University of Nebraska-Kearney, 25 West Street, Kearney, 68849, NE, USA

Corresponding author email: bokenvl@unk.edu

### **Abstract**

*A case study was conducted for Yavatmal district of Maharashtra state of India where dryland agriculture dominates and where a significant number of farmers have committed suicides in recent years due to the lack of support systems necessary to manage an agrarian crisis. Using monthly temperature and the precipitation data during 2001-2013 period, a weather-based index was developed for the main crops of the district (sorghum, soybean, and pigeon pea; cotton was excluded) to assess the agrarian crisis due to low crops yields, in a more objective and less disputable way that could be preferred by a crop insurance company. While the mean value of WI was 1.0, its range was 0.64 to 1.32 for pigeon pea, from 0.94 to 1.12 for sorghum, and from 0.31 to 1.72 for soybean. These ranges could be further divided appropriately into qualitative categories of to define agrarian crisis for the purpose of designing crop insurance plans to support farmers at their hard times thus making agricultural profession more sustainable.*

**Key words:** crop yield, drought, farmer suicide, Maharashtra.

### **INTRODUCTION**

Ensuring agricultural risks in developing countries is a relatively new phenomenon that has not spread its roots due to various reasons, for example:

- (i) farmers are not well educated and not adequately aware of the credit options available to them;
- (ii) the average farm size is very small and the farmers income is hardly sufficient to support the basic needs and as a result farmer may not have disposable income to pay for the insurance premiums.

When crops fail due to droughts that occur in most countries (Boken et al., 2005), farmers are unable to return the money they borrow for buying farming inputs.

If the natural calamities strike for successive years, an average farmer's financial condition deteriorates so much that some of the farmers who are unable to cope with the stress even commit suicides although there are several factors responsible for suicide occurrence (Dongre & Deshmukh, 2012; Kale et al., 2015) Due to liberalization or globalization of agriculture trade, there has been significant fluctuation in the market prices of commercial

crops and in the input costs of cultivating these crops thus increasing the risk levels for farmers. Small farmers with the lack of education and access to credit are unable to manage risks and end up even committing suicides.

The goal of this study is to mitigate the sufferings the poor farmers face due to natural hazards in India, so that their financial conditions don't reach a dismal level due to agricultural risks. One of the solutions to address this paramount issue is to provide crop insurance to farmers. While insurance in other sectors (such as, life, business, health etc.) in India is rather common, albeit mostly in urban areas, the insurance in the agricultural sector is lagging far behind. The assessment of crop damages that may be claimed by farmers is also difficult to verify and may be disputable, which may discourage an insurance company from venturing into the agricultural sector successfully.

In recent years, researchers have come up with an idea of a more objective and an index-based insurance (Berhani et al., 2013; Arshad et al., 2015; Black et al., 2015) insuring weather or other variables that affect crop yields and for which the reliable data are available.

Support systems and decision making innovative approached are required to withstand drought conditions and ensure food security (Enenkel et al., 2015).

In this study, a weather-based index (WI) is developed by examining the relationship between weather variables and crop yields.

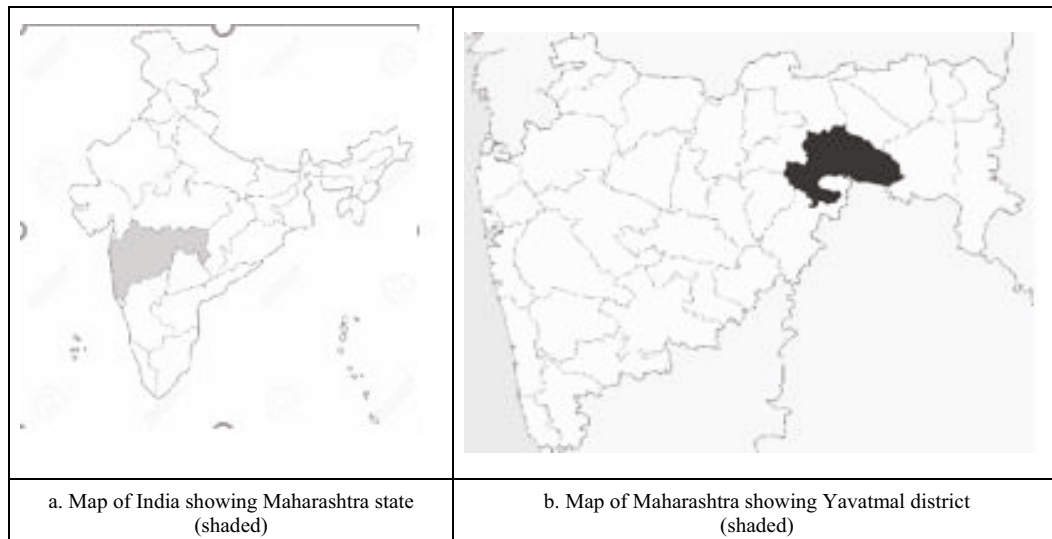


Figure 1. The location of the study area

### Study Area

The study was conducted for Yavatmal district, Maharashtra, India, where the number of farmers-suicides was higher than in any other district of the state in recent years. Maharashtra is the state with maximum number of farmer-suicides in India accounting for almost half the number of farmer-suicides occurred in the entire country in 2014 as per the report by the National Crime Records Bureau (2019)

The boundaries of Yavatmal district (Figure 1) lie between  $19.26^{\circ}$  and  $20.42^{\circ}$  north latitudes and between  $77.18^{\circ}$  and  $79.90^{\circ}$  east longitudes covering about 13.6 thousand  $\text{km}^2$ . The average annual temperature for the district is about  $25^{\circ}\text{C}$  with the average maximum temperature of  $45^{\circ}\text{C}$  and the minimum temperature of  $5.6^{\circ}\text{C}$ . Dryland agriculture dominates the district as the irrigated area accounts for less than 8% of the total cropped area (<http://kvkyavatmal.pdkv.ac.in/districtprofile/>). Farmers plant various crops but cotton, sorghum, soybean, and pigeon pea are the main crops accounting for more than 80% of the total cropped area.

### MATERIALS AND METHODS

The following data were collected from different sources for developing a weather-based index.

#### *Weather data*

The monthly precipitation data were collected from the VDSA database maintained at the International Crops Research Institute for the Semi-Arid Tropics ([vdsa.icrisat.ac.in](http://vdsa.icrisat.ac.in)) for the 2000-2011 period; the data for the remaining 2012-2015 period were purchased from the India Meteorological Department ([imd.gov.in](http://imd.gov.in)).

#### *Agricultural data*

The harvested area, yield, and production of different crops planted in the district were collected from the VDSA database as well though the original source of the data was the Directorate of Economics and Statistics, Ministry of Agriculture and Farmers Welfare, Government of India (<https://eands.dacnet.nic.in>).

The above data were used for developing the weather-based index by first examining their relationships with crop yields.

*Yield versus weather relationship*

A correlation analysis was conducted between the yield (production per unit area) of a crop and the variables relating to monthly temperature and precipitation during the main cropping season, the *Kharif* season (June/July to September/October). The variables included the temperature averaged for June and July

( $T_{ij}$ ), the total precipitation for June and July ( $P_{ij}$ ), the temperature averaged for August and September ( $T_{as}$ ), the total precipitation for August and September ( $P_{as}$ ), and the number of the rainy days during June through September ( $NR_{js}$ ).

Table 1 presents the coefficients of correlations between crop yields and these weather variables, which were considered for developing a weather-based index capable of indicating if the crop yield in a year was lower or higher than the multi-year average yield.

Table 1. The correlation coefficients between weather-based variables and the yields of the main crops for Yavatmal district, Maharashtra, India

Crops	Weather-based variables					Multiple regression, $R^2$
	$T_{ij}$ ( $^{\circ}C$ )	$P_{ij}$ (mm)	$T_{as}$ ( $^{\circ}C$ )	$P_{as}$ (mm)	$NR_{js}$	
Pigeon pea	0.19	0.21	0.49	0.36	0.20	0.75
Sorghum	0.34	-0.19	-0.08	0.00	0.03	0.37
Soybean	0.20	0.45	-0.19	0.59	0.55	0.84
Cotton	-0.38	-0.36	-0.39	-0.47	-0.11	

$T_{ij}$ = the temperature averaged for June and July,  $T_{as}$ = the temperature averaged for August and September,  $P_{ij}$ = the total precipitation in June and July,  $P_{as}$ = the total precipitation in August and September,  $NR_{js}$ = the number of the rainy days in June through September.

Table 2. The derivation of weather-based index for different crops of Yavatmal district, Maharashtra, India; cotton was excluded due to high fluctuations in its yields caused by non-weather-related reasons

Year*	Pigeon pea				Sorghum			Soybean			
	Yield (kg/ha)	Selected weather-based variables		Weather-based Index, WI	Yield (kg/ha)	Selected variable	Weather-based Index, WI	Yield (kg/ha)	Selected weather-based variables		Weather-based Index, WI
		$T_{as}$	$P_{as}$						$P_{ij}$	$P_{as}$	
2001	1268.3	26.9	452.7	1.25	1094.2	27.7	0.99	1298.9	404.3	452.7	1.02
2002	1014.1	26.1	414.4	1.11	1180.8	31.4	1.12	1359.4	509.2	414.4	1.17
2003	804.1	24.9	455.6	1.17	1028.7	28.1	1.00	1449.4	534.2	455.6	1.35
2004	651.5	24.9	410.6	1.05	981.8	27.8	0.99	536.6	322.4	410.6	0.74
2005	807.1	25.5	422.1	1.11	768.7	28.9	1.03	1122.8	670.3	422.1	1.57
2008	601.2	25.8	240.0	0.64	967.7	28.2	1.01	332.6	228.6	240.0	0.31
2009	689.8	26.2	216.7	0.58	524.4	28.9	1.03	405.9	253.7	216.7	0.31
2010	743.3	24.6	520.8	1.32	764.4	27.9	1.00	1375.8	472.8	520.8	1.37
2011	864.8	24.1	275.2	0.68	1285.5	26.3	0.94	1346.4	562.2	275.2	0.86
2013	736.3	25.2	418.1	1.08	320.0	25.1	0.90	548.3	737.9	418.1	1.72
Mean	818.1	25.4	382.6	1.00	891.6	28.0	1.00	977.6	469.6	382.6	1.00

\*Due to data inconsistency, WI couldn't be developed for 2012 and 2013.

*Derivation of weather-based index*

In order to develop a weather-based index that has a reasonably strong relationship with the crop yield, the variables that were more significantly related with crop yields were short listed to be used for developing the weather-based index. Based on the coefficients of correlation shown in Table 1, the short-listed variables turned out to be  $T_{as}$  and  $P_{as}$  for pigeon

pea,  $T_{ij}$  for sorghum, and  $P_{ij}$  and  $P_{as}$  for soybean. Cotton was excluded from the analysis because farmers had adopted genetically modified varieties of cotton (Guere & Sengupta, 2011) that produced very high yields in the first year but were unable to sustain the promised yields in subsequent years thus causing high fluctuation in yields due to non-weather-related reasons (Figure 2).

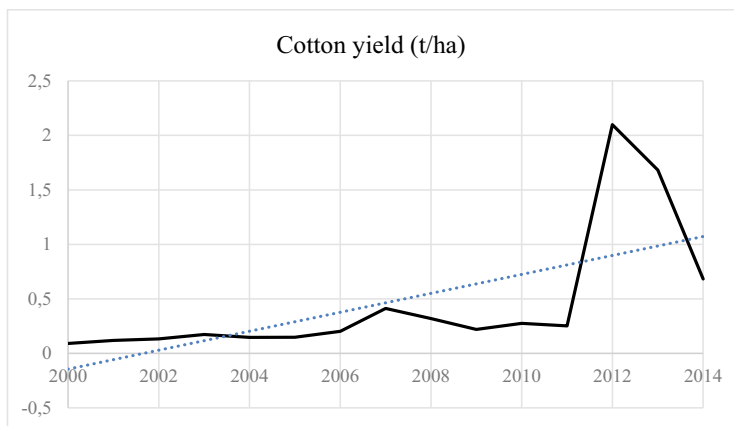


Figure 2. Abnormal fluctuation in cotton yields during 2008-2015

The deviation from the average yield was found a simple and a practical indicator to reflect drought or low crop-yield conditions (Boken, 2009).

For each of the short-listed variables, a new variable was created by dividing the annual value of the variable by the multiyear mean or average value of the variable as shown in Table 2. In case of pigeon pea and soybean, the two new variables were then multiplied to develop the weather-based Index, WI. For example, the WI for soybean was defined as follows:

$$WI = (P_{ij} / P_{ij\_avg}) * (P_{as} / P_{as\_avg}) \quad (1)$$

Where:

- $P_{ij}$  and  $P_{as}$  are the short-listed variable for soybean;
- $avg$  subscript refers to the mean or average value of the variable for the 2001-2013 period considered in this study.

## RESULTS AND DISCUSSIONS

The yearly values of WI for main crops (excluding cotton) are shown in Table 2. The average of WI as developed above turned out to be 1.0. A value of WI lower than 1.0 indicated a lower than the average crop yield and a value higher than 1.0 indicated a higher than the average crop yield. A lower than 1.0 value for WI means that the farmers may deserve to receive pay-out as per their insurance plans. WI ranged from 0.64 to 1.32 for pigeon pea, from 0.94 to 1.12 for sorghum, and from 0.31 to 1.72

for soybean. The WI ranges could be further divided into qualitative categories of agricultural drought conditions or agrarian crisis, such as mild, moderate and severe crisis. Eventually, the pay-out amount could be determined to make the crop insurance a sustainable venture supporting farmers at a time of agricultural crisis.

## CONCLUSIONS

The weather variables showing stronger relationships with crop yields were selected for developing weather-based index to be used in a crop insurance method in order to indicate the level of an agrarian crisis relating to agricultural drought conditions. This will help determine pay-outs to farmers more objectively, in a less disputable way.

The selected variables were the average temperature during August-September and the total precipitation during August-September for pigeon pea, the average temperature for June-July for sorghum, and the total precipitation for June-July and the total precipitation in August-September for soybeans. While the mean value of WI was 1.0, its range was 0.64 to 1.32 for pigeon pea, from 0.94 to 1.12 for sorghum, and from 0.31 to 1.72 for soybean. These ranges could be further divided appropriately into qualitative categories of to define agrarian crisis for the purpose of designing crop insurance plans to support farmers at their hard times thus making agricultural profession more sustainable.

## REFERENCES

- Arshad, M., Amjath-Babu, T. S., Kächele, H., Müller, K., (2016). What drives the willingness to pay for crop insurance against extreme weather events (flood and drought) in Pakistan? A hypothetical market approaches. *Climate and Development*, 8(3), 233–244.
- Berhane, G., Clarke, D., Dercon, S., Hill, R. V., Taffesse, A. S. (2013). Insuring against the Weather. Ethiopia Strategy Support Program UU, Research Note 20. Ethiopian Development Research Initiative. International Food Policy Research Institute.
- Black, E., Tarnavsky, E., Maidment, R., Greatrex, H., Mookerjee, A., Quaife, T., Price, J. (2015). Exploiting Satellite-Based Rainfall for Weather Index Insurance: The Challenges of Spatial and Temporal Aggregation. Conference Proceedings. *1<sup>st</sup> International Electronic Conference on Remote Sensing*, 22 June-5 July.
- Boken, V. K. (2009). Improving a drought early warning model for an arid region using a soil moisture index. *Applied Geography*, 29(3), 402-408.
- Boken, V. K., Cracknell, A. P., Heathcote, R. L. (Editors), (2005). *Monitoring and Predicting Agricultural Drought: A Global Study*. Oxford University Press, New York, 472 pp.
- Dongre, A. R. Deshmukh, P. R. (2012). Farmers' suicide in the Vidarbha region of Maharashtra, India: a qualitative exploration of their causes. *Journal of Injury and Violence*, 4(1), 2–6.
- Enenkel, M., See, L., Bonifacio, R., Boken, V., Chaney, N., Vinck, P., You, L., Dutra, E., Anderson, M. (2015). Drought and food security– Improving decision-support system via new technologies and innovative collaboration. *Global Food Security*, 4, 51–55.
- Gruère, G., Sengupta, D. (2011). Bt cotton and farmer suicides in India: an evidence-based assessment. *Journal of Development Studies*, 47(2), 316–337
- Kale, N. M., Khonde, S. R., Mankar, D. M. (2014). Socio-economic, psychological and situational causes of suicides of farmers in Vidarbha region of Maharashtra. *Karnataka Journal of Agricultural Science*, 27(1), 40–46.
- The National Crime Records Bureau, Government of India Available: [www.ncrb.gov.in](http://www.ncrb.gov.in), Accessed: January 15, 2019.

## DETERMINING STOCKPILE VOLUMES USING PHOTOGRAMMETRIC METHODS

**Tudor SALAGEAN<sup>1</sup>, Elemer-Emanuel SUBA<sup>1,2</sup>, Ioana Delia POP<sup>1</sup>, Florica MATEI<sup>1</sup>,  
Jutka DEAK<sup>1</sup>**

<sup>1</sup>University of Agricultural Sciences and Veterinary Medicine Cluj-Napoca,  
3-5 Calea Manastur Street, Cluj-Napoca, Romania

<sup>2</sup>Technical University of Civil Engineering Bucharest, 122-124 Lacul Tei Blvd,  
Bucharest, Romania

Corresponding author email: popioana@usamvcluj.ro

### **Abstract**

*Stockpile volume measurement is very important, especially in highway construction sites. Monitoring inventories, as well as keeping records of stockpiles, is one of the key elements in the success and optimizing the construction site works. Inventories in the case of construction sites are constantly changing; the raw material stored is on the one hand supplied by the suppliers and on the other hand transported and used on the site. Within this paper we aim to compare different methods of measuring and determining volumes. We also develop a workflow for UAV photogrammetric measurements and compare the volumes obtained with different specialized software. Using different software even on the same UAV data set, we obtained relatively similar results, the differences being due mainly to the different 3D modelling of the surfaces. To determine as precisely as possible highway construction sites, stockpile volumes the UAV photogrammetric method is the most precise in terms of the accuracy of the results obtained. This method also saves a lot of time on the site and is also risk free.*

**Key words:** drone, photogrammetric, point cloud, stockpile volume, UAV technology.

### **INTRODUCTION**

Determining stock volumes is an activity of particular importance.

Monitoring inventories, as well as keeping records of raw materials as accurate as possible, is one of the key elements in the success of the works.

Inventories in the case of construction sites are constantly changing; the raw material stored is on the one hand supplied by the suppliers and on the other hand transported and used on the site. We can compute the stockpile volumes using various methods like: terrestrial measurements using a total station, GNSS techniques, photogrammetry and the newest technology, laser scanning (Raevaa et al., 2016).

In order to manage efficiently a stockpile, it is required a fast and accurate data gathering. Gaining up-to-date information consists of continuous surveying the constantly changing shape of the stockpile and its elements and computes the volume. Monitoring could take

place weekly, monthly or every 3 months (Mazhrakov, 2007).

The UAV techniques combine aerial and terrestrial photogrammetry but also introduce low-cost alternatives to the classic methods (Carvajal et al., 2011).

Comparing to classical volume measurement methods, close range photogrammetry is a more efficient method. The time required for collecting spatial information is much reduced. The accuracy of the volume calculation is proportional to the presentation of the land surface. The presentation of the surface on the other hand is dependent on the number of coordinated points, their distribution and its interpolation (Raevaa et al., 2016).

### **MATERIALS AND METHODS**

Nowadays UAV platforms are becoming more and more accessible, and photogrammetry is used frequently.

Classical measurements, which are very time consuming, can be easily replaced by laser

scanning, UAV measurements and other automated workflows.

In this paper we used various techniques and instruments. First for determining the position of the ground control points we used two dual band (L1 L2) GNSS receivers, in base rover-radio setup. The base station is presented in Figure 1. The base point was marked with a FENO Landmark, as presented in Figure 2. We chose to mark the exact position of the base station, as we determined it with static GNSS measurements, and we plan to use it for numerous surveys performed during the monitoring of the stockpile. We chose the location of the base station outside the perimeter for safety reasons so that the workers won't disturb it.



Figure 1. Dual band GNSS receiver - base station



Figure 2. Base point - FENO Landmark

For the photogrammetric work we used a Phantom 4 Pro Drone (Figure 3), having an on board, 20-megapixel camera with 1" CMOS sensor.



Figure 3. DJI Phantom 4 Pro Drone

For processing the data, we used various software products like: Dronedeploy, Agisoft Photoscan, Global Mapper and AutoCad.

Usually specialized software determines the pile volume(s) by calculating the volume of a pile as defined by an area feature by creating sample elevations along the perimeter of the selected area feature to form the 'base' surface. The elevation values for each sample will be where the elevation value from where the sample point intersects with the loaded elevation model (Global Mapper Help, 2017).

The sample spacing is determined by the width of the area feature and the height of the pile. It will be 1/200 th of the width of the selected area feature, or 1/200 th of the height of the pile - whichever is the smallest interval. For example, a pile that is 50 m width by 40 m tall will have its boundary resample at 0.2 m spacing ( $40 \text{ m} / 200 \text{ m} = 0.2 \text{ m}$ ) (Global Mapper Help, 2017).

The volumes are then calculated by creating a terrain surface from the pile area, calculating the area surface from the generated terrain surface, and then subtracting from the actual terrain (Global Mapper Help, 2017).

To use the Pile Volume measurement tool, we will need an area feature that encompasses the hill or pile we would like to measure the volume of, or you will need to digitize a new area feature around the pile. The area feature does not need to have elevations defined for vertices, as the elevation values to calculate the Pile Volume will be derived from the generated samples (Global Mapper Help, 2017).

For a more accurate measurement, we need to make sure the area feature fully encloses the pile or hill, without having a lot of space around the perimeter (Global Mapper Help, 2017).

## RESULTS AND DISCUSSIONS

Within this paper we determined the stockpile volume from A3 highway construction site from Abram, Romania. The new A3 highway it's part of the national highway routes and this specific section is 60 km long which connects Bors (border to Hungary) and Suplacu de Barcau. This particular section has two major material stockpiles, one in Abram at km 21.7, and another in Salard at km 50.5, so that the distance that the vehicles most cross for delivering materials is minimized as much as possible. As a first step we picked the location and marked the ground control points inside the perimeter, so that the GCP's are evenly distributed (Figure 4).



Figure 4. Ground control points location

The next step we made is planning the flight. We programmed the drone using Dronedeploy for a flight at 100 m above ground and a front overlap of 75% and side overlap of 65%.

Because the drone takes as reference the take-off point, we didn't get the same results as programmed.

In Figure 5 it can be seen the location and the actual overlap of the cameras.

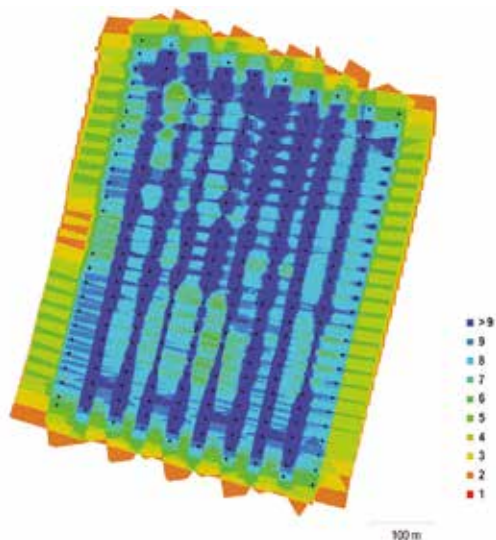


Figure 5. Camera locations and image overlap

Due to the GNSS receiver precision, and the Ground control points marking, we obtained a total planimetric error of 0.01701m. The total altimetry error was 0.0110m as it is presented in Table 1.

Table 1. Ground control points and errors (RMSE)

GCP	XYerror (m)	Zerror (m)	Projections	Error (pix)
2066	0.02231	0.0103	10	0.3860
2067	0.02582	-0.0304	6	0.3130
2068	0.01892	-0.0066	11	0.2090
2069	0.00538	0.0092	7	0.2220
2070	0.00944	-0.0023	10	0.2460
2071	0.01807	0.0014	10	0.2000
2072	0.01844	0.0010	8	0.2820
2073	0.01238	0.0063	7	0.1390
2074	0.01756	-0.0100	8	0.2080
1148	0.01939	-0.0042	8	0.2610
1153	0.00618	-0.0022	6	0.2390
<b>Total</b>	<b>0.01701</b>	<b>0.0110</b>		<b>0.2550</b>

Regarding the fact that we are intending to compute stockpile volumes, we are more interested in altimetry, so we consider the results satisfactory to compute the volumes. The block compensation of the aero-triangulation error was computed as root mean square error (RMSE) (Vorovencii, 2010) as it results from the equations 1 to 5.

Average square error:

$$\sigma_0 \pm \sqrt{\frac{|FF|}{r}} \quad (1)$$

Where r - compensation redundancy.

$$r = 3(n'_R + n'_L) - (n_M + 3n_L) \quad (2)$$

- $n_M$  - no. stereomodel blocks;
- $n_L$  - no. pass points;
- $n'_R$  - total no. of control points appearances on  $n_M$  models;
- $n'_L$  - total no. of control points appearances on  $n_L$  models.

The root mean square errors in control pass and sparse points are calculated as follows:

$$e_R \pm \sqrt{\frac{[v_{n'_R}^2 + v_{n'_L}^2 + v_{n'_C}^2]}{3n'_R}} \quad (3)$$

$$e_L \pm \sqrt{\frac{[v_{n'_R}^2 + v_{n'_L}^2 + v_{n'_C}^2]}{3n'_L}} \quad (4)$$

$$e_C \pm \sqrt{\frac{[v_{n'_C}^2 | v_{n'_C}^2 | v_{n'_C}^2]}{3n'_C}} \quad (5)$$

After obtaining the digital elevation model in Agisoft, we could compute the volume, directly, just by making a perimeter for the stockpile and then determining the exact volume. We performed a case study on the site of the new A3 highway, on the two stockpiles, one at km 21.7 in Abram, and another at km 50.5 in Salard. The stockpiles were specifically numbered as shown below in Figure 6. According to the requests of the beneficiary constructor, all the results will be reported with these names, and numbering of the stockpile, so that we could better keep the inventory of the crushed stone and other materials stored there.

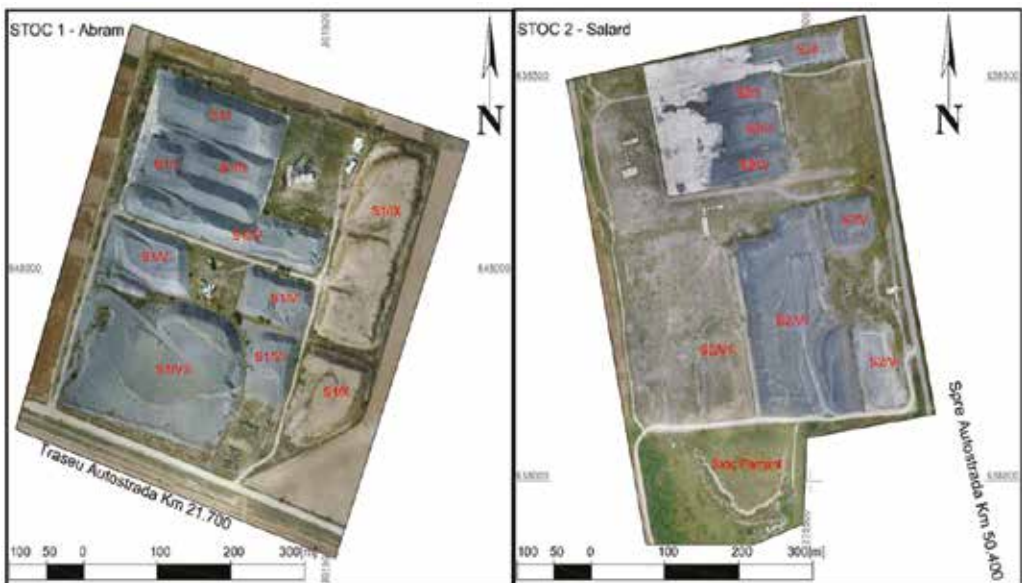


Figure 6. Stockpiles taken into the case study

We performed the volume computation using directly Agisoft Photoscan. The surface used for volume computation was the DEM, derived

from the dense point cloud. In order to compute the volume, we had to draw a polyline, determining the contour of the stockpile. This

polyline was drawn on the orthophotomap. In Figure 7 the volume computation for stockpile plot 1 is presented.

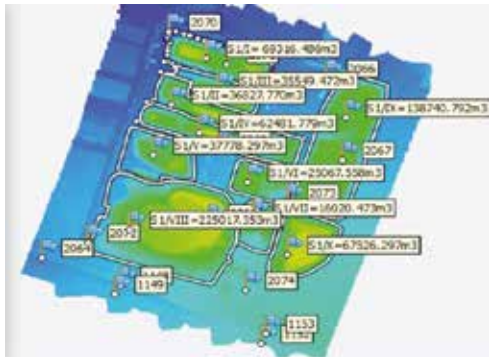


Figure 7. Stockpile volume computation using Agisoft Photoscan

For determining the right value for stockpile volume, we have to choose from a set of options in Agisoft Photoscan. The software computes the volume above the best fit plane, the volume above mean level, and the volume above a custom level. If the stockpile is inaccessible from the margins, or it is very close to other stockpiles, than we cannot use the option of computing a best fit plane. We will have to find a custom level and compute the volume above that. In our case, the stockpiles were mostly disposed above a concrete plane, of which level we determined by measuring the extremities, so we were able to find a custom level above which we made the volume computation.

In order to validate the results, we used two more software to process and compute volumes. We used Dronedeploy to reprocess all photos and determine the volumes, and we also used Global Mapper.

In Figures 8 and 9 we presented the stockpiles and volume computation using Dronedeploy.

As a third comparable value we made the volume computation in Global Mapper. For obtaining the 3D model, we generated a DEM from the point cloud exported from Agisoft Photoscan. Global Mapper computes volume dividing the surface into more sections, as it was presented before at materials and methods. In Figure 10 it can be seen a cross section in Global Mapper, and in Figure 11 the volume computation for a stockpile.



Figure 8. Stockpile 1 presented in Dronedeploy



Figure 9. Stockpile volume computation using Dronedeploy

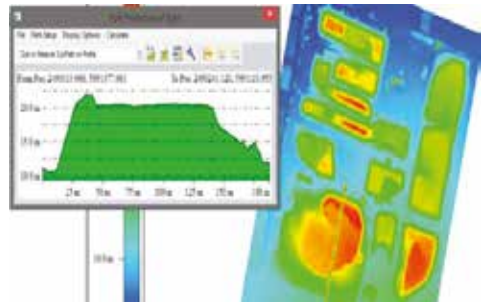


Figure 10. Cross section of a stockpile Global Mapper

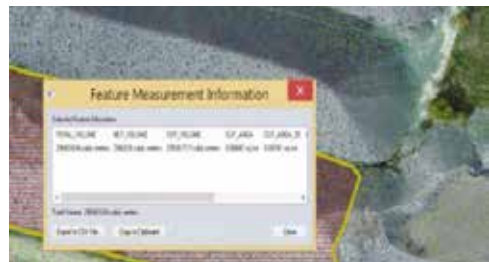


Figure 11. Volume computation Global Mapper

After computing the volume using three different software, we compared the obtained results. We had differences up to 3.07%, mostly because of the vectorisation of the

surface area taken into study, and the difference between applied volume calculation methods. The results are presented in Table 2.

Table 2. Stockpile 1 Volumes and differences using the three software solutions

Stockpile	1. Volume Dronedeploy [m <sup>3</sup> ]	2. Volume Agisoft [m <sup>3</sup> ]	2. Volume Global Mapper [m <sup>3</sup> ]	Difference % (1, 2)	Difference % (1, 3)	Difference % (2, 3)
S1/I	69316.486	70092.831	70711.333	1.120	1.990	0.875
S1/II	36827.770	36246.628	36540.334	-1.578	-0.793	0.804
S1/III	35549.472	35094.794	35260.642	-1.279	-0.823	0.470
S1/IV'	62481.779	63856.378	63329.792	2.200	1.328	-0.831
S1/V	37778.297	38265.259	38080.593	1.289	0.790	-0.485
S1/VI	25067.558	24727.642	24807.918	-1.356	-1.050	0.324
S1/VII	16020.473	16337.999	16189.081	1.982	1.032	-0.920
S1/VIII	225017.353	218514.351	219869.155	-2.890	-2.356	0.616
S1/IX	138740.792	134481.450	135253.688	-3.070	-2.593	0.571
S1/X	67526.297	68167.797	68173.891	0.950	0.950	0.009

## CONCLUSIONS

As shown in the Table 2, there are no significant differences in volume computation by using different software.

Agisoft Photoscan computes the closest volume, comparing to Global Mapper, but Dronedeploy is more different than the others, maximum variation determined was 3.07%.

If it is to put in balance, those 3% regarding to the 138740.792 square meters is not significant at all, as per the total surface of the stockpile it would generate less than 1cm in height difference.

Comparing to classical methods, the UAV photogrammetric method is safer for the operator, and in the same time is much more cost efficient, as the measurements are made really quick. The UAV photogrammetric method, we can say it's more accurate, as it captures all the details regarding the stockpile, it could be said that we obtain a model, stone by stone. By classical methods we never capture all the characteristic elements of the stockpile, for example small gaps or hills. we usually capture a general surface, and we just ignore the small details, as it is much more time consuming to get all the small characteristics, and in fact it doesn't count as much in percent's regarding the whole volume.

Comparing the volume determination using UAV photogrammetric methods to the classical ones, where usually u measure a number of cross sections, and then approximate the volume by multiplying the cross sections surface with the distance between them, we can easily say that by classical methods we lose much more details than using the UAV photogrammetric method. Those details represent much more than those 3% difference from the software, thereby we can affirm that any software used is closer to reality than the classical volume computation.

## REFERENCES

- Carvajal, F., Aguera, F., Perez, M. (2011). Surveying a Landslide in a Road Embankment Using Unmanned Aerial Vehicle Photogrammetry. ISPRS, XXXVIII-1/C22, 201–206.
- Raeva, P. L., Filipova, S. L., Filipov, D. G. (2016). Volume computation of a stockpile – a study case comparing GPS and UAV measurements in an open pit quarry. The International Archives of the Photogrammetry, Remote Sensing and Spatial Information Sciences, XXIII ISPRS Congress, Prague, Czech Republic, XLI-B1, 999–1004.
- Vorovencii, I. (2010). *Fotogrammetrie*. Matrixrom, Bucharest, Romania, ISBN 978-973-755-580-9.
- \*\*\* (2017) Global Mapper Help, Blue Marble Geographics <https://www.bluemarblegeo.com>

## SUSTAINABLE ARCHITECTURE: RESTORATION OF THE FACADES OF HISTORIC BUILDINGS USING MODERN METHODS

**Bogdan ERGHELEGIU, Alexandra TRIF, Raluca-Margareta MANEA**

University of Agronomic Sciences and Veterinary Medicine of Bucharest, 59 Marasti Blvd,  
District 1, Bucharest, Romania

Corresponding author email: [erghelegiubogdan@gmail.com](mailto:erghelegiubogdan@gmail.com)

### **Abstract**

*This paper presents a comparative study of different methods used in building front reconstruction. It compares modern methods of automatic image acquisition and processing of building fronts which have been subject to degradation. The first method presented involves using data captured with a drone. The drone captured multiple photos which have been stitched together using software to create an orthophoto map. This map was then used to vectorize the image, by using the Vector Magic software which automatically transforms a raster into a vector network. The second method presented takes a different approach by creating a point cloud of the building directly with the help of the Leica Scan Station 2. A comparative study is presented, by showing the advantages and disadvantages of both methods, as well as their similarities and differences.*

*We can note from this study that a reliable solution for conservation and restoration of historical buildings is available by combining modern technology and known software solutions.*

**Key words:** facade, restoration, Point Cloud, Vector Magic.

### **INTRODUCTION**

Buildings' façade mapping is one of the most important procedures in urban design as provides the basis for the urban scene analysis and the evaluation of the quality of the built environment. The current most used procedure for mapping a buildings' facade capturing photographs, scaling them with measured distances and then manually tracing the façade edges using CAD software (Attya & Habib, 2013).

This method is limited by the omission of the geo-referencing process which makes it possible to add the façade maps as details to mass-block 3D city models.

Enriching 3D city models with building's façade details is crucial for many applications such as urban scene analysis, heritage conservation, urban recognition and visual navigation among many others (Attya & Habib, 2013).

The digital 3D survey of building façades represents a well-established issue, which has been improved in the last 15 years thanks to the introduction of several active and passive digital systems (Carnevali et al., 2018).

The introduction of light UAVs (Unmanned Aircraft Vehicle) or RPAS (Remotely Piloted Aircraft Systems) equipped with digital camera seems to be in such sense the best solution to acquire hidden or unreachable building areas, overcoming terrain limitations (Carnevali et al., 2018).

Compared with aerial photogrammetry, close range photogrammetry and particularly architectural photogrammetry isn't limited to vertical photographs with special cameras.

The methodology of terrestrial photogrammetry has changed significantly, and various photographic acquisitions are widely in use (Grussenmeyer et al., 2002).

Close range photogrammetry is a technique for obtaining geometric information, e.g. position, size and shape of any object that was imaged on photos before (Grussenmeyer et al., 2002).

3D surface information can be obtained efficiently via remote sensing technologies applied to UAVs at close range domain. Spectral images provide spectral features whereas LiDAR point clouds contain 3D spatial features (Popescu et al., 2017).

The building that is the subject of the study is one of the oldest buildings belonging to the university, where chemistry classes are held.

## MATERIALS AND METHODS

### Standard Method

The measurements were taken with a Leica Scan Station 2 (Figure 1). 3D Laser Scanning, also known as terrestrial LIDAR, has been commercially available for several years, providing a detailed, reliable, and accurate solution to many surveying and measurement problems (Marinescu et al., 2013; Popescu et al., 2015).



Figure 1. Leica Scan Station 2

Terrestrial laser scanners produce a dense point cloud of an object's surface.

For many applications a reconstruction which is as close to the original as possible is required. The most typical example is the visualization of the scanned data. In many respects, laser scanning follows the same general surveying process as other instruments: data is collected in the field, adjusted to the appropriate coordinate system, and relevant features can be extracted to produce deliverables ranging from topographic maps, coordinate values, 2D or 3D CAD drawings (Marinescu et al., 2013).

### Image acquisition

DJI Phantom 3 Professional drone was used. The drone flew on a single altitude band with the camera pointing perpendicularly to the facade of the building. It took off from the ground and flew in parallel with the building

until it reached the roof (Figure 2) (Erghelegiu et al., 2018).



Figure 2. DJI Phantom 3 Professional

The building that is the subject of the study is one of the oldest buildings belonging to the university (Erghelegiu et al., 2018).

### Data process

The photogrammetric data were processed in Vector Magic and AutoCAD software.

Vector Magic analyses the image and automatically detects appropriate settings to vectorize it with, and then goes ahead and traces out the underlying shapes in full colour.

Vector Magic uses the blending to make the vector result resemble the input image as closely as possible (Figure 3) (<https://vectormagic.com/>)



Figure 3. Automatic vectorization

Vector Magic carefully traces out every pixel in image, slicing each edge pixel at precisely the right spot to re-create the intention of the original.

Graphics recognition is conceded with the analysis of graphics-intensive documents, such as technical drawings, maps or schemas. Vectorization, i.e. raster-to-vector conversion, is of course a central part of graphics recognition problems, as it deals with converting the scanned image to a vector form suitable for further analysis. Many

vectorization methods have been designed throughout the years, and several software packages are available. Thus, in one sense, the basic raster-to-vector conversion problem might be solved. However, there is still a major problem of precision, robustness and stability of the vectorization processes (Tombre et al., 1998; 1999; 2000).

## RESULTS AND DISCUSSIONS

As a result of taking pictures with the help of the drone, we obtained the orthophoto map which includes the facade of the building following the steps in the scientific article published last year by Erghelegiu et al., 2018.

Thus, continuing the research, we digitized the obtained image automatically through the Vector Magic processing software.

The vectorization process takes a minute or two, depending on how fast processor is. Once it is done, we will find the result on the "Review result" page. On this page, we can quickly reprocess the image with slightly changed settings, or we can edit it manually.



Figure 4. Computing the vector map.

The first step involved the insertion of the desired image and the selection of the accuracy parameters that are desired for a fairer vectorization of the façade (Figure 4).



Figure 5. Removing background vectors

After obtaining the automatic result, we proceed to the next step, namely the one in which the vectors that are not part of the studied object will be removed, vectors such as those representing the background of the image (Figure 5).

The segmentation editor works in a similar manner to Microsoft paint, or any other simple bitmap editor. It allows the user to make manual edits to a coarse, pixel-aligned version of the vector image. This is particularly useful for correcting mistakes like this one, where the wrong shapes are connected.



Figure 6. Exporting vectors in dxf format

The result obtained can be exported in several formats, as well as the one in "\*.dxf" compatible with CAD software. This step is exemplified in Figure 6.



Figure 7. Preview of vectors-network

Here is another view that shows the outlines from the vector image superimposed over the original bitmap image. As we can see, nodes are generally placed in very sensible locations, and the vector image very closely follows the actual shape boundaries in the original bitmap. That the edges in the vector image slice right through the anti-aliasing in the original bitmap is one of the best features of Vector Magic in comparison to other auto-tracing tools. Figure 7

shows the vector network superimposed over the image layer for a more objective analysis.

That takes us to the page for saving our vectorized result to the hard disk or dragging and dropping it on another program. In this case, we've elected to use the "Quick Save" feature. Quick save allows us to save the vectorized result to the specified directory and using the specified file format with a single click.

The next step is the standard method of determining point cloud on the building façade as a comparison with the previous method.

Terrestrial laser scanning technology allows measurement of a large number of points placed on the object monitored without the need for them to be accessible but only visible. The principle of laser scanning system is very simple; the scanner emits a laser beam that is reflected from the object. When measuring a characteristic point on the surface of the object, three observations are made: slope distance and two angles - horizontal angle and vertical angle (Calin et al., 2015).

In AutoCAD, we can create models in a conventional way. AutoCAD, however, comes with a programming environment (more than one), with which we can create a set of instructions, including the rules and constraints of the design (as well as parameters defining certain aspects of the design), which can be used to build the model. We can use these instructions to always build a model from scratch, each time using the same parameters, or experimenting with different ones.

We can create a TIN surface from points within RCS format point cloud scan files and RCP format point cloud project files created with Autodesk® ReCap™.

We can use the Create Surface from Point Cloud command to create a surface from several point clouds, selecting only the areas that we want to include and filtering out non-ground points, so they are not included in the resulting surface. When using this command, we can select entire point clouds or areas of point clouds to include in the surface. We can select areas of point clouds by using window selections, by defining polygon areas, or by selecting existing closed polylines in the drawing.

In the following figure we can analyse the result obtained by scanning the facade and obtaining the cloud of points (Figure 8).



Figure 8. Point cloud of the facade

The point cloud renders every detail of the facade very precisely with a modelled surface precision (noise) of 2 mm, an scan resolution of 6 mm (Gaussian - based) for position and 4 mm (FWHH - based) for distance at a range of 0 m-50 m, the maximum range being 300 m at 90% (134 m at 18%) and a maximum instantaneous scan rate up to 50.000 points/sec.

A point cloud is a large collection of points acquired by 3D laser scanners or other technologies to create 3D representations of existing structures.

Point cloud files support the design process by providing real-world context where we can recreate the referenced objects or insert additional models. Once a point cloud is attached to a drawing, we can use it as a guideline for drawing, change its display, or apply a colour stylization to distinguish different features.

Sectioning a point cloud provides another way for us to extract the geometry from it. The PCEXTRACTSECTION command identifies the underlying 2D geometry in the point cloud and creates a 2D line drawing. By default, the geometry is created on a plane coincident with the section plane (Fei Dai & Ming Lu, 2008). We can define the geometry that we want to extract, the layer on which it is created on, the colour of the resulting 2D lines or polylines, the width of the polylines, and the tolerance settings.

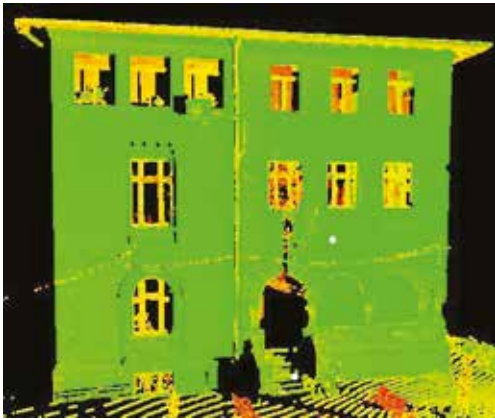


Figure 9. Facade Model from Point Cloud

Deliverables can be extracted straight from the point cloud without further processing, or by first creating a 3D surface model from the point cloud and extracting the deliverables from this surface model (Figure 9).

Building models can be explicit. Every aspect of the model is well-defined and can be described, typically independently without referring to other parts of the model. In a computer model in which a building is represented explicitly, we can, for example, get the coordinates of any point in the building, and from this information, even create various representations (such as plans and sections, renderings, physical models), and even create the real building. During the design process, where decisions about the building are being made as the model is being built, aspects of the model are built, tested (by various methods), and continually modified (Neil et al., 2008).

## CONCLUSIONS

Both methods are usable in the reconstruction of building fronts. The method presented in this study which uses a laser scanner to create a point cloud of the building front is more accurate and precise, when compared to the method which involves using images captured by drone.

It is recommended to use the drones to acquire images of a building with complex details and 3D laser scanning of those elements. The two methods are complementary.

The 3D scanning method is a precise method that can recreate the facade of the building with

superior accuracy using the cloud points taken, but at the same time it also presents disadvantages through the high price of the instrument and related software, as well as a thorough knowledge of the data processing.

The greatest advantage is the using a point cloud we have the possibility to extract any information we need to determine surfaces or other details.

3D models of building components or construction resources have been largely created by computer-aided-design (CAD) or by proprietary code for virtual reality development. Such 3D modelling methods entail accurate definition of points, lines and their relationships in the spatial coordinate system. Unlike CAD modelling, the surveying technique of photogrammetry takes a completely different approach by deriving metric information about an object through measurements conducted on photographs of the object. The very basic technique of photogrammetry is effective and computationally simple. With much less efforts, digital cameras and photogrammetry software have made possible 3D reconstruction of an object in digital form (coordinates and derived geometric elements). The resultant 3D models may well satisfy application needs in construction simulation visualization.

The method in which the drone was used to acquire images is less precise but faster, and the software used is cost-effective and easy to use. Thus, depending on the desired accuracy, one of the two methods can be used.

It is recommended to study the facade of the building before acquiring the data and to determine the best method according to the complexity of the details to be recreated. In some cases, both methods can be used to increase the quality of the final product.

Architectural façade mapping is one of the important tasks in wide range of geospatial applications. Existing 3D mass-block city model was used in this research to obtain control points for façade mapping. In order to reconstruct the facades of buildings, both 3D scanning and photogrammetric methods using drones can be used, and the images are further processed with software such as those presented.

## ACKNOWLEDGEMENTS

The authors would acknowledge the Faculty of Land Reclamation and Environmental Engineering for support and allowing the acquisition of the oldest building belonging to the University of Agronomic Sciences and Veterinary Medicine of Bucharest. We also want to thank for the use of the equipment and the software that belong to the university.

## REFERENCES

- Attya, H., & Habib, A. (2013). Options for medium-accuracy architectural facades mapping from terrestrial Photogrammetry. ASPRS 2013, Annual Conference Baltimore, Maryland, March 24-28, 2013.
- Calin, M., Damian, G., Popescu, T., Manea, R., Erghelegiu, B., Salagean, T. (2015). 3D modeling for digital preservation of Romanian heritage monuments. *Agriculture and Agricultural Science Procedia*, 6, 421–428.
- Carnevali, L., Ippoliti, E., Lanfranchi, F., Menconero, S., Russo, M., Russo, V. (2018). Close-range mini-UAVS photogrammetry for architecture survey. The International Archives of the Photogrammetry, Remote Sensing and Spatial Information Sciences, XLII-2, 2018 ISPRS TC II Mid-term Symposium "Towards Photogrammetry 2020", 4-7 June 2018, Riva del Garda, Italy.
- Erghelegiu, B., Trif, A., Manea, R. M., Boasca, A. (2018). The Restoration and Remodelling of Facades - A Permanent Necessity for the Conservation of History. Sciendo, International Conference Agriculture for Life, Life for Agriculture 2018, DOI: 10.2478/alife-2018-0057.
- Fei, Dai & Ming, Lu (2008). Photo-based 3D modeling of construction resources for visualization of operations simulation: case of modeling a precast façade. Proceeding WSC '08 Proceedings of the 40<sup>th</sup> Conference on Winter Simulation (pp. 2439–2446), Miami, Florida, December 07-10, 2008
- Grussenmeyer, P., Hanke, K., Streilein, A. (2002). Architectural photogrammetry (pp. 300–339). Chapter in *Digital Photogrammetry*, edited by M. KASSER and Y. EGELS, Taylor & Francis.
- Marinescu, C. C., Trif, A. (2013). 3D laser scanning for surveying application. *Journal of Young Scientist*, Vol. 1, ISSN 2344-1283, 227–232.
- Neil C. Katz, Skidmore, Owings & Merrill LLP. (2008). Parametric modeling in AutoCAD. A version of this article appeared in AECbytes in 2007.
- Popescu, G., Balota, O. L., Iordan, D. (2015). Direct georeferencing application of aerial photogrammetry using a GNSS/IMU/SENSOR System. Albena, Bulgaria, 18-24 June 2015, SGEM Conference Proceedings ISBN 978-619-7105-34-6/ISSN 1314-2704, Book 2, Vol.1, pp 1043–1050.
- Popescu, G., Balota, O. L., Iordan, D. (2017). Increasing land classification accuracy using unmanned aerial vehicles (uavs) with multispectral LIDAR sensor. Project: Fast system of monitoring and interactive mapping.
- Tombre, K., Ah-Soon, C., Dosch, P., Habed, A., and Masini, G. (1998). Robust and Off-the-shelf Methods for Graphics Recognition (pp. 406–408). In Proceedings of the 14<sup>th</sup> International Conference on Pattern Recognition, Brisbane (Australia), Aug. 1998.
- Tombre, K., Ah-Soon, C., Dosch, P., Masini, G., and Tabbone, S. (1999). Stable and Robust Vectorization: How to Make the Right Choices (pp. 3–16). In Proceedings of 3<sup>rd</sup> International Workshop on Graphics Recognition, Jaipur (India), Sept. 1999. Revised version to appear in a forth coming LNCS volume.
- Tombre, K., Tabbone, S. (2000). Vectorization in graphics recognition: to thin or not to thin. Proceedings 15<sup>th</sup> International Conference on Pattern Recognition. ICPR-2000, DOI: 10.1109/ICPR.2000.906024

## INVESTIGATION OF ANIMAL ORIGIN BIOGAS POTENTIAL USING GEOGRAPHICAL INFORMATION SYSTEMS: EAST MEDITERRANEAN REGION CASE

Ozan ARTUN<sup>1</sup>, Burak SALTUK<sup>2</sup>

<sup>1</sup>Cukurova University, Vocational School of Karaisali, 01770, Adana, Turkey

<sup>2</sup>Siirt University, Faculty of Agriculture, Biosystem Engineering Department, 56100, Siirt, Turkey

Corresponding author email: oartun@cu.edu.tr

### Abstract

*Animal breeding is one of the agricultural activities in Turkey. The animal manure can be used as an organic material in producing biogas. The energy needs of agricultural enterprises can be met by establishing biogas production facilities in these enterprises. In this study, it was aimed to determine the potential areas in the East Mediterranean region of Turkey which is suitable for biogas plants. The East Mediterranean covers Adana, Hatay, Kahramanmaraş and Osmaniye provinces. In this context, the borders of the provinces (Adana, Hatay, Kahramanmaraş and Osmaniye) subjected to the study and the topographic properties of the region were drawn using ARCMAP 10.3 software. In this study, it was aimed to determine the obtainable biogas energy fields and the current situation in the provinces in the East Mediterranean region. Furthermore, the number of cattle in the East Mediterranean region for the years 2013-2017 was benefited from in this framework. The potential biogas areas in each province were determined and these areas are tried to be interpreted. The areas that are suitable, non-suitable or partially suitable for biogas energy production were determined. The finding that a total of 7634583.885 tons of annual wet manure can be obtained in the study area was obtained. It was determined that a total of 3193690103 MJ biogas energy amount can be obtained per year from this wet manure.*

**Key words:** biogas, cattle manure, East Mediterranean region, GIS.

### INTRODUCTION

One of the most important branches of agricultural production is animal (meat and milk) production. Although the main output of modern production is seen as meat and milk in cattle-breeding facilities, the manure and wastes that animals give to the environment can be accumulated in the storage structures and energy can be obtained, but they are left uncontrolled to the external environment. This situation causes soil and water pollution as well as loss of energy that can be obtained by recycling (biogas) from these wastes. Biogas is one of the most advantageous methods to eliminate and recycle waste from livestock.

The energy in the universe is present and constant since the beginning of time. At the beginning of each transformation of the energy used, the energy that was initially used is consumed so as not to be recovered (Akova, 2008).

Turkey is a country of agriculture and livestock. Studies on biogas began in Turkey

in 1957. After 1975, soil, water and biogas production activities carried out under the General Directorate of Rural Services in the 1980s were supported by some international agreements, but in 1987 they were cut for an incomprehensible reason. Turkey's biogas potential of 17.3 million TEP/year is estimated to be level (Öztürk, 2005).

Biogas typically refers to a gas produced by the biological breakdown of organic matter in the absence of oxygen. Biogas originates from biogenic material and is a type of bio fuel.

The continuing use of fossil fuels and the effect of greenhouse gases (GHGs) on the environment have initiated research efforts into the production of alternative fuels from bio resources. The amount of GHG emissions in the atmosphere is rising, with carbon dioxide (CO<sub>2</sub>) being the main contributor. In addition, the global energy demand is increasing rapidly, with approximately 88% of the energy produced at the present time being based on fossil fuels (Anonymous, 2014; 2015).

Anaerobic digestion (AD) is expected to meet with increasing success due to the low cost of available feedstock's and the wide range of uses for biogas (i.e., for heating, electricity, and fuel). Biogas production is growing in the European energy market and offers an economical alternative for bio energy production. A study by Achinas et al. (2017) provides an overview of biogas production from lignocelluloses waste, thus providing information toward crucial issues in the biogas economy.

On a farm that feeds 200 cows, 200 cattle per day  $\times$  62 l/day/cow = 12400 l fertilizer/day occurs (Öztürk, 2017).

Gas produced by biogas production is not a pure gas. The content of this gas includes approximately 55-75% CH<sub>4</sub> gas, 25-45% CO<sub>2</sub> gas, 1-10% hydrogen gas (H<sub>2</sub>), 0-0.3% nitrogen (N<sub>2</sub>) gas and 0-3% hydrogen sulphide gas (H<sub>2</sub>S) (Weiland, 2010).

Digester volume for typical livestock operation cubic feet per gallon:

- Swine (500 head): 2500/20000;
- Dairy (75 head): 1950/15000;
- Poultry (15000 birds): 5550/42000;
- Beef (300 head): 4050/30400 (Fulhage et al., 1993).

Since the smell of animal fertilizers used in biogas production is lost during the process and many elements threatening human health are eliminated, it will provide a clean and healthy environment for people living in areas where biogas production is carried out (Kumbur et al., 2015).

Since biogas acquisition is mainly based on the decomposition of organic substances, vegetable wastes or animal fertilizers can be used as the main ingredient. Today, biogas production has a wide range of diameters; meets the heating and kitchen expenses of a single house, and is made up of generators with electricity generation (Anonymous, 2018c)

According to the data of 2018 in Turkey, there are 68 business units working with biomass energy (Anonymous, 2018a).

The fact that fertilizers and wastes from animal production are not stored properly and are not used to convert them into energy cause both losses of income and environmental pollution. The pollution that occurs in the

environment due to the energy is caused by burning of carbon and its derivatives and the gases formed in this case; mix into the air, water and soil.

Environmental contamination is the result of the deterioration of the ecological balance in nature, and harm to humans and other living things (Karabulut, 2000).

Keeping environmental impacts at a minimum level of damage requires being sensitive to waste management. In addition, it is necessary to bring animal wastes to the economy. Based on this, the amount of manure obtained from animals according to the type of animals is as follows:

- 3.6 tons/year wet manure from 1 cattle;
- 0.7 tons/year wet manure from 1sheep;
- 0.022 tons/year of manure are obtained from 1 poultry.

Based on these values, it consists:

- 33 m<sup>3</sup>/year biogas from a ton of cattle manure,
- 58 m<sup>3</sup>/year of biogas from a ton of sheep manure,
- 78 m<sup>3</sup>/year biogas from a ton of poultry manure (Koçer, 2006).

Waste and biogas are produced as a result of decay of fertilizers and other substances by microorganisms. Biogas consists of a mixture of methane, carbon dioxide and other gases. Biogas and natural gas are similar. Biogas; can be used as fuel in heating or electricity production. The heating requirement depends on the season, not comparable to the production of fertilizers and biogas. Therefore, biogas is frequently used in electricity production. The electricity produced is used on the farm and surplus electricity can be sold (Öztürk, 2017). Biogas production is an excellent way of using organic waste for energy generation, followed by the recycling of the digested substratum (digested) as fertilizer (Comparetti et al., 2013)

Biogas is a cheap, environmentally friendly energy and fertilizer source and provides waste recovery. As a result of biogas production, weed seeds that can be found in animal manure lose their germination. After biogas production, wastes are not destroyed and they are transformed into a more valuable organic fertilizer (Gizlenci & Acar, 2008).

With 1 m<sup>3</sup> biogas it is possible to:

- Keep working a 60-100-watt lamp for 6 hours;
- Cooking 3 meals for a family of 5-6 people;
- Obtain calories equivalent to 0.7 kg of petrol;
- Run a horsepower engine for 2 hours;
- Obtain 1.25 kWh electrical energy (Öztürk, 2017).

Through biogas; natural balance is maintained by preventing soil, water and air pollution. In addition, wastes from biogas production are used as fertilizer in agriculture (Çanka, 2011).

## MATERIALS AND METHODS

The study was carried out in the East Mediterranean region of Turkey and it covered four provinces (Adana, Hatay, Kahramanmaraş and Osmaniye) (Figure 1). Adana province is located in the northeast of the Mediterranean region and has a surface area of 13844 km<sup>2</sup>. Hatay province is located at the eastern end of the Mediterranean region and is the border province of Syria. The

surface area of Hatay province is 5867 km<sup>2</sup>. The northern part of the province of Kahramanmaraş is quite mountainous and has a surface area of 14525 km<sup>2</sup>. Osmaniye province is surrounded by Amanos Mountains in the east and southeast and Taurus Mountains from the west to the north. The surface area of Osmaniye province is 3215 km<sup>2</sup>.

In this study area, the areas suitable for biogas energy production and the obtainable biogas energy amounts are trying to examine. Furthermore, the number of cattle in the region and the amount of animal waste and biogas were determined. The present number of cattle of 4 provinces (Adana, Hatay, Kahramanmaraş and Osmaniye) and their districts taken from the literature data and the Veterinary Information System (VETBIS) of the Ministry of Food, Agriculture and Livestock for the years 2012-2017 (Anonymous, 2018b).



Figure 1. Map of Turkey (a) and the study area (b)

In the study, Geographic Information Systems (GIS) were used to create database for cattle numbers, animal waste and biogas amounts in the provinces and districts of the East Mediterranean region. It is a known fact that GIS technologies are very useful applications for capturing, storing, manipulating, analyzing, managing, and presenting all types of spatial and environmental data (Glass, 2001).

In the study, the UTM map projection and WGS 84 datum are selected as the reference system and all maps and data were transferred to the chosen projection and datum using ArcMap 10.3 software (ESRI, 2010). In the

study, it was aimed to assess the presence of cattle, and animal waste and biogas amounts in the provinces in question, on the basis of districts, in the Geographical Information System environment. For this purpose, the places in question were digitized in the GIS environment as a polygon first within the limits of the province and then the district boundaries. In order to make an examination of each province independently of other provinces, all boundaries were divided on the basis of the provinces as a separate layer. Similarly, the districts of each province were divided in the form of district boundaries as a

separate layer. The database (attribute data) was created by entering the numbers of cattle supplied from the VETBIS system to all these layers prepared.

In this study, the places that are suitable for establishing biogas units were shown on the maps created on the basin by determining the animal waste and biogas amounts on the basis of districts by means of benefiting from the present cattle number for 2015 obtained from the VETBIS system and the related literature (Anonymous, 2018b).

Hill (1982) and Ekinci et al. (2010) are reported that, it is very important to determine the capacity before projecting biogas facilities. In the study area, the calculation of biogas production quantities was performed taking into account the use of whole manure produced. An average amount of 43 kg·day<sup>-1</sup> of manure obtained from mature cattle can be taken as a basis, for the calculation of the amount of manure.

While producing the prediction map of the study area, the districts with cattle between 0 and 1000 heads were determined to be the areas not potential for biogas and coloured in orange (●), and the districts with cattle between 1000 and 10000 heads were determined to be potential biogas production areas and coloured in yellow (●). Again, the districts with more than 10000 heads of cattle were determined to be high-potential biogas production areas and coloured in green (●).

## RESULTS AND DISCUSSION

When the provinces in the study area were compared with each other, it was seen that Adana and Kahramanmaras provinces take an important place both in terms of land area and animal numbers. In the study area, the total number of cattle was determined to be 173945 in Adana province, 147898 in Kahramanmaras province, 107272 in Hatay province and 57128

in Osmaniye province for year 2017 (Table 1). Upon examining the study area, it was determined that livestock breeding was performed at a lower level in Osmaniye province. In the study area, it was determined that the number of cattle slightly decreased due to population density; however, biogas production has not changed.

The number of animals in the study area has increased arithmetically in the last 5 years. In particular, the province of Kahramanmaras which in the inner parts of the region and the Feke, Saimbeyli districts of Adana province and Tufanbeyli district on the border with Kayseri province have a potential in terms of obtaining biogas from livestock enterprises. As the livelihoods of these districts are fruit growing and livestock breeding, biogas planting in these areas can meet the needs of the region and can prevent especially the pollution caused by livestock. Due to the existence of usable river sources at the borders of the three districts and especially the winter precipitation is too much in these areas, it is very important to protect the water resources in the region. Seyhan River is used for irrigation of Cukurova delta and it is the most important water source of the region therefore the pollution control of the river is very important. In this context, one or several biogas plants to be established will generate electricity and heat and provide economic benefits to the region. As a result of biogas production, the smell of animal manure disappears unimaginable and the resulting product is transformed into a more valuable organic fertilizer. Methane gas, one of the worst greenhouse gases produced in biogas plants, is converted to CO<sub>2</sub> by burning. In addition, it helps to reduce the effectiveness of the disease factors that threaten human health, provides a significant loss of effectiveness of the diseases that threaten groundwater and creates healthier, hygienic living spaces.

Table 1. Number of cattle in the East Mediterranean Region provinces between the years 2013-2017

Province	Total Number of Cattle				
	2013	2014	2015	2016	2017
Adana	190955	152687	172641	174209	173945
Hatay	102262	97469	93761	89765	107272
Kahramanmaras	102080	127093	129860	134854	147898
Osmaniye	66209	51335	53006	50793	57128

There are various ways to calculate the amount of wet manure and obtainable biogas energy in the literature. In the study area, the amount of wet manure and obtainable biogas energy were calculated for the year 2017, according to Hill (1982) and Ekinçi et al. (2010) using the number of cattle, and the results are given in Table 2.

In the calculation made according to Hill (1982) and Ekinçi et al. (2010), it was determined that the highest amount of wet manure and obtainable biogas energy was in Adana province. Adana province was followed by Kahramanmaraş, Hatay and Osmaniye provinces, respectively (Table 2).

Table 2. The amount of potential wet manure and obtainable biogas energy in the Eastern Mediterranean Region provinces

Province	Total Number of Cattle (2017)	Average Amount of Wet Manure (kg/year)	Amount of Obtainable Biogas Energy Mj/year
Adana	173945	2730066775	1142487244
Hatay	107272	1683634040	704572661.7
Kahramanmaraş	147898	2321259110	971408079.7
Osmaniye	57128	896623960	375222117.8

The calculation method of Hill (1982) and Ekinçi et al. (2010) was also used separately for the districts of all provinces in the study area, and the amounts of wet manure and potential biogas energy of these districts were calculated.

With these calculations, the appropriate places where biogas energy production facilities could be established in the provinces of the East Mediterranean region are trying to be determined. Also the suitability maps are evaluated in the GIS environment.

The highest animal population in the study area is in Adana province and it is especially concentrated in Sarıçam and Yüreğir districts. According to the VETBIS records for the year 2017, the cattle amount of Sarıçam and Yüreğir districts in Adana constitutes 29.76% of the current population of cattle in Adana province.

Thus, biogas production facilities built in the region, such as these districts, can reduce the amount of input in the operator's energy costs and will increase the productivity. Due to the fact that animal breeding is concentrated in this region, there is a 1 MW biogas production facility established by Adana Municipality in Kozan district in 2017.

In addition, Seyhan, Kozan, Ceyhan and Tufanbeyli districts are also seen as a potential biogas production area. The number of cattle in these six districts constitutes approximately 70.26% of the total number of cattle in Adana province. In the study it was determined that

biogas plant investments would also be appropriate in these regions.

In the study, a slight decrease was observed in the number of cattle in the province of Adana between years 2013-2017. This is due to increased input costs and reduced pastures.

When 2017 data are analysed, it is determined that 43.60% of Adana province are very convenient and 56.40% of them are potential for biogas production (Figure 2).

It is also determined that 1142487244 Mj/year of biogas based electrical energy can be obtained in Adana province.

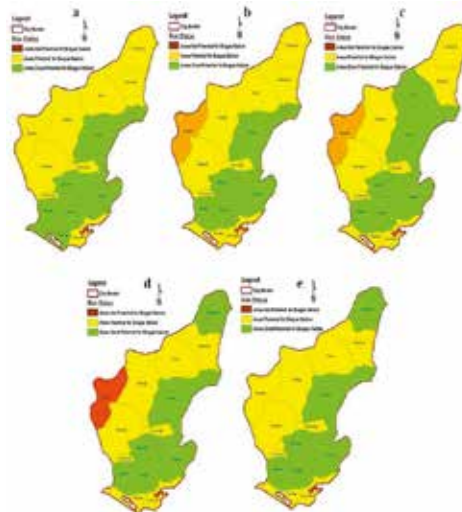


Figure 2. Potential Biogas Energy Fields in Adana province (a. 2013; b. 2014; c. 2015; d. 2016; e. 2017)

Central, Samandag and Kirikhan districts constitute 41.66% of the total animal husbandry potential of Hatay province. It is determined that the planned biogas plants should be built in these districts (Figure 3). It was determined that the electrical energy of 704572661.7 Mj/year would be obtained in Hatay province, depending on the wet manure supplied from this source.

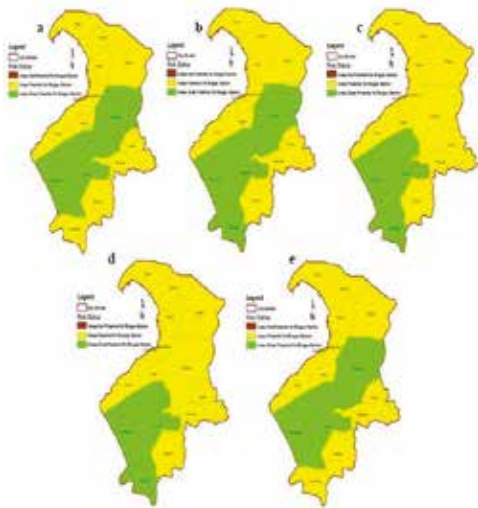


Figure 3. Potential Biogas Energy Fields in Hatay province (a. 2013; b. 2014; c. 2015; d. 2016; e. 2017)

Because of the low total number of cattle, the potential biogas production sites of Osmaniye province are limited. Kadirli, Central and Duzici districts account for 74.58% of the total animal husbandry potential of Osmaniye province (Figure 4).

According to 2017 data it was determined that 96.03% of Osmaniye province is suitable for biogas production and 3.97% are not suitable for biogas production.

In Kahramanmaraş province, 48.26% of all provincial cattle are located in the Afsin, Elbistan and Dulkadiroglu districts.

It was determined that 90.65% of Kahramanmaraş province are suitable for biogas production and 9.35% are not suitable for biogas production. 971408079.7 Mj/year of biogas based electrical energy can be obtained annually from the biogas facilities that can be installed in Kahramanmaraş province (Figure 5).

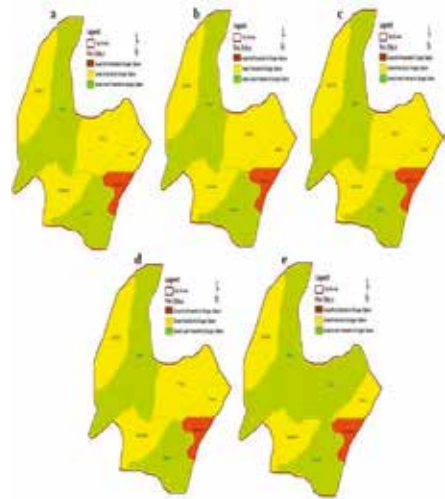


Figure 4. Potential Biogas Energy Fields in Osmaniye province (a. 2013; b. 2014; c. 2015; d. 2016; e. 2017)

According to the information in "Final Renewable Energy Sources" list of Turkey in 2018, there are 62 facilities that obtain biomass energy and these are diversified as landfill gas, biogas, vegetable and animal wastes. In the study area there are two facilities in Adana and Kahramanmaraş that have a power capacity of 1840 MWm/Mwp and 1232 MWm/Mwp respectively. When the number of cattle in the study area is evaluated, it is seen that this number is below the potential.

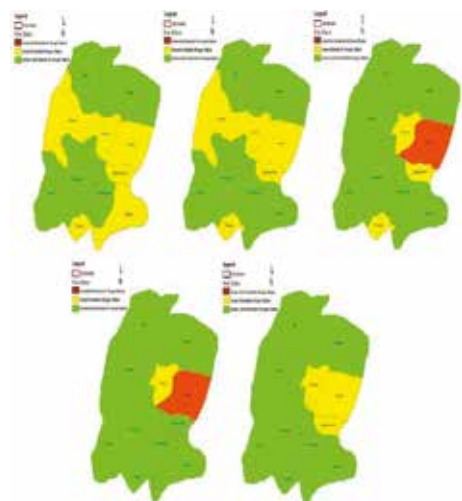


Figure 5. Potential Biogas Energy Fields in Kahramanmaraş province (a. 2013; b. 2014; c. 2015; d. 2016; e. 2017)

In the study area, it was determined that the total potential biogas energy of 21654515836 MJ/year would be obtained from approximately 7631583.9 tons of animal manure.

## CONCLUSION

The appropriate biogas production sites were trying to be determined in the study area for the years 2013-2017, using the ARCMAP 10.3 software. In this context the given number of cattle and their wet manure production values are used. As a result, the regions, where the number of cattle is high, are identified as the areas suitable for potential biogas production. In addition, the amounts of biogas energy per year 2013-2017 are calculated from the existing cattle numbers in these years, in the East Mediterranean Region. Upon examining the animal capacities of the provinces in the study area, Adana (35.77%) and Kahramanmaraş (30.42%) provinces are those with the highest number of animals in the basin. Thus, biogas energy production studies can be prioritized in these two provinces starting from Adana province. Upon examining the districts in the study area, the districts with the highest number of animals in Adana province are Sarıcam Yüreğir, Seyhan and Kozan districts. In the year 2017, there are 95.374 heads of cattle for the biogas energy production areas to be established in this region. Considering that cattle manure can be collected from these animals, the number of animals needed for biogas energy production areas can be easily fulfilled from this region. Thus, the information that Adana province is the most suitable area for biogas energy production was obtained. Furthermore, Elbistan and Afsin districts of Kahramanmaraş province were also determined as one of the most suitable regions for biogas energy production with a total number of cattle of 50220. It was concluded that biogas energy production facilities to be established in this area will prevent the random collection of animal manure, as well as provide input for the enterprises in an economic sense.

When the fertilizer produced as a result of livestock activities is converted into production, energy production causes pollution

and economic losses. This is also the case if fertilizer is used in plant feeding, not stored and left in indiscriminate environment. As a matter of fact, any pollution (such as litter material, slaughtering wastes, discharge to rivers, etc.) used in agriculture and livestock activities and resulting from activities reaches the levels that threaten the world. In particular, both environment ministries in the European Union candidate countries such as Turkey and in the world are making very strict controls in this regard.

As a result, in this study where the livestock potential is taken as the main material and the potential effects are investigated, it is very important to provide fertilizer storage, especially in areas close to or near the water resources in the basin, to promote the establishment of biogas facilities by making cooperatives in the potential areas.

## REFERENCES

- Achinas, S., Achinas, V., Euverink, G. J. V. (2017). A Technological Overview of Biogas Production from Biowaste <https://doi.org/10.1016/J.ENG.2017.03.002>
- Akova, İ. (2008). *Renewable energy sources* (In Turkish). Nobel Press, Ankara.
- Anonymous (2014). United Nations Environment Programme. The emissions gap report 2014: A UNEP synthesis report Final report, UNEP, Nairobi
- Anonymous (2015). International Energy Agency World energy outlook special report 2015: Energy and climate change Final report, OECD/IEA, Paris
- Anonymous, (2018a). Final List of Renewable Energy Resources (In Turkish) (Accessed date) 26.02.2018. <https://www.epdk.org.tr/Detay/DownloadDocument?id=vCeOhQftrjs=>
- Anonymous (2018b). Turkish Statistical Institute data (Accessed date) 26.02.2018 <https://biruni.tuik.gov.tr/medas/?kn=101&locale=tr>
- Anonymous (2018c). Biogas Investments Development Association (In Turkish) (Accessed date) 26.02.2018. <http://www.biyogazder.org/>
- Comparetti, A., Febo, P., Greco, C., and Orlando, S. (2013) Current state and future of biogas and digestate production. *Bulgarian Journal of Agricultural Science*, 19(1), 1–14, Agricultural Academy.
- Çanka Kılıç, F., (2011). Biogas, It's Importance, General Condition and Place in Turkey (In Turkish). *Engineer and Machine*, 52(617), 94–106.
- Esri (2010). The mapping and analytics platform data (Accessed date) 26.02.2018 <https://www.esri.com/en-us/arcgis/>
- Ekinci, K., Kulcu, R., Kaya, D., Yaldiz, O., Ertekin, C., Ozturk, H. (2010). The Prospective of Potential Biogas Plants that can utilize Animal Manure in

- Turkey. *Energy Exploration & Exploitation*, 28(3), 187–206.
- Fulhage, C. D., Sievers, D., Fischer, J. R. (1993). Generating Methane Gas from Manure. *Agricultural Publication G01881*, Department of Agricultural Engineering, University of Missouri-Columbia.
- Glass, G. E. (2001). *Geographic Information Systems in Infectious Disease Epidemiology* (pp. 231–253). Aspen Publishers.
- Gizlenci, Ş., Acar, M. (2008). Energy Crops and Biofuels (Biodiesel, Bioethanol, Biomass). *Sectoral Report on Energy Plants and Biofuels* (In Turkish). Karadeniz Directorate of Agricultural Research Institute, Samsun.
- Hill, D. T. (1982). A comprehensive dynamic model for animal waste methanogenesis. *Transaction of the ASAE*, 25(5), 1374–1380.
- Karabulut, Y. (2000). *Energy Resources of Turkey*. Ankara University Press, Ankara.
- Koçer, N., Öner, C., and Sugözü, İ. (2006). Livestock Potential in Turkey and Biogas Production (In Turkish). Fırat University, Eastern Anatolia Research Center, Eastern Anatolia Studies, 17-20, Elazığ.
- Kumbur, H., Özer, Z., Özsoy, H. D., Avcı, E. D. (2015). Comparing the Potential Environmental Effects of Conventional and Renewable Energy Sources in Turkey (In Turkish) III. *Renewable Energy Symposium*, 19-21 October, Mersin, Turkey.
- Öztürk, M. (2005). Biogas Production from Animal Fertilizer (In Turkish). Ministry of Environment and Urbanization, Ankara
- Öztürk, M. (2017). Production of compost from animal manure and waste (In Turkish). Ministry of Environment and Urbanization, Ankara
- Weiland, P. (2010). Biogas Production: Current State and Perspectives. *Applied Microbiology and Biotechnology*, 85, 849–860

## A COMPARISON OF BIOCLIMATIC FACTORS EFFECT FOR CUTANEOUS LEISHMANIASIS CURRENT STATUS BETWEEN EASTERN MEDITERRANEAN REGION AND TIGRIS BASIN OF TURKEY BY USING ECOLOGICAL NICHE MODELING

Ozan ARTUN, Hakan KAVUR

Cukurova University, Vocational School of Karaisali, 01770, Adana, Turkey

Corresponding author email: hkavur@cu.edu.tr

### Abstract

*Cutaneous leishmaniasis (CL) is known as tropical and subtropical neglected vector-borne disease in the Old World. Despite the fact that the Eastern Mediterranean Region and Tigris Basin are an endemic area of CL, unfortunately their bio-climatic and environmental variables are relatively poorly understood.*

*The aim of the present study were determining the distribution of disease into endemic foci and comparison of variables in terms of CL epidemiology. For this purpose, extracted numbers of environmental variables from different sources and determined 3044 CL cases' location information obtained from the ministry of health database to are used for modeling of the CL current probability of occurrence. The ecological niche model (ENM) analysis was used for this purpose. ENM analyses are made by using ArcGIS and MaxEnt softwares to explore the ecological conditions of the disease. Our results emphasized that CL current the area under the curve (AUC) value were found 0.868, 0.918 and 0.924 in Adana, Mersin (East Mediterranean Region) and Diyarbakir (Tigris Basin) respectively. Also, BIO1, BIO4, BIO5, BIO9, BIO10 and DEM were found related to the presence of native human cases of CL in East Mediterranean Region. BI O2, BIO4 and BIO11 were found to correlate with CL probable distribution in Tigris Basin. Consequently, there were relationship between temperature data and disease epidemiology for both areas. Also, comparison results of the study could be a reference to the health ministry's CL and vector control studies*

**Key words:** cutaneous leishmaniasis, ecological niche modeling, MaxENT, bioclimatic factors, Eastern Mediterranean Region, Tigris Basin.

### INTRODUCTION

All clinical types of leishmaniasis are vector-borne diseases caused by parasites protozoan from the genus *Leishmania* (Trypanosomatida: Trypanosomatidae). Accordance with the leishmaniasis epidemiology information; reported in large areas of the tropics, sub-tropics, and the Mediterranean basin, including more than 98 countries, where there are a total of 350 million people at risk and 12 million cases of infection.

Leishmaniasis presented two clinical forms in Turkey:

- Visceral leishmaniasis (VL), the most severe and fatal in almost all cases (if is left untreated),
- Cutaneous leishmaniasis (CL) which has a tendency towards spontaneous resolution (Ok et al., 2002; Singh, 2004).

There were two well-known CL high endemic foci in Turkey caused two different *Leishmania* Ross, 1903 (Kinetoplastida:

Trypanosomatida) species. *Leishmania infantum* Nicolle, 1908 (Kinetoplastida: Trypanosomatida) is responsible for both clinical forms occurred many cities of the Mediterranean Region (Mainly Adana, Antalya and Mersin) while *Leishmania tropica* Wright (Kinetoplastida: Trypanosomatidae) causes CL in Tigris Basin (Mainly Diyarbakir and Sanliurfa) of Turkey (Ok et al., 2002). *L. infantum* and *L. tropica* transmitted by dominant species *Phlebotomus tobbi* Adler & Theodor (Diptera: Psychodidae) and *Phlebotomus sergenti* Parrot, respectively in two focused endemic region (Alptekin et al., 1999; Simsek et al., 2007; Svobodova et al., 2009; Kavur & Artun, 2017).

46.003 new cases were reported in our country between 1990 and 2010. 96% of these cases were reported from Şanlıurfa, Adana, Osmaniye, Hatay, Diyarbakir, Icel and Kahramanmaraş provinces (Sucakli & Saka 2007; Gurel et al., 2012).

Related environmental data obtained from different sources have been used for the analyzing of infectious diseases predicted epidemiology by using geographic information systems technologies (Ostfeld et al., 2005). Ecological niche models (ENM) investigations carried out with basic and powerful computers could be used for estimation modeling of various species distributions, environmental requirements, epidemiological status of some neglected diseases (Ostfeld et al., 2005; Philips 2006). Also ENM, including maximum entropy (MaxEnt) present-only data, is widely used in ecology and biodiversity conservation in modeling species distribution and diseases such as malaria and leishmaniasis (Elith et al., 2006).

The aim of this study, comparison of CL current status between Mediterranean Region and Tigris Basin, specifically selected foci in terms of bioclimatic factors and patients report number and locations using MaxENT and ArcGIS software.

## MATERIALS AND METHODS

### Study Area

We selected three endemic foci (Mersin, Adana and Diyarbakir) in two geographical regions, because of the high number of CL patients reported before.



Figure 1. CL cases location and study areas of East Mediterranean Region (Adana and Mersin Province)

Mersin is Turkey's 11<sup>th</sup> major city and it is located in the Eastern part of the Mediterranean Region. Mersin's basin is 15.853 km<sup>2</sup> in area. The South and North aspect of Mersin are Mediterranean sea and East Taurus Mountains, respectively.

Also, Mersin has 13 districts and its altitude is 100 m. It is located at 36°48'43.575" north latitude and 34°38'29.331" east longitude. Mersin has a population of 1.814.468 according to the latest population data in 2018 (TSI 2018) (Figure 1).

Adana is located in the eastern part of the Mediterranean Region of Turkey and it is the fifth major city of Turkey. The city has a human population of 2.220.125. Its basin is 14,032 km<sup>2</sup> in area. Adana has fifteen districts and it is located at 37.002 latitude and 35.329 longitude (UTM Zone 36N - WGS84) (TSI, 2018) (Figure 1).

Diyarbakir is the 12<sup>th</sup> largest city in Turkey, is located in the Northern part of the Tigris Basin. Its basin is 15168 km<sup>2</sup> and generally surrounded by mountains.

The central part of Diyarbakir is slightly pitted and is surrounded by the tributaries of the Southeastern Taurus. Diyarbakir, which has 17 districts, has a height of 674 m. The city of Diyarbakir is located at 37°54'39" North latitude and 40°14'12" East longitude. As of the end of 2018, its population is 1.732.396 (TSI, 2018) (Figure 2).

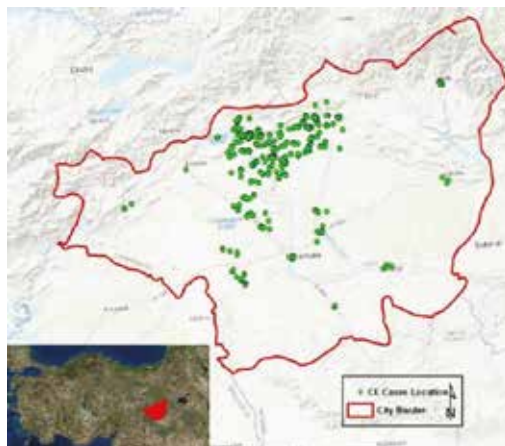


Figure 2. CL cases location and study areas of Tigris Basin (Diyarbakir Province)

### Bioclimatic and Environmental Parameters

The environmental data included three variables derived from remotely sensed data and 19 bioclimatic (bioclim) variables (Table 1). The current variables were downloaded from WorldClim website, version 1.416. The bioclimatic variables all had a nominal

resolution of approximately 1 km<sup>2</sup>. The current data were developed from monthly average climate data between 1950 and 2000 using observed data. The current bioclimatic variables describe the climatic conditions such as temperature, isothermality, annual precipitation.

Table 1. Bioclimatic and environmental data

Name of Data	Description
BIO1	Annual mean temperature (°C)
BIO2	Mean diurnal range [mean of monthly (max temp - min temp)] (°C)
BIO3	Isothermality (BIO2/BIO7) (x100)
BIO4	Temperature seasonality (standard deviation x100)
BIO5	Max temperature of warmest month (°C)
BIO6	Min temperature of coldest month (°C)
BIO7	Temperature annual range (BIO5-BIO6) (°C)
BIO8	Mean temperature of wettest quarter (°C)
BIO9	Mean temperature of driest quarter (°C)
BIO10	Mean temperature of warmest quarter (°C)
BIO11	Mean temperature of coldest quarter (°C)
BIO12	Annual precipitation (mm)
BIO13	Precipitation of wettest month (mm)
BIO14	Precipitation of driest month (mm)
BIO15	Precipitation seasonality (coefficient of variation)
BIO16	Precipitation of wettest quarter (mm)
BIO17	Precipitation of driest quarter (mm)
BIO18	Precipitation of warmest quarter (mm)
BIO19	Precipitation of coldest quarter (mm)
Alt	Altitude from the sea level (m)
Slope	Slope in degrees obtained from altitude (%)
Aspect	Aspect in degrees obtained from altitude (Direction)

### Obtaining CL Cases Data and Map Producing

The population data and CL patient numbers of 3 provinces and 39 districts (Adana: 15,

Mersin: 10 and Diyarbakir: 14) of the study areas between 2008-2015 were accessed from related institution's databases (TMOH, 2016), (Table 2).

Table 2. Cutaneous Leishmaniasis Cases in Adana, Mersin and Diyarbakir Provinces between 2008-2015

Districts/Years	2008	2009	2010	2011	2012	2013	2014	2015	Total
ADANA	216	330	371	315	179	219	232	118	1980
MERSIN	98	108	70	64	46	38	52	92	568
MEDITERRANEAN	314	438	441	379	225	257	284	210	2548
DIYARBAKIR	93	73	154	86	41	8	22	19	496
TIGRIS	93	73	154	86	41	8	22	19	496
TOTAL	407	511	595	465	266	265	306	229	3044

### Ecological Niche Modeling

In the study, we used the distribution of cases as if it was a vector sand fly species for producing ENM of CL (Abdullah et al., 2017). We can identify the distribution of sand flies in an understandable manner with the same environmental variables used to model the

distribution of CL. Recently, the maximum entropy model is used for this purpose. Maximum entropy (MaxEnt) models were utilized in this study using the MaxEnt v3.3.3 software. Maxent software is freely downloadable at <http://www.cs.princeton.edu/~schapire/maxen>.

For the ENM, a file was prepared for proven vector species *P. tobii* with several environmental variables in ASCII format and entered into MaxEnt software. Totally 3044 CL cases were included for the modeling construct the remaining 25% data were used in testing the model (Sofizadeh et al., 2017). The software was used with its default parameters with 10,000 as the maximum number of background absences, 0.00001 convergent thresholds, 15 replicates and 5000 as the maximum numbers of iterations and a logistic output presenting a continuous presence probability ranging from 0 to 1. A Jackknife procedure was worked to calculate the contribution of each variable in the modeling process. The area under the curve (AUC) and receiver operating characteristic curve (ROC) was found for the model (Phillips et al., 2006). Also a probability threshold representing the 10th percentile training presence points was selected as a cutoff probability used to convert continuous probability maps for today. For novel CL model, Maxent software was used that based on a maximum entropy algorithm. The Jackknife test has played an important role in the calculation of the most

contributed variables in producing model. In the conducted study, we focused in four contributed variables with the highest percentage, to better understanding of environmental requirements of CL, which were set apart from others. For model prediction in the current, the area under the curve (AUC) which categorized as higher predictive power ( $AUC > 0.5$ ), random chance ( $AUC = 0.5$ ) and worse than random ( $AUC < 0.5$ ), and receiver operating characteristic curve (ROC) was found.

## RESULTS AND DISCUSSION

Total 2548 CL patients were reported in 25 districts of two cities in the Eastern Mediterranean Region between 2008 and 2015. Also 496 CL cases reported in Diyarbakir, located in Tigris Basin. Produced model's AUC values were calculated as 0.868, 0.918 (Figure 3) and 0.924 (Figure 4) in Adana Mersin and Diyarbakir, respectively. This means, for the model prediction in the current, the area under the curve (AUC) categorized as higher predictive power ( $AUC > 0.5$ ) for both three provinces.

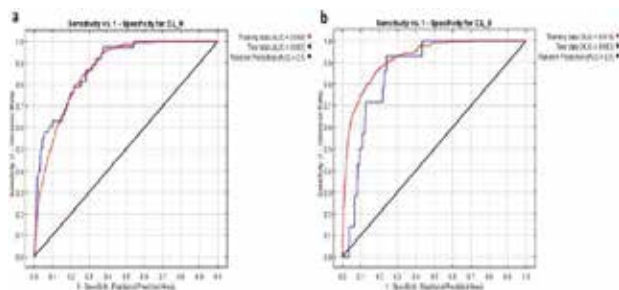


Figure 3. AUC values of MaxEnt model for CL cases in the Eastern Mediterranean Region: a) Adana; b) Mersin

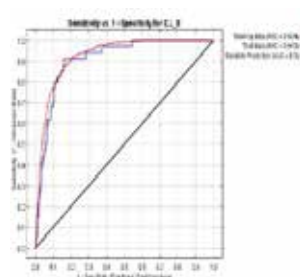


Figure 4. AUC values of MaxEnt model for CL cases in Tigris Basin (Diyarbakir)

Our results included estimation of CL cases possible distribution in the present in two endemic geographical foci, were emphasized in Figures 5 (a, b) and 6. The maps predict that, CL cases epidemiology marked in yellow and red will expanding the central and southeastern parts of Adana (Karaisali, Seyhan

and Kozan districts), central and northeastern parts of Mersin (Mut, Silifke and Tarsus districts) in the Eastern Mediterranean Region. Also, Northern parts of Diyarbakir, especially coast of the Tigris river, are more risky in terms of CL than other areas in Tigris Basin.

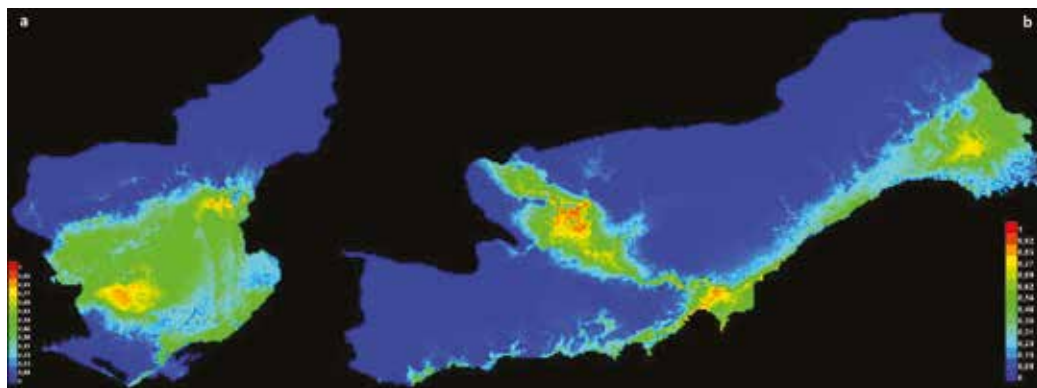


Figure 5. CL cases probable epidemiology in East Mediterranean Region: a) Adana; b) Mersin

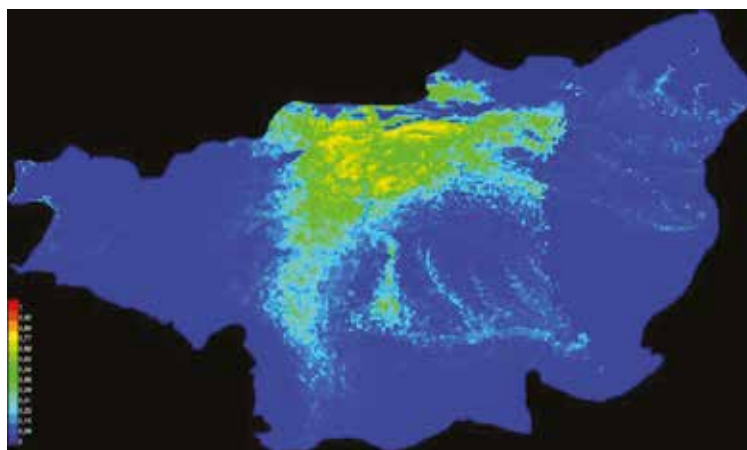


Figure 6. CL cases probable epidemiology in Tigris Basin (Diyarbakir)

In the determination of the most effective factors in the distribution of CL cases in current time, Jackknife analysis was performed with 19 bioclimatic variables and three geographic variables (Table 1). The cross comparison of 22 data groups revealed that, 9 variables were effective with higher contribution to CL distribution.

However, BIO1 (Annual mean temperature), BIO4 (Temperature seasonality) and DEM (Digital elevation model) were significantly associated with the presence of native human CL cases in the current time in Adana.

BIO5 (Max temperature of warmest month), BIO9 (Mean temperature of driest quarter) and BIO10 (Mean temperature of warmest quarter) were found more effective factors in CL cases distribution in Mersin. In Diyarbakir, BIO2 (Mean diurnal range), BIO4 and BIO11 (Mean temperature of coldest quarter) were detected found to be more effective factors.

In accordance with our MaxENT results, the total accuracy (training gain) of the model in the presence of all variables were approximately 0.92 and 1.42 in Adana and Mersin respectively. Also, it calculated as 1.41 for in Diyarbakir (Figures 7 and 8).

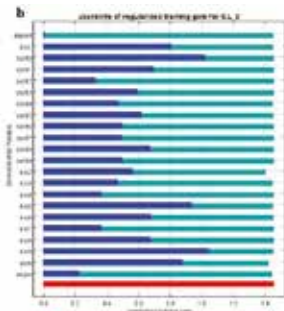
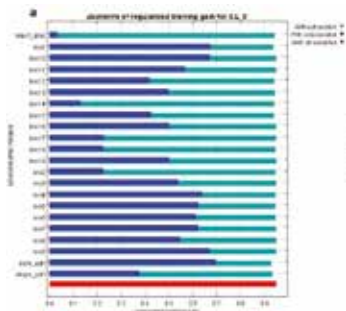


Figure 7. Regularized training gain for CL in East Mediterranean Region: a) Adana; b) Mersin

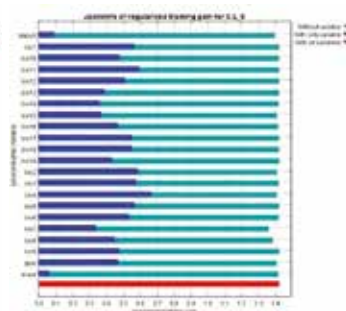


Figure 8. Regularized training gain for CL in Tigris Basin

In evaluation of the most effective bioclimatic and environmental variables in epidemiology of native CL cases in current time for both geographical endemic foci.

In the Eastern Mediterranean Region we observed 5 bioclimatics and one environmental variables were related to neglected diseases called leishmaniasis. In Adana occurrence of CL cases were currently

directly related to BIO1, BIO4 was found positive and negative inclined with CL patients probable occurrence and DEM was found inversely related to CL cases distribution (Figure 9.a, Figure 9.b and Figure 9.c). BIO5, BIO9 and BIO10 were found directly related with the CL cases occurrence in Mersin (Figure 9.d, Figure 9.e and Figure 9.f).

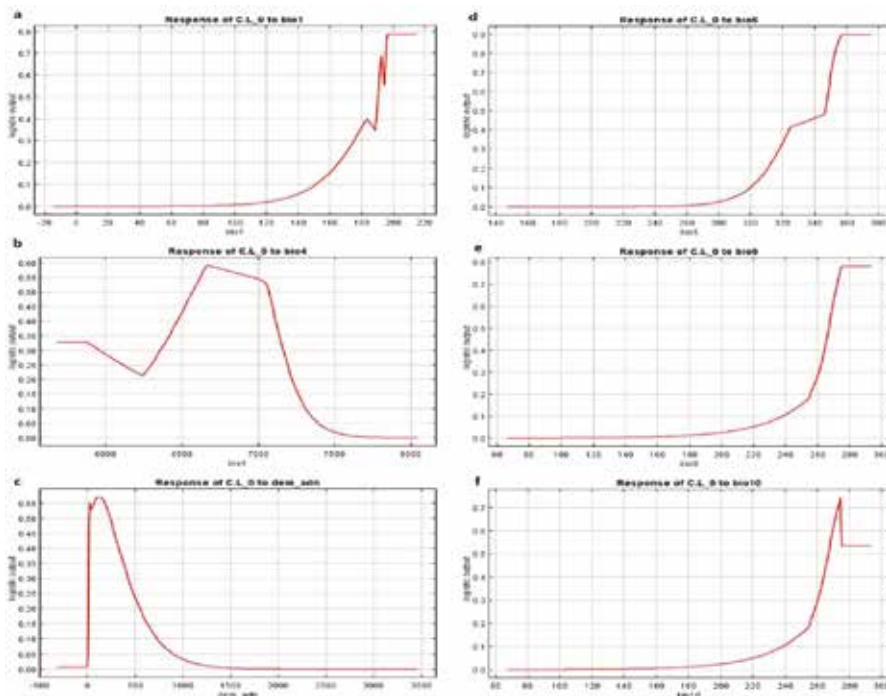


Figure 9. Response of CL cases to significantly associated in East Mediterranean Region: a) Annual mean temperature in current; b) Temperature seasonality in current; c) Digital elevation model in current; d) Max temperature of warmest month; e) Mean temperature of driest quarter; f) Mean temperature of warmest quarter.

In Tigris Basin (Diyarbakir), BIO2, BIO4 and BIO11 were found positive and negative

inclined with CL cases distribution (Figure 10).

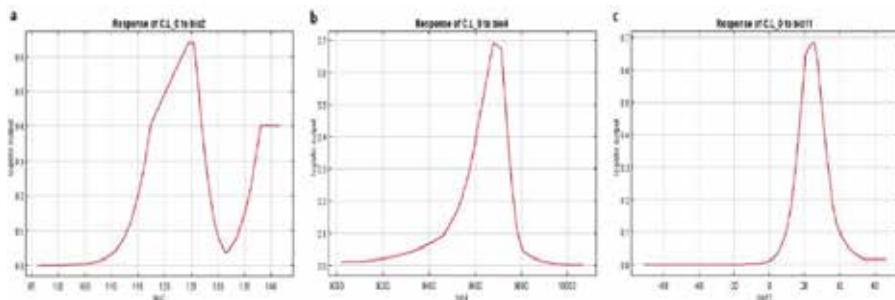


Figure 10. Response of CL cases to significantly associated in Tigris Basin: a) Mean diurnal range; b) Temperature seasonality; c) Mean temperature of coldest quarter

Especially low socioeconomic level peripheral areas of focused cities, have high number CL patients in two endemic foci of Turkey. Various computer software, included geostatistical tools, used epidemiological prediction of disease in current and future projection. The present MaxENT model helps us to better understanding of comparison of CL current status between two focused endemic foci.

In our study, ecological niche models were compared for two endemic areas and only data from CL patients were used. Although data on the patient and disease agent are theoretically used in risk analyzes, the models produced by MaxENT are preferred, especially in countries where records of CL cases are not accurately reported (Abdullah et al., 2017; Adegboye et al., 2017).

In the present model, it was found that all the three calculated AUC values were above 0.5 and the predictive power was very high (Philips et al., 2006).

When the current model is taken into consideration, it is seen that the Mediterranean Region is more risky than the Tigris Basin in terms of possible increasing in distribution of CL.

When two bio-climatic data were compared for two endemic areas, it was observed that the temperature data of the cold seasons were associated with CL distribution in Tigris Basin. On the contrary, in the Eastern Mediterranean Region where temperate seasons conditions are dominant, it is observed that the bio-climatic data of the hot period is more correlated with CL distribution.

In previous studies, which predict the future distribution of the disease, it is foreseen that the disease will spread to larger areas than the current distribution of the disease, especially in Adana and Diyarbakır (Artun, 2018; Artun & Kavur, 2019).

Totally 3044 CL cases information, reported between 2008 and 2015, were included in this study while 3671 patients were added in a previous study in Bangladesh. In addition AUC value of the Eastern Mediterranean Region were calculated as 0.868, 0.918 and Tigris Basin's AUC was 0.924. These values were close to visceral leishmaniasis prediction (VL) AUC value in Bangladesh, calculated as 0.842. Differently, influential variables were LST (Land use/land cover category), Normalized difference vegetation index (NDVI), Precipitation seasonality, Precipitation of the warmest quarter, Drainage and General soil type (GST) (Abdullah et al., 2017).

In the former study included, the information of the CL patients reported in Iran between 2007-2016, prediction of the possible distribution the vector of the disease and the its reservoir, the AUC values were estimated as high as the AUC value in our model and were calculated as 0.955 and 0.914, respectively, for the two living things (Shiravand et al., 2018).

In conclusion, bioclimatic data are likely to be compatible with each other in the ecological models of the vector sand fly and the disease it infects. The study focusing on CL epidemiology comparison of two endemic foci in Turkey is thought to contribute to the literature as a new study by ENM.

## ACKNOWLEDGMENTS

We thank to Scientific Research Projects Coordination Unit of Cukurova University, which supported our study with a project ID of “FBA-2018-10679” and the Metropolitan Municipality of Adana, Turkish Republic Ministry of Health and Turkish Statistical Institute.

## REFERENCES

- Abdullah, A. Y., Dewan, A., Shogib, R. I., Rahman, M., Hossain, F. (2017). Environmental factors associated with the distribution of visceral leishmaniasis in endemic areas of Bangladesh: modeling the ecological niche. *Trop. Med. Int. Health*, 45, 1–15.
- Adegboye, A. O., Adegboye, M. (2017). Spatially Correlated Time Series and Ecological Niche Analysis of Cutaneous Leishmaniasis in Afghanistan. *Int. J. Environ. Res. Public Health*, 14(309), 1–14.
- Alptekin, D., Kasap, M., Lüleyap, U., Kasap, H., Aksoy, S., Wilson, M. L. (1999). Sand flies (Diptera: Psychodidae) associated with epidemic Cutaneous Leishmaniasis in Şanlıurfa, Turkey. *J. Med. Entomol*, 36, 277–281.
- Artun, O. (2018). Ecological Niche Modeling for understanding the bioclimatic factors for current and projected scenario of Cutaneous Leishmaniasis in Adana, Turkey. *J. Vector Borne Dis.*, 55(4), 246–254.
- Artun, O., Kavr, H. (2019). Kutanöz Leishmaniasisin Gelecek Projeksiyonunu Ekolojik Niş Modelleme Kullanarak Belirleme: Diyarbakır İli Örneği. *Journal of the Institute of Science and Technology*, 9(2), 562–570.
- Elith, J., Graham, C. H., Anderson, R. P., Dudik, M., Ferrier, S., Guisan, A.,... Zimmermann, N. E. (2006). Novel methods improve prediction of species' distributions from occurrence data. *Ecography*, 29, 129–151.
- Gurel, S. G., Yesilova, Y., Olgen, M. K., Ozbel, Y. (2012). Cutaneous Leishmaniasis in Turk. *Soc. Parasitol*, 36, 121–9.
- Kavr, H., Artun, O. (2017). Geographical Information Systems in Determination of Cutaneous Leishmaniasis Spatial Risk Level Based on Distribution of Vector Species in Imamoğlu Province, Adana. *J. Med. Entomol*, 54(5), 1175–1182.
- Ok, Z., Balcioglu, I. C., Ozkan, A. T., Ozensoy, S., Ozbel, Y. (2002). Leishmaniasis in Turkey. *Acta Trop*, 84, 43–48.
- Ostfeld, R. S., Glass, G. E., Keesing, F. (2005). Spatial epidemiology: An emerging (or re-emerging) discipline. *Trends Ecol. Evol*, 20, 328–336.
- Phillips, S. J., Anderson, R. P., Schapire, R. E. (2006). Maximum entropy modeling of species geographic distributions. *Ecological Modelling*, 190, 231–259.
- Shiravand, B., Ali, A., Tafti, D., Bojd, A. A. H., Almodaresi, S. A., Mirzaei, M., Abai, M. R. (2018). Modeling spatial risk of Zoonotic Cutaneous Leishmaniasis in Central Iran. *Acta Trop.*, 185, 327–335.
- Simsek, F. M., Alten, B., Caglar, S. S., Ozbel, Y., Aytekin, A. M., Kaynas, S.,... Rastgeldi, S. (2007). Distribution and altitudinal structuring of phlebotomine sand flies (Diptera: Psychodidae) in southern Anatolia, Turkey: their relation to human cutaneous leishmaniasis. *J. Vector Ecol.*, 32, 269–279.
- Singh, S. (2006). New developments in diagnosis of leishmaniasis. *Indian J. Med. Res.*, 123, 311–30.
- Sucakli, M. B., Saka, G. (2007). Epidemiology of Cutaneous Leishmaniasis in Diyarbakir. *Turk. Soc. Parasitol.*, 31(3), 165–169.
- Svobodova, M., Alten, B., Zidkova, L., Dvorak, V., Hlavackova, J., Myskova, J. (2009). Cutaneous leishmaniasis caused by *Leishmania infantum* transmitted by *Phlebotomus stobbi*. *Int. J. Parasitol.*, 39, 251–256.
- Turkish Ministry of Health (TMOH) (2016). Leishmaniasis data of Adana province, Turkey. MoH, Ankara, Turkey.
- Turkish Statistical Institute (TSI) (2018). Population database of Turkey.

## MAKING A DIGITAL DATABASE REGARDING LAND ANTI-EROSION ORGANIZATION WORKS AND ITS DISSEMINATION THROUGH THE CARRY MAP EXTENSION

Maria-Olivia MOLDOVAN, Marcel DIRJA, Iulia-Diana GLIGA (ARION),  
Mihai VOEVOD

University of Agricultural Sciences and Veterinary Medicine of Cluj-Napoca,  
3-5 Calea Manastur Street, 400372, Cluj-Napoca, Romania

Corresponding author email: maria-olivia.moldovan@usamvcluj.ro

### *Abstract*

*The purpose of this study is to make an inventory of works regarding anti-erosion organization and land improvements that have been designed in the body known as Feleac Farm, in Cluj-Napoca, Romania. After consulting execution projects, estimates for various categories of works and documents from the archive of S.C.H. Cluj-Napoca, an inventory was made of works fighting surface soil erosion (canals that intercept runoff, outlets, chutes, collector and absorbent drain pipes in view of collecting groundwater, leveling) and works fighting deep soil erosion. The existing cartographic material was first scanned in order to be used in the GIS platform, then georeferenced. The digital database was created starting from vector database structures, based on the graphic primitive's dot, line, polygon, and from tabular database structures, attribute. In order to visualize and access data for information and field orientation for the evaluation of the current state of works, data has been disseminated through the Carry Map ArcGIS extension.*

**Key words:** databases, dissemination, fighting erosion, GIS, works.

### INTRODUCTION

In order to establish the proper measures and works needed to eliminate the excess moisture from the slopes, several factors have to be considered such as: factors which enhance the excess water, soil permeability, the terrain configuration, territorial organization, anti-erosion works (Dirja & Budi, 2006).

The area in the country covered with works necessary for preventing soil erosion is around 2.226.469 ha, the main constructions being coastal, marginal and leading drainage channels, organizing valleys and ravines, anti-erosion roads, dams and thresholds, chutes, culverts, anti-erosion forestry plantations, support walls and shore consolidation works, outlets, collector and absorbent drain pipes. Land improvement works, such as drainage works, from A.N.I.F. administration, foretell a surface of 3.085.895 ha spread throughout Romania, the main constructions being represented by evacuation channels, main and collector channels respectively secondary and tertiary channels, evacuation pumping stations, bridges and culverts, weirs and chutes. The underground drainage network consists of

40.660 km of collector drains and absorbent drains. When slopping lands are concerned, the issue regarding eliminating the excess moisture and the soil erosion must be taken into consideration, as well as landslides control and prevention works if it is needed.

According to Dirja (2000), improving the surface water runoff regime and improving the soils natural drainage must be ensured by landscaping works regarding slopping lands with excess moisture.

Horizontal drainage is the most efficient work for lands with a permanent water excess. For lands with lower water permeability, besides leveling works, a network of coastal channels and sloped land waves must be built. These works ensure to intercept water leaks from the slopes, leading them towards the outlets, which lead the collected water into a natural emissary or evacuation collector channel.

For good water runoff regularization from the slopes, within the study area certain works have been designed within the complex consisting of channels, outlets, chutes, leveling works.

The considered study area, marked by the red outline (Figure 1), is located at the southern extremity of the cadastral limit of the city Cluj-

Napoca, Cluj County. This zone contains the spatial extension of the frame known as Feleac Farm, which was under the property of S.C.H. Cluj-Napoca (S.C.H. – Horticultural Research Station Cluj-Napoca).

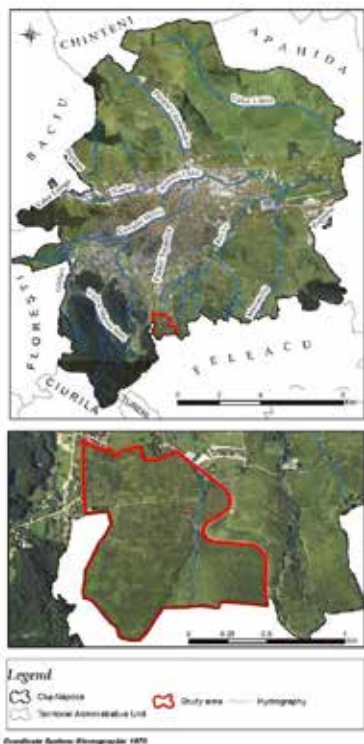


Figure 1. The geographical location of the study area, Cluj-Napoca

## MATERIALS AND METHODS

After consulting the existing documents from the S.C.H. Cluj-Napoca archive, an inventory regarding design works, water runoff regularization works, anti-erosion landscaping works, which are grouped into surface anti-erosion landscaping works and depth anti-erosion landscaping works was created. For an improved data access and analysis, the existing plans within the S.C.H. Cluj-Napoca archive, which were created from 1966 to 1971, were converted from an analog format to a digital one, thus results a database as well as a digital archive. The first step into creating the digital database is scanning the documents, followed afterwards by georeferencing the cartographic

materials for a better territorial identification of the entities which are to be represented. For an improved management over the database and due to the spatial entities, that needed to be represented, a File Geodatabase file was created along with Feature dataset as well as Feature Classes, each specific to the type of vector entities they were to contain. The coordinate system used for representing the database was Stereographic 1970 and the program used to create the database was ArcGIS 10.2. The dissemination was done based on the drawings, as well as on the Carry Map plug-in for ArcGIS. The Carry Map application allows visualizing spatial databases and interrogating them, by using a mobile device with an Android operating system and the Carry Map Observer application installed on it.

## RESULTS AND DISCUSSIONS

For the Feleac Farm frame, the soil nature, slope and the pluviometric regime have favored the surface and depth erosion process. After conducting some studies, the soil degradation process was presented as follows:

Table 1. The situation regarding the soil degradation process

Degradation process	Area ha
Surface erosion	
Second degree	56.33
Third degree	30.91
Forth degree	7.59
Trenches and ravines which have to be levelout	0.52
Active trenches and ravines	1.09
Active landslides	4.13
Stabilized landslides	30.91

The torrential formations are represented by trenches and ravines. Depending on the direction in which the water drains, the shores for these formations are alternately partially consolidated. The transported solid material is represented in big part by sand and bolders, due to the fact that it is dislodged from the upper third part of the slope, where the soils have a slight sandy texture.

When the landslides from the within the study frame are concerned, these are of two types as follows. In the lower and upper thirds there are old landslides, geological, with a sliding bed at

great depth, where the petrographyc sublayer is represented by marl and clay. These kind of landslides are reactivated in isolated points, small areas, where the groundwater appears every day. In the ravines area, due to the depth of their bottom, the soils slide towards the ravines thread because they have no support.

All the works were dimensioned to the evacuation flow rate corresponding to the study and design year,

$Q_{10\%} = 0.049 \text{ m}^3/\text{s}/\text{ha}$ , determined with the following formula:

$$Q = 0.167 \times i \times K \times F \quad (1)$$

where:

$i$  - rain intensity having a 10% insurance [mm/min];

$K$  - drainage coefficient;

$F$  - collecting surface [ha].

Upstream, besides roads, there were designed marginal slopped channels. They serve, on one hand to protect the roads and on the other they are a part of the controlled slope water evacuation network, in order to collect pelicular leaks and to direct the water towards outlets and streams. The slope for the marginal channels was calculated taking into account the flow rate and speed, so that the water speed will be between the limits of non-erosion and non-clogging, according to the consolidation type for every channel. According to the dimensioning calculus based on the hydrological studies and the 10% insurance, there were designed the following types of channels: 5 types of slopped marginal channels consolidated with grass furrows, a type of slopped coastal channels, a small pier downstream and a type of marginal slopped channel consolidated with concrete tiles (Figure 2).

In the areas where the channel slope exceeds the maximum allowed non erosion speed some drops were designed in order to reduce the slope and to ensure that the drainage speed is below the non-erosion speed.

The collected and transported water by the channels are directly evacuated in an emissary or will be evacuated through a series of outlets to the nearest emissary. These were located on the thread of the natural water drainage concentration zones on the line with the highest grade. Depending on the flow rate, speed and location the following were designed: 3 types

of outlets consolidated with grass furrows, having a shore with a slope of 1: 3; one type of outlet consolidated with grass furrows having a shore slope of 1: 1.5; 1 type of outlet having a shore slope of 1: 1; 1 type of outlet consolidated with concrete tiles having a shore slope of 1: 1.5 (Figure 3).

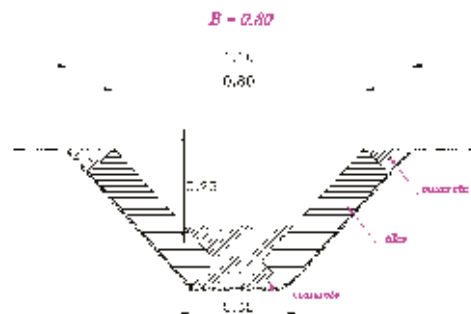


Figure 2. Slopped channel consolidated with concrete tiles, trapezoidal section:  
 $B = 0.80 \text{ m}$ ,  $b = 0.30 \text{ m}$ ,  $H = 0.25$ ,  $1/\text{m} = 1/1$

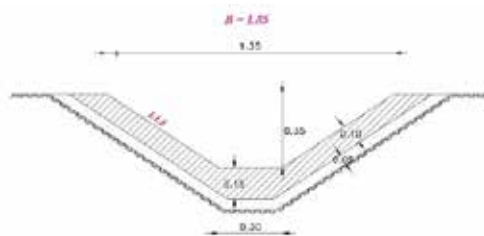


Figure 3. Outlet consolidated with concrete tiles, trapezoidal section:  
 $B = 1.35 \text{ m}$ ,  $b = 0.30 \text{ m}$ ,  $H = 0.35$ ,  $1/\text{m} = 1/1.5$

In order to capture the water coming from the groundwater, 2 types of drains were designed: collector drains and absorbent drains.

The collector drains are located on the line with the highest grade, in the depression areas, collecting the water transported by the absorbent drains (Figure 4).

The absorbent drains were designed both for water stagnation zones, at the base of the slope break lines, as well as in the inside of the excess groundwater zones.

The absorbent drains are designed to be build out of perforate concrete tubes having a longitudinal slope between 2 and 3 percent. They are located around 50 centimeters below the impervious layer, having on the downstream wall a screen of clay to prevent

water passing downstream of the drain (Figure 5).

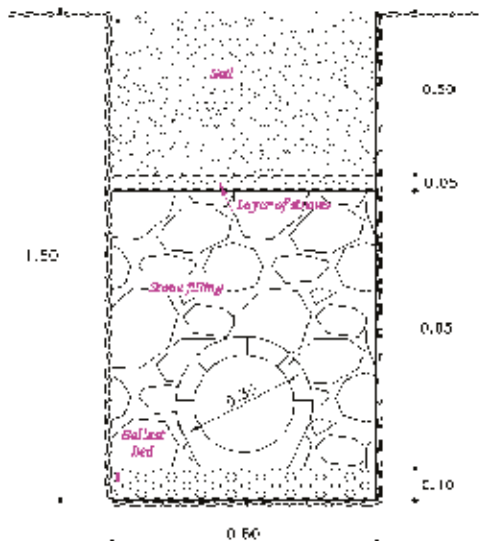


Figure 4. Collector drain

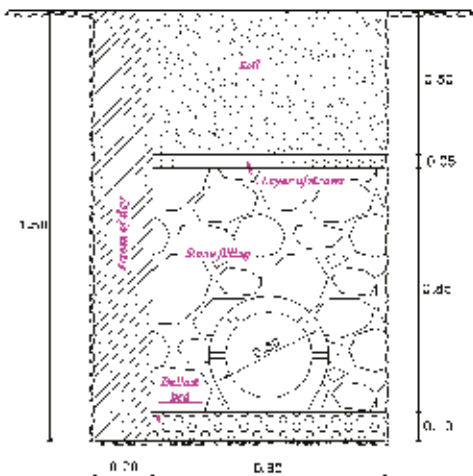


Figure 5. Absorbent drain

In order to equalize the slope, several leveling works have been designed, abolishing water stagnation on the slopes, an essential factor to producing landslides.

Reducing the parcel grade where necessary is done using terraces, which contribute to adjust the slope drainage through a higher infiltration capacity and reducing the water drainage speed.

Combating depth erosion is resolved in the project depending on the nature of trenches and ravines. On the great ravine, concrete steps and a dam made out of a stone wall were designed. The concrete steps are located on the active sectors of the ravine and on the sectors where a reactivation tendency is noted.

Thus, an inventory of all the works, including data regarding their number but also the dimensioning elements, was created.

In order to have a good data management, when the drawings are concerned, the existing analog material from the S.C.H. archive was scanned, resulting a TIFF image with 100025 x 9450 pixels dimensions and a 300 dpi horizontal and vertical resolution. This image was subjected to the georeferencing process to the Stereographic Projection 1970 (Figure 6).

During the georeferencing process several control points, common points, which are easily identifiable both in the field and on the scanned drawing, represented by elements stable in time, such as road intersections, were identified.



Figure 6. Georeferenced situation plan

Elements regarding the land use, parcels, contour lines, limit, roads, lakes, streams,

culverts, outlets and drains were vectorized and had their principle attributes attached, which include name, type, length and surface. The symbols used are in conformity with the map legend and for a better visualization and identification of the elements, the Label feature has been activated (Figure 7).

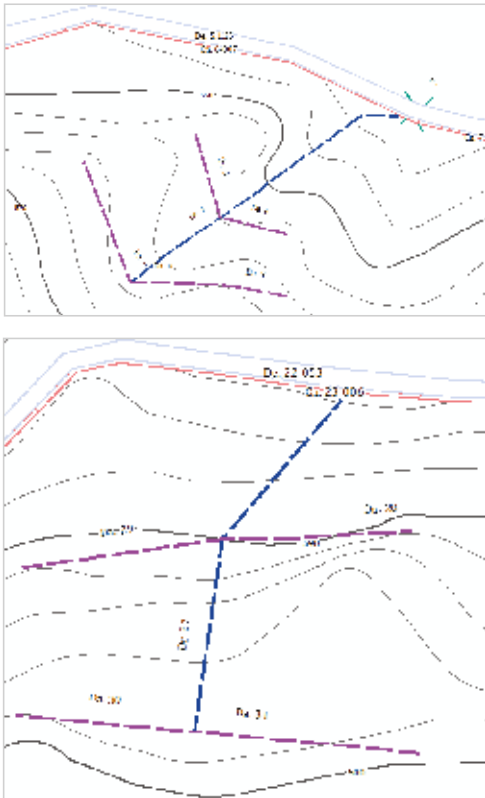


Figure 7. Sections of the designed works plan

The visualization, interpretation and analysis of the databases materialized in drawings; thematic maps are facilitated by integrating them as stand-alone applications. The applications integrate both the symbolized databases as well as their related attributes. During the present paper the dissemination was done based on the drawings, but also on the Carry Map plug-in for ArcGIS. The Carry Map plug-in is available for free for 14 days and it can run multiple operating systems such as: Windows 2000/XP/7/10 - the *Create Desktop Win 32 version* option; Windows Mobile - the *Create Windows Mobile*

*version* option; Android and iOS - the *Create Map file* option (Bilasco et al., 2017).

The file which runs on the Windows operating system (Figure 8) allows visualizing and interrogating databases, the possibility to measure on the map, the printing option, etc.

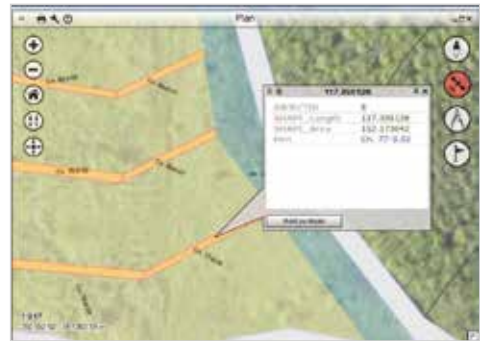


Figure 8. The Carry Map Interface

Once the cmf file type was accessed on a mobile device (Figure 9) it allows consulting, identifying and analyzing on the field without having to use analog maps, thus facilitating the users work because in most cases the drawings have big dimensions, such as A0 format or custom.

Furthermore, the application's importance consists in the ability to localize the user on the map if the mobile device has a GPS sensor.



Figure 9. Carry Map Observer

## CONCLUSIONS

Creating a digital database in the field of land improvements has a major importance because it facilitates the access to spatial and non-spatial data, converting plans from an analog format to a digital one thus leading to creating a complex database for this field.

The works inventory with related attributes is necessary because it represents the founding stone for the studies being conducted in the area.

Disseminating databases through the Carry Map application allows for an easier field identification of all the represented entities, for the established purposes: evaluating the condition of the works, proposals and recommendations for anti-erosion landscaping and eliminating excess humidity.

## REFERENCES

- Bilasco, S., Moldovan, M. O., Rosca, S. (2017). *Aplicatii G.I.S. in administratia publica locala*. Cluj-Napoca, RO: Risoprint Publishing House.
- Dirja, M. (2000). *Combaterea eroziunii solului*. Cluj-Napoca, RO: Risoprint Publishing House.
- Dirja, M., Budiu, V. (2006). *Imbunatatiri funciare. Combaterea excesului de umiditate pe terenurile agricole*. Cluj-Napoca, RO: AcademicPress Publishing House.
- \*\*\*<http://www.anif.ro/patrimoniu/>

## RESEARCHES REGARDING THE USE OF G.I.S. TECHNOLOGIES IN MODELLING AND SPATIAL ANALYSIS OF THE VARATEC MINING COMPLEX, MARAMURES COUNTY

Petruța SOLCAN<sup>1</sup>, Tudor SALAGEAN<sup>2</sup>, Elemer-Emanuel SUBA<sup>3</sup>, Marioara ILEA<sup>2</sup>

<sup>1</sup>University of Petroșani, Faculty of Mine, 20 Universitatii Street, Petrosani, Romania

<sup>2</sup>University of Agricultural Sciences and Veterinary Medicine of Cluj-Napoca, Faculty of Horticulture, 3-5 Calea Manastur Street, Cluj-Napoca, Romania

<sup>3</sup>Technical University of Civil Engineering of Bucharest, Faculty of Geodesy, 122-124 Lacul Tei Blvd, Bucharest, Romania

Corresponding author email:tudor.salagean@usamvcluj.ro

### Abstract

*The purpose of this paper is to use GIS techniques for the modelling and spatial analysis of Varatec mining complex, Maramures County. The practical result of this paper, consists in the creation of the GIS database and the integration into it of maps and plans from the mining complex. A spatial analysis of a mine field is based on the effectiveness of a GIS database which will lead to 3D modelling and the representation of the topography. Among the parameters used will be slope and slope orientation or aspect because the slope determines the intensity and type of processes that model the substrate ground, and the slope orientation leads to the evolution of geomorphological processes due to climatic factors that are not evenly dispersed over the land area: solar radiation, sun exposure, precipitation and temperatures. Regarding the mining exploitation, an important element is the land use category, which was taken over by expeditious methods from the L-35-013-A-a Orthophotoplan. Another desirable aspect in this case study is the integration of the general plan from Varatec mining complex into the GIS database and spatial modelling, but also making thematic map on the main geological layers in the Varatec mining complex in order to highlight the applicability of GIS technologies in mining. The various modifications and the evaluation of the subsidence processes within the mining complex can be analysed over the years through remote sensing methods, but especially during the period when the mining complex was closed following the closure action organized by CNMPN REMIN.*

**Key words:** GIS, mining, modelling, spatial analysis.

### INTRODUCTION

Situated approximately in the centre of Maramures county (Figures 1 and 2), the Varatec mine, near the Varatec peak, 1351 m high was closed by CNMPN REMIN in 2006 according to the Decision no. 644/2007 approving the final closure and monitoring the environmental factors after the closure of some mines and quarries, the 10<sup>th</sup> stage (www.remin.ro).

This paper will use the Varatec mining field as a case study in GIS modelling.

Mine is the unit production of a mining enterprise which, through its mining works and facilities, provides for the extraction of useful minerals, aeration, illumination and water evacuation. There are 3 types of deposits (Covaci St., 1972):

1. Group I include deposits and the known parts of them, with a simple structure and a constant thickness.
2. Group II includes deposits with a more complicated structure of variable thickness, in which the determination of the reserves from A category is more expensive.
3. Group III includes very complicated fields with very variable thicknesses.

Mining topography is closely related to geographic information systems or GIS as it helps to manage the mining activity by integrating the results into a database that can easily be accessed by a user. An efficient management is based on technical information, including topographical ones; an effective technical data management tool is represented by a geospatial database such as the Geographic Information System (Manu C.S.).

It is possible to quantify the novelty of the present paper because it enrolls in the current trends regarding the mining management.

## MATERIALS AND METHODS



Figure 1. Framing the study area: Maramures County and the contour of Varatec mine complex

The general plan of the mine contains all mining works from all horizons of exploitation or research and in all layers, with stratigraphic and tectonic details opened by sterile and useful works. There are not shown the short-term preparatory work, such as: risings, training, pre-essays, channels, etc. on this plan (Radulescu et al., 2017). From this plan, there are eight galleries, a blind pit and over 30 risings.



Figure 2. Varatec Mine

**Galleries** are horizontal mining works with a slope of less than 7s/1000m, much longer than the cross section. It is used for transport, ventilation, water evacuation, piping installation, electrical cable installation, etc. (Popa A. et al., 1986). Types of galleries: Coastal galleries digging into a hillside (mountain) to open a reservoir. Depending on the angle they make with the direction of the deposit, they can be transverse (perpendicular

to the direction of the deposit), directional (in the direction of the deposit, or parallel to it) and diagonal (making an angle with the direction of the deposit). The tunnel is a horizontal mining work, which has two exits on the opposite slopes of a hill or mountain.

The puncture gallery (or the crossing gallery) is transversely cut from the bed to the roof of the deposit.

The pre-work gallery is executed in the deposit, depending on the method of exploitation chosen (Popa A. et al., 1986).

According to the general plan of the mine, there are: the Varatec transversal gallery, the Babeica transversal gallery, the coastal gallery I, II and III, the Jelenszki gallery, the Borcut gallery and other 1090 gallery.

**Risings** are executed after puncturing the deposits with cross-galleries. Are mining works less inclined than pits, with two or three compartments (exploration or exploitation) and linking two horizons, compartmenting the deposit in panels. It is used for research as well as for exploitation (Aron et al., 1986).

**Blind pit** makes the connection between two or more horizons without having an exit (Lețu et.al., 1986).

## RESULTS AND DISCUSSIONS

GIS modelling and spatial analysis will take into account certain parameters such as slope, slope orientation, land use category and mine horizons.

### 1<sup>st</sup> Parameter: Slope

Based on the digital elevation model of the mining field, the slope of the terrain was calculated. As can be seen in Figure 3, the mining field has a slope that exceeds 35 degrees. It is an important parameter because slope determines the intensity and the type of processes that model the substrate ground, determining the stability of the whole mine.

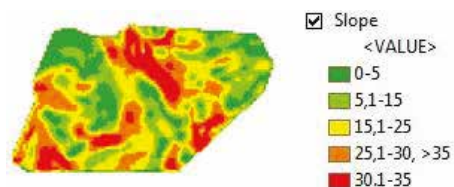


Figure 3. Slope

## 2<sup>nd</sup> Parameter: Slope Orientation

Based on the digital elevation model of the mining field, the slope orientation was calculated as seen in Figure 4. This parameter leads to the evolution of geomorphological processes due to climatic factors that are not evenly dispersed over the land area: solar radiation, sun exposure, precipitation and temperatures, very important to consider in the preparation and opening of the minefield.

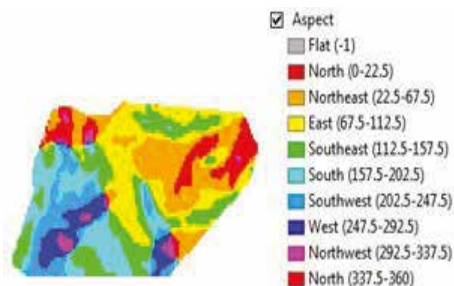


Figure 4. Slope orientation

## 3<sup>rd</sup> Parameter: Land use in the mining complex

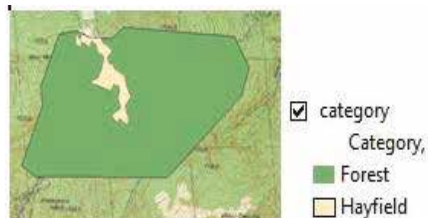


Figure 5. Land use in Varatec Mine Complex



Figure 6. Orthophotomap L-35-013-A-a and the contour of the mine

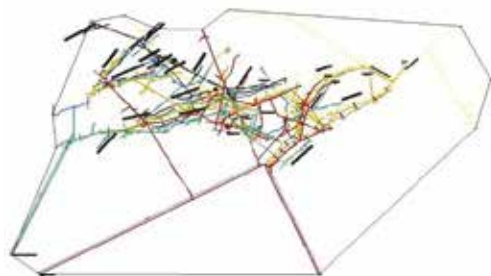


Figure 7. The horizons the mine

It is made through expositive methods directly on Orthophotomap L-35-013-A-a (Figure 6). First of all, the Orthophotomap was georeferenced in ArcMap, a new polygon shape file was created and edited and the result can be observed in Figure 6. 10% of the mine complex is hayfield and 90% forest as seen in Figure 5.

## Horizons of the mine

The horizons of the mine vary as follows: there are horizons on the surface and underground at different levels ranging from +70 meters and -295 meters (Figure 8).

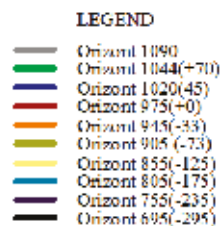


Figure 8. Horizons of the mine, between +70 and -295 m

In order to create a topographic map in ArcMap a hill shade and contour lines must be created.

A hill shade is a greyscale 3D representation of the surface, with the sun's relative position taken into account for shading the image (Figure 9).

This function uses the altitude and azimuth properties to specify the sun's position (<http://desktop.arcgis.com/en/arcmap/10.3/manage-data/raster-and-images/hillshade-function.html>).



Figure 9. Hill shade

The contour lines for topographic map can be seen in Figure 10. Because the altitude in the mining complex is between 861 and 1351 meter, there are intermediate lines and index lines (thicker) that go from 900 to 1300 meters, at 100 meters interval.



Figure 10. Contour lines

Based on the contour lines, a TIN (Triangular irregular networks) surface is created. It has been used by the GIS community for many years and are a digital means to represent surface morphology. It is form of vector-based digital geographic data and are constructed by triangulating a set of vertices (points). The vertices are connected with a series of edges to form a network of triangles (<http://desktop.arcgis.com/en/arcmap/10.3/manage-data/tin/fundamentals-of-tin-surfaces.htm>). TIN created only for the Varatec mine complex can be observed below, in Figure 11 with the elevation distributed in 8 classes.



Figure 11. TIN surface

## CONCLUSIONS

This paper work was aimed at accentuating the importance of GIS in mining works. Before starting such work, there are some factors that should be taken into consideration and this type of spatial analysis can be achieved with GIS in order to estimate the degree of land degradation.

In order to quantify the value of the probability of degraded land, Government Decree 447/2003 proposed a method that refers to an analysis of quantitative and qualitative terms. The model validation is possible using morphological and morphometric parameters derived from digital elevation model (DEM) (Petrea et al., 2014).

Overall, the maps and plans integrated in a database can easily be consulted by a user.

## REFERENCES

- Covaci, S. (1972). *Exploatarea zacamintelor de substante minerale utile in subteran*. Editura Tehnica, Bucuresti.
- Letu N., si colaboratorii (1986). *Constructia lucrarilor miniere vertical, Vol IV*. Litografia Institutului de Mine Petrosani.
- Manu, C.S. (2018) . *Metode geodezice si topografice utilizate in managementul activitatilor miniere de la suprafata*. Teza de Doctorat, Universitatea din Petrosani.
- Petrea, D., Bilasco, S., Rosca, S., Vescan I., Fodorean. I. (2014). The determination of the landslide occurrence probability by GIS spatial analysis of the land morphometric characteristics (case study: the Transylvanian Plateau). *Carpathian Journal of Earth and Environmental Sciences*, May 2014, 9(2).
- Popa, A., Fodor, D., Letu, N., Popa, V., Ilias, N., Simionescu, A.,... Spafiu, G., (1986). *Manualul Inginerului de mine, Vol III*. Editura Tehnica, Bucuresti.
- Radulescu, A. T. G. M., Radulescu, V. M. G. M., Radulescu, G. M. T., Stefan, O., Arsene, C. (2017). *Topografie miniera*. UT Press.
- <http://www.graiul.ro/2017/07/08/la-baiut-apele-de-mina-se-deverseaza-direct-in-rau/>
- <http://desktop.arcgis.com/en/arcmap/10.3/manage-data/raster-and-images/hillshade-function.html>
- <http://desktop.arcgis.com/en/arcmap/10.3/manage-data/tin/fundamentals-of-tin-surfaces.htm>
- [www.remin.ro](http://www.remin.ro)

## ANALYSIS OF THE INFLUENCE OF OROGRAPHICAL FACTORS ON THE PLANIMETRIC ACCURACY OF POINTS DETERMINED USING GPS IN FORESTED AREAS

Cornel Cristian TERESNEU, Maria Magdalena VASILESCU

Transilvania University of Brasov, 25 Eroilor Street, Brasov, Romania

Corresponding author email: [vasilescumm@unitbv.ro](mailto:vasilescumm@unitbv.ro)

### Abstract

*This research aims to identify the manner in which orographically factors influence the horizontal precision of GPS coordinates. The study area is a mountainous region in the Bran locality, mainly covered with spruce forests. Data was collected using the Stop&Go method with post-processing, using two GPS receivers (Trimble Pro XH and Pro XT). Data was stratified considering the following criteria: orography (valley, slope, crest) and aspect (S-N, E-V). Field data was post-processed and the resulting precisions were analysed using the Statistica software. The influencing factors were analysed individually, but also in different combinations. The best accuracy was obtained for points located on crests, followed by points on slopes (which had a good precision) and finally points in valleys (which had acceptable or low precision).*

**Key words:** GIS, GPS, mountainous forests, statistical analysis.

### INTRODUCTION

This research paper aims to highlight the factors that influence the horizontal precision of point positioning using GPS equipment in a forest environment. The study area is represented by the mountainous forests of the Bran-Moeciu area (Figure 1). There are numerous studies carried out in this area, which analysed the point coordinates precision depending on category (forest, border, forest road, open wood and alpine barren zone) (Teresneu et al., 2014), the precision of coordinates for points on the edge of forest canopy (Teresneu & Vasilescu, 2015) and the implications on the area of forest parcels (Teresneu et al., 2011). For this study, the methods and means used in similar studies were considered, which highlighted that in a forest environment the number of visible satellites is much lower (Wang et al., 2014), the tree canopy considerably lowers the precision of coordinate calculation (Ordenez Galan et al., 2011; 2013; Weilin et al., 2000; Zhang et al., 2014), the presence of a snow layer further decreases positioning accuracy (Janez et al., 2004), the vegetative season greatly influences this precision (Dogan et al., 2014; Sawaguchi et al., 2003). For this paper the positive aspects

offered by remote sensing were not taken into account (Vorovencii, 2014a, 2014b).

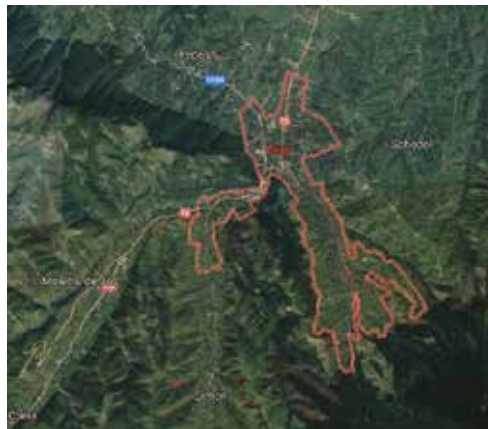


Figure 1. Study area

### MATERIALS AND METHODS

Materials used for this study are: cadastral maps with forest boundaries, corroborated with parcel descriptions from the forest management plan; two GPS receivers, type *Trimble Pro XT* and *Trimble Pro XH*.

Direct measurements were made to determine the coordinates of over 2700 points (the specific method used was *Stop&Go* with post-

processing). Data was downloaded from the GPS receivers using the *Trimble GPS Pathfinder Office*, and for post-processing the Top GEOCART Brasov permanent station was used. Data was stratified considering the following criteria: orography, regardless of the presence of forest (valley, slope, crest), aspect (S-N, E-V), spruce forest for the three orographic classes (valley, slope, crest), spruce forest for the two aspect classes (S-N, E-V), beech forest for the three orographic classes (valley, slope, crest), beech forest for the two aspect classes (S-N, E-V).

This data was then processed using the Statistica software, by calculating the common statistical indices (minimum, maximum, mean, standard error of mean, mode, frequency of mode, standard deviation, coefficient of variation).

A GIS project for the study area was created in which the coordinates of points determined with GPS receivers were imported.

## RESULTS AND DISCUSSIONS

Experimental data was represented graphically and the relative cumulative frequencies were assigned to the categories of horizontal precision values. In this way, allotments for the orographic factors and aspects can be observed in Figure 2.

As the two graphs show, exponential distributions are obtained, with some tendency of normalization.

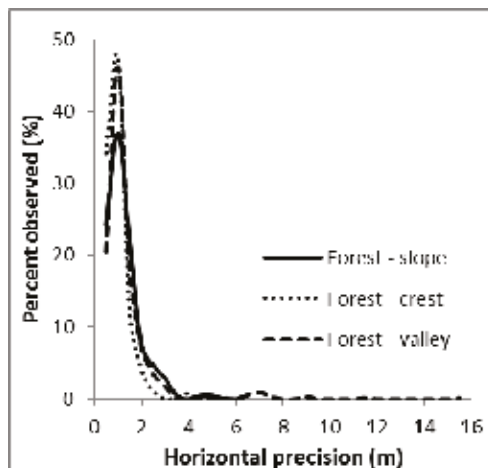


Figure 2. Influence of orography

Next, a series of statistical indices were calculated: minimum, maximum, mean, standard error of mean, mode, standard deviation and coefficient of variation (Table 1). It can be seen that factor were analysed individually, but also in groups of two and three, respectively.

Table 1. Calculation of statistical indices

Categories	Valid N	Mean	Mode	Minimum	Maximim	Std Dev	Coef Var
Valley	205	0.99	0.4	0.2	7.5	0.84	85.64
Slope	781	1.00	0.5	0.2	8.2	0.74	74.50
Crest	10	0.54	0.5	0.4	0.8	0.11	19.91
S-N	626	0.96	0.5	0.2	8.2	0.81	84.27
E-V	370	1.04	0.4	0.2	5.4	0.68	64.77
Spruce-Valley	144	0.96	0.5	0.2	3.9	0.60	62.13
Spruce-Slope	570	0.94	0.5	0.2	8.2	0.69	73.40
Spruce-Crest	10	0.54	0.5	0.4	0.8	0.11	19.91
Spruce-S-N	437	0.95	0.5	0.2	8.2	0.72	76.22
Spruce-E-V	277	0.95	0.4	0.2	3.3	0.59	62.57
Spruce-Slope-S-N	293	0.94	0.5	0.2	8.2	0.78	82.62
Spruce-Slope-E-V	277	0.95	0.4	0.2	3.3	0.59	62.57
Beech-Slope-S-N	128	0.96	0.6	0.4	6.8	0.82	85.95
Beech-Slope-E-V	93	1.33	Multiple	0.6	5.4	0.82	61.47

Analysis of the obtained results leads to the conclusion that the horizontal accuracy for points located on crests (regardless of the type of analysed forest) have a lower variation, with points on slope having an intermediate value and points in valleys a relatively large one.

If mean is considered, we can state that it is better for points located on crests (regardless of forest type), the other two situations having a lower accuracy. As for aspect, it can be seen that the differences are practically meaningless.

Mode has relatively small amplitude, from 0.4 in various situations to 0.6 for points located on slopes and an S-N aspect. Mode also has a multiple value in the case of beech stands located on slopes with an E-V aspect.

Furthermore, statistical indices such as median, quartiles and percentiles were analysed (Table 2). Graphical representation of orographically and aspect factors are shown in Figure 3.

Analysis of the two representations shows that a better horizontal accuracy is obtained for points located on crests, relative to the other two conditions. Furthermore, a minor influence of the aspect factor is shown.

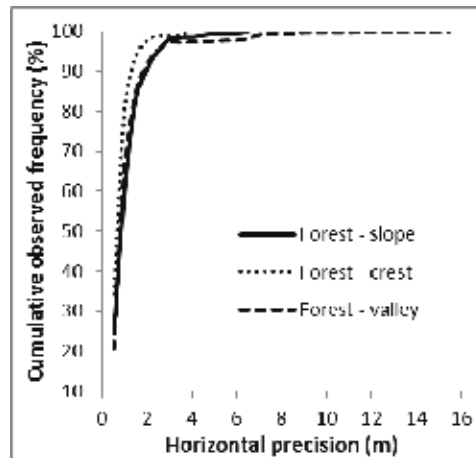


Figure 3. Relative frequencies - orography

Table 2. Calculation of median, quartiles and percentiles

Categories	Median	Lower Quartile	Upper Quartile	Percentile 90	Percentile 95
Valley	0.8	0.5	1.2	1.7	2.1
Slope	0.8	0.5	1.2	1.8	2.3
Crest	0.5	0.5	0.6	0.7	0.8
S-N	0.8	0.5	1.1	1.8	2.1
E-V	0.9	0.6	1.3	1.85	2.4
Spruce-Valley	0.8	0.5	1.2	1.8	2.1
Spruce-Slope	0.7	0.5	1.1	1.8	2.3
Spruce-Crest	0.5	0.5	0.6	0.7	0.8
Spruce-S-N	0.8	0.5	1.2	1.8	2.1
Spruce-E-V	0.7	0.5	1.2	1.8	2.3
Spruce-Slope-S-N	0.7	0.5	1.1	1.8	2.1
Spruce-Slope-E-V	0.7	0.5	1.2	1.8	2.3
Beech-Slope-S-N	0.7	0.6	0.95	1.7	2
Beech-Slope-E-V	1.1	0.9	1.4	2	3.1

## CONCLUSIONS

To conclude, it can be said that orography has the greatest influence on point positioning accuracy. Especially high accuracies are obtained on crests, where satellite signals are considerably better. Somewhat lower accuracies are obtained for points located on

slopes, and the worst accuracies are obtained in valleys, where satellite signals are weakest.

Furthermore, if the valley has an S-N aspect, then accuracy is even worse.

Regarding the influence of aspect on horizontal precision for GPS positioning of points, it can

be said that, in all cases, sunny aspect is the most favourable.

## REFERENCES

- Dogan, U., Uludag, M., Demir, D.O. (2014). Investigation of GPS positioning accuracy during the seasonal variation. *Measurement*, 53, 91–100.
- Janez, G., Adrados, C., Joachim, J., Gendner, J. P., Pepin, D. (2004). Performance of differential GPS collars in temperate mountain forest. *Comptes Rendus Biologies*, 327, 1143–1149.
- Ordóñez Galan, C., Rodríguez Perez, J. R., García Cortez, S., Bernardo Sanchez, A. (2013). Analysis of the influence of forestry environments on the accuracy of GPS measurements by means of recurrent neural networks. *Mathematical and Computer Modelling*, 57(7-8), 2016–2023.
- Ordóñez Galan, C., Rodríguez Perez, J. R., Martínez Tores, J., García Nieto, P. J. (2011). Analysis of the influence of forestry environments on the accuracy of GPS measurements by using genetic algorithms. *Mathematical and Computer Modelling*, 54(7-8), 1829–1834.
- Sawaguchi, I., Nishida, K., Shishiuchi, M., Tatsukawa, S. (2003). Positioning precision and sampling number of DGPS under forest canopies. *Journal of Forest Research*, 8, 133–137.
- Tachiki, Y., Yosimura, T., Hasegawa, H., Mita, T., Sakai, T., Nakamura, F. (2005). Effects of polyline simplification of dynamic GPS data under forest canopy on area and perimeter estimation. *Journal of Forest Research*, 10, 419–427.
- Teresneu, C. C., Vasilescu, M. M. (2015). Testing the accuracy of the GPS locations as a pre-requisite of forest cadastre related bordering issues. In *Lucrarile Sesiunii stiintifice nationale: Padurea si dezvoltarea durabila*. Editura Universitatii Transilvania din Brasov, 356–361.
- Teresneu, C. C., Vorovencii, I., Vasilescu, M. M. (2014). Statistical study on the accuracy of determining points coordinates in mountain forests from Bran-Brasov, Romania. In 14th SGEM Geoconference on Informatics, Geoinformatics and Remote Sensing. *Conference Proceedings*, 3, 893–900.
- Teresneu, C. C., Vasilescu, M. M., Hanganu, H., Vlad-Draghici, H. G., Tamaa, Șt. (2011). A GIS analysis regarding the implications of redetermining forestry geodetic markers positions. In *GeoPreVi 2011, Geodesy present and future*. Bucharest, RO: Conspress Publishing House, 355–364.
- Vorovencii, I. (2014). A change vector analysis technique for monitoring land cover changes in Copsa Mica, Romania, in the period 1985–2011. *Environmental Monitoring and Assessment*, 186(9), 5951–5968.
- Vorovencii, I. (2014). Detection on environmental changes due to windthrows using Landsat 7 ETM+ satellite images. *Environmental Engineering and Management Journal*, 13(3), 565–576.
- Wang, H., Zhan, X., Zhang, Y. (2008). Geometric dilution of precision for GPS single-point positioning based on four satellites. *Journal of Systems Engineering and Electronics*, 19(5), 1058–1063.
- Weilin, L., Buo, X., Yu, L. (2000). Applications of RS, GPS and GIS to Forest Management in China. *Journal of Forestry Research*, 11, 69–71.
- Zhang, H., Zheng, J., Dorr, G., Zhou, H., Ge, Y. (2014). Testing of GPS Accuracy for Precision Forestry Applications. *Arabian Journal for Science and Engineering*, 39(1), 237–245.

## WEB PLATFORM SOLUTION FOR SMART FARMING MANAGEMENT

Andreea CALUGARU<sup>1,2</sup>, Petre LEU<sup>2</sup>, Andreea DAMALAN<sup>2</sup>, Doru MIHAI<sup>1</sup>

<sup>1</sup>University of Agronomic Sciences and Veterinary Medicine of Bucharest, 59 Marasti Blvd,  
District 1, Bucharest, Romania

<sup>2</sup>ESRI Romania, 25 Washington Street, District 1, Bucharest, Romania

Corresponding author email: [acalugaru@esri.ro](mailto:acalugaru@esri.ro)

### Abstract

*In the last decades, technology has evolved rapidly across all industries. As expected, farming has also benefit from the digital transformation era, becoming more technology-driven. Nowadays, farmers use smart devices to gain knowledge about their crops and livestock, to make predictions and take better actions, improving efficiency and production. However, a great challenge of the present is combining and integrating data from a variety of data sources, in a manner that is both easy to use and understand. This paper presents a solution for integrating and analysing data collected from smart agriculture sensors inside a web platform. The solution allows the user to visualize metrics regarding productivity, crop stage, make predictions, take actions and deploy field workers for planned activities. The first part of the paper introduces the research farms of the University of Agronomic Sciences and Veterinary Medicine. These were used as part of the study, being spread across the country, with different types of soils, terrain and crops. Further, we introduce a series of data collected from the farms, including drone imagery data collected in 2017 and 2018, respectively. Finally, we present the web platform, its functionality and the workflows that allows a smart farming management.*

**Key words:** crops, environment engineering, IOT, livestock, GIS, sensors, smart farming, web GIS.

### INTRODUCTION

The 21<sup>st</sup> century is marked by the digital revolution. Accessible, easy-to-use technology has increased the social and economic opportunities around the world. Also, is the direct cause of this fast rhythm of development that has not been achieved in human society until now. Access to information, education and financial instruments has led to economic growth worldwide. We have a better living due to the technology that improves our daily basic tasks, we travel faster, we have mobility with jobs, we can even work remote. Added to that, we have access to medical and life insurance, modern medical plans, which all contribute to a better life expectancy.

In this context, United Nations announced last June that the world's population had exceeded 7.6 billion inhabitants, and by 2050 is estimated the number will grow by another 2.3 billion people. With that increase in the number of inhabitants, demand for the food sector will increase proportionately. However, some measures need to be taken to cover global needs. First, it should be taken into consideration that as a cause of the increased

living standards and the automation of various industries, people have concentrated around towns. Only few have remained in the rural area and still maintain an agricultural activity that ensures their own needs as well as the commercialization of the products.

The unprecedented development of the society has left a strong footprint on the planet that does not come at a low cost. According to the UN, by the middle of this century, the effects of global warming will intensify strongly and will bring about significant changes; higher average temperatures, changing rainfall patterns, increased levels of seas and oceans, and increased frequency and intensity of extreme weather phenomena. If added to the possible emergence of resistant diseases and pests, the effects will strongly impact the agricultural sector and, implicitly, the food sector. Unfortunately, the most exposed population is also the one that is struggling now with damaged lands and those from developing countries (Koester, 2015). Thus, over the next decade, society will have to address the demand for food, while at the same time ensuring sustainability of the natural resources for the next generations. The solution lies also

in the digital revolution. New, autonomous technologies have been developed to modernize agricultural practices: mechanical systems for watering, sowing, fertilizing and harvesting. To monitor crops, UAVs equipped with multispectral cameras are now widely used, capable of providing complete information on crop health status. The system can be complemented by a network of sensors placed in the field to retrieve information about air and soil conditions. All integrated into a platform easily accessible anytime, anywhere, from any device, will generate disruptive changes in current farming practices.

### **Sharing Data and Knowledge**

Despite the development opportunities presented, there are of course also many barriers to the adoption of these modern agricultural practices. The high costs of such a system, as well as limited knowledge, might represent barriers, especially in developing countries. This context can produce a gap between the large agricultural associations, capable of supporting implementation efforts and small farmers. On the other hand, the public sector can gain from the data collected for the purpose of monitoring and controlling (Kaushik, 2017). So, it is expected to get involved in the financial and education tools for farmers. At the same time, this would be a great opportunity to lay the foundation for a platform of collaboration and selling agricultural products.

Romania is a member of the European Union and is subject to its regulations. Thus, according to the Inspire Directive (2007/2/CE), which entered effect on May 15th, 2007, we are responsible for reporting to the CE a series of 34 spatial data sets. One of these themes is Agricultural and Aquaculture Facilities and refers to *"physical instruments and constructions with permanent or semi-permanent occupation (inland or outland) that are related to agricultural and aquaculture activities"* (Inspire Directive). In Romania, the Agency for Payments and Intervention for Agriculture (APIA), is the body charged by Ministry of Agriculture and Rural Development (MARD) for the collection and delivery of INSPIRE data sets related to agriculture. This naturally came about because the agency has

the role of collecting information on agricultural parcels in the LPIS system, based on which farmers are granted financial aid. In addition to activities related to cultivating soils, producing crops and manning the land in good agricultural and environmental condition, APIA also deals with harvesting, milking, breeding animals, holding animals for farming purposes. There were some cases where farmers misrepresented locations and areas of plots, land use or livestock farms and have paid compensation perhaps even higher than the subsidies originally received from APIA. From our experience, these cases occurred due to uncertain land situations, misunderstanding of the reporting process, and non-recognition on the map of own land.

### **Aim**

A GIS system would primarily help farmers make asset management - in order to have a clear picture of the areas they cultivate. Not always what they cultivate is in their property, there are cases when lands are leased. It is essential for a farm that administers large areas of land to know the legal/contractual situation of each plot. Then, it is very important that alongside this information there is data on what is cultivated on these lands (Schaller, 1992). This will help them not only when reporting to APIA, but also to ensure sustainable agricultural practices through crop rotation. The overview of available surfaces, as well as other sets of data as: soil quality data, irrigation system, or irrigation channel location, allow the farmer to make the best strategy for the next crop season. Technological equipment and people also play a very important role. If equipped with GPS, then the control and monitoring of field operations is also ensured by integrating them into the GIS system (Yousefi Reza, Mohammad Razdari, 2015). Most of the time, even the best strategies are diverted by unforeseen events, even in the current climate, when we record more and more weather abnormalities. In order to obtain the planned production, the farmer must ensure that the plant development parameters are assured. The most basic analysis of this type is the NDVI. It can be obtained from satellite imagery or high-resolution images taken from drones, depending on the surface and the

culture being targeted. The results, combined with the parameters of the ground sensor network, represent the trustworthy decision support that will improve or even save the harvest in critical years (Delenne et al., 2010). From our experience so far, we have found that some farmers are well educated in what precision farming means. Many own some of component or more of the presented system. The problem we have identified is that they administer them individually and there is no integration to allow them to correlate the data. The purpose of our study is to build a web platform that performs asset management, field operation, analysis and decision support that is easy to implement and can serve as a tool for collaborating and selling products on a farm.

## MATERIALS AND METHODS

### Location

The study focuses on the nine research centers of the University of Agronomic Sciences and Veterinary Medicine of Bucharest (USAMVB) as follows: Belciugatele/Moara Domneasca Training Center; Pietroasa Vine-Growing Research and Development Center; Istria Farm and Istria Nursery Farm; Stoenesti Research and Development Farm and the lands of Pietrosani - Giurgiu and Teleorman, Borcea and Fetesti - Ialomita County, Gradistea and Cuza Voda - Calarasi County. All nine centres are spread across the south-est part of the country (Figure 1) and have special plots for vegetable crops, orchards and livestock's farms.



Figure 1. Map of the research areas of USAMVB

Their complexity from the perspective of the crop and agricultural works diversity make them ideal for a GIS Management Platform.

### System architecture

The proposed system was designed to support the collection, storage, manipulation and analysis of spatial data in a web interface. Implementation was accomplished using proprietary Esri solutions, but similar results can be obtained using open source tools.

### Data

The base of the proposed system is represented by the data storage format, the geodatabase format. It is preferred in favour of other storage formats (shp) because it allows for complex behaviours between spatial object classes. From simple functionality's such as the ability to declare domain values across fields to subtype classification, to attachments, relationship classes, and topology that provide the attribute and spatial integrity of data. It also provides support for SQL and the creation of complex query expressions (De Filippis et al., 2010). Finally, it allows viewing, editing, and querying data by multiple users simultaneously, without generating conflicts.

Most of the project data was digitized and organized into spatial objects classes, geodatabase storage subdivisions. The raster's obtained after processing the photogrammetric flight were also managed in the same geodatabase. After building the structure, we migrated the data on parcels and which existed in various formats. After loading them into the geodatabase and running the topology to check for any fault data, we proceed to upload it to the server. From here, data was deployed as web services on the web map and finally on the web application.

### UAV

A special step in the project was considered for flying the drone and obtaining high resolution imagery of the crops. The images were taken over the period of two years 2017 and 2018, respectively, from June to September. In 2017, we used a classic rgb camera for taking the pictures, and next year with a Sequoia multispectral camera in order to obtain information about the health of the plants. We will be repeating the flights this year, this time at shorter intervals - monthly / bimonthly, in order to watch the crops in different stages of development. The drone used is eBee from

SenseFly, a fixed wing UAV, suitable for precision farming (Figure 2).



Figure 2. eBee Drone and cameras

### Web

The web map is a dynamic map, optimized for use on the internet in order to display geographic information and facilitate user interaction with it.

Also, whatever you click on the map, displays the information available in the geodatabase regarding that object.

The purpose of the map is to add and view data, to collect and integrate information from the field (people, agricultural vehicles and sensor network), and to allow simple data queries. In the context of our project, the final web application consumes this web map (Figure 3).

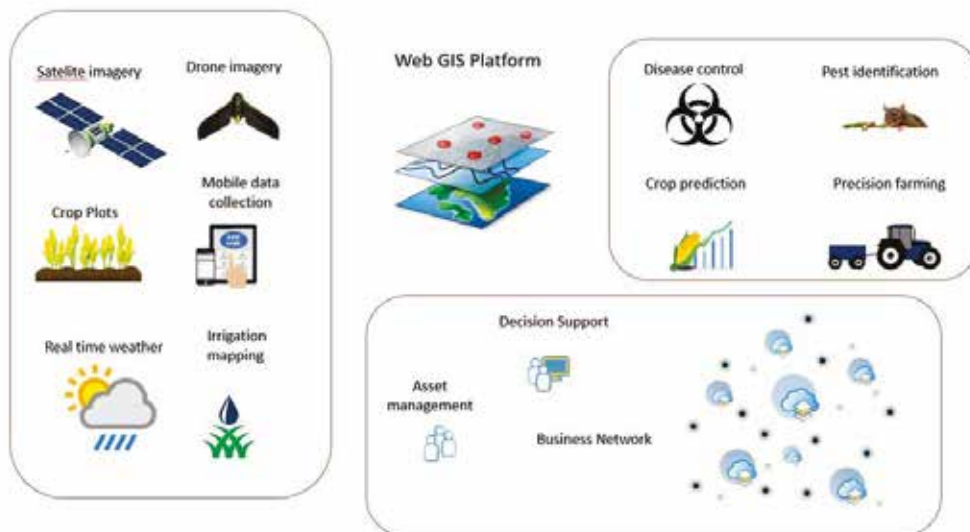


Figure 3. System Architecture of Proposed Platform

## RESULTS AND DISCUSSIONS

The initial processing of images in order to obtain photogrammetric products was done with the Pix4D software. In the first year, we only had the standard camera that the drone comes with. So, we were able to obtain only the basic photogrammetric products - orthomosaic, point cloud, DSM and DTM. Even so, we were able to easily detect gaps in corn and wheat

crops just before harvesting (Figure 4). Their main cause is the soil texture. However, there were also some anomalies due to the way the seeds were sown. Next year, 2018, we used the Sequoia multispectral camera with sensors in Green, Red, Near Infrared and Red Edge bands, and the photogrammetric products we have obtained allowed us to do more complex analyses (Tang L. & Tian L.F., 2013).

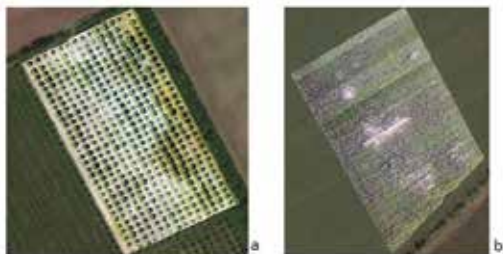


Figure 4: a) Fruit trees; b) Corn crops

For example, using Envi and the Crop Science module, we were able to obtain, in addition to the vegetation indices, the number of trees in an orchard, and the condition of each's health (Figure 5 and Figure 6).

Along with these high-resolution images, we also integrated Sentinel 2 satellite imagery. Sentinel-2, 10, 20, and 60 m Multispectral, Multitemporal, 13-band imagery services are

rendered on-the-fly and available for visualization and analytics.

After postflight processing of images and running vegetation health analyzes, the rasters have been published as tiled package services for the online use alongside vector data sets.

At the same time, another data service has been prepared and published that will allow field teams to collect and transmit real-time information on plant observations and possible pest invasions.

All data services have been merged at the level of a web map which was used in the deployment of the web application (Figure 7).

Various widgets were added for generating and printing crop maps, charts about crops and planted areas as well as tools for querying other pieces of information.

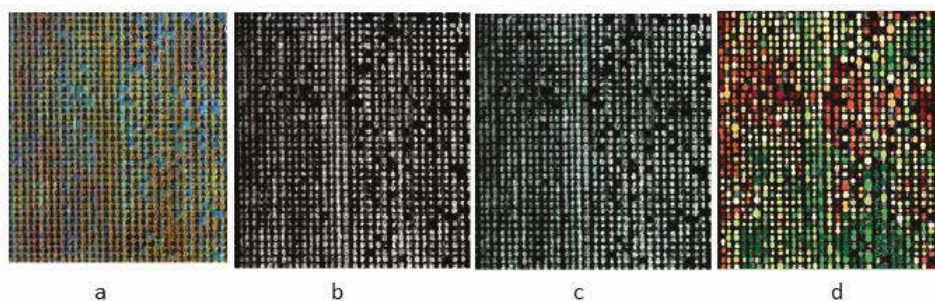


Figure 5: a) Picture of an orchard taken with multispectral camera; b) Individual trees automatically counted - detected locations marked with green circles; c) Individual trees identified by colour: green = healthy, red = poor, yellow-orange = between values; d) The analysis obtained by running hot spot analysis - green areas represent trees with a better state than the average, red - trees with a worse state than the average

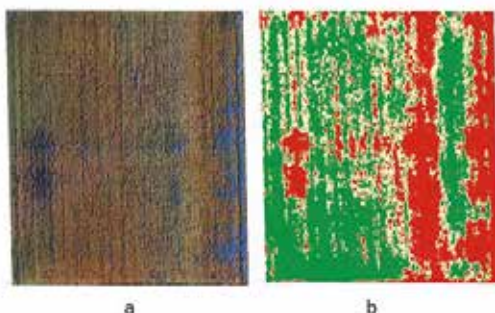


Figure 6: a) Picture of a corn crop taken with multispectral camera; b) The analysis obtained by running hot spot analysis - green areas represent plants with a better state than the average, red - plants with a worse state than the average

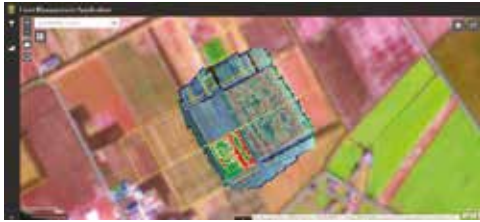


Figure 7. Web Application integrating all data sets

## CONCLUSIONS

Since the beginning of the 21st century, the global agricultural market has evolved significantly, but naturally, to serve the increased demand. Since the financial crisis in 2008, international commodity trade has been slow due to slow financial recovery. However, agricultural trade proved to be more resilient than fuel, mineral and manufactures.

The digital revolution in the agricultural sector will revolutionize the way the spatial data on crops and livestock farms are collected, stored, analysed and used. GIS platforms that integrate data from various farm sources will become important tools in the hands of decision-makers. Today we are seeing more and more equipment for use on farms with built-in GPS, automatic irrigation systems and specialized weather stations. All this is no longer news for farmers.

The period will bring challenges to analysing the data produced by these systems. The sensors we have today around us: satellites, drones, mobile devices, air and soil sensors produce a huge amount of data today. Therefore, in the coming years we will have to train the machines for the integrated analysis of these very large sets of data to produce forecasts and plant needs.

## REFERENCES

- Aliev, Khurshid et al. (2018). Internet of Plants Application for Smart Agriculture. *International Journal of Advanced Computer Science and Applications*, 9(4), 421–29. <http://thesai.org/Publications/ViewPaper?Volume=9&Issue=4&Code=ijacsa&SerialNo=58>.
- Çaylı, Ali, A Nafi Baytorun, and Ali Selçuk Mercanlı (2018). The Feasibility of a Cloud-Based Low-Cost Environmental Monitoring System Via Open Source Hardware in Greenhouses Açık Kaynaklı Donanım İle Bulut Tabanlı ve Düşük Maliyetli Bir Çevre Koşulları İzleme Sisteminin. *21(3)*: 323–38.
- Cuca, Branka et al. (2016). How Can Space Make a Difference for the Agriculture Sector. Technical report.
- Delenne, Carole, Sylvie Durrieu, Gilles Rabatel, and Michel Deshayes. (2010). From Pixel to Vine Parcel: A Complete Methodology for Vineyard Delineation and Characterization Using Remote-Sensing Data. *Computers and Electronics in Agriculture*, 70(1), 78–83.
- FAO 2013. Sourcebook on Climate-Smart Agriculture, Forestry and Fisheries Climate-Smart Agriculture Sourcebook. Food and Agriculture Organization of the United Nations. <http://www.fao.org/docrep/018/i3325e/i3325e00.htm>.
- De Filippis, T, Rocchi, L., Fiorillo, E., and Genesisio, L. (2010). A WebGIS Application for Precision Viticulture: From Research to Operative Practices. *International Archives of the Photogrammetry, Remote Sensing and Spatial Information Sciences - ISPRS Archives*, 38 (4W13). [www.scopus.com/inward/record.uri?eid=2-s2.0-84923875558&partnerID=40&md5=37f393e26aa64b566c36619eabc5ad75](http://www.scopus.com/inward/record.uri?eid=2-s2.0-84923875558&partnerID=40&md5=37f393e26aa64b566c36619eabc5ad75).
- Kaushik, Anjali (2017). GIS Based Decision Support Systems in Government. *Proceedings of the 10th International Conference on Theory and Practice of Electronic Governance - ICEGOV '17* (January 1995), 366–74. <http://dl.acm.org/citation.cfm?doid=3047273.3047391>.
- Koester, Ulrich (2015). Agricultural Transition in Post-Soviet Europe and Central Asia after 25 Years Markets and Morality: The Relevance for Transforming the Agricultural Sector in Transition Countries. [https://www.iamo.de/fileadmin/documents/sr\\_vol79.pdf](https://www.iamo.de/fileadmin/documents/sr_vol79.pdf).
- Kumar, K., Santosh, and Suresh Babu, D. B. (2017). A Web GIS Based Decision Support System for Agriculture Crop Monitoring System-A Case Study from Part of Medak District. *Journal of Remote Sensing & GIS*, 05(04).
- Tang, L., and Tian, L. F.(2013). Plant Identification in Mosaicked Crop Row Images for Automatic Emerged Corn Plant Spacing Measurement. *Transactions of the ASABE*, 51(6), 2181–91.
- Maguire, David J., and Paul A. Longley (2005). The Emergence of Geoportals and Their Role in Spatial Data Infrastructures. *Computers, Environment and Urban Systems*, 29(1 SPEC.ISS.), 3–14.
- Manescu, Camelia et al. (2016). Analysis of the Importance of Agriculture Sector in Romanian Economy. *Scientific Papers, Series Management, Economic Engineering in Agriculture and Rural Development*, 16(1), 271–77.
- Schaller, Joerg (1992). GIS Application in Environmental Planning and Assessment. *Computers, Environment and Urban Systems*, 16(4), 337–53.
- Sladić, Dubravka, Aleksandra Radulović, and Miro Govedarica (2014). Application of Service Oriented Gis in Agriculture. *Research Journal of Agricultural Science*, 46(3), 59–67.
- Tetis, Cirad U M R, and Irstea U M R Tetis (2015). Identifying Cropped Areas in Small Growers Agricultural Regions.

## SHADOWS CORRECTION METHODS FOR LANDSAT SATELLITE IMAGES

Bianca BADULESCU<sup>1</sup>, Alexandru Marin MATACHE<sup>2</sup>, Luciana VRANCUTA<sup>1</sup>,  
Silviu MUSAT<sup>1</sup>, Sevastel MIRCEA<sup>1</sup>, Nicolae PETRESCU<sup>2</sup>

<sup>1</sup>University of Agronomic Sciences and Veterinary Medicine of Bucharest, 59 Marasti Blvd,  
District 1, Bucharest, Romania

<sup>2</sup>Valahia University of Targoviste, 2 Carol I Blvd, Targoviste, Romania

Corresponding author email: bianca.badulescu@yahoo.com

### Abstract

*This article aims to present the problem about the topographic effects produced by the shadow in the mountain area. The existence of this phenomenon creates confusion between the components of a scene, cause difficulty in establishment with precision the types of land use because the surfaces covered with the same type of vegetation being totally different shown. In this case, even if they represent the same category of use of the land, the pixels found under the shadow have different digital values compared to the sunny ones. Topographic correction, which eliminates the terrain effect caused by the topographic relief, is one of the fundamental steps in data pre-processing. The diminution of the topographic effects can be achieved through various methods which have as result getting clear images by highlighting the information in the shadow. The reflected radiance in topographically complex areas is severely affected by variations in topography; thus, topographic correction is considered a necessary pre-processing step when retrieving biophysical variables from these images. It was assessed the performance of three topographic corrections: Cosine, C-Correction and Minnaert. The performance of topographic corrections on the images was assessed by visual comparison and spectral response analysis. In the majority of cases, C method performed best in terms of eliminating topographic effects comparing with the Cosine and Minnaert methods, which showed the poorest performance.*

**Key words:** topographic correction, Landsat satellite images, shadow.

### INTRODUCTION

In the rugged mountainous terrain, topographic effects distort severely the spectrum features of land surface. Slopes facing toward the sun receive more radiation and appear brighter than slopes facing away from the sun. Not only is illumination modified by topography, but the proportion of light reflected toward the satellite also varies with the geometry of sun, target and viewer. There are many of topographic effects that can cause topographic variation in the mountain area, including terrain shadow, slope effect, aspect effect, surrounding-reflected irradiance, and displacement of image points for high resolution image. Therefore, the process of topographic normalization may be critical in areas of rugged terrain, and is a preliminary step for the quantitative evaluation of the multispectral satellite imagery (Zhang et al., 2011). The operational use of remote sensing data is often limited due to sensor variation, atmospheric effects as well as topographically induced illumination effects

(Ekstrand, 1996; Twele & Erasmi, 2005). Topographic normalization is therefore, especially in rough terrain, important for improving analysis of remote sensing data (e. g. image classification). Although numerous topographic normalization methods have been proposed in the past, none of them has been found to be universally applicable and therefore topographic normalization is still a pre-processing issue rarely used (Füreder, 2010). The intensity of illumination on the surface depends on the orientation of the surface in respect to the sun. Different slope and aspect angles are inducing variable illumination angles and thus diverse reflection values. Areas of high relief therefore show high radiometric variation. Depending on topography reflection values within one land cover type can vary a lot. The illumination variations result in lower reflection values in the shadow and higher values in the sun for the same land cover class. Hence, reflection values of different land cover types in equal conditions of illumination can be more similar than within one land cover type in

shadow and sun, leading to problems in image segmentation and possible misclassifications (Twele & Erasmi 2005; Civco, 1989). Topographic normalization methods try to compensate for the topographically induced illumination variations in advance (Füreder, 2010). Till now, a variety of topographic correction models have been proposed. Methods for correcting the topographic effect may be grouped into two categories: 1) Empirical correction methods models which mainly correct the solar direct radiance affected by topography, such as solar direct radiance affected by topography, such as ratio model, cosine model, Minnaert model, sun-canopy-sensor (SCS) model, and C model; 2) Radiative transfer models for mountainous area, which employ a radiative transfer code to obtain a deterministic description of the correction of topographic effects. The advantage of the second method is that scene-dependent empirical parameters are avoided. Introducing some terrain factors slope and azimuth, illumination angle, horizon, and view factors for radiation from sky and terrain with the help of the digital elevation model (DEM), investigators have done a lot of work (Yanli Zhang & Xin Li, 2011).

## MATERIALS AND METHODS

The selected study area is located in Bucegi Mountains, which are located in central Romania, south of the city Brasov. They are part of the Southern Carpathians group of the Carpathians Mountains. It is characterized as rugged terrain, which has slope ranging from 0 to 254 degrees with an average of 170, the altitude ranging from 1600 m to 2400 m above sea level. The mean annual air temperature is 1.8°C and the mean annual precipitation is about 1200 mm/year.

In preparation of this work they were used Landsat 4-5 TM and Landsat 8 OLI / TIRS satellite images, which were downloaded through [theearthexplorer.usgs.gov](http://theearthexplorer.usgs.gov) portal. Choosing the right area is an essential thing, because the image must include the whole area studied, respectively Bucegi Mountains (Figure 1). Since a single image was not sufficient to cover the area, there were downloaded two images, respectively WRS Path 183, WRS Row

28/WRS Path 183, WRS Row 29, taking into account the visibility, cloud coverage and time for optimal comparison. The first step in the pre-processing stage was radiometric calibration, to correct brightness, reflection and image brightness temperature.



Figure 1. Study area

Correction methods of topographic effects of the land are known in the specialty literature and rely on using the slope and orientation got from the land digital pattern processing (DTM). These leads, eventually, to the topographic normalization of satellite image, being used on extended areas in the forestry fund, and the success is differentiated depending on the aimed objectives because the topographic effects cannot be entirely removed. The image, even if it is corrected, can be altered by “topographic residues” due to sub-corrections or by “negative topographies” because of super-corrections, effects that are allotted to over-simplification by the photometric model, neglecting the diffuse light and lack of accuracy of the digital pattern (Vorovencii, 2005).

The simplest method for compensating the topographic induced variable illumination is building of band ratios wherefore no additional data is required. It is based on the assumption that the relative topographic effect is similar in all bands and the quotient of two bands can compensate for this. This method does not

account for the diffuse irradiance, which depends on each band, and therefore can only partly compensate the topographic effect, provided that the atmospheric path radiance is eliminated in advance (Ekstrand, 1996). A further disadvantage in terms of multispectral classification is the loss of spectral resolution when using band ratios (Riano et al., 2003). Real topographic correction methods try to model the illumination characteristics of a horizontal surface by means of a DEM. For this purpose, it is required to calculate the local solar incident angle ( $i$ ), the angle between the current position of the sun (depending on solar zenith angle and solar azimuth) and the local surface (terrain slope and aspect) (Figure 2).

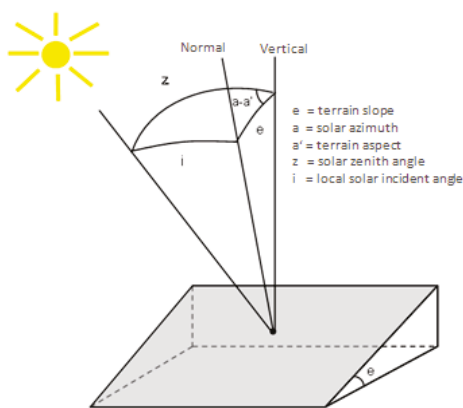


Figure 2. Angles necessary for computing the incident angle (based on Teillet et al., 1982)

The illumination ( $\cos i$ ) can be computed as follows:

$$\cos i = \cos e \cos z + \sin e \sin z \cos (a-a') \quad (1)$$

where:

- $i$  - local solar incident angle;
- $e$  - slope angle;
- $z$  - solar zenith angle;
- $a$  - solar azimuth angle;
- $a'$  - aspect angle.

The value of  $\cos i$  varies from -1 to +1, whereas a value  $< 0$  indicates shadowed slopes, which do not receive direct irradiance (Ekstrand, 1996).

The topographic correction methods can be classified in two categories according to their assumption of reflection characteristics of surfaces: Lambertian and non-Lambertian methods. Lambertian methods like the cosine correction are assuming a surface, which reflects the incident radiation in all directions equally, neglecting the atmospherically influences. Non-Lambertian methods are actually not physically based but try to model the diffuse irradiance by means of constants of the bidirectional reflectance distribution function (BRDF), which describes reflection characteristics of surfaces. The amount of the correction depends on the wavelength. So, the assessment of the constants for each band separately is required. The topographic effect is thereby most dominant in the near infrared band (Civco, 1989). As reflection characteristics are related to the land cover, the constants should also be calculated for each land cover individually (Twele & Erasm, 2005; Teillet et al., 1982; Bishop et al., 2003), resulting in a respectable effort (Füreder, 2010).

### Cosine correction

The cosine correction, which neglects the diffuse irradiance, only considers the solar zenith angle and the local solar incident angle for computation of the local illumination (Füreder, 2010). This is an empiric statistic method relying on a significant correlation between a dependent variable and one or more independent variables (Vorovencii, 2005). This method is frequently used because of its implementation in many software programs but it strongly over-estimates the influence of direct irradiance in areas of high incident angles and is therefore problematical for steep and sun-averted slopes, which appear brighter than sunfacing slopes (Civco, 1989; Twele & Erasm, 2005; Teillet et al., 1982).

$$L_H = L_T \frac{\cos z}{\cos i} \quad (2)$$

where:

- $L_H$  - reflectance of a horizontal surface;
- $L_T$  - reflectance of an inclined surface;
- $z$  - solar zenith angle;
- $i$  - local solar incident angle.

### Minnaert correction

The most common non-Lambertian topographic correction method is the Minnaert correction, which is based on the ideas of Minnaert (1941), who initially proposed a semi-empirical equation for describing the roughness of the moon's surface. The Minnaert correction extends the cosine correction as follows (Füreder, 2010):

$$L_H = L_T \left( \frac{\cos z}{\cos i} \right)^k \quad (3)$$

where:

$L_H$  - reflectance of a horizontal surface;

$L_T$  - reflectance of a inclined surface;

$z$  - solar zenith angle;

$i$  - local solar incident angle;

$k$  - Minnaert constant.

The constant  $k$  models the extent, to which a surface is Lambertian. It is determined by linear regression between reflection values of the input image ( $L_H$ ) and the angles ( $i$  and  $e$ ). The value of  $k$  lies between 0 and 1, whereas 1 characterises a Lambertian surface (Füreder, 2010).

### C-correction

This semi-empirical approach, developed by Teillet et al. (1982), is similar to the Minnaert correction. The factor  $c$  should model the diffuse irradiance and compensate the over correction effects of the cosine correction (Twele et al., 2006). The factor  $c$  can be derived from the quotient of the gradient and intercept from the regression line:

$$L_H = L_T \frac{\cos z + c}{\cos i + c} \quad (4)$$

where:

$L_H$  - reflectance of a horizontal surface;

$L_T$  - reflectance of an inclined surface;

$z$  - solar zenith angle;

$i$  = local solar incident angle;

$c = \frac{b}{m}$  for  $L_T = m \cdot \cos i + b$ ;

$m$  - gradient of regression line:  $L_T - \cos i$ ;

$b$  - intercept of regression line:  $L_T - \cos i$ .

## RESULTS AND DISCUSSIONS

For reducing the topographic effect, cosine-correction, Minnaert correction and C-

correction were tested, in two different software programs - ENVI 5.2 and Rstudio, R version 3.2.0.

The Rstudio program comprises `topocorr` function, which implements several different methods for topographic correction of remote sensing data. There are currently eight methods available: "cosine", "improvedcosine", "minnaert", "c-correction" (first four from Riano et al., 2003), "minslope" (Minnaert with slope correction, also from Riano et al., 2003), "gamma" (Richter et al., 2009), "SCS" (Gu & Gillespie, 1998; Gao & Zhang, 2009), "illumination" (uncorrected illumination) (R documentation) (Canty, 2014).

`topocorr(x, slope, aspect, sunelev, sunazimuth, method = "cosine", na.value = NA, GRASS.aspect = FALSE, IL.epsilon = 0.000001)` - this function was used for the available topographic correction methods to compensate for the effects of slope and aspect on reflectance from the land surface (Canty, 2014).

For the topographic normalization, a DEM (Digital Elevation Model) with 30 m spatial resolution has been downloaded, corrected and calibrated (Figure 3). As the quality of the topographic normalization is highly depending on the spatial resolution of the DEM the resolution should be at least as fine as the satellite image (Civco, 1989).

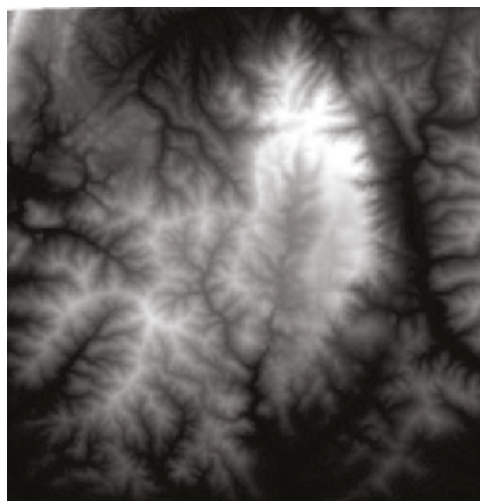


Figure 3. Digital Elevation Model

Also, for the result validation there were needed slope map (Figure 4) and hill shade map (Figure 5), which were extracted from DEM.



Figure 4. Slope map



Figure 5. Hill shade map

As primary results, it was obtained that the topographic variability has been removed and given a more 'flat' impression than the non-corrected image (Figures 6, 7, 8 and 9). To evaluate the correction, we randomly compared the spectral response in a point sample from corrected and uncorrected images from shady slope. These results suggest that in the uncorrected image the apparent reflectance of forest on the shady slope is very low.



Figure 6. Original image



Figure 7. C-correction



Figure 8. Minnaert correction

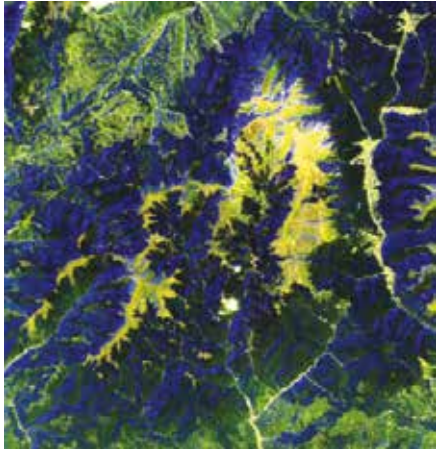


Figure 9. Cosine correction

Spectral differences (Figure 11) between original and topographic normalized image should be low, otherwise it would be a sign of over- or under correction (Figure 10). Slopes facing away from the sun should get higher values, sun-facing slopes respectively lower values. An effective topographic correction should reduce spectral variances and standard deviation and retain the mean (Law & Nichol, 2004).



Figure 10. Image before/after correction

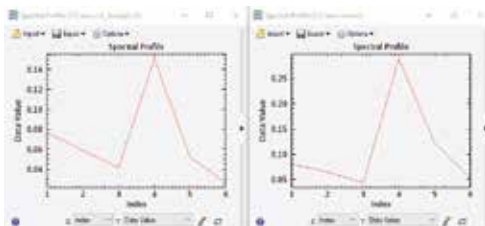


Figure 11. Spectral profile on original/corrected image

## CONCLUSIONS

In this study, the results of these three different topographic methods were analysed visually and from the perspective of spectral response. The visual analysis clearly indicates that the C-correction strongly overcorrects weakly illuminated areas like slopes facing away from the sun whereas they appear brighter than sun-facing slopes. Instead of reducing spectral variances, the normalized image appears more distorted (Füreder, 2010). As already observed in other studies (Meyer et al., 1993; Twele et al., 2006) the cosine correction and the Minnaert correction visually do not show major differences and could successfully reduce the topographic effect, which implicates the loss of the three-dimensional impression. Overcorrection of mountain ridges, where illumination is very low, is also showed here. Topographically normalized satellite images can, in general, obtain better classification results (Meyer et al., 1993; Colby, 1991; Riano et al., 2003; Twele et al., 2006). The reason for the non-perfect correction lies probably in some reasons. First, the DEM generated from the satellite images may have small errors because of lacking ground control points (Zhang & Li, 2011). A higher resolution of the DEM could compensate the topographic effect better, whereby also smaller illumination variations could be corrected (Füreder, 2010). Second, some of the areas lie in so deep a shadow and thus have very dark pixel values, which lead to no reliable estimations can be obtained (Zhang & Li, 2011).

## REFERENCES

- Bishop, M. et al., (2003). Remote sensing and geomorphometry for studying relief production in high mountains. In: *Geomorphology*, 55, 345–361.
- Canty, M. J. (2014). *Image Analysis, Classification and Change Detection in Remote Sensing, with Algorithms for ENVI/IDL and Python* (Third Revised Edition). Taylor and Francis CRC Press.
- Civco, D. L. (1989). Topographic normalization of Landsat Thematic Mapper digital imagery. *Photogrammetric Engineering Remote Sensing*, 55, 1303–1309.
- Colby, J. D. (1991). Topographic normalization in Rugged Terrain. *Photogrammetric Engineering and Remote Sensing*, 57(5), 531–537.
- Ekstrand, S. (1996). Landsat TM-based Forest Damage Assessment: Correction for Topographic Effects.

- Photogrammetric Engineering & Remote Sensing*, 62(2), S. 151–161.
- Erasmı, S. et al. (2004). Mapping deforestation and land cover conversion at the rainforest margin in central Sulawesi, Indonesia. *EARSeL eProceedings*, 3, S. 388–397.
- Füreder, P. (2010). Topographic correction of satellite images for improved LULC classification in alpine areas, *Grazer Schriften der Geographie und Raumforschung Band*, 45, 187–194
- Law, K., Nichol, J. (2004). Topographic correction for differential illumination effects on Ikonos satellite imagery. In: *International Archives of Photogrammetry Remote Sensing and Spatial Information Sciences*, 35, S. 641–646.
- Meyer, P. et al. (1993). Radiometric Corrections of Topographically induced Effects on Landsat TM Data in Alpine Terrain. Remote Sensing Laboratories. Department of Geography Zürich.
- Meyer, P., Iiten, K. J., Kallensberger, T., Sandmeier, S., Sandmeier, R. (1993). Radiometric correction of topographically induced effects on Landsat TM data in analpine environment. *ISPRS J. Photogrammetric Remote Sensing*, 48(4), 17–28.
- Riaño, D. et al. (2003). Assessment of Different Topographic Corrections in Landsat-TM Data for Mapping Vegetation Types. In: *IEEE Transactions on Geoscience and Remote Sensing*, 41(5), S. 1056–1061.
- Richter, R. (2009). Atmospheric/Topographic Correction for Satellite Imagery. Report DLR-IB 565-01/09/2009.
- Richter, R. (1997). Correction of atmospheric and topographic effects for high spatial resolutionsatellite imagery. *International Journal of Remote Sensing*, 18(5), 1099–1111.
- Teillet, P., Guindon, B., Goodenough, D. (1982). On the slope-aspect correction of Multispectral Scanner Data. In: *Canadian Journal of Remote Sensing*, 8(2), S. 84–106.
- Twele, A. et al. (2006). The effect of stratified topographic correction on land cover classification in tropical mountainous regions. In: *ISPRS 2006*.
- Twele, A., Erasmı, S. (2005). Evaluating Topographic Correction Algorithms for Improved Land Cover Discrimination in Mountainous Areas of Central Sulawesi. In: Erasmı S., B. Cyffka und M. Kappas (Ed.) (2005): *Remote Sensing & GIS for Environmental Studies (= Göttinger Geographische Abhandlungen)*, 113, S. 287–295. Göttingen.
- Vorovencii, I. (2005). *Researches concerning using possibilities of satellite images inforest planning works*. Doctor’s thesis. Transilvania University of Braşov.
- Vorovencii, I. (2005). Removal of Topographic Effects from Satellite Images (p 1–6).
- Zhnag, Y., Li, X. (2011). Topographic Normalization of Landsat TM Images in Rugged Terrain Based on the High-resolution DEM Derived from ASTER-PIERS Proceedings, Suzhou, China, September 12-16, 712–716.

## ADVANTAGES OF REALISTIC REPRESENTATION OF A GEOGRAPHIC AREA BY COMBINING OPTICAL AND LiDAR DATA CAPTURED WITH UAVs

Gabriel POPESCU<sup>1</sup>, Octavian Laurentiu BALOTA<sup>1</sup>, Daniela IORDAN<sup>1</sup>, Daniel ILIE<sup>2</sup>

<sup>1</sup>University of Agronomic Sciences and Veterinary Medicine of Bucharest, 59 Marasti Blvd, District 1, Bucharest, Romania

<sup>2</sup>Prosig Expert SRL, 62A Soseaua Mihai Bravu, Corp B, District 2, Bucharest, Romania

Corresponding author email: gabrielpopescu2013@gmail.com

### Abstract

*The paper aimed to present the advantages of realistic representation of a geographic area by combining optical and LiDAR data captured with UAVs. LiDAR data and aerial images, both captured with an UAV, have their own unique advantages and disadvantages and it is natural to integrate those two data sets for a good realistic representation of a geographic area in terms of horizontal and vertical accuracy. Compared with aerial images, LiDAR data provide more accurate height information but less accurate boundaries. Aerial images provide more extensive planimetric information such as high-resolution texture and colour information. Although 3D height information can be estimated from one or several images by the use of several photogrammetric methods, the height information extracted from aerial images is still relatively less accurate. The realistic representation of a geographic area in the virtual environment, was verified for validation in the Cernica Dam area, checking the spatial data sets used (LiDAR and optical). We used for data validation, the ground truth, given by GNSS measurements in the field, and the experimental results indicate that this combination improves the overall accuracy from 94% to 97%.*

**Key words:** LiDAR, mapping, photogrammetry, UAVs.

### INTRODUCTION

The use of Unmanned Aerial Vehicles (UAVs), named also drones, is still only in its infancy but with a rapid development in the last few years. UAV industry is still mainly dominated by start-ups. Unmanned aerial systems, composed by UAV + LiDAR + Digital Photo Camera + IMU + GNSS, constitute an increasingly important segment of engineering. Mapping and surveying drones provide an easy-to-deploy platform for aerial views of an area of interest. Currently there are some factors limiting the use of drones regarding operation time and development of regulation in many countries. UAVs contribute to the production of valuable 3D and image data for needs in various engineering projects, urban planning or scientific research.

As is well known, photogrammetry is a well-established technique for acquiring dense 3D geospatial information about objects and phenomena. In fact, the method is as old as modern photography, dating back to the middle of the 20<sup>th</sup> century. The science has continued

to evolve over time, of course, and – especially in view of the recent advancements in computer vision and machine learning – the technology is no longer as simple as it may seem. Developers of photogrammetric software and equipment face the challenge of providing the mapping and surveying community with solutions that are sophisticated, yet also meet high customer expectations in terms of user-friendliness.

LiDAR (Light Detection and Ranging) technology is based on LASER (Light Amplification by Stimulated Emission of Radiation) scanning through the use of optically directed LiDAR beams to collect object information in direct 3D measurements. This allows the system trajectory (position and attitude), to be produced robustly and accurately. Prior to the mid-1990s years, GNSS-IMU technology was not affordable for commercial use. Since then, however, the market for devices has exploded, especially with the development of fibre-optic gyroscopes (FOG) and micro electro-mechanical systems (MEMS) technologies. Also, the build-up of nationwide GNSS base station networks has

contributed to the success of LiDAR in surveying and mapping in all its variety.

LiDAR, so effective in topographic mapping, makes possible the capability to direct 3D measurements to the target and penetration of the beam through vegetation to collect information from objects and the ground beneath. The light wave front passing through the vegetation produces information on the vegetation as a side product.

Dense and geometrically accurate point cloud offers photographic 3D capture of the reality for mapping, modelling and monitoring. Spectral information from LiDAR have significant implications on automated data interpretation (Wim van Wegen, 2019).

Keeping account of advantages and disadvantages of the two technologies, there is a growing tendency to combine them both (Table 1).

Table 1. Some applications which are using photogrammetry, LiDAR and both together

	Photogrammetry only	LiDAR only	Combination of both
Topographic mapping	60%	6%	34%
Cadastral Surveying	54%	19%	27%
Generation of DEMs	27%	46%	27%
3D City Models	30%	19%	51%
Agriculture	55%	18%	27%
Archeology	47%	9%	44%
Forestry	30%	26%	44%

More than half of the users rely on photogrammetry plus LiDAR for the creation of 3D city models, in agriculture, in archaeology, in forestry and others are also high-ranking applications. For example, in forestry, LiDAR-derived DEMs and photogrammetric canopy surface measurements are both suitable for providing relevant geospatial information relating to forest canopy structure. Contrary to LiDAR, photogrammetry cannot penetrate vegetation canopy, but photogrammetric matching of digital aerial images is a cost-effective and reliable solution.

## MATERIALS AND METHODS

The data collected by authors and used for the realization of the realistic representation of a geographical area were as follows:

- LiDAR point clouds obtained using UAV;
- Color digital aerial images taken with UAV;
- GNSS measurements in field checkpoints (GCPs).

The Flow Diagram (Figure 1), or otherwise the technological flow, is nothing more than a schematic presentation of the steps leading to the construction of the final product being analysed, which is the realistic representation of a geographical area.

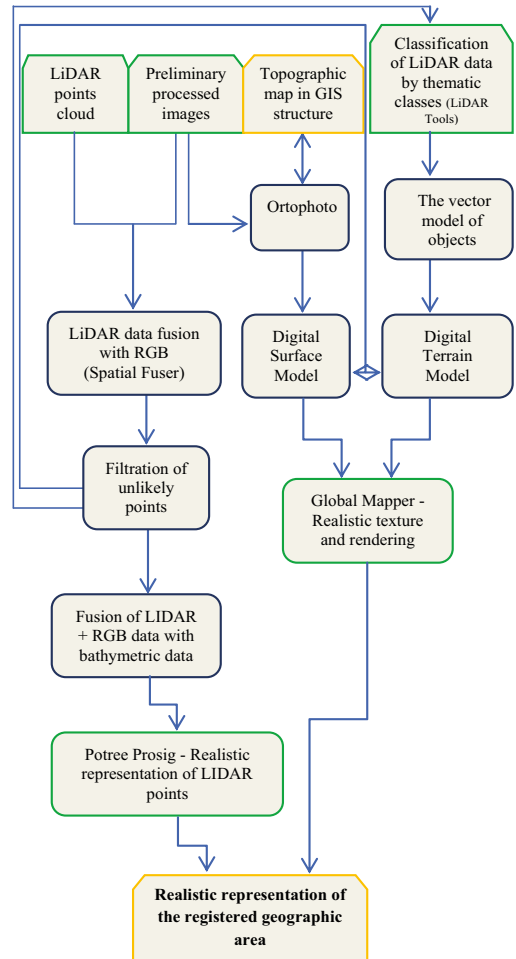


Figure 1. Workflow diagram to obtain the product "realistic representation of a geographical area"

The diagram presented is a review of all the steps that need to be taken when it is desired to obtain a virtual-realistic model of representing or monitoring an area of interest, such as those hard-to-reach areas, or areas for which a

modelling realistic in particular of urban objects.

## RESULTS AND DISCUSSIONS

Conceptually, the realistic representation of a geographic area is a new product that comes to the user with a reproduction of the analyzed area, in a digital format that is more in line with reality. The main use of the final product is to use it in various simulations of intervention in case of natural disasters, or even simulations of natural disasters (floods, earthquakes, fires, landslides, etc.).

The product, which can be generated entirely or only for certain thematic interest classes, is based on scanning techniques with the LiDAR-UAV system and the automatic and fast processing of data, all performed in accordance with the principles of photogrammetry. The product allows us to perform various types of measurements on the virtual image, determinations that reflect true field values.

The realistic representation of a geographic area, in our case in the Cernica Dam area (Figure 2), was made using: the point cloud LiDAR with RGB, the optical digital colour images and the digital topographic map in the GIS structure, the vector object model and the digital terrain model (DTM).



Figure 2. Cernica Dam area, chosen and tested for realistic representation

In the following Figure 3, several photographic pictures in the field and LiDAR point clouds from the model from the Cernica Dam area are presented for comparison.



Figure 3. In-field photographic images (on the left) and LiDAR point clouds in the model (on the right)

The realistic representation of the purchased LiDAR data is the merging of LiDAR data with the images recorded in the field. This method involves the generation of LiDAR point cloud with RGB merging the two datasets. Follow point cloud classification in grades points credible or anomalies. Upon completion of these processes, the generated point cloud is used in the realistic representation of the area with the Potree-Prosig application.

Optical data were recorded by the Sony A6000 camera, which was attached to the CPU and mounted on the DJI MATRICE M600 PRO as images with the “.arw” extension. This data format is a very professional one, representing the image to its maximum, uncompressed quality, but unfortunately this format was impossible to use in the next stages of obtaining a realistic representation. In order to be able to merge optical data with LIDAR data, these optical images were converted to “.jpg”

format images using Image Converter. By using the same application, radiometric corrections can be made (correcting shadows or brightness too high).

The working mode in generating the realistic representation of the Cernica Dam area is checked using the Portree-Prosig software, as shown in the following figures.

Three ways in which a realistic representation of a geographic area can be achieved in the presented workflow (Figure 1), using the LiDAR and optical data purchased with the MATRICE M600 PRO - LiDAR SCOUT UAV system. These representations were made in the following way: the first is based on the geometrically and physically calibrated LiDAR cloud and pre-processed RGB optical images, the second was obtained from the RGB optical images and the topographical map in the GIS structure, and the third is a realistic presentation based on the collage made of two models (the vector model of urban objects and the digital model of the land).

In Figure 4, it is shown the transformation of the LiDAR point cloud in realistic representation for the Cernica Dam area tested for validation with the Potree-Prosig software.

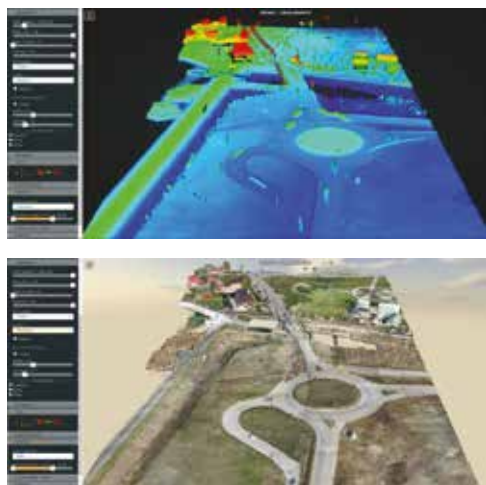


Figure 4. Transformation, with the Potree-Prosig software, of the LiDAR point cloud in realistic representation, for the Cernica Dam

For optical images, the final processing involves: obtaining preliminary oriented photograms using the Spatial Fuser application (using the camera file “.cam” and the

navigation file “.nav”) and Agisoft PhotoScan Professional, orthorectification of images (correcting images based on 3D Mesh dense points), georeference (based on ground control points, determined at the data acquisition stage). All these steps, of the final processing of the optical data, lead to the obtaining of the georeferenced orthophotoplan (Figure 5).

For the “.las” file it was further elaborated: a data filter by extracting from the calibrated data set the unreliable points (those anomalies) by applying the integrated algorithms in the LiDAR Tools application, followed by an extraction of the digital models of the field (Digital Elevation Model) and surface function (Digital Surface Model) by using the same LiDAR Tools software, digital models shown in Figure 6 (for DSM) and in Figure 7 (for DEM).



Figure 5. Orthophotoplan for the verified area at the resolution of 5cm/pixel

UAV LiDAR and photogrammetry are both viable methods for capturing point clouds for 3D modelling of the ground or space-object in general. Although both methods produce point clouds, the manner of capturing data differs in many ways, resulting in point clouds with differing characteristics.

LiDAR is a technology that is based on laser beams. It shoots out laser and measures the time it takes for the light to return. It is so called active sensor as it emits its energy source rather than detects energy emitted from objects on the ground.

Photogrammetry, on the other side, is a passive technology, based on images that are transformed from 2D into 3D cartographic models. It uses the same principle that human

eyes or 3D videos do, to establish a depth perception, allowing the user to view and measure objects in three dimensions. The limitation of photogrammetry is that it can only generate points based on what the camera sensor can detect illuminated by ambient light. LiDAR uses lasers to make measurements, while photogrammetry is based on captured images, that can be processed and combined to enable measurements (Buczowski A., 2018).

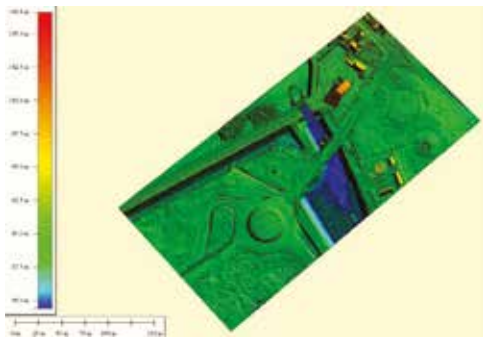


Figure 6. The Digital Surface Model (DSM) for the Cernica Dam area

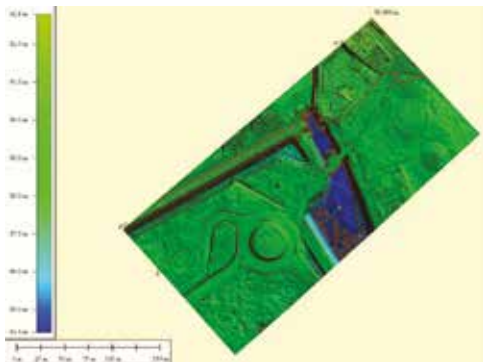


Figure 7. The Digital Elevation Model (DEM) for the Cernica Dam area.

The LiDAR and optical data fusion process was performed in the Spatial Fuser application developed by the Phoenix LiDAR integrator and delivered with the LiDAR system. The application uses the LiDAR Mill processed flight path, optical images converted to the "jpg" format, the droning camera file, and the non-processed LiDAR file in "ldr" format. Following this merger, a LiDAR point cloud with RGB color was obtained for each LiDAR

point, the colour taken from the optical images (Figure 8).



Figure 8. Making realistic virtual model of the area after texture, in the Global Mapper

The final product, shown in Figure 9, was obtained by merging all the materials resulting from the previous stages (orthophoto and the cloud of points representing the ground points) and the realistic representation of a geographic area can be obtained in several variants of coordinate systems and data formats.

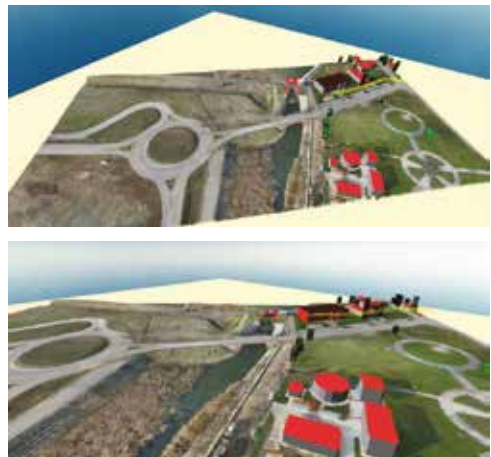


Figure 9. Making the realistic vectorial model using urban objects, DTM and the georeferenced orthophotos

The advantages of additional LiDAR surveying, face to photogrammetry, include:

- (1) LiDAR provides a more accurate digital terrain model (DTM) when vegetation is present;
- (2) LiDAR data can be processed faster than UAV photogrammetry and much higher productivity can be achieved;
- (3) LiDAR is expected to produce better reliability than photogrammetry over weakly

textured surfaces (although a thorough data comparison still has to be performed to confirm this).

## CONCLUSIONS

Data that is captured by either photogrammetric or LiDAR mapping technology is gathered in a point cloud. An often-heard question is whether photogrammetric point clouds are superior to LiDAR ones, or vice versa. The best answer is probably that there is no clear-cut answer; it depends on the application. Although LiDAR mapping may deliver a higher level of detail, photogrammetry is usually sufficiently detailed for large areas, for example. The fairest conclusion is that each system has advantages and disadvantages. Our research reveals that photogrammetry is a far more popular geodata acquisition technology for mapping projects than LiDAR (photogrammetry 75%, LiDAR 25%). However, the demand for LiDAR solutions is growing and LiDAR, in particular, is an often-used method for the generation of digital elevation models (DEMs). Our experimental results indicate that the combination of photogrammetry with LiDAR improves the overall accuracy from 94% to 97%.

Briefly, high accuracy in Photogrammetry is related to photo resolution, camera calibration, angles, photo orientation quality, photo redundancy and targets/markings precision.

Ease of use and low costs will make photogrammetry accessible to a wider range of users, including non-traditional photogrammetry users. There also seems to be a growing demand for software that is able work with LiDAR, aerial photography and UAV data in a single-window environment. In the future, it is very important to achieve the interoperability between data formats and/or sensor formats from different manufacturers and the rise of UAVs in the geomatics field will require new adjustments from providers of photogrammetric solutions.

The clear development trends are towards automated systems and real-time data processing. Also, longer operation times for UAVs are achieved with improved avionics,

battery life and indigenous ideas for hybrid drones with 2-4 hours' flight time. Small but high-performance sensors and real-time data are the most relevant needs for drones, and typically limited project areas do not necessitate the presence of a GNSS-IMU. Data are processed to a local coordinate system using techniques prevailing within the robotics community. With ever-smaller and more capable GNSS-IMUs and decreasing prices, it happens that direct georeferencing reduces the effort for ground control.

3D mapping using photogrammetry and LiDAR has huge potential in many applications because data attributes are significantly discriminated and delineated with excellent accuracy and speed by involving limited manpower which is less time consuming and relatively economical (Ahmad Firoz et al., 2017).

The final conclusion of our study is the same with Aleks Buczkowski's: "When comparing LiDAR and photogrammetry, it is a key to understand that both technologies have their applications as well as limitations, and in the majority of use cases they are complementary. None of these technologies is better than the other and none of them will cover all the use cases" (Buczkowski A., 2018).

## ACKNOWLEDGEMENTS

This investigation and research work was carried out by authors through the Romanian firm Prosig Expert SRL, with the support of the National Authority for Science, Technology and Innovation from Romania.

## REFERENCES

- Ahmad, F., Uddin, Md. M., Goparaju, L. (2018). 3D Mapping by Photogrammetry and LiDAR in Forest Studies. *World Scientific News*, 95, 224-234.
- Buczkowski, A. (2018). Drone LiDAR or Photogrammetry? Everything you need to know. <http://geoawesomeness.com/drone-lidar-or-photogrammetry-everything-your-need-to-know/>, uploaded 6/1/2018.
- Wim van Wegen (2019). Which Photogrammetry Solutions Are Surveyors Waiting For Geomares Publishing. *The Global Magazine for Geomatics*, 33.

## PROTEIN SOURCES FOR ANIMAL FEED: YEAST BIOMASS OF BEER AND/OR WINE - REVIEW

Corina DUMITRACHE, Florentina MATEI, Diana Iuliana BARBULESCU, Mihai FRINCU,  
Valerica TUDOR, Lucian Nelutu HIRJOABA, Razvan Ionut TEODORESCU

University of Agronomic Sciences and Veterinary Medicine of Bucharest, 59 Marasti Blvd,  
District 1, Bucharest, Romania

Corresponding author email: razvan.iteodorescu@gmail.com

### Abstract

*This paper relates to studies regarding the influence of cultivation's substrates (carbon source - molasses, glucose, methanol, malt extract, nitrogen source yeast extract, phosphorus source monobasic and dibasic phosphates), inoculum (inoculation rate and inoculum age - CFU / ml), bioprocess parameters (temperature, aeration, rate of stirring) on the development of wine and / or brewing yeast biomass. Biomasses of brewing and / or wine yeast obtained (active and inactive) have been proven to be a rich source of protein (SCP) and mono-oligosaccharides (MOS) in different feed recipes compared to other protein sources (soybean meal, corn) for animal feed. It has been demonstrated that yeast biomass obtained with use in feed recipe has beneficial effects on animal health (ruminants, pigs, horses, poultry).*

**Key words:** feed recipe, protein, yeast.

### INTRODUCTION

Yeast is a unicellular eukaryotic organism with many nutritional benefits. Because of their high nutritional value, they are part of animal nutrition supplements (Shurson G.C., 2018; Ingrid Marie Håkenåsen, 2017). In 1996 yeasts, bacteria, fungi and algae have been used to develop new feed recipes. The protein thus obtained from microbial sources was called "Single Cell Protein" - SCP (Anamika Malav et al., 2017). Although SCP's have been successfully marketed for decades in the UK, optimal fermentation conditions are still under scrutiny by many researchers. From the studies performed, it was found that the fermentation conditions and media used had a major effect on the yield (g/l) and the productivity (g/l·h<sup>-1</sup>) of SCP's (Fatemeh S., Reihani S., 2019; Hezarjaribi M., 2016).

The manufacturing process of many products are dependent on processes triggered and sustained by microorganisms. Wine, beer, sake, and bread are just some examples of yeast-dependent products, especially *Saccharomyces cerevisiae* species (Rocio Gomez-Pastor et al., 2011).

*Saccharomyces cerevisiae* yeasts have demonstrated beneficial health effects over the years due to their vitamin content (especially vitamin

B) and their role in the production of microbial proteins,  $\beta$ -glucans and mannans (Jach M.E. et al., 2015).

Globally, it is estimated that approximately 0.4 million metric tons of yeast biomass is produced, of which 0.2 million are bakery yeast (Rocio Gomez-Pastor, 2011).

Due to the protein content and probiotic properties of yeasts of the species *Saccharomyces cerevisiae*, yeast biomass is an option to consider for animal feed. (Suarez & Guevara, 2018).

The major components of the yeast cell wall are polysaccharides. In *Saccharomyces cerevisiae*, up to 90% of the cell wall's dry weight are  $\alpha$ -mannan and  $\beta$ -D-glucan polysaccharides with properties to interact with the host's immune system (Kogan G., Kocher A., 2007). Another growth promoter taken into consideration today is mannan oligosaccharides (MOS). MOS is derivate from yeast cell wall of *Saccharomyces cerevisiae* species (Brendemuhl & Harvey, 1999).

The cell wall of yeast, 26-32% of dry weight, is a structural component that gives yeast the form and specific rigidity. The literature specifies the immune cell stimulation property of beta-glucan in the cell wall of the yeast. In addition, the MOS, another yeast cell wall component, has been successfully used to

prevent diarrhea in weaning pigs (EURASYP, 2016).

The yeast cell wall typically contains 15-30% Beta-Glucan and 15-30% MOS, representing an effective alternative for antibiotic-growth promoters. (Ronel Jay & Conejos V., 2012).

The present review presents the importance of yeast biomass in the feed recipe as a beneficial effect on animal health.

### **Yeast used for biotechnological process in order to obtain active and inactive biomass yeast**

In the market for fodder products, there are numerous yeast-based supplements marketed and used in animal feed for sources of nutrients, nutraceutical compounds, and probiotics or as participants in different nutritional functions (Middelbos, 2007).

Yeast has vegetative states that predominantly reproduce by budding or fission and do not form their sexual state within or on a fruit body. They can be defined as basidiomycetous, ascomycetous or as unicellular fungi (Kurtzman & Fell, 1998). Yeasts are widespread in nature, but they do not appear totally random, they form communities in specific habitats - especially areas where they are vineyards (Lachance & Starmer, 1998).

Currently, there are about 60 different types of yeast composed of about 500 different species. Species distribution is based on variation in cell morphology, metabolism of different substrates, and different reproduction processes (Stone, 2006).

Of all kinds of yeast, only a few species are used commercially. Typical commercial yeast applications include alcoholic beverages (beer, wine and spirits), soft drinks (root beer, kvass, kombucha, kefir, mauby), bread and food baking, bioremediation, (to generate carbon dioxide for plant growth in the aquarium), food additives and flavouring agents, scientific research, and genetic engineering prophecies (Shurson, 2018).

In order to obtain a source of SCP, fermentations with substrates as carbon source - molasses, glucose, methanol, malt extract and nitrogen source yeast extract, is used. The biomass resulted represents a protein source and a most part of the yeast is reach in MOS.

### **Cultivation methods**

Yeast production uses fermentative processes (Chandrani-Wijeyaratne & Tayathilake, 2000). It was involving the incubation of selected strains of microorganisms in environments that meet the needs of these microorganisms, with the aim of growing the culture followed by separation processes (Gour Suman, 2015).

To maximize the final product, the literature describes the efforts made to evaluate the effects on fermentation of the various factors: pH, temperature, incubation period, dissolved oxygen, aeration rate, carbon and nitrogen sources (Chandrani-Wijeyaratne & Tayathilake, 2000).

One of the yeast strains that has proven useful over time in fermenting on various substrates is *Saccharomyces cerevisiae*.

This strain is considered very useful in animal feed considering its probiotic nature (Suarez, 2018).

An example of this process is given by G.G. Fonseca et al., 2007, with ATCC 26548 yeast (CBS 6556, NCCY 2597, NRRLy 7571). This yeast strain was cultivated in YPD medium (yeast extract,  $10 \text{ g} \times \text{l}^{-1}$ ; peptone,  $20 \text{ g} \times \text{l}^{-1}$ ; glucose,  $20 \text{ g} \times \text{l}^{-1}$ ).

### **Inoculum preparation**

Regarding the preparation of the inoculum, this was prepared in 250 ml Erlenmeyer flasks with 100 ml medium sterilized at  $121^\circ\text{C}$  for 15 minutes. The composition of the medium was:  $150 \text{ g} \times \text{l}^{-1}$  sucrose,  $6 \text{ g} \times \text{l}^{-1}$  yeast extract,  $5 \text{ g} \times \text{l}^{-1}$  monobasic potassium phosphate,  $5 \text{ g} \times \text{l}^{-1}$  ammonium chloride,  $1 \text{ g} \times \text{l}^{-1}$  magnesium sulphate (Erika Vieira, 2013).

### **Fermentation**

The outcome of the fermentation is affected by the substrate used (Spalvins, 2017).

### **Molasses and glucose**

Regarding the carbon source, molasses is the most used in the production of yeast (especially for the production of bakery yeast). Molasses is a by-product of the sugar industry that contains about 55% fermentable sugars. Its composition includes sucrose, glucose, fructose, raffinose, melibiose and galactose.

### **Methanol**

In addition to conventional materials such as molasses, fruit and vegetable wastes and unconventional substrates such as petroleum by-products, natural gas, ethanol, and methanol have been used.

### **Malt extract and molasses**

Due to the cost of cane molasses, different medium was used. The yeast biomass results achieved from malt medium and from molasses medium were not very different (Ragheb et al., 2015).

### **Nitrogen source yeast extract**

As with the carbon source, the use of different sources of nitrogen can increase the yield of yeast production.

A positive effect on yeast production has yeast extract, peptone and soybean meal, whereas urea can have a negative effect (Zhao G., 2010).

Fermentation with yeast extract in 0.5% concentration yielded maximum yield. Significant increase in growth could be observed with the increase in nitrogen source and phosphorus source (monobasic and dibasic).

### **Effects of initial $\text{KH}_2\text{PO}_4/\text{K}_2\text{HPO}_4$ concentration on biomass production**

In 2017, Nicolas Ouedraogo determined the effects of the initial concentration of  $\text{KH}_2\text{PO}_4/\text{K}_2\text{HPO}_4$  on the fermentation medium on the growth of biomass production by experimenting with concentrations of  $\text{KH}_2\text{PO}_4/\text{K}_2\text{HPO}_4$ . This concentration was changed between 0.1 and 0.5 g of  $\text{l}^{-1}$  inoculum (inoculum rate and inoculum age - CFU/ml).

In general, type of microorganism used, incubation temperature, incubation time, shake rate, chemical structure, and availability of carbon source from different substrates were considered and were monitored in various works. However, inoculum size, inoculum age, pH, and aeration rate are also important factors for which their effects on the SCP production need to be investigated (Fatemeh S. et al, 2019).

The optimal pH for most strains of *Saccharomyces cerevisiae* is 4.5 (Rose, 1987). The required amount of raw molasses, nitrogen and phosphorus salts was calculated based on

the spreadsheet simulator. The molasses purity was 56% as determined by sugar HPLC (fructose, glucose and sucrose) and Brix analysis. (Erika Vieira, 2013).

The degree of SCP (Single Cell Protein) production depends on the type of substrate used and also on media composition (Spalvins, 2017).

After fermentation, the culture media is separated, purified and dried.

Depending on the drying process, the yeast obtained may be active or inactive.

Active yeast can be obtained by lyophilization or by fluidized bed dryer and inactive yeast results by spray drying or rolled drums process.

An investigation of the optimization of parameters of an industrial continuous fluidized bed dryer for the production of instant active dry yeast was made by Hamidreza Akbari et al. (2012).

Example for active yeast used for feed animal:

Active Yeast - A-YEAST™ Yeast Culture provides a boost in rumen fermentation, production and feed efficiency, while mitigating the effects of heat stress (<https://ahanimalnutrition.com/species/dairy/products/a-yeast>). Levucell® SC is active dry yeast for use as a direct fed microbial in ruminant feeds. It is a unique strain exclusively selected to improve rumen function. RumiSacc is a commercial live yeast culture. It contains live yeast and autolyzed yeast (Sakine Yalçin, 2011).

*Saccharomyces cerevisiae*, *Candida robusta* and *Hansenula polymorpha* were taken in study in batch fermentation in order to study profile of yeast growth and biomass accumulation. Maximum cell density was reached after 24 h and amounted to 178.22 g WCW per litre of medium, corresponding to 36.4 g/l CDW.

It was established the bioprocess flowsheet at micropilot level in order to obtain a viable proteic biomass with yeast mixed culture (*Saccharomyces cerevisiae*, *Candida robusta* and *Hansenula polymorpha*).

Yeast single-cell protein (SCP) is a high nutrient feed substitute (Burgents et al, 2004). Among these, most popular are yeast species *Candida* (Bozakouk, 2002), *Hansenula*, *Pichia*, *Torulopsis* and *Saccharomyces*.

Active dry yeast is comprised of 15-25 billion live yeast cells (colony forming units; CFU's) per gram (Stone, 2006). The three most common processing methods include tunnel dried yeast (granular powder), fluid-bed dried yeast (quick rise yeast in oval shaped spheroids), and rotolouver dried yeast (produces small spheres or balls). The tunnel dried and fluid-bed drying methods are most common in the U.S., while the rotolouver drying method is more common in Europe and Latin America (NPCS Board of Consultants and Engineers, 2011). Of these drying processes, fluid-bed drying has become the most popular because it causes less damage to yeast cells, and thus, maintains their viability. In the 1960's, yeast biomass-producing plants contributed to the technology of producing large amounts of active dry yeast (ADY), and its use rapidly spread to European countries (Reed & Nagodawithana, 1988). Nowadays, modern industries require very large amounts of selected yeasts to obtain high quality reproducible products and to ensure fast, complete fermentations. (Rocio Gomez-Pastor, 2011).

Beside the content of proteins, yeast biomass is a good source of B-complex vitamins, nucleic acids and minerals.

Commercial brewer's yeast is inactive yeast remaining after the brewing process with an inexpensive nitrogen source with good nutritional characteristics and a very bitter taste (Bekatorou, Psarianos, & Koutinas, 2006).

Yeast single-cell protein (SCP) is a high-nutrient feed substitute (Burgents et al., 2004). Among these, most popular are yeast species *Candida* (Bozakouk, 2002), *Hansenula*, *Pichia*, *Torulopsis* and *Saccharomyces* (Gour Suman, 2015).

## ANALYSES

### Determination of dry cell weight

According to Gaensly F. (2014), the dry cell weight can be determined by drying the yeast biomass at 60°C after centrifuging 10 ml of sample at 6000 rpm until the biomass reach a constant weight.

Another method was used by De Sous et al. (2006), the method assumes that at the end of the fermentation yeast biomass was collected. The collected biomass was centrifuged at 6000x G/min at 4°C and washed two times

with distilled water. The resulting precipitate was dried in oven at 105°C for 4 h and the yeast biomass was measured with an analytical balance.

### Biomass determination

The biomass concentration was determined by turbidity measurements at 610 nm, correlated to dry weight from duplicate samples (5 ml, taken in the middle and at the end of cultivation) which were centrifuged (5000x G, 10 min), washed twice with distilled water, and dried for at least 24 h at 110°C. The specific growth rate was calculated from the biomass measurements, as well as from the heat measurements, since during anaerobic exponential growth, the rate of heat production is directly correlated to the specific growth rate.

**Total protein content** was determined with samples of freeze-dried cells (prepared as described previously (Gurakan, 1990), resuspended in 3 ml of 1M NaOH, by a modified biuret method (Verduyn, 1991). The A555 was measured, and bovine serum albumin (Amersham Life Science, Little Chalfont, England) was used as a standard).

Sugar content was measured by a saccharometer (Dujardin-Salleron, France), phosphate concentration was measured according to the micro determination method (Chen P.S., 1956; Ehab El-Helow et al., 2015)

**Total carbohydrates** could be determined through the colorimetric method from Dubois et al. (1958).

**Total lipids** could be extracted through the procedure of Blight and Dyer (1959) and after that determined gravimetrically (Sidney Becker Onofre, 2017).

The results concerning the content of protein and lipid from different yeast biomass are shown in the Table 1.

### MOS analyses

Yeast cell wall is a non-specific stimulator of the immune system in both human and animals which is generally composed of 30-60% polysaccharides (beta-glucan and mannan sugar polymers), 15-30% proteins, 5 - 20% lipids and a small amount of chitin. Most of the protein is

linked to the Mannan-OligoSaccharides (MOS) and is referred to as the Mannoprotein complex (Aguilar-Uscanga & Francois, 2003; Huang et al., 2005; Klis et al., 2006).

MOS is derived from the cell wall of the yeast *Saccharomyces cerevisiae* (Linn. Brendemuhl & Harvey, 1999).

#### **Extraction of crude mannan oligosaccharides**

For the extraction of the MOS, 5 g of dry yeast were used. Extraction with 1% NaOH (50 ml) was performed at 100°C for 2 h. After cooling, the solution was diluted with HCl solution until pH 7 reached.

After filtration, the mannan oligosaccharides were precipitated by adding 200 ml (4 volumes) of ethanol absolute. The precipitate was washed with ethanol absolute and diethyl ether dissolved in water, dialyzed against 2 changes of water and subsequent drying (Huang et al., 2010; Al-Manhel, 2017).

**Application:** The potential effect of mannanoligosaccharides on the intestinal immune system, combined with the high concentration of mannan components in dry yeast cell wall (YCW), may make YCW preparations useful functional dietary ingredients in pet foods by improving intestinal health and resistance against intestinal upset (Middelbos I.S., 2007). Benefit from adding yeast to the diets of monogastric animal can be illustrated based on that yeast cells containing mannan in the outer layer of their cell wall (Ofek et al., 1977). Mannan has anti-adhesive properties that can help in the adhesion of bacteria to epithelial of mucous membranes. Addition of yeast also can stimulate the immunity of animals. (Qamar et al., 2001). Yeasts are also known to contain other essential microelements that participate in the physiological and metabolic processes in human organism, such as Zn, Cu, Mn (Barbulescu et al., 2010), Fe (Pirman & Oresnik, 2012).

#### **Yeast– ingredients for animal feed**

MOS-fed animals had greater height compared with the control and the doxycycline-fed animals. The corresponding improvement in digestibility was correlated with the increase in

height due to their high correlation coefficient ( $r = 0.70-0.87$ ). MOS is therefore an effective alternative for antibiotic-growth promotants. (Jay Ronel V. Conejos, 2012). Mannan-Oligo-Saccharide (MOS), another constituent of Yeast Cell Wall, has been demonstrated to prevent diarrhoea in weaning pigs.

The quality of viable yeast biomass obtained by the protocol performed by Campeanu Gh. et al. (2002) is good and it could be used as probiotic product for animal nutrition. *Saccharomyces cerevisiae* known also as the brewer's yeasts or baker's yeasts is one of the well-known and commercially significant yeast species (Håkenåsen, 2017). In animals, *Saccharomyces cerevisiae* in their diets are known to play several vital roles including prevention of diarrhea and mortality, boosting of immune system, performance, milk production, fiber degradation and nutrient digestability, adsorption of toxic metal such as cadmium, stabilization of rumen pH and microorganisms (Sylvester Chibueze Izah, 2018).

In addition, yeast strain, production conditions and processing, could affect the chemical composition and the biological availability of the yeast. The yeast included in the feed in the present experiment was dried and hence inactivated as a probiotic.

#### **CONCLUSIONS AND FUTURE PERSPECTIVE**

The quality of yeast biomass produced in the mentioned conditions by Campeanu Gh. et al. (2002) is high and allow its use as additive in animal fodder.

The beneficial effects of *Saccharomyces cerevisiae* have been demonstrated by research in the field and are largely due to the vitamin B complex and the mineral content, but also due to its role in the production of microbial proteins,  $\beta$ -glucans and mannans (Jach M.E., 2015).

*Saccharomyces cerevisiae* yeast has been used in animal feed in different proportions as part of the diet, 10% in cattle, sheep and 5% in the birds (Caridad Suarez, 2018). Since it has a good composition of amino acids, e.g. high levels of lysine, threonine and leucine and, also, high levels of B-complex vitamins, *Saccharomyces cerevisiae* may be a satisfactory

alternative to soybean meal in animal diets, provided it has nontoxic or antinutrient properties (Winkler, 2011). 50 kg/tonne of soybean meal = 48.5 kg/tonne of corn + 1.5 kg/tonne of L-Lysine HCl (<http://www.fao.org/3/y5019e/y5019e0a.htm>)

**Yeast can be a protein source for animal feed (ruminants, pigs, horses, poultry).**

For future studies, the aim is to obtain new yeast biomass of beer and/or wine (Figure 1) as a potential source of protein for feed animals.

Table 1. Chemical composition of brewer's yeast biomass and wine yeast biomass

Yeast biomass	brewer's yeast biomass - <i>Saccharomyces cerevisiae</i>	<i>Candida utilis</i>	<i>K. marxianus</i> ATCC	Wine yeast
Protein (% N × 6.25)	49.63 ± 2.43	54.8 ± 0.12	54.6 ± 1.5	-
Lipids	4.64 ± 0.52	15.12 ± 0.98	5.2 ± 0.2	6.06 ± 0.2
Ashes	7.98 ± 0.76	8.1 ± 0.18	3.0 ± 0.2	-
Total Carbohydrates	31.55 ± 4.32	2.8 ± 0.2	26.5 ± 0.8	28.42 ± 0.31
References	Sideney Becker Onofre, 2017	Ouedraogo et al., 2017	Gustavo Graciano Fonseca, 2007	Chiselita Oleg, et al., 2004),

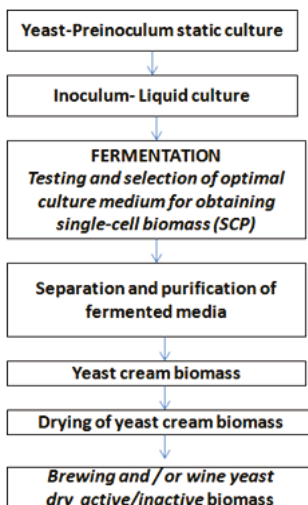


Figure 1. Fermentation process for obtaining dry active/inactive yeast biomass.

**ACKNOWLEDGMENTS**

This work was supported by the project 20PFE/2018 "Dezvoltarea Centrului pentru valorificarea superioara a subproduselor rezultate din fermele viti-vinicole", Programul 1 - Dezvoltarea sistemului national de cercetare-dezvoltare, Subprogramul 1.2 – Performanta institutionala – Proiecte de dezvoltare institutionala – Proiecte de finantare a excelentei în CDI, PNCDI III.

**REFERENCES**

Aguilar-Uscanga, B., & Francois, J. (2003). A study of the yeast cell wall composition and structure in

response to growth conditions and mode of cultivation. *Letters in Applied Microbiology*, 37(3), 268–274. doi:10.1046/j.1472-765x.2003.01394.

Akbari H., et al. (2012). Optimization of baker's yeast drying in industrial continuous fluidized bed dryer. *Food and Bioproducts Processing*, 90(C1), January, 52–57.

Al-Manhel, A. J., Niamah, A. K., (2017). Mannan extract from *Saccharomyces cerevisiae* used as prebiotic in bioyogurt production from buffalo milk, International. *Food Research Journal*, 24(5), 2259–2264.

Analytical Chemistry (1956), 28(3), March 1, ACS Publications, Washington, D.C., 350–356.

Barbulescu, I. D., et al. (2010). Obtaining yeast biomass enriched with copper, zinc and manganese. *Romanian Biotechnological Letters*, 15(1).

- Blight, E. G., Dyer, W. J. (1959). A rapid method of total lipid extraction and purification. *Canadian Journal of Biochemistry and Physiology*, 37(7), 911–917.
- Bozakouk, A. H. (2002). Acid hydrolysis of Phragmites austral: is powder for production of single cell protein by *Candida utilis*. *J. Res.*, 98, 876–897.
- Bradford, M. (1976). A Rapid and Sensitive Method for the Quantitation of Microgram Quantities of Protein Utilizing the Principle of Protein-Dye Binding. *Analytical Biochemistry*, 72(1-2), 248–254. doi:10.1006/abio.1976.9999
- Brendemuhl J. H., Harvey M. K. (1999). Evaluation of Bio-Mos (mannan oligosaccharide) in diets for pigs. *15 th Annual Symposium in Biotechnology in the Feed Industry*. Lexington, Kentucky. U.K., Nottingham University Press, 1202–1208.
- Burgents, J. E., et al. (2004). Disease resistance of Pacific white shrimp, *Litopenaeus van namei*, following the dietary administration of a yeast culture food supplement. *Aquacult. J. Microbiol.*
- Campeanu, G. H., et al. (2002) Biotechnological studies concerning the obtaining of biomass with probiotic role from yeasts and bacteria. *Roum. Biotechnol. Lett.*, 7(4), 795–802
- Caridad S., Guevara C. A. (2018). Probiotic Use of Yeast Saccharomyces Cerevisiae in Animal Feed. *Res J Zool*.
- Chen, P. S., Toribara, T. Y., & Warner, H. (1956). Microdetermination of Phosphorus. *Analytical Chemistry*, 28(11), 1756–1758. doi:10.1021/ac60119a033.
- Chiselița O, et al. (2008). Componenta biochimică a drojdiilor din sedimente vinicole. *Buletinul Academiei de Științe a Moldovei. Științele vieții*. 1(304), 132–137. ISSN 1857-064X.
- Dubois, M., et al. (1958). Colorimetric method for determination of sugars and related substances.
- Ehab R El-Helow, et al. (2015). Economic production of baker's yeast using a new Saccharomyces cerevisiae isolate. *Biotechnology & Biotechnological Equipment*, 29(4), 705–713.
- Erika, V., et al. (2013). Yeast biomass production: A new approach in glucose-limited feeding strategy. *Braz J Microbiol.*, Oct. 30, 44(2), 551–8.
- EURASYP - European Association for Specialty Yeast Products  
[http://www.yeastextract.info/public/documents/yeast-products/yeast\\_cell\\_wall.pdf](http://www.yeastextract.info/public/documents/yeast-products/yeast_cell_wall.pdf)
- Fatemeh S., et al. (2019). Influencing factors on single-cell protein production by submerged fermentation: A review. *Electronic Journal of Biotechnology*, 37, 34–40.
- Fernanda G. (2014). The uptake of different iron salts by the yeast Saccharomyces cerevisiae. *Brazilian Journal of Microbiology*, 45(2), Aug., 491–4.
- Ferreira, M. P. L. V. O., et al. (2017). Brewer's Saccharomyces yeast biomass: Manufacturing Process. *International Journal of Environment, Agriculture and Biotechnology (IJEAB)*, 2(2), March-April, <http://dx.doi.org/10.22161/ijeab/2.2.2> ISSN: 2456-1878.
- Ferreira, I., et al. (2010). Brewers Saccharomyces yeast biomass: Characteristics and potential applications. *Trends in Food Science & Technology*, 21(2), 77–84. doi:10.1016/j.tifs.2009.10.008
- Fonseca, G. G., et al. (2007). Physiology of the yeast *Kluyveromyces marxianus* during batch and chemostat cultures with glucose as the sole carbon source. *FEMS Yeast Res.*, 7, 422–435
- Gurakan, T., et al. (1990). Proposals for a standardized sample handling procedure for the determination of elemental composition and enthalpy of combustion of biological material. *Thermochimica Acta*, 172, December 1, 251–266.
- Håkenåsen, M. I. (2017). Feed intake, nutrient digestibility, growth performance and general health of piglets fed increasing levels of yeast. Master's Thesis. 30 ECTS, Faculty of Biosciences, January 1991, Volume 59, Issue 1, pp 49–63 |
- Hezarjaribi, M, Ardestani, F, Ghorbani, H. (2016). Single cell protein production by Saccharomyces cerevisiae using an optimized culture medium composition in a batch submerged bioprocess. *Appl Biochem Biotechnol*, 179(8), 1336–45.
- Huang, G. L., et al. (2010). Extraction and deproteinization of mannan oligosaccharides. *Zeitschrift für Naturforschung, C* 65, 387–390.
- Izah, C. S. (2017). Potentials of Yeast Biomass Production from Food Processing Wastes Effluents *EC Nutrition*, 8(3), 72–74.
- Jach, M. E., et al. (2015). Dietary supplements based on the yeast biomass. *Current topics in nutraceutical research*, 13(2), 83–88, ISSN 1540–7535.
- Jolly, N. (2006). The Role and Use of Non-Saccharomyces Yeasts in Wine Production, *South African Journal for Enology and Viticulture*, January.
- Klis, F. M., et al. (2006). Cell wall construction in *Saccharomyces cerevisiae*. *Yeast*, 23, 185–202.
- Kogan, G., Kocher, A. (2007). Role of yeast cell wall polysaccharides in pig nutrition and health protection, *Livestock Science*, 109, 161–165.
- Kurtzman, C. P., Fell, J. W. (1998). Definition, classification and nomenclature of the yeasts. In: Kurtzman, C.P. & Fell, J.W. (eds). *The yeasts, a taxonomic study*. Elsevier Science Publishers, Amsterdam.
- Lachance, M. A., Starmer, W. T. (1998). Ecology of yeasts. In: Kurtzman, C.P. & Fell, J.W. (eds). *The yeasts, a taxonomic study*. Elsevier Science Publishers, Amsterdam.
- Malav, A., et al. (2017). A critical review on single cell protein production using different substrates. *International Journal of Development Research*, 7.
- Middelbos, I. S. (2007). Adose-response evaluation of spray-dried yeast cell wall supplementation of diets fed to adult dogs: Effects on nutrient digestibility, immune indices, and fecal microbial populations. *J. Anim. Sci.* 85, 3022–3032, doi:10.2527/jas.2007-0079
- Middelbos, I. S., et al. (2007). Evaluation of fermentable oligosaccharides in diets fed to dogs in comparison to fiber standards. *J Anim Sci.*, Nov., 85(11), 3033–44.

- NPCS Board of Consultants & Engineers (2011). *Handbook on Fermented Foods and Chemicals*. Asia Pacific Business Press Inc., Oct. 1.
- Ofek, et al. (1977). Adherence of *Escherichia coli* to human mucosal cells mediated by mannose receptors. *Nature*, 265(5595), March, 623–5.
- Onofre, B. S., et al. (2017). Chemical Composition of the Biomass of *Saccharomyces cerevisiae* (Meyen ex E. C. Hansen, 1883). Yeast obtained from the Beer Manufacturing Process. *Int. Journal of Environment, Agriculture and Biotechnology*, 2(2), March-April, 0558–0562 DOI: 10.22161/ijeab/2.2.2.
- Ouedraogo, N., et al. (2017). Effect of mineral salts and nitrogen source on yeast (*Candida utilis* NOY1) biomass production using tubers wastes. *African Journal of Biotechnology*, 16(8), February 22, 359–365.
- Ouédraogo, N., et al. (2012). Essai de production de protéines d'organismes unicellulaires par des souches de levures à partir de résidus de tubercules de patate douce et d'igname. *Biotechnol. Agron. Soc. Environ.*, 16(4), 463–467.
- Pirman, T, Orešnik, A. (2012). Fe bioavailability from Fe-enriched yeast biomass in growing rats. *Animal*, 6(2), 221–6. doi: 10.1017/S1751731111001546.
- Qamar, A, et al. (2001). *Saccharomyces boulardii* stimulates intestinal immunoglobulin A immune response to *Clostridium difficile* toxin A in mice. *Infect Immun.*, 69(4), 2762–5.
- Reed, G., Nagodawithana, T. W. (1988). Technology of Yeast Usage in Winemaking. *Am. J. Enol. Vitic.*
- Rocio, G.P., et al. (2011). Recent Advances in Yeast Biomass Production, [www.intechopen.com](http://www.intechopen.com).
- Ronel, V. J. et al. (2012). Mannan Oligosaccharides from Yeast (*Saccharomyces cerevisiae*) Cell Wall Improves Nutrient Digestibility and Intestinal Morphology of Growing Pigs [*Sus domesticus* (Erxleben)]. *Philippine Agric. Scientist*, 95(3), 305–311.
- Rose, A. H. (1987). Responses to the Chemical Environment. In: Rose, A. H and Harrison, J.S. (eds), *The Yeast, Volume 2*. 2<sup>nd</sup> edition (pp. 5–40). Academic Press, New York.
- Shurson, G. C. (2018). Yeast and yeast derivatives in feed additives and ingredients: Sources, characteristics, animal responses, and quantification methods. *Animal Feed Science and Technology*, 235, 60–76.
- Spalvins, K., et al. (2018). Single cell protein production from waste biomass: review of various agricultural by-products. *Agronomy Research*, 16(S2), 1493–1508.
- Stone, C. W. (2006). Yeast products in the feed industry: a practical guide for feed professionals. Yeast Products in the Feed Industry, <https://en.engormix.com/feed-machinery/articles/yeast-products-in-feed-industry-t33489.htm>
- Suman, G., et al. (2015). Single Cell Protein Production: A Review. *Int. J. Curr. Microbiol. App. Sci.*, 4(9), 251–262.
- Toride, Y. Lysine and other amino acids for feed: production and contribution to protein utilization in animal feeding. (<http://www.fao.org/tempref/docrep/fao/007/y5019e/y5019e07.pdf>)
- Uçkun Kiran, E., et al. (2015). Platform chemical production from food wastes using a biorefinery concept. *J Chem Technol Biotechnol*, 90(8), 1364–79, <https://doi.org/10.1002/jctb.4551>.
- Verduyn, C., et al. (1991). A theoretical evaluation of growth yields of yeasts. *Antonie van Leeuwenhoek*, 59(1), January, 49–63.
- Wijeyaratne, S. C., Jayathilake, A. N. (2000). Characteristics of two yeast strains (*Candida tropicalis*) isolated from *Caryota urens* (Kithul) toddy for single cell protein production. *Journal of the National Science Foundation of Sri Lanka*, 28(1), 79, doi:10.4038/jnsfsr.v28i1.2936.
- Winkler, B., et al. (2012). Effect of the type of substrate on the chemical composition and productivity of a protein concentrate of yeast origin. *Cien. Inv. Agr.*, 39(3), 425–434.
- Yalçın, S., et al. (2011). The Nutritive Value of Live Yeast Culture (*Saccharomyces cerevisiae*) and Its Effect on Milk Yield, Milk Composition and Some Blood Parameters of Dairy Cows. *Asian-Aust. J. Anim. Sci.*, 24(10), 1377–1385.
- Zhao, G., Zhang, W., Zhang, G. (2010). Production of single cell protein using waste capsicum powder produced during capsanthin extraction. *Lett. Appl. Microbiol.*, 50, 187–91.

## COMPARE OF THE TECHNICAL MEANS WHEN ADMINISTERED OF PLANT EXTRACTS FOR CONTROL OF R PESTS OF OIL SEED RAPS

Dimitar KEHAYOV, Nedyalka PALAGACHEVA

Agricultural University of Plovdiv, 12 Mendelev Blvd, Plovdiv, Bulgaria

Corresponding author email: dkechajov@mail.bg

### **Abstract**

*With a view protection of rapeseed during flowering of pest and conservation of the main pollinators on crop plants namely bees are looking for alternative means of control. In this connection under field tested plant extracts: walnut (*Juglans regia* L.), wild walnut (*Ailanthus altissima* Swing.), tobacco (*Nicotiana tabacum* L.), against adult pollen beetle (*Meligethes aeneus* F.) and blossom beetle [*Tropinota (Epicometis) hirta* Poda]. Exploring held in 2018 in experimental rape fields in Southern Bulgaria. Experiment was conducted in 3 repetitions and 6 variations aim parameters. The following were: the type of sprayer and the plant extract at the same concentration of solutions. The results of conduct a studies show that high effectiveness against adults pollen beetle (*M. aeneus*) and blossom beetle (*T. hirta*) occurs with the use of plant extracts. It is established, influence both on the type of sprinkler, and the nature of the plant extract.*

**Key words:** oil seed raps, pests, plant extracts, sprayers.

### **INTRODUCTION**

Enhanced use of insecticides for controlling the pest of cultural plants lead to distortion the ecological equilibrium and in many cases until the resistance emerges insects to certain plant protection products. On the other hand, the type of sprinkler used in treatment is also a problem. As a result, the search for new ways to protection of its production restrict the use of chemical preparations.

During flowering key pests on oil seed rape are: pollen beetle (*Meligethes aeneus* F.), blossom beetle [*Tropinota (Epicometis) hirta* Poda]. They are directly threatened yield, under favorable conditions are massively multiplied. The pollen beetle (*M. aeneus*) in separate years may compromise the harvest, because you lose it reach 30-80%, and in some cases 100% (Hansen, 1996; Coll et al., 1998; Mason & Huber, 2002; Heimbach et al., 2007; Kazachkova, 2007; Wegorek & Zamoyska, 2008; Ahmanl et al., 2009; Farkas & Kondor, 2014; Erban et al., 2017).

A number of authors, Pavela (2005; 2006; 2009), Pavela et al., (2009a; b), Zabka et al., (2009), Nerio et al., (2010), in their research, found that essential oils derived from plant species exhibit insecticidal, fungicidal and

bacterial action. As in most cases the essential oils exhibit activity against pests (Isman, 2000; Nerio et al., 2010). On the one hand by the insecticidal effect of plant extracts reducing the density of the enemy, but on the other cause antifungal activity (Pavela, 2011).

Pavela (2011) tested the insecticidal activity of essential oils from 9 plant species: *Carum carvi* L., *Cinnamomum osmophloeum* Kaneh., *Citrus aurantium* L., *Foeniculum vulgare* Mill., *Lavandula angustifolia* L., *Mentha arvensis* L., *Nepeta cataria* L., *Ocimum basilicum* L., *Thymus vulgaris* L. against adult's pollen beetle. The results of the monitoring show that the tested essential oils exhibit high efficacy and cause of death of adult insects. Plant extracts of caraway (*Carum sarvi* L.) and thyme (*Thymus vulgaris* L.) exhibit the highest efficiency from 65.6 to 63.8%.

Based on their observations Hummelbrunner and Isman (2001) and Pavela (2008) found that essential oils of vegetable origin can cause not only mortality, they also affect fertility and lifespan of their enemies.

Recent years have witnessed the constant development of agricultural sprayers, with the availability of accessories such as electronic controls, GPS, plant sensors and air assistance along the spray boom. However, little is known

about these modifications in relation to the efficiency of the pest and disease control (Bauer & Raetano, 2003; Van de Zande et al., 1994).

It's the literature Nuytens et al. (2006), that the size of the sprinkler, the pressure of the solution, the speed of movement and the height of the bar significant influence on the performance of the sprayer.

Studies have been made Bauer and Raetano (2003) to assess the degree of coverage when treating legumes with a classic sprayer of a Twin System. No improvement was found the degree of coverage when applying air support. Pascuzzi (2013) has established the degree deposition of the working fluid on the foliage from vineyards at work with pneumatic sprinkler.

Several experiments have been carried out observations at work on fan and pneumatic sprinklers in fruit species. (Panneton & Lacasse, 2004; Pezzi & Rondelli, 2000; Dekeyser et al., 2013; Doruchowski et al., 2002). Experimental results show, that the distribution of the sprayed liquid is directly related with the airflow from sprinklers. Sprayers, equipped with pneumatic sprinklers are more effective ecological to work in these plantations.

They were not in the literature found results for work of sprayers, equipped with pneumatic sprinklers, in field crops.

Thus, purpose of this study is to establish insecticidal activity of some plant extracts against pollen beetle (*Meligethes aeneus* F.) and blossom beetle [*Tropinota (Epicometis) hirta* Poda], such as are used different types of sprinklers.

## MATERIALS AND METHODS

The research was held in 2018 in the area of Opan, Yambol, Southern Bulgaria in rape seed of the hybrid variety "Xenon" at size of Experimental parcels 25 m<sup>2</sup>. Under field conditions were tested plant extracts of: walnut (*Juglans regia* L.), wild walnut (*Ailanthus altissima* Swing.) and tobacco (*Nicotiana tabacum* L.) for controlling of key pests in oil seed raps during flowering: pollen beetle (*Meligethes aeneus* F.) and blossom beetle [*Tropinota (Epicometis) hirta* Poda], when

used two types of sprinklers: cranked and pneumatic.

Experience is bet in six variants and three iteration: Variant I - treatment crocked sprinkler with wild walnut extract; Variant II - treatment crocked sprinkler with tobacco extract; Variant III - treatment crocked sprinkler with walnut extract; Variant IV - treatment pneumatic sprinkler with wild walnut extract; Variant V - treatment pneumatic sprinkler with tobacco extract; Variant VI - treatment pneumatic sprinkler with walnut extract; Variant Control - treatment with one of the commonly used insecticides for chemical control of pollen beetle. In everyone variants marked 10 plants.

To determine the degree of coverage close to the inflorescence of each of the marked plants are put a sheet watermarking paper. Immediately after treatment, with the help of planner, the area covered by the solution is counted. This area is attributed to the total area of the leaves reflects degree of coverage (%).

Efficiency of the plant extracts were carried out on the 3<sup>rd</sup> and 7<sup>th</sup> day.

Main parameters, the following were: efficacy of plant extract and degree of coverage in colour area in dependence the type of sprayer used, at the same concentration of the solutions.

Received results were processed mathematically by dispersion analysis and comparing average values.

## RESULTS AND DISCUSSIONS

Average data for the degree of coverage and for the efficacy of plant extracts of the experiments and the results obtained in them are presented in Table 1.

Table 1. Results of the experiments

Sprinkler	Plant extract	Grade on coverage, %	Efficacy %	
			3 <sup>rd</sup> day	7 <sup>th</sup> day.
Cranked	wild walnut	43.6	67.4	80.5
Cranked	walnut	44.6	33.4	42.1
Cranked	tobacco	44.6	38.7	45.1
Pneumatic	wild walnut	64.3	68.2	83.4
Pneumatic	walnut	64.0	40.3	57.3
Pneumatic	tobacco	64.0	41.6	52.4
Cranked	insecticide	44.0	64.5	81.3

With the above data a dispersion analysis was performed for the influence of the independent variables on the degree of coverage and efficacy. About the degree of coverage, the following results were obtained (Tables 2 and 3).

Table 2. Dispersion analysis for influence of the species of the sprinkler on the degree of coverage

	SS	Degr. of	MS	F	p
<b>Intercept</b>	20106.67	1	20106.67	128888.9	0.000001
<b>sprinklers</b>	678.87	1	678.87	4351.8	<b>0.000001</b>
<b>Error</b>	0.78	5	0.16		

Table 3. Dispersion analysis to influence the type of extract on the degree of coverage

	SS	Degr. of	MS	F	p
<b>Intercept</b>	17065.16	1	17065.16	86.68312	0.002623
<b>extract</b>	89.05	3	29.68	0.15078	<b>0.922730</b>
<b>Error</b>	590.61	3	196.87		

In regard to the degree of coverage has been proven statistical difference at significance level  $p = 0.000001$ , which is much less than the limit value - 0.05.

There is a clear division into the quality of work of both types of sprinkler independently of the type of working solution (Figure 1).

With pneumatic sprinkler it is about 20% larger in comparison with a slit.

This is due to the fact that, in the case of a pneumatic sprinkler, the air jet crashes the working fluid of very small drops with approximately equal size (about 50  $\mu\text{m}$ ) and more in number. This enables them to be better placement on the treated surface, with cover of a larger area than it.

In the slit sprayer drops are with considerably larger diameter (150 to 300  $\mu\text{m}$ ), as a result of which is obtained and worse coverage in the same amount of spitting solution.

From the analysis it is established, that kind of extract has no effect the degree of coverage.

There is no statistically proven difference, because the calculated level of significance  $p = 0.92273$  is much higher than the acceptable 0.05.

For efficacy of plant extracts on the 3<sup>rd</sup> and 7<sup>th</sup> days according to the type of sprinkler were obtained the following results (Tables 4 and 5).

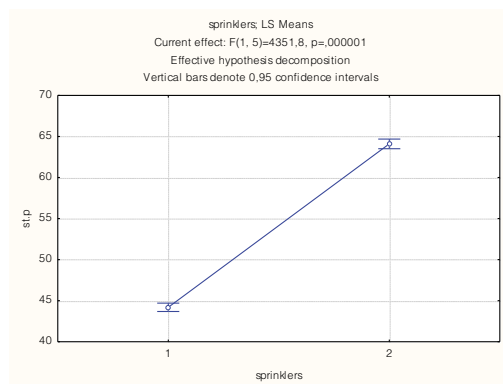


Figure 1. Comparison of average values of degree of coverage at the two sprinklers

Table 4. Dispersion analysis for influence type of sprinkler on the efficacy of plant extract on day 3

	SS	Degr. of	MS	F	p
<b>Intercept</b>	17498.97	1	17498.97	62.13477	0.000528
<b>sprinklers</b>	1.60	1	1.60	0.00569	<b>0.942806</b>
<b>Error</b>	1408.15	5	281.63		

Table 5. Dispersion analysis for influence type of sprinkler on the efficacy of plant extract on day 7

	SS	Degr. of	MS	F	p
<b>Intercept</b>	27483.05	1	27483.05	70.41460	0.000394
<b>sprinklers</b>	7.68	1	7.68	0.01968	<b>0.893915</b>
<b>Error</b>	1951.52	5	390.30		

From Tables 4 and 5, that the level of significance is 0.942806 for 3 days and 0.893915 on day 7, this gives us reason to say, that there is not statistically proven difference for influence the type of sprinkler on the efficacy of plant extracts.

For efficacy of plant extracts of 3 and 7 days the following results (Tables 6 and 7).

It is statistically proven ( $p = 0.004807$ ) that plant extracts show different efficacy.

Table 6. Dispersion analysis of the efficacy of plant extracts on day 3

	SS	Degr. of	MS	F	p
<b>Intercept</b>	17522.60	1	17522.60	1855.552	0.000028
<b>extract</b>	1381.42	3	460.47	48.762	<b>0.004807</b>
<b>Error</b>	28.33	3	9.44		

Graphical comparison performed of the mean values (Figure 2) that the wild walnut extruder (b) has the same efficiency with that of control (a) chemical preparation.

Extracts of walnut and tobacco are lower efficiency as they have close values.

Table 7. Dispersion analysis of the efficacy of plant extracts on day 7

	SS	Degr. of	MS	F	p
<b>Intercept</b>	27394.76	1	27394.76	561.4830	0.000165
<b>extract</b>	1812.83	3	604.28	12.3852	<b>0.033879</b>
<b>Error</b>	146.37	3	48.79		

The results are similar to the 3<sup>rd</sup> day.

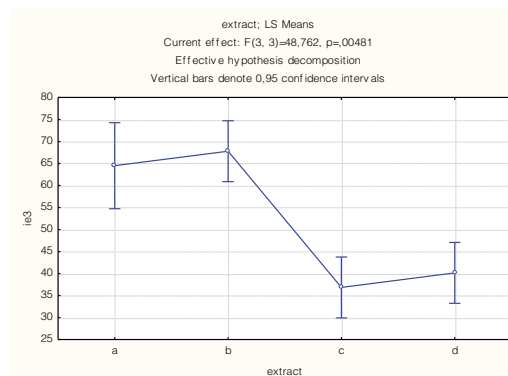


Figure 2. Comparison of the mean efficacy values for the different extracts

## CONCLUSIONS

As a result of conducted research can be done the following conclusions:

- Significant influence on the degree of coverage type of uses sprinkler;
- The walnut extract is c equal insecticidal efficacy as the control (chemical used). The efficacy of tobacco and walnut extracts is unsatisfactory.

## REFERENCES

Ahmanl, I., Lehrman, A., Ekbom, B. (2009). Impact of herbivory and pollination on performance and competitive ability of oilseed rape transformed for pollen beetle resistance. *Interactions*, 3,105–113.

Bauer, F., Raetano, C. (2003). Air-assisted boom sprayer and spray deposition on bean plants. *Sci. Agric. (Piracicaba, Braz.)*, 60(2), Piracicaba.

Coll, C., Booth, E. J., Sutherland, K. G. (1998). Pest and diseases control requirements for spring oilseed rape in northern climates. Brighton Crop Protection Conference, *Pests & Diseases, Volume 3*, Proceeding of an International Conference, Brighton, UK, 16-19 November, 1059–1064.

Dekeyser, D., et al. (2013). Assessment of orchard sprayers using laboratory experiments and computational fluid dynamics modeling. *Biosystems Engineering*, 114, 157–169

Doruchowski, G., et al. (2002). Spray Depozit, spray Loss and biological Efficacy of chemicals Applied with spraying Techniques in black Currants. *Electronic Journal of Polish Agricultural Universities*, 5(2).

Erban, T., Harant, K., Chalupnikova, J., Kocourek, F., Stara J. (2017). Beyond the survival and death of the deltamethrin-threatened pollen beetle *Meligethes aeneus*: An in-depth proteomic study employing a transcriptome database. *Journal of Proteomics*, 281–289.

Farkas, I., Kondor, Zs. (2014). The shaggy Rosenkaefer *Epicometis (Tropinota) hirta* in winter raps - increasing damage. 55. *Austrian Plant Protection Days*, 26.11. and 27.11.2014, 45–46.

Hansen, L. M. (1996). Blossom beetles in oilseed rape - monitoring and threshold, Danske Planteværnskonference. Sygdomme og skadedyr., 139–143.

Heimbach, U., Muler, A., Thieme, T. (2007). First Steps to analyse pyrethroid resistance of different oilseed rape pests in Germany. *Nachrichtenblatt des Deutschen Pflanzenschutzdienstes*, 58, 1–5.

Hummelbrunner, L. A., Isman, M. B. (2001). Acute, sublethal, antifeedant, and synergistic effects of monoterpenoid essential oil compounds on tobacco cutworm, *Spodoptera litura* (Lep., Noctuidae). *J.Agric. Food Chem.*, 49(2), 715–720.

Isman, M. B. (2000). Plant essential oils for pest and disease management. *Crop Prot.*, 19, 603–608.

Kazachkova, N. I. (2007). *Genotype analysis and studies of parathyroid resistance of the Oilseed rape (Brassica napus) Insect pest Pollen beetle (Meligethes aeneus)*. Thesis of Swedish University of Agriculture Sciences, 1–20.

Nerio, L. S., Olivero-Verbel, J., Stashenko, E. (2010). Repellent activity of essential oils:a review. *Bioresour. Technol.*, 101, 372–378.

Nuittens, D. et al. (2006). Experimental study of factors influencing the risk of drift from field sprayers, Part 2: Spray application technique. *Aspects of Applied Biology*, 77.

Panneton, B., Lacasse, B. (2004). Effect of air-assistance configuration on spray recovery and target coverage for a vineyard sprayer. *Canadian Biosystems Engineering*, 46: 2.13-2.18

Pascuzzi, S. (2013). The effects of the forward speed and air volume of an air-assisted sprayer on spray deposition in tendone trained vineyards. *Journal of Agricultural Engineering*, XLIV, 125–132

Pavela, R. (2005). Insecticidal activity of some essential oils against larvae of *Spodoptera littoralis*. *Fitoterapia*, 76, 691–696.

Pavela, R. (2006). Insecticidal activity of essential oils against Cabbage aphid (*Brevicoryne brassicae*). *JEOBP*, 9(2), 99–106.

Pavela, R. (2008). Acute and synergistic effects of some monoterpenoid essential oil compounds on the house fly (*Musca domestica* L.). *JEOBP*, 11, 451–459.

Pavela R., (2009). Larvicidal property of essential oils against *Culex quinquefasciatus* Say (*Diptera: Culicidae*). *Ind. Crop Prod.*, 30(2), 311–315.

- Pavela, R. (2011). Insecticidal and repellent activity of selected essential oils against of the pollen beetle, *Meligethes aeneus* (Fabricius) adults. *Industrial Crops and Products*, 34(1), 888–892.
- Pavela, R., Sajfrtova, M., Sovova, H., Karban, J., Barnet, M. (2009a). The effects of extracts obtained by supercritical fluid extraction and traditional extraction techniques on larvae *Leptinotarsa decemlineata* Say. *J. Essent. Oil Res.*, 21, 367–373.
- Pavela, R., Vrchotova, N., Triska, J. (2009b). Mosquitocidal activities of thyme oils (*Thymus vulgaris* L.) against *Culex quinquefasciatus* (Diptera: Culicidae). *Parasitol. Res.*, 105(5):1365–1370.
- Pezzi, F., Rondelli, V. (2000). The Performance of an Air-assisted Sprayer operating in Vines. *Journal of Agricultural Engineering Research*, 76, 331–340
- Van De Zande, J. C., Meier, R., Van IJzendoorn, M. T. (1994). Air-assisted spraying in winter wheat-results of deposition measurements and the biological effect of fungicides against leaf and ear diseases. In: *British Crop Protection Conference - Pests and Diseases, Brighton, 1994*. Proceedings Brighton: BCPC, 1994. 313–315
- Węgorzek, P., Zamoyska, J. (2008). Current status of resistance in pollen beetle (*Meligethes aeneus* F.) to selected active substances of insecticides in Poland. *Bull. OEPP/EPPO Bull.*, 38, 91–94.

## INFLUENCE OF SOME FACTORS ON THE GAS FLOW PRODUCED BY HHO GENERATOR

**Dimitar KEHAYOV, Georgi KOMITOV, Ivan IVANOV**

Agricultural University of Plovdiv, 12 Mendeleev Blvd, Plovdiv, Bulgaria

Corresponding author email: gkomitov@abv.bg

### **Abstract**

*Natural resources are an energy source, the restoration of which becomes extremely slow. In Global terms, there is an energy crisis with distinct peaks and lows, which compels all sides to seek lasting solutions in terms of energy balance. To meet their energy needs, many countries are planning a more rational use of energy and the development of renewed energy sources (RES) to replace part of the fossil fuels.*

*As a variant of a renewable energy source, the Brown's gas can also be considered. The efficiency of Brown's generator is justified by the clear decomposition of the hydroxyl group and the amount of gas produced.*

*This article examines the influence of two factors on the flow rate of receiving Brown's gas. Two different electrolytes are used with different concentration and different current force from the power source. Conducted experiment is planned for B2 plan. It is decided the optimization task with a global maximum and it is found the meanings of the factors that give the maximum value of the gas flow rate.*

**Key words:** HHO gas, gas flow rate, planned experiment, RES, optimization.

### **INTRODUCTION**

In recent years, there has been strong interest in creating and using different types of alternative fuels. One of these fuels is HHO gas (Brown's gas). A number of authors have demonstrated that the addition of HHO gas to traditional fuels (diesel or gasoline) leads to improved operational and environmental performance of the internal combustion engines (Yilmaz A. et al., 2010; Levente B. et al., 2015; Chakrapani K., Neelamegam P., 2011; De Silva T. et al., 2015;

<https://www.doc-developpement-durable.org/>). Advantages of HHO gas are: a compact and easy-to-use device for receiving it, perfect blend of fuel flammability based on air and hydrogen, allowing easy engine start at any ambient temperature, the calorific value (140 MJ/kg) his exceed more than 3 times this item on natural methane gas, absolute ecological safety-exhaust gases are converted into water, 4-7 times greater burning rate compared to the petrol mixture without detonation with a high degree of compression; the ability to synchronize the work of some stunt in combined generator, allows to increase the performance of your device several times

(Shalbaev K. et al., 2017; Malinowska M., 2015).

Its drawbacks are: the high cost of components for gas storage and transportation, the amount of hydrogen fuel tank is comparable with the parameters of the vehicle, the high explosive atmosphere of gas should exclude the possibility for the leakage; retrofitting of gas stations and the production of hydrogen fuel is now 4 times more expensive than the production of gasoline; the ability to burn when hydrogen comes into contact with the hot exhaust manifold. Therefore, it is proposed to use the engines and combustion systems with the remote location of the intake manifold from the exhaust pipe, hydrogen engines emit significantly more nitrogen oxides from gasoline engines.

As a source of HHO gas is used a low volume electrolytic cell. The electrolyte fluid is KOH or NaOH with different concentration (De Silva T. et al., 2015;

<https://www.doc-developpement-durable.org/>). Electrolysis runs under a constant, at low voltage of 10-14 V. An important element is the use of a suitable power supply control module for the generator (Yilmaz A. et al., 2010; Balawender K. et al., 2016).

Water was split by electricity to form its various elements, oxygen and hydrogen. When HHO mixture was ignited, both explosion and implosion occurred to form water, releasing the energy that was found in the bonds of the two elements in the form of heat (Yilmaz A. et al., 2010).

On the basis of the literature, it was found that there is insufficient data of characteristics for the HHO gas production.

The purpose of this study is to determine the optimal values of current power and electrolyte concentration used to achieve maximum flow of HHO gas.

## MATERIALS AND METHODS

Applying the cybernetic method of the "black box", a model of the experiment presented in Figure 1.



Figure 1. Model of experiment:  
 $W_D$ -process of obtaining HHO gas; C-concentration of electrolyte; I- force current power; D-gas flow

A two-factor B2 experiment is planned. The independent variables of this experiment are: electrolyte concentration (C) and current strength (I). Sodium (NaOH) and potassium (KOH) bases, each with three different concentrations, are used as the electrolyte. The power of the current also changes to three levels. Table 1 presents the factors and their variation levels.

Table 1. Factors and variation levels

Factors	Variation levels		
X - Electrolyte concentration, %	10	15	20
Y - Power of current, A	10	12.5	15

Attempts to determining the flow of generated HHO gas are carried out at the Department of Agricultural Mechanization in Agricultural University - Plovdiv on a research test stand (Figure 2).

The power supply is fulfilled with an adjustable DC source with a capacity of 12 V and 20 A. The HHO gas generator (1) used in the circuit is made up of two cells connected in electrical parallel connection with one pipeline. The generator's electrolyte container is connected to the atmosphere to reduce hydraulic losses. The gas produced by the HHO generator on the pipelines (4) passes through the water filter (3) and from there is directed to the flowmeter (5) for direct flow measurement.

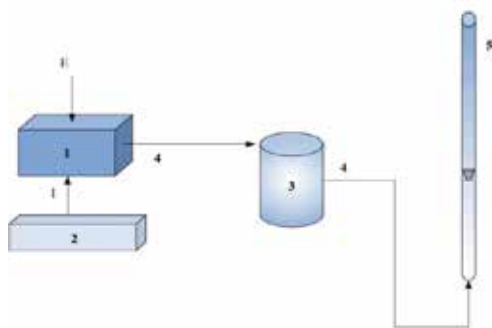


Figure 2. Scheme of test stand:  
 1-generator of HHO; 2-power source; 3-water filter; 4-pipes; 5-rotameter

The used rotameter is manufactured by the company "SKC", model "CHROMSERVIS" with a range of (0-5) l/min. The rotameter's protective case is removed and it is levelled to avoid errors at reading the values. With the obtained results in the experiments carried out a regression analysis using the software Statistica v.7 and the regression models for each of the electrolytes were constructed. The obtained models are illustrated with regression graphs and surfaces.

## RESULTS AND DISCUSSIONS

The results of the experiments are reflected in Table 2.

For both electrolytes the change in the flow rate of the generated gas is not one-way. With an increase in the concentration of 10% to 15% there is an increase in the flow, then from 15% to 20% decreases.

As the current increases in both electrolytes, the amount of gas generated increases one-sided.

The general observation is that, within the range of the observed factors change, KOH electrolyte determines a gas flow higher than when NaOH is used.

Table 2. Results of the experiments

Nº of experience	X, %	Y, A	D <sub>NaOH</sub> , l/h	D <sub>KOH</sub> , l/h
1	20	15	80	100
2	20	12.5	60	27.5
3	20	10	50	15
4	15	15	140	190
5	15	12.5	115	140
6	15	10	20	110
7	10	15	50	190
8	10	12.5	35	32.5
9	10	10	10	22.5

After the regression analysis by B2 plan, the following results were obtained:

- For electrolyte NaOH, the results of experiments are shown on Table 3.

For this electrolyte, the amount of gas generated is mainly influenced by the power of the current.

The regression model has the form (1):

$$D = 0.398 \cdot Y^2 \quad (1)$$

The flow of HHO for using NaOH electrolyte is graphically shown in Figure 3.

The debit is linear increase only with increase of current.

Table 3. Regression analysis for flow using NaOH electrolyte

Regression Summary for Dependent Variable: D <sub>NaOH</sub> : R= 0.90332014; R <sup>2</sup> = 0.81598728; Adjusted R <sup>2</sup> = 0.79298569; F(1,8)=35.475; p=0.00034						
	Beta	Std. Err.	B	Std. Err.	t (8)	p-level
Y <sup>2</sup>	0.903320	0.151663	0.398101	0.066839	5.956111	0.000340

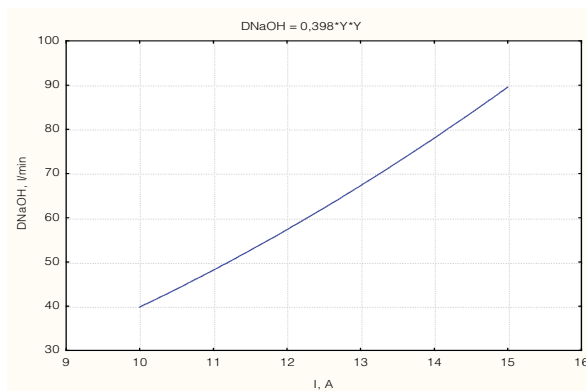


Figure 3. HHO gas flow for using NaOH electrolyte

Table 4. Regression analysis for flow for using KOH electrolyte

Regression Summary for Dependent Variable: D <sub>KOH</sub> : R= 0.98457257; R <sup>2</sup> = 0.96938316; Adjusted R <sup>2</sup> = 0.94488968; F(4,5)=39.577; p<0.00056						
	Beta	Std. Err.	B	Std. Err.	t (5)	p-level
X	12.9552	2.940868	95.643	21.71127	4.40524	0.006988
X <sup>2</sup>	-7.7727	1.705232	-3.289	0.72166	-4.55813	0.006067
Y <sup>2</sup>	8.0441	1.551205	5.483	1.05740	5.18574	0.003508
Y	-12.5926	2.809162	-114.106	25.45482	-4.48269	0.006503

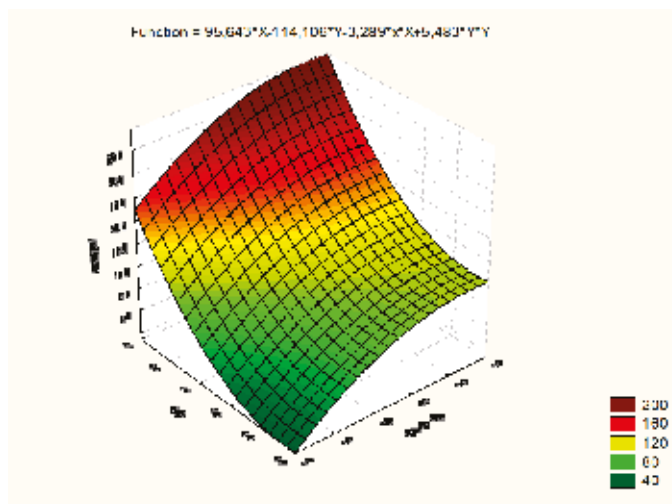


Figure 4. HHO gas flow for using KOH electrolyte

- For using electrolyte KOH, the results of experiments are shown on Table 4.

The amount of gas generated is affected to the equal extent by the current and electrolyte concentration

The regression model has the form (2):

$$D = 95,643 * X - 114,106 * Y - 3,289 * X^2 + 5,483 * Y^2 \quad (2)$$

The flow of HHO for using KOH electrolyte is graphically shown in Figure 4.

The figure shows that the highest flow rate is obtained at the maximum values of the electrolyte concentration and the current strength.

## CONCLUSIONS

On the basis of the experiments and analysis carried out, the following conclusions can be drawn:

The flow of the generated HHO gas is higher for using KOH electrolyte.

For both electrolytes (NaOH and KOH), the flow increases as the current increases.

Maximum debit for both electrolytes is obtained at 15 A current.

## REFERENCES

- Balawender, K., Jaworski, A., Kusewski, H., Ustrzyski, A. (2016). Badania wpływu zasilania z dodatkiem gazu hho na wybrane parametry użytkowe silnika spalinowego o zapłonie samoczynnym; autobusy; 6,757–760.
- Chakrapani, K., Neelamegam, P. (2011). Optimization of Fuel Consumption using HHO in NDL Technique Verified FRGA. *Journal of Theoretical and Applied Information Technology*, 31(2), 140–146.
- De Silva, T., Senevirathne, L., Warnasooriya, T. (2015). HHO Generator - An Approach to Increase Fuel Efficiency in Spark Ignition Engines. *European Journal of Advances in Engineering and Technology*. 2(4), 1–7.
- Levente, B., Lelea, D., Birsan, N. (2015). Stand for Experimental Evaluation of Effects of Hydrogen Use in Internal Combustion Engines. *Problemele energeticii regionale*, 1(27) *Termoenergetica*, 70–78.
- Malinowska, M. (2015). Ocena możliwości zastosowania gazu Browna w okrętownictwie. *ZESZYTY NAUKOWE AKADEMII MORSKIEJ W GDYNI*, 91, 103–113.
- Shalbaev, K., Uralov, D., Ladnorg, Z., Torgaev, R. (2017). Drigately na benzino-vodorodnoy smesi dlya avtotransporta respubliky Kazahstan, Material XLI Mezhdunarodnoy nauchno-prakticheskoy konferentsii KazATK im. M. Tynyshpaeva na temu: *Innovatsionnie tehnologii na transporte: obrazovanie, nauka, praktika*, tom 1, 383–388.
- Yilmaz, A., Uludamar, E., Aydin, K. (2010). Effect of hydroxy (HHO) gas addition on performance and exhaust emissions in compression ignition engines. *International Journal of Hydrogen Energy*, 35, 11366–11372
- [https://www.doc-developpement-durable.org/file/Energie/hydraulique/HHO\\_Generator\\_Plans\\_pile\\_a\\_combustible.pdf](https://www.doc-developpement-durable.org/file/Energie/hydraulique/HHO_Generator_Plans_pile_a_combustible.pdf)

## ADVANTAGES OF USING THE ELECTRO-KINETIC METHOD FOR SOIL DEPOLLUTION

**Maria POPA, Loredana Irena NEGOTA, Bogdan Petre ARNAUTU**

Petroleum-Gas University of Ploiesti, 39 Bucharest Blvd, Ploiesti, Prahova, Romania

Corresponding author email: mariapopa2007@gmail.com

### **Abstract**

*In the present paper the electro-kinetic depollution is compared with the thermal depollution. The need for a high degree of depollution for soils contaminated with liquid petroleum products is complemented by the economic need not to destroy the pollutant. The study contains a set of experimental data of laboratory activity to compare a new method of depollution with already known and industrially applicable methods. Thermal methods of depollution, combustion and desorption, are methods that have a high degree of depollution, but destroy the pollutant. Electro-kinetic depollution is based on physical principles that cause the migration of the pollutant for the purpose of collecting it without destroying it. The paper presents comparatively the degree of depollution rates achieved by the three methods and the costs obtained for them. In addition, for the electro-kinetic method particular attention has been given to both the recovery of pollutants and the properties of the water used in the process so that it does not become a new source of pollution.*

**Key words:** *depollution, electro-kinetics method, petroleum products, soil.*

### **INTRODUCTION**

Soil is the environmental factor that connects the other two factors with which man is directly connected and without whom life would not be possible: water and air.

A possible soil pollution can have effects on both the ground and the water through the water circuit in nature, but also the air through the evaporation phenomenon.

With the development of refineries and the discovery of new deposits of crude oil, soil pollution has grown, affecting all the stages of crude oil transformation into finished product, starting with extraction, and continuing with transport and refining.

Soil depollution is a difficult action because of the fact that existing technologies have a high cost, and affordable ones have a fairly long time, when the soil is unusable. There is a constant concern of authors in finding new forms of decontamination and, where appropriate, existing ones can be upgraded (Popa et al., 2016; 2017; 2018).

In the present paper there are presented by comparison three technologies of depollution, two thermics methods, already existing and with industrial applicability and a new methodphysically, which has not yet been

implemented at industrial level but the results obtained show it as a feasible alternative in the field of technologies of depollution. The idea started from literature data, in which the authors presented various possibilities for electric depollution (Streche et al., 2013). Also, variants of the use of electrodes have been studied and an attempt has been made to set up such an installation (Han et al., 2004; Li et al., 2018; Lysenco et al., 2018; Ren et al., 2014; Risco et al., 2016). Thus, a new depollution stand presented by the authors was designed (Popa M. & Negoita L.I., 2018).

### **MATERIALS AND METHODS**

Thermal decontamination methods applied at the laboratory level are achieved by: direct contact with the combustion flame and by heating without contact with the flame upon desorption. We considered from the outset the complete combustion of the pollutant when applying the combustion, so a degree of depollution of 100%. Experimental assemblies are shown in Figures 1 and 2.

For electro-kinetic (EK) method we needed an experimental assembling consisting of 9 electrodes (eight anodes and one cathode), a known volume vessel in which we tracked the

effect of the electrode field created by the electrodes and a source that transformed the alternating current in continuous current of 5 and 12V (Popa M. & Negoita L.I., 2018). Experimental assembly is shown in Figure 3.



Figure 1. Experimental installation for combustion



Figure 2. Experimental installation for desorption

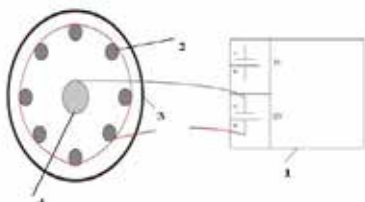


Figure 3. Experimental installation for electro-kinetic method: 1-power source; 2- anode; 3- vessel with soil; 4-cathode

In addition, for analysis we used the kit CRISON CM35 for determining the water properties before and after use. This kit is presented in Figure 4.



Figure 4. Kit CRISON CM35 for water analyser

## RESULTS AND DISCUSSIONS

In order to have results to report the efficiency of the electro-kinetic method, we have operated the modules for combustion and desorption depollution.

For combustion, we used a sample of 100 g of soil to determine organic material and a sample of soil contaminated with 5% diesel oil. The operating time of the combustion was 30 minutes, after which an organic material content of 16.8% lost by incineration and a 100% depollution rate was obtained (Table 1).

Table 1. Combustion results

Sample	Mass of the sample after combustion, g	Weight lost by combustion, g	Degree of depollution %
Sample witness	83.2	16.8 (organic material)	100
Contaminated, 5% diesel	78.2	21.8 (16.8 g organic material + 5 g diesel oil)	

For desorption, we also used a sample of 100 g of soil to determine organic soil material and a sample contaminated with 5% diesel oil.

The desorption module operating time was the same as for the 30 minutes of combustion. We obtained an organic material lost by desorption of 5.6% and a degree of depollution of 80% (Table 2).

Table 2. Desorption results

Sample	Mass of the sample after desorption, g	Weight lost by desorption, g	Degree of depollution, %
Sample witness	94.4	5.6 (organic material)	80
Contaminated 5% diesel oil	90.4	9.6 (5.6 g organic material + 4 g diesel oil)	

For electrokinetic decontamination, the electrodes were arranged as in Figure 3. In attempting to develop such a method, the first step was to "make" electrodes in a variation as close as possible to the recommendations of the specialists (Streche et al., 2013).

The electrodes are connected to a current source that allows operation at two different voltages: 5V and 12V.

The experiments started with the 5V voltage. In the first phase, the soil sample was polluted with 5% diesel oil.

The soil sample was then watered for four days, as follows: in the first three days with 200 ml of water and on the fourth day with 100 ml of water.

In total, 700 ml of water was used. All this time, the source was powered.

The total volume of water collected on the fifth day was 150 ml (Figure 5).

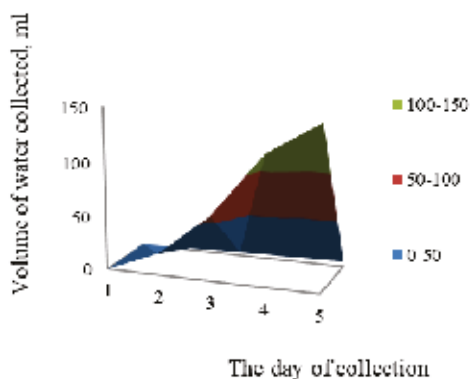


Figure 5. Water collected after 5 days

After five days it was found that at the 5 V voltage and the 5% diesel oil concentration, no pollutant was moved to the cathode.

For this reason, the concentration of the pollutant was considered too low and increased from 5 to 10% for the diesel oil pollutant, but the supply voltage also increased from 5 to 12V.

In the electro-kinetic process we used distilled water to generate the electroosmosis phenomenon, an essential factor alongside electromigration and electrophoresis.

The volumes of soil, distilled water and diesel introduced and subsequently partially collected, are shown in table below (Table 3).

An experimental without electrodes module was also used.

Table 3. Decontamination degrees and water usage for EK method

Working days for 12V 10% diesel oil		Sample soil 1800g soil + 200g diesel oil (240 ml)	
		With electrodes	Without electrodes
Day 1	Water used	300 ml	300 ml
Day 2		300 ml	300 ml
Day 3		300 ml	300 ml
Day 4		300 ml	300 ml
On days 5 and 6 the current was not stopped. Only the water supply was interrupted.			
Collected on day 7	Water	540 ml	500 ml
	Diesel oil	50 ml	30 ml
Decontamination degree, %		21	12.5

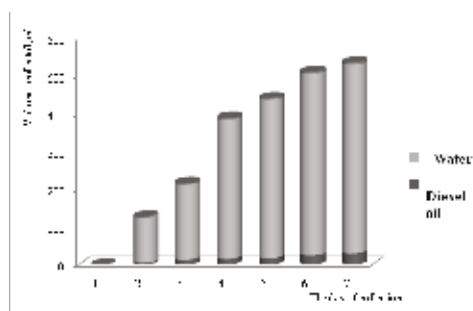


Figure 6. The time variation of collected volumes

Following the passage of water through soil types and especially under the influence of the electric field, it changes its properties. The way water changes its characteristics is important due to the fact that after treatment of the soil and water it must be subjected to the initial properties. The modified water properties allow us to categorize it as the wastewater to be treated (Table 4).

Table 4. Properties of water (used and clean)

Properties	Clean distillate water	Water from electrode module	Water from witness module	Potable water
pH <sup>27°C</sup>	7.84	11.72	10.17	7.15
Conductivity <sup>27°C</sup>	0.272 mS/cm	4.49 mS/cm	0.608 mS/cm	1.342 mS/cm
Salinity <sup>27°C</sup>	10.34 mg/l	2.36 mg/l	294 mg/l	661 mg/l

## CONCLUSIONS

Based on the results obtained, referring to the properties of the soils and in comparison with the methods already known, we can state the following:

The method of electro-kinetic depollution is a method which allows the recovery of a certain proportion of the pollutant.

The electro-kinetic depollution method can only be used as a preliminary method of depollution.

The lack of results after 5V operation and the occurrence of a degree of depollution, but especially the collection and separation of the used water pollutant at 12V, can be considered to operate at a higher voltage to obtain depollution degrees, respectively a higher recovery.

There is a degree of depollution and recovery of the larger product in the presence of the electric field than in the absence of it.

The degree of depollution of the new method is inferior to the degree of depollution of the thermal methods, but recovering polluting products by using the electro-kinetic depollution method constitutes an economic advantage.

## REFERENCES

Han, S. J., Kim, S. S., Kim, B. I. (2004). Electroosmosis and porepressure development characteristics in lead contaminated soil during electrokinetic remediation. *Geosciences Journal*, 8, 85–93.

Li, D., Ji, G., Hu, J., Hu, S., Yuan, X. (2018). Remediation strategy and electrochemistry flushing&reduction technology for real Cr(IV)-contaminated soils. *Chemical Engineering Journal*, 334, 1281–1288.

Lysenko, L., L., Shen, A., E., Rynda, E., F. (2018). Prevention of Groundwater Pollution by Using the

Electroosmotic Flushing of Soilsystems. *Journal of Water Chemistry and Technology*, 40, 102–107.

Popa, M., Onutu, I. (2016). Studies on the Seed Germination after Thermal Decontamination of Crude Oil Polluted Soils. *Agriculture and Agricultural Science Procedia*. Available online at [www.sciencedirect.com](http://www.sciencedirect.com), 10/2016, <https://doi.org/10.1016/j.aaspro.2016.09.014>.

Popa, M., Negoita, L. (2016). Comparative studies on remediation techniques in laboratory of soils contaminated with liquid petroleum products, SIMIECOIND The environment and industry, 187–192, <https://doi.org/10.21698/simi.2016.0024>.

Popa, M., Negoita, L., Oprescu, E., Radulescu, S. (2017). Laboratory studies on accidental pollution and soil remediation techniques, SIMIECOIND The environment and industry, 49–55, DOI: <http://doi.org/10.21698/simi.2017.0006>.

Popa, M., Negoita, L. I. (2018). New laboratory techniques on soil decontamination, *SIMI ECOIND Incd Ecoind* – international symposium – simi 2018, The environment and industry, Proceedings book, Section Sustainable Environmental Technologies, 69–75, DOI: <http://doi.org/10.21698/simi.2018.fp08>.

Popa, M. (2017). *Tehnologii de depoluare a solurilor contaminate*. Editura UPG Ploiesti.

Ren, L., Lu, H., He, L., Zhang, Y. (2014). Enhanced electrokinetic technologies with oxidation-reduction for organically-contaminated soil remediation, *Chemical Engineering Journal*, 247, 111–124.

Risco, C., Lopez-Vizcaino, R., Saez, C., Yustres, A., Canizares, P., Navarro, V., Rodrigo, M. A. (2016). Remediation of soils polluted with 2,4-D by electrokinetic soil flushing with facing rows of electrodes: A case study in a pilot plant. *Chemical Engineering Journal*, 285, 128–136.

Risco, C., Rodrigo, S., Lopez, Vizcaino, R., Yustres, A., Saez, C., Canizares, P., Navarro, V., Rodrigo, M. A. (2016). Removal of oxyfluorfen from spiked soil using electrokinetic soil flushing with linear row of electrodes. *Chemical Engineering Journal*, 294, 65–72.

Streche, C., Istrate, I. A., Badea, A. (2013). The treatment of diesel contaminated soil by DCTs methods. *UPB Scientific Bulletin, Series C: Electrical Engineering*.

## BIO-INGREDIENTS BASED ON SPENT INDUSTRIAL YEAST BIOMASS

Simona-Ioana MARINESCU<sup>1,8</sup>, Daniela Eliza MARIN<sup>2</sup>, Zsuzsa JÓKAI<sup>3</sup>,  
Márta ÜVEGES<sup>3</sup>, Madalina ALBU KAYA<sup>4</sup>, Vasile BUNDOC<sup>5</sup>,  
Mihály DERNOVICS<sup>6</sup>, Hajnalka HINGYI<sup>7</sup>, Mihaela BEGEA<sup>1,9</sup>,  
Iuliana Diana BARBULESCU<sup>1,8</sup>

<sup>1</sup>Pharmacorp Innovation, 313 Splaiul Unirii Street, 030138, Bucharest, Romania

<sup>2</sup>Laboratory of Animal Biology, National Research and Development Institute for Biology and Animal Nutrition, Balotesti (INCDBNA-IBNA), 1 Calea Bucuresti, Balotesti, 077015, Ilfov, Romania

<sup>3</sup>Szent István University, Faculty of Food Science, Department of Applied Chemistry, Budapest, Hungary

<sup>4</sup>Collagen Department, INCDTP - Division Leather and Footwear Research Institute, 93 Ion Minulescu Street, 031215, Bucharest, Romania

<sup>5</sup>S.C. Avicola Lumina S.A, 3 Tulcei Street, 907175, Constanta, Romania

<sup>6</sup>Hungarian Academy of Sciences' Department of Plant Physiology, Centre for Agricultural Research, 2462 Martonvásár, Hungary

<sup>7</sup>Adexgo Ipari, Kereskedelmi és Szolgáltató Kft. 8230 Balatonfüred, Hungary

<sup>8</sup>University of Agronomic Sciences and Veterinary Medicine of Bucharest, 59 Marasti Blvd, District 1, 011464, Bucharest, Romania

<sup>9</sup>University Politehnica of Bucharest, Faculty of Biotechnical Systems Engineering, Department of Biotechnical Systems, 313 Splaiul Independentei, 060042, Bucharest, Romania

Corresponding author email: barbulescudia@yahoo.com

### Abstract

*The paper relates to obtaining new bio-ingredients based on wine/brewing yeast biomass rich in polyphenols, which can be used for feed purpose. The drying process by lyophilization of yeast biomass was performed in the pilot phase in order to obtain active yeast and the content of total polyphenol and protein was also determined. Inactivation of yeast by drum dryers with rolled drums was also achieved and the content of total polyphenol and protein from spent brewing yeast and mixture of this with new bio-ingredients based on wine/beer yeast biomass was performed. A content of 580-930 mg/100 g (referred to gallic acid) was obtained for yeast that accumulates total polyphenol at pilot level, 320 mg/100 g (referred to gallic acid) dry spent brewing yeast and 310 mg/100 g (referred to gallic acid) for mixture (the yeast obtained at pilot level and spent brewing yeast). It was also noticed that the content of protein at pilot level for yeast that accumulates protein at pilot level was 41.24 g/100 g, 45.73 g/100 g for spent brewing yeast and 42.85- 43.39 g/100 g of protein from mixed yeasts.*

**Key words:** bioingredient, new materials, polyphenols, protein, yeast.

### INTRODUCTION

Yeast has been used for thousands of years to produce food and beverages such as beer, wine, sake and bread. Despite the fact that *S. cerevisiae* remains by far the most commonly used species of yeast, other unconventional yeasts such as the *Scheffersomyces jamb*, *Yarrowia lipolytica*, *Kluyveromyces lactis* and *Dekkera bruxellensis* have also supported the contributors to industrial fermentation processes (Steensels et al., 2014). *Dekkera*

species are also important in the bread and brewing industry. When high levels occur, food spoilage occurs. However, small amounts of *Dekkera* contribute to the desired metabolites in bread, lambic beer, ale and kombucha tea (Schifferdecker, 2014).

Beer production inevitably leads to the generation of different wastes and by-products. The most common by-products are spent grains, spent hops and spent yeast, which are generated from the main raw materials used to produce beer.

From environmental point of view, the disposal of industrial by-products is a solution to pollution problems (Mussatto, 2009).

For example, yeast can be used for accumulation of organic minerals such as selenium, zinc, copper in biomass. By optimizing media factors such as sucrose, yeast extract,  $MnSO_4$ ,  $ZnSO_4$ ,  $CuSO_4$ , vitamins,  $FeCl_3$ , (Barbulescu et al, 2010) yeast biomass enriched with  $1145.8 \text{ mg} \times \text{l}^{-1}$  copper,  $1143.4 \text{ mg} \times \text{l}^{-1}$  zinc and  $33.9 \text{ mg} \times \text{l}^{-1}$  manganese has been obtained.

Most of the spent brewer's yeast, a waste product, is used as a source of protein, B vitamins, and minerals in animal feed production. Spent brewer's yeast is a good source of inexpensive protein (45-60%), B vitamins, minerals (York & Ingram, 1996; Ferreira et al., 2010; Jarmolowicz et al., 2013; Waszkiewicz R., 2013; Bartłomiej et al., 2016).

Spent brewing yeast has been studied as source of polyphenols as well. Total analysis of polyphenols and total flavonoids was performed using the spectrophotometric method described by (Vijayalaxmi et al., 2015), with some changes, and the polyphenols were isolated from the spent brewer's yeast by applying various aqueous extraction solutions, water or ethanol/water (20/80) at different extraction temperatures (León-González et al, 2017).

## MATERIALS AND METHODS

The preinoculum, inoculum and fermentation processes were static; the wine and brewing processes selected yeasts used for pitching are obtained from a maintenance culture that is harvested on medium based on yeast extract. The method for preparation of preinoculum, inoculum and the fermentation process were described by Barbulescu et al (2018) in Figures 1a-1d.



Figure 1a. Selection of yeast colonies



Figure 1b. Selected yeast colonies



Figure 1c. Preinoculum obtainment - Yeast cultures developed at agar slant



Figure 1d. Inoculum development at orbital shaker

The mixture between liquid spent brewing yeast and consortium wine and brewing yeast obtained at pilot level was done by a specific technique and a protocol for homogenization.

The culture fermented media was a subject of the post-fermentation process comprising the following steps (Figures 2 and 2a-2d):



Figure 2. Fermented media

1) Separation of biomass by centrifugation.



Figure 2a. Centrifugation of fermented media



Figure 2b. Biomass of separated yeast by centrifugation

2) Washing the biomass.



Figure 2c. Washing with distilled water of yeast biomass

3) Drying the biomass by lyophilisation/drier drum.

**Method for separation of wet cell yeast by culture medium**

Post-fermentation processing:

- *Separation of fermented media:* The easiest and fastest way to perform yeast biomass separation from the fermentation medium is to apply centrifugation, by which separation of the yeast cells from the culture medium and metabolites occurs;
- *Washing of biomass:* To remove the culture medium retained between yeast cells, it is necessary to wash the separated biomass two or three times with distilled water.

The washing is done by vigorous stirring followed by centrifugation and discharging the wash water. The volume of the wet cell biomass was used to estimate the cell concentration in the broth, taking into account that the mass of the dry cells (g) is about 25% of the volume of the wet cells (ml) (Vieira et al., 2013).

The centrifugal cells were washed with distilled water and centrifuged twice after being transferred to pre-weighed dishes. The biomass was dried at  $60 \pm 5^\circ\text{C}$  at a constant weight (Vieira et al., 2013)



Figure 2d. Wet yeast biomass

During the drying process, the cells that are excessively dry are inactive, unlike those where drying is not so advanced and, therefore, remain active. This is primarily due to the drying conditions and is related to the homogeneity of the material to be dried.

**Drying the wet biomass by lyophilisation**

The yeast biomass was freeze-dried using a Delta 2-24 LSC lyophilizer (Martin Christ, Germany) as following: the yeast biomass were

put into Petri dishes and initially frozen at  $-40^{\circ}\text{C}$  for 8 hours followed by main freeze-drying at  $-40^{\circ}\text{C}$  and 0.1 mbar for 10 hours. Then the temperature increased in steps to  $10^{\circ}\text{C}$  during 10 hours, to  $20^{\circ}\text{C}$  during other 8 hours and to  $30^{\circ}\text{C}$  for 8 hours at same pressure, 0.1 mbar. The final freeze-drying lasted 3 hours: 1 hour at  $30^{\circ}\text{C}$  and 0.001 mbar followed by 2 hours until temperature reached  $35^{\circ}\text{C}$ . After 48 hours of freeze-drying (Table 1 and Figure 3) the obtained dried yeast biomass was sent to analysis.

Table 1. Yeast biomass lyophilization program

No. phase	Stage of the lyophilization process	Time, hours	Shelf temperature, $^{\circ}\text{C}$	Pressure mbar
1	Freezing *	8	$-40$	1000
2	Main freeze-drying	10	$-40$	0.1
3	Main freeze drying	10	10	0.1
4	Main freeze drying	8	20	0.1
5	Main freeze drying	8	30	0.1
6	Final freeze drying	1	30	0.001
7	Final freeze drying	3	35	0.001

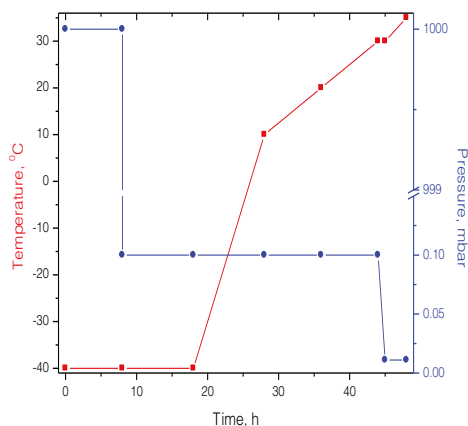


Figure 3. Lyophilization program

**Drying the wet biomass using drum dryers (drying of spent brewing yeast and mixture of yeast biomass to obtain inactive yeast)** (Figure 4).

The raw material to be subjected to the drying process, in order to obtain dried yeast biomass, is the spent yeast resulted from the brewing

process in the form of yeast milk. It was used using a dryer with drum dryers. Drum dryers are heat-transfer conduction.

A heating medium (generally steam) is sent to the rotating drum (cylinder) and the liquid material is fed to the heated drum to evaporate and concentrate and at the same time the liquid material is blocked on the surface of the drum in the form of a film, evaporated and dried.

Dry materials are continuously scraped with a knife. The mixture of yeast biomass was dried by inactivation with a specific technology. The dry yeast biomass is presented in the form of a brownish-brown powder with a bitter-sweet taste, having the specific smell and aroma of yeast.

The time for drying is shorter when the liquid spent yeast or the mixtures of yeast biomass are not exposed to high temperatures for a long period.



Figure 4. Dry yeasts biomass samples

**Methods of determination of moisture (%) and crude protein (CP) for yeast biomass**

Standardized methods were used, in accordance with Regulation (EC) No. 152 (2009). The moisture and crude protein (CP) were determined from the biomass in accordance with recognized standardized methods (SR 8613-1: 2009, SR 8613-6: 2009).

**Method for total polyphenols determination**

Total polyphenols were analyzed by Folin-Ciocalteu method.

About 250 mg of samples were weighted in a centrifuge tube, and 10 ml of water were added. After that, the samples were centrifuged at 6000 rps for 20 minutes.

The supernatant was separated and centrifuged again at 12000 rps for 15 minutes.

Gallic acid was used to prepare the standard curve. The working reagent was prepared by diluting a stock solution of Folin-Ciocalteu's

phenol reagent with distilled water (1:10, v/v). Sodium carbonate solution was prepared by mixing 7.42 g Na<sub>2</sub>CO<sub>3</sub> with 100 ml distilled water (0.7 M).

Methanol solution was prepared in ration 4:1 with distilled water. Samples (the supernatant resulted from the second centrifugation) (50 µl) were aliquoted into test cuvettes, 200 µl of methanol solution and 1250 µl of prepared Folin-Ciocalteu's phenol reagent was added.

After a few minutes, 1000 µl of saturated sodium carbonate solution-Na<sub>2</sub>CO<sub>3</sub> (7.5% w/v in water) was added. The mixture was then incubated at 50<sup>0</sup>C for 5 min.

Afterwards, the absorbance of the reaction mixture was measured at 760 nm using a Spectronic Helios Gamma UV Visible spectrophotometer (Thermo Fisher Scientific). The results were expressed as mg GA/100 g of dry yeast sample.

## RESULTS AND DISCUSSIONS

Three pilot biomass samples based on consortium of wine and brewing yeast and dried by lyophilisation (S1, S2, S3) were taken in the study for the assessment of protein and total polyphenols.

The difference between these samples is based on the inoculum ratio (results not presented in this paper).

The biomass samples S1 and S2 have been further mixed with spent brewing yeast (as wet biomass), and the bioingredients S1 mixture and S2 mixture have been obtained.

Table 2 illustrates the characterisation of biomass samples as regards the content in polyphenols, and the content of crude protein and moisture is presented in Table 3.

It was observed the higher content of total polyphenols in the sample S1 (Table 2).

Table 2. Content of total polyphenol from different samples of yeasts biomass (average values)

Samples	Moisture, %	Crude protein, g/100g
S1	11.5	41.24
S2	11.61	35.76
S1 mixture	9.62	43.39
S2 mixture	7.32	42.85
Spent brewing yeast	5.69	45.73

Table 3. Content of protein and moisture from yeast biomass

Samples	Total polyphenol, mg/100g (referred to gallic acid)
S1	930
S2	760
S3	580
Control dry spent brewing yeast	310
S1 mixture	340
S2 mixture	330

The concentration of total polyphenols in the mixture samples is decreased because of the mixture with spent brewing yeast, in order to be valorised as a polyphenol source for the feed receipts for laying hens.

The polyphenol content in the spent brewer's yeast was found between 0.23 and 2.9 mg of gallic acid/g by León-González et al. (2017), these results being comparable with those presented in this paper.

The content of polyphenols was highly dependent on the treatment applied to the spent brewing yeast (lyophilized and air-dried yeast). The content of crude protein for mixture samples was higher in comparison with the content of crude protein for the spent brewing yeast.

## CONCLUSIONS

This study demonstrated the possibility of utilisation of spent brewing yeast for feed receipts. The new bioingredients are good source of polyphenols and protein.

The higher content of protein was noticed for the S2 mixture.

The drying using drum dryers is preferable because the method is economic and efficient.

The mixture obtained was taken into study in order to set up a new feed receipt formula that has been tested on laying hens (results not presented).

The yeast biomass is a good and cheap source of protein and polyphenols.

## ACKNOWLEDGEMENTS

This work is financially supported by EUREKA 94/2017, EUREKA\_16-1-2017-0006 project (project ID 11700, ZINCOPPYEAST).

We also thank the company AGSIRA SRL for providing samples of post-fermentation brewing yeast biomass.

## REFERENCES

- Barbulescu, I. D., et al (2010). Obtaining yeast biomass enriched with copper, zinc and manganese. *Romanian Biotechnological Letters*, 1, January, 5008–5016.
- Barbulescu, I. D., Üveges, M., et al. (2018). Fermentative technological research for obtaining zinc enriched yeasts. *Nonconventional Technologies Review*, 4, 10–15
- Ferreira, I. M. P. L. V. O., Pinho, O., Vieira, E., Tavarela, J. G. (2010). Brewer's *Saccharomyces* yeast biomass: characteristics and potential applications. *Trends in Food Science and Technology*, 21, 77–84.
- León-González, M. E., Gómez-Mejía, E., Rosales-Conrado, N., Madrid-Albarrán, Y. (2018 Nov.). Residual brewing yeast as a source of polyphenols: Extraction, identification and quantification. *Food Chem.*, 30(267), 246–254. doi: 10.1016/j.foodchem.2017.06.141. Epub 2017 Jun 27.
- Jarmołowicz, S., Zakęś, Z., Siwicki, A., Terech-Majewska, E., Kowalska, A., Partyka, K., Hopko, M. (2013). Immunomodulatory effect of dietary brewer's yeast extract in *Sander lucioperca* juveniles against the challenge of *Aeromonas salmonicida*. *Aquaculture International*, 21, 939–945.
- Solange I. Mussatto (2009). Biotechnological Potential of Brewing Industry By-Products, *Biotechnology for Agro-Industrial Residues Utilisation* (pp. 313–326), P. Singh nee' Nigam, A. Pandey (eds.). *Biotechnology for Agro-Industrial Residues Utilisation*, DOI 10.1007/978-1-4020-9942-7 16
- Pod Pora, B., Świdorski, F., Sadowska, A., Rakowska, R., and Wasiak-Zys, G. (2016). Spent Brewer's Yeast Extracts as a New Component of Functional Food, 554 *Food Technology and Economy, Engineering and Physical Properties*, *Czech J. Food Sci.*, 34(6), 554–563, doi: 10.17221/419/2015-CJFS.
- Schiffederdecker, A. J., Dashko, S., Ishchuk, O. P., and Piškur, J. (2014 Sep.). The wine and beer yeast, *Dekkera bruxellensis*, *Yeast.*, 31(9), 323–332
- Steensels, J., Snoek, T., Meersman, E., Nicolino, M. P., Voordeckers, K., and Verstrepen, K. J. (2014 Sep). Improving industrial yeast strains: exploiting natural and artificial diversity. *FEMS Microbiol Rev.*, 38(5), 947–995.
- Vieira, É. D., Maria da Graça, S., Andrietta, S. R. (2013). Yeast biomass production: a new approach in glucose-limited feeding strategy. *Brazilian Journal of Microbiology*, 44(2), 551–558.
- Vijayalaxmi, S., Jayalakshmi, S. K., Sreeramulu, K. J. (2015 May). Polyphenols from different agricultural residues: extraction, identification and their antioxidant properties. *Food Sci Technol*, 52(5), 2761–2769.
- York, S. W., Ingram, L. O. (1996). Ethanol production by re-combinant *Escherichia coli*, KO11 using crude yeast au-tolysate as a nutrient supplement. *Biotechnology Letters*, 18, 683–688.
- Waszkiewicz-Robak, B. (2013). Spent brewer's yeast and beta-glucans isolated from them as diet components modifying blood lipid metabolism disturbed by an atherogenic diet. In: Baezin R.V. (ed.): *Lipid Metabolism. Croatia, InTech Pub*: 261–290. SR 8613-1: 2009 - Food concentrates. Part 1: Determination of moisture SR 8613-6: 2009 - Food concentrates. Part 6: Determination of nitrogen.





ISSN 2285 – 6064  
ISSN-L 2285 – 6064